9-18-2014

Navigation Solution for a Multiple Satellite and Multiple Ground Architecture

Abraham M. Leigh

NAVIGATION SOLUTION FOR A MULTIPLE SATELLITE AND MULTIPLE GROUND ARCHITECTURE

DISSERTATION

Abraham M. Leigh, Captain, USAF

AFIT-ENY-DS-14-S-1

DEPARTMENT OF THE AIR FORCE
AIR UNIVERSITY

AIR FORCE INSTITUTE OF TECHNOLOGY

Wright-Patterson Air Force Base, Ohio

The views expressed in this dissertation are those of the author and do not reflect the official policy or position of the United States Air Force, the Department of Defense, or the United States Government.

AFIT-ENY-DS-14-S-1

NAVIGATION SOLUTION FOR A MULTIPLE SATELLITE AND MULTIPLE GROUND ARCHITECTURE

DISSERTATION

Presented to the Faculty

Graduate School of Engineering and Management

Air Force Institute of Technology

Air University

Air Education and Training Command

in Partial Fulfillment of the Requirements for the

Degree of Doctor of Philosophy in Astronautical Engineering

Abraham M. Leigh, B.S., M.E.

Captain, USAF

September 2014

AFIT-ENY-DS-14-S-1

NAVIGATION SOLUTION FOR A MULTIPLE SATELLITE AND MULTIPLE GROUND ARCHITECTURE

DISSERTATION

Abraham M. Leigh, B.S., M.E.
Captain, USAF

Approved:

/signed/	7 May 2014
Jonathan T. Black, PhD (Chairman)	Date
/signed/	10 Apr 2014
William E. Wiesel, PhD (Member)	Date
/signed/	22 Apr 2014
Mark E. Oxley, PhD (Member)	Date
/signed/	30 Apr 2014
David B. Goldstein, PhD (Member)	Date

Accepted:

/signed/	3 Jun 2014
ADEDEJI B. BADIRU PhD Dean, Graduate School of Engineering and Management	Date

AFIT-ENY-DS-14-S-1

Abstract

This research presents the phased development of an algorithm to plan impulsive orbital maneuvers based on the relative motion between multiple satellites and multiple ground locations. The algorithm leverages the state transition matrix derived from the equations of motion and the equations of variation for the non-spherical Earth and air drag effects. The algorithm determines the impulsive maneuver to achieve the user-defined terminal conditions. The first phase solves for the first burn of an orbital transfer between user-defined altitudes. The optimum trajectory is determined and compared to the first burn in a Hohmann Transfer. The results are expanded to include varying the inclination and eccentricity of the initial orbit. The second phase solves for the minimum time trajectory resulting from a fixed fuel maneuver to transfer a satellite between user-defined altitudes. The results include the transfer time and transfer angle for the minimum time trajectory. The third phase places a satellite within a sphere, of user-defined radius, centered on a non-maneuvering satellite within a constrained time. The results are presented for prograde orbits. An empirical method to determine the optimum ΔV is provided. The fourth phase places a satellite within the overlapping spheres, of user-defined radii, centered on multiple non-maneuvering satellites, within a constrained time. Empirical methods are presented to determine the separation distance and optimum ΔV. The final phase culminates by delivering a satellite within the overlapping spheres, centered on multiple non-maneuvering satellites and ground locations, constrained by range and elevation angle, within a constrained time. An empirical model to calculate the optimum ΔV is shown. All results illustrate mission design trade-offs including ballistic coefficient, orbit inclinations, eccentricity and orbit sizes.

To my Wife and Kids

Acknowledgments

Thank you very much to my advisor, Dr. Jonathan Black. His guidance and wisdom helped shape and bound the problem into a manageable project that has resulted in this successful document. I also appreciate the countless discussions with him about losing the forest through the trees.

I also want to thank my family, friends and the rest of my class including the guys in the Outhouse. Special thanks to Dan Showalter for numerous 'chalk-talks' to work through some of the abstract components of this research.

Abraham M. Leigh

Table of Contents

Page

Page

Page

List of Figures

List of Tables

List of Symbols

Symbol	Definition
A	cross-sectional area normal to velocity direction (m^2)
a	orbit semi-major axis (km)
a_T	transfer orbit semi-major axis (km)
$\vec{d}_{DRAG}$	air drag acceleration ($\frac{km}{s^2}$)
$\partial\vec{d}_{DRAG}$	partial derivative of air drag vector
a_R	semi-major axis ratio
B^*	ballistic coefficient ($\frac{m^2}{kg}$)
C_D	coefficient of drag
E	eccentric anomaly (rad)
e	orbital eccentricity
$\bar{e}$	error vector
a_R	semi-major axis ratio
e_T	eccentricity of transfer orbit
H	scale height
$\|\vec{h}\|$	Specific angular momentum magnitude ($\frac{km^2}{s}$)
$h_X(t_0)$	component of specific angular momentum in X direction ($\frac{km}{s}$)
$h_Y(t_0)$	component of specific angular momentum in Y direction ($\frac{km}{s}$)
$h_Z(t_0)$	component of specific angular momentum in Z direction ($\frac{km}{s}$)
h_0	base altitude (km)
h_{ellp}	height above the elliptical (km)
$\mathbf{I}$	identity matrix
i	orbital inclination (deg)
i_R	inclination ratio

Symbol	Definition
J_2	Earth's 2nd zonal harmonic
m	satellite mass (kg)
N	number of cooperative satellites
p	number of ground locations
$\mathbf{Q}$	weight matrix
$R_\oplus$	radius of the Earth (km)
$\partial\vec{R}_X$	partial derivative of x component of position vector
$\partial\vec{R}_Y$	partial derivative of y component of position vector
$\partial\vec{R}_Z$	partial derivative of z component of position vector
$\vec{R}_{Sat1}$	position vector for Satellite 1 (km)
$\lvert\vec{R}\rvert$	Position magnitude (km)
$\dot{R}$	change in position vector ($\frac{km}{s}$)
R_{Sat1_X}	component of final position vector for Satellite 1 in x direction (km)
R_{Sat1_Y}	component of final position vector for Satellite 1 in y direction (km)
R_{Sat1_Z}	component of final position vector for Satellite 1 in z direction (km)
R_{Sat2_X}	component of final position vector for Satellite 2 in x direction (km)
R_{Sat2_Y}	component of final position vector for Satellite 2 in y direction (km)
R_{Sat2_Z}	component of final position vector for Satellite 2 in z direction (km)
R_{t_0}	initial altitude for Satellite 1 (km)
R_{t_f}	desired/final altitude for Satellite 1 (km)
$R_X(t_0)$	initial position x component for Satellite 1 (km)
$R_Y(t_0)$	initial position y component for Satellite 1 (km)
$R_Z(t_0)$	initial position z component for Satellite 1 (km)
$\mathbf{S}$	scaling matrix
$\mathbf{T}$	T matrix for differential control algorithm

Symbol	Definition
$\tilde{T}$	intermediate **T** matrix
$\vec{u}$	control vector
∂u	variation of the control vector
$\vec{V}_{REL}$	relative velocity vector ($\frac{km}{s}$)
$\partial\vec{V}_X$	partial derivative of x component of velocity vector
$\partial\vec{V}_Y$	partial derivative of y component of velocity vector
$\partial\vec{V}_Z$	partial derivative of z component of velocity vector
$\vec{V}_{Sat1}$	velocity vector for Satellite 1 ($\frac{km}{s}$)
$\lvert\vec{V}\rvert$	Velocity magnitude ($\frac{km}{s}$)
$\dot{V}$	change in velocity vector ($\frac{km}{s^2}$)
$V_X(t_0^-)$	initial velocity x component for Satellite 1 ($\frac{km}{s}$)
$V_Y(t_0^-)$	initial velocity y component for Satellite 1 ($\frac{km}{s}$)
$V_Z(t_0^-)$	initial velocity z component for Satellite 1 ($\frac{km}{s}$)
$X_{Sat1}(t_0^-)$	Satellite 1 state vector at $t = 0^-$
$X_{Sat1}(t_0^+)$	Satellite 1 state vector at $t = 0^+$
β	starting angle for 2^{nd} satellite
γ	user defined ground sphere radius (km)
Δt	transfer time update (s)
ΔV_X	component of maneuver in x direction ($\frac{m}{s}$)
ΔV_Y	component of maneuver in y direction ($\frac{m}{s}$)
ΔV_Z	component of maneuver in z direction ($\frac{m}{s}$)
ΔV_{Sat1_X}	component of maneuver in x direction for Satellite 1 ($\frac{m}{s}$)
ΔV_{Sat1_Y}	component of maneuver in y direction for Satellite 1 ($\frac{m}{s}$)
ΔV_{Sat1_Z}	component of maneuver in z direction for Satellite 1 ($\frac{m}{s}$)
ϵ	Specific mechanical energy ($\frac{km^2}{s^2}$)

Symbol	Definition
η	user defined satellite sphere radius (km)
$\vec{\Lambda}$	satellite sphere miss vector (km)
Λ_X	component of satellite sphere miss vector in X direction (km)
Λ_Y	component of satellite sphere miss vector in Y direction (km)
Λ_Z	component of satellite sphere miss vector in Z direction (km)
μ	Earth's gravitational parameter ($\frac{km^3}{s^2}$)
ρ	atmospheric density ($\frac{kg}{m^3}$)
ρ_0	nominal atmospheric density ($\frac{kg}{m^3}$)
$\vec{\Upsilon}$	ground sphere miss vector (km)
Υ_X	component of ground sphere miss vector in X direction (km)
Υ_Y	component of ground sphere miss vector in Y direction (km)
Υ_Z	component of ground sphere miss vector in Z direction (km)
Φ	State Transition Matrix (STM)
ϕ	upper right portion of STM
ϕ_{GS}	ground location angle off of $\hat{I}$
Ω	Right Ascension of the Ascending Node (deg)
ω	Argument of Perigee (deg)
$\vec{\omega}$	Earth's rotation rate vector ($\frac{rad}{s}$)
$\omega_\oplus$	Earth's rotation rate ($\frac{rad}{s}$)

List of Acronyms

Acronym	Definition
ORS	Operationally Responsive Space
DoD	Department of Defense
TMN	T-Matrix Navigation
BC	Ballistic Coefficient
DU	Distance Unit
TU	Time Unit
COEs	Classical Orbital Elements
STM	State Transition Matrix
EOM	Equations of Motion
EOV	Equations of Variation
LEO	Low Earth Orbit
GEO	Geostationary Orbit
GTO	Geostationary Orbit Transfer
RAAN	Right Ascension of the Ascending Node
ROM	Rough-Order-of-Magnitude
LCM	Least Common Multiple
PQW	Perifocal Coordinate System

NAVIGATION SOLUTION FOR A MULTIPLE SATELLITE AND MULTIPLE GROUND ARCHITECTURE

I. Introduction

1.1 Motivation

Significant effort and capital has been placed into the concepts regarding responsive space and space superiority. The need for responsive space capabilities is recognized throughout the Department of Defense (DoD). Specifically, this need led to the establishment of the Operationally Responsive Space (ORS) Office with a charter to be the "agent for change" [2] for how the DoD moves into the future regarding its space capabilities. Additional resources are leveraged at numerous levels for the ability to better monitor, understand and control the space domain.

Though the concepts of responsive space superiority are unbounded, most attention has been focused towards the design, development and deployment of new hardware to meet emerging needs[2]. However, this hardware continues to consistently leverage the infrastructure that is already in place. Therefore, little forethought has been placed in significant modification to, or the development and implementation of a new infrastructure or concepts to specifically execute a responsive space superiority mission. One significant capability of the necessary architecture is to provide the ability to relay both satellite telemetry and payload communications between a ground station and the collection satellite during a responsive space scenario. Additional capability is to analytically predict satellite separation distances between multiple satellites as well as develop maneuver sequences in complex dynamic scenarios.

Addressing these types of responsive space superiority scenarios requires a new paradigm of thinking. Therefore, it is the intent of this research to pass on to the reader a concept for optimizing the necessary maneuvers between a single satellite and a number of cooperative satellites including ground locations while satisfying defined criteria.

The study of astrodynamics and the theory of optimal orbital maneuvering is nothing novel. The literature is robust in forms and methods of establishing and solving optimal control problems applying to the minimization of both time and fuel for satellite applications. The literature presents both continuous and impulsive thrust models with the objectives of minimizing both time and fuel. The literature is full of many forms and applications of solving the "problem of orbit determination from two positions and time"[3] known as Lambert's Problem. Specifically, Lambert's Problem is regarded as a problem "of considerable interest to modern astrodynamics since it has direct application in the solution of intercept and rendezvous..."[3]. Significant research has been completed with a focus on the algorithms necessary for satellite and missile intercept and rendezvous. One such research topic was that of Chioma. Chioma presents an algorithm to satisfy the repeated satellite intercept mission[4]. Chioma's algorithm, called T-Matrix Navigation, provides the foundation for this research. It is the focus of this research to enhance the T-Matrix Navigation algorithm to present a new algorithm to ultimately demonstrate the ability to optimize the desired geometry between multiple satellites and ground locations.

Throughout this research the algorithm complexity will build from one maneuvering satellite and one cooperative satellite to the more general one maneuvering satellite with multiple cooperative satellites with multiple ground locations. It is also the intent of this research to provide a foundational argument for the optimality of the T-Matrix Navigation algorithm. Although optimality was argued by Chioma[4], this research will present a more general case for optimizing both orbital transfer time and fuel expended.

1.2 Research Objectives

The overall vision of this research is to provide an algorithm that optimizes the necessary impulsive thrust maneuvers to achieve the user-defined geometry between multiple satellites as well as multiple ground locations. By successfully completing the objectives below, this vision can be realized. There are four main objectives to be met and presented from this research. They are broken into areas that are addressed throughout the chapters of this document.

1. Demonstrate the robust optimality of the T-Matrix Navigation (TMN) algorithm. (Chapters 5 and 6)

   (a) Demonstrate a fixed time minimum fuel maneuver similar to the first burn of a Hohmann Transfer. (Illustrated in Figure 1.1 and presented in Chapter 5).

   (b) Demonstrate a constrained fuel minimum time maneuver. (Illustrated in Figure 1.2 and presented in Chapter 6).

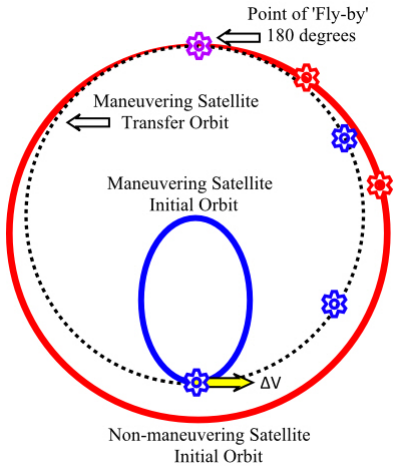

Figure 1.1: Minimum Fuel Solution (Objective 1a) Illustrated.

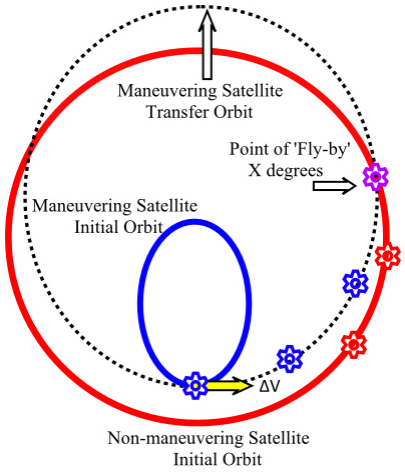

Figure 1.2: Minimum Time with Fixed Fuel Solution (Objective 1b) Illustrated.

2. Demonstrate an optimized maneuver strategy for one maneuvering satellite with one cooperative non-maneuvering satellite. (Chapter 7)

   (a) Develop algorithm to solve for separation distance and ΔV with established geometric criteria between satellites. (Illustrated in Figure 1.3 and presented in Chapter 7).

3. Demonstrate an optimized maneuver strategy for one maneuvering satellite with *'N'* non-maneuvering cooperative satellites. (Chapter 8)

   (a) Develop algorithm to solve for separation distance and ΔV with established geometric criteria between multiple satellites. (Illustrated in Figure 1.4 and presented in Chapter 8).

4. Demonstrate an optimized maneuver strategy for one maneuvering satellite with *'N'* non-maneuvering cooperative satellites and *'p'* ground locations. (Chapter 9)

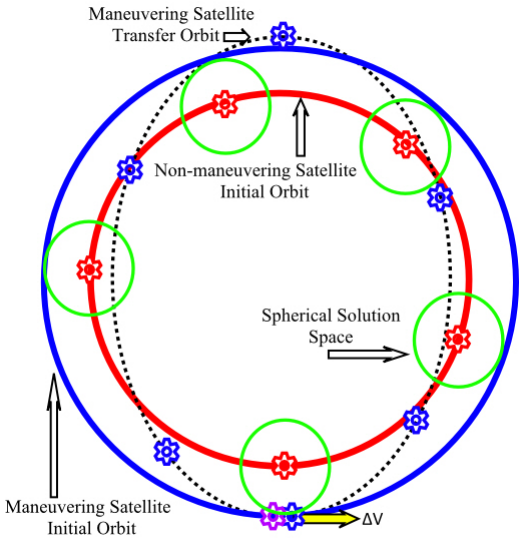

Figure 1.3: Single Satellite: Spherical Separation Distance Solution (Objective 2) Illustrated.

(a) Develop algorithm to solve for separation distance and ΔV with established geometric criteria between multiple satellites and multiple ground locations. (Illustrated in Figure 1.5 and presented in Chapter 9).

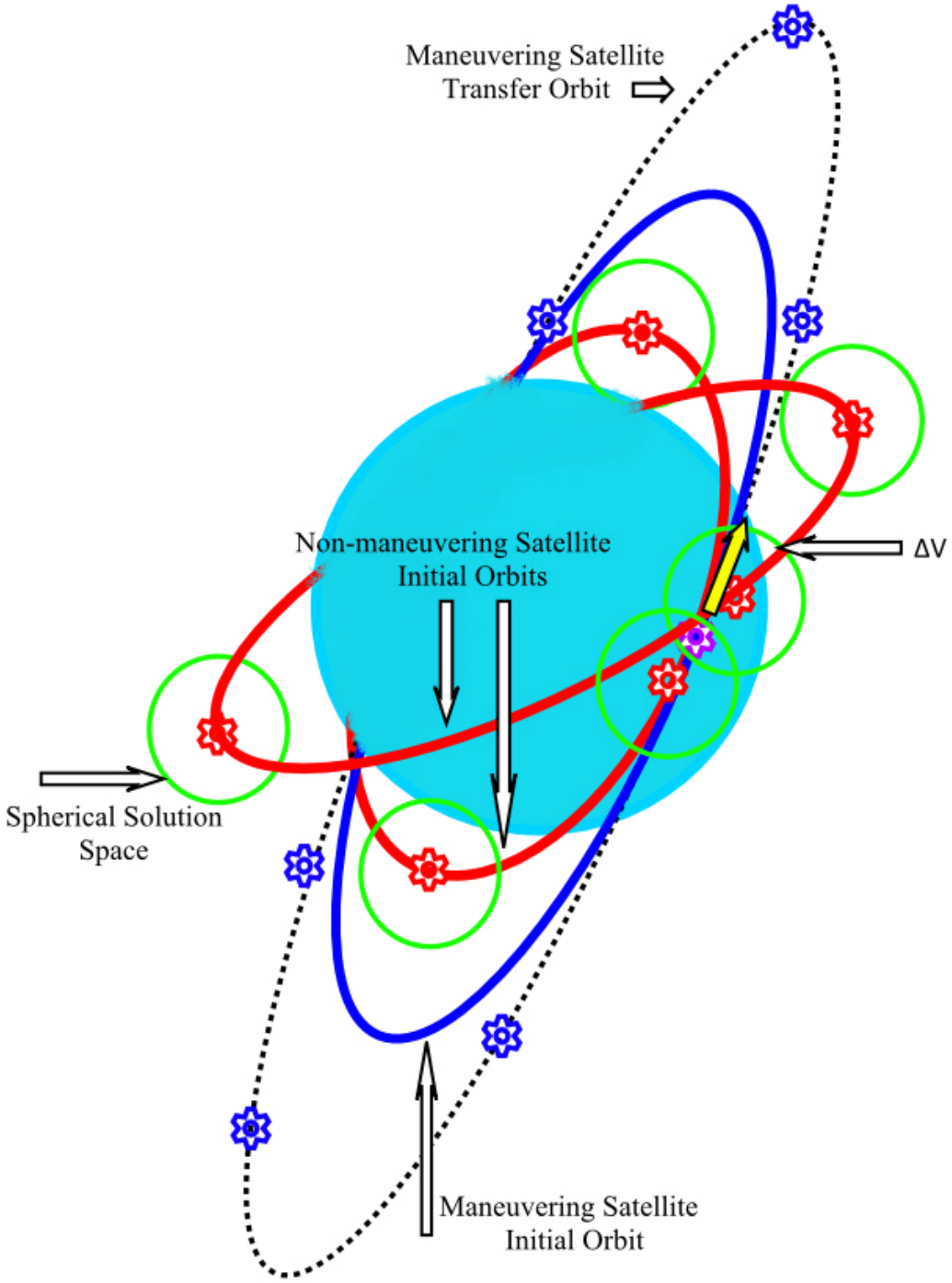

Figure 1.4: Multiple Satellites: Spherical Separation Distance Solution (Objective 3) Illustrated.

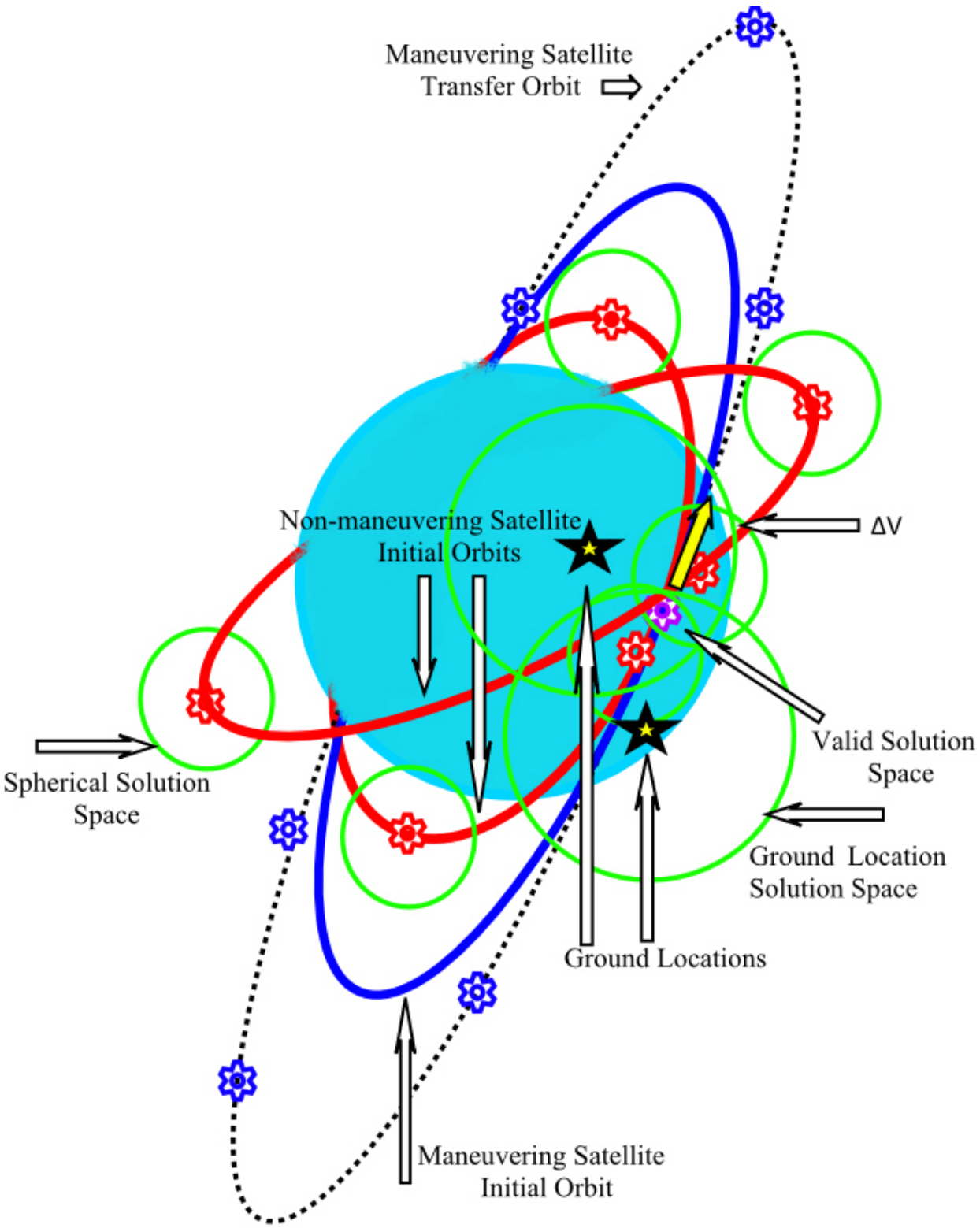

Figure 1.5: Multiple Satellites and Multiple Ground Locations Solution (Objective 4) Illustrated.

II. Literature Review

2.1 Lambert's Problem

Lambert's problem is to determine the trajectory connecting specified initial and terminal position vectors over a specified transfer time [5]. It is regarded as a significant problem in the field of astrodynamics [3]. Many sources exist highlighting means to solve Lambert's Problem. Lambert's Problem is recognized as a target / intercept astrodynamics problem. This research will leverage various characteristics of Lambert's Problem.

Engles and Junkins [6] use a Kustaanheimo-Stiefel Transformation to solve the first order oblate Earth, J_2, perturbed solution to Lambert's Problem. Lawton and Martell [7] demonstrate their ability to solve Lambert's Problem in a ballistic missile boost phase targeting algorithm by reducing residual velocity errors to place the interceptor on a nearly exact intercept path.

Lawton and Byrum [8] highlight the necessity of discerning between the two possible Lambert Solutions in their algorithm to intercept ballistic missiles. They address the possibility of achieving the "lofted or depressed" [8] solutions. Lawton and Byrum introduce the model in which Lambert's Problem is solved by identifying moving targets and interceptors, vs fixed position vectors [8]. Lawton and Byrum [8] demonstrate one of the earliest applications of Lambert's Problem as a target intercept problem. Bate, Mueller and White [3], Kaplan [9], Vallado [10], Prussing and Conway [11] provide an excellent derivation of the traditional Lambert's Problem and highlight the most significant drawback.

Bate, Mueller and White highlight that if the two position vectors are collinear, then a unique solution to Lambert's Problem does not exist [3]. This limitation is also validated by Chioma [4]. The limitation means that if the initial position vector is also the final position vector, representing one orbital revolution later with no perturbations or maneuvers, as

designed the Lambert algorithms will not converge to a viable solution. The algorithm would determine that it would need an infinite ΔV to accomplish the transfer [3, 10]. The work developed and demonstrated by Chioma [4] and Geisel [12] demonstrate the ability to overcome the limitation presented within Lambert's Problem.

Vallado provides several algorithms to solve Lambert's Problem with examples in Reference[10]. Curtis [13] combines the challenge of solving Lambert's Problem with a Gauss method of preliminary orbit determination, which is also addressed by Boulet [14] demonstrating numerical examples. Prussing and Conway [11] also demonstrate examples of solving Lambert's Problem utilizing a Gauss method for orbit determination.

The work presented throughout this document represents a form of satellite navigation, which is an expanded capability from the basic Lambert's Problem and its solutions. Understanding the implementation and limitations of the Lambert's Problem solutions is the foundation for this work.

2.2 Optimal Control Problem

This research will deliver an optimized solution to a complex system of nonlinear differential equations. In order to appreciate the optimality of that solution an in-depth review of nonlinear optimal control problems is necessary. This includes the means necessary to present and solve a nonlinear optimal control problem. Specifically, presenting and solving nonlinear optimal control problems that relate to satellite orbital maneuvers.

2.2.1 Optimal Control Problem Definition.

The ability to build and analyze a nonlinear optimal control problem is established by Kirk[15] and Bryson[16]. An in-depth analysis is provided which presents the ability to tailor each nonlinear optimal control problem to its own uniqueness. Significant challenges exist to establish a suitable optimal control problem for spacecraft trajectories. However, optimizing space trajectories has shown significant development by the community. Conway[17] highlights a summary of these developments, including strengths and

weaknesses of the various techniques. Conway and Paris [18] break the optimization problem down and analyze the importance of the correct initial guess. Izzo [19] discusses the possibilities and challenges of establishing a global minimum. Specifically, he addresses the importance of using multiple algorithms to check for various solutions before declaring global optimality. One such challenge of the various algorithms is explained by Jo and Prussing [20]. They establish a procedure to apply second-order necessary and sufficient conditions using a transition matrix and Ricatti equation. Ultimately, the dynamic optimization problems are broken down into static problems, which can be directly solved using algorithms from Arora[21]. One such example is to use the Broyden-Fletcher-Goldfarb-Shanno quasi-Newton algorithm to optimize hyperbolic intercepts as demonstrated by Gilbert, Howe, Lu and Vinh [20].

2.2.2 Hohmann Transfer.

The literature is full of information regarding the Hohmann Transfer. Prussing and Chiu [22] highlight the limitations of declaring the Hohmann Transfer the minimum fuel solution. Boden[23], Humble[24], Vallado[10], Sellers[25], Bate, Mueller and White[3], Wertz[26], Sidi[27], Curtis[13] and Kaplan[9] all give sufficient justice to the minimum fuel construct of the Hohmann Transfer. Kaplan[9] derives the proof for the Hohmann Transfer's optimality.

2.2.3 Certainty Control.

The concept of certainty control is introduced by Alfano [28]. He highlights a form of an optimal control problem based on controlling an interceptor to a reducing radius sphere target over each iteration to minimize the initial impulsive velocity change required for intercept. Alfano and Fasha [29] modify the methodology to a problem of constraining the final state of an intercept trajectory to a projected error target state. Alfano enhances the algorithm to replace the shrinking sphere with a shrinking ellipsoid [30]. An application of

this control is demonstrated by Lawton, Martell and Jesionowski [31] to minimize terminal state error for ballistic missile intercept.

2.2.4 Minimum Time/Minimum Fuel Continuous/Impulsive Thrust Trajectory Optimization Models.

Minimum time spacecraft trajectory optimization problems do not frequently appear in the literature, especially evaluations modeling impulsive thrust. The opposite is true for the continuous thrust models. Thorne [32] develops a minimum time optimal control problem utilizing continuous thrust. He also introduces the concept of deriving and propagating the variational equations of motion to accurately integrate reference trajectories. Jezewski [33] develops a model for time-optimum guidance equations of motion for planetary ascent and descent trajectories. Again, Jezewski's approach models continuous thrust applications without perturbation effects.

The converse is true of the literature for the minimum fuel case. Specific to the application at hand, Ng, Brietfeller and Ledebuhr [34] derive a cost function that harnesses the multi-objective nature of trajectories. Their approach introduces a model to both minimize the time and control effort with a known target trajectory and an unknown target trajectory. Their overall objective is to minimize the total fuel usage against the desire to achieve an earlier intercept time citing a boost phase ballistic missile intercept application. Other well-researched topics include the maximum payload to orbit application. Specifically, Deaton, Lomas and Mullins[35] provide a summary of the potential benefits of incorporating a wait time before executing a minimum fuel maneuver.

Alfano and Thorne [36] demonstrate a method to produce minimum fuel trajectories between coplanar circular orbits while using constant, continuous thrust. This line of methodology is enhanced by Kluever [37]. Kluever utilizes an orbital averaging method for solving the Lagrange Planetary equations of motion to ultimately demonstrate the viability of a minimum time, low-thrust orbital transfer. Kechechian [38] redefines the problem into

an unconstrained transfer and then one with altitude constraints throughout the maneuver. Overall, Kechechian introduces the reader to a method utilizing constraints in an optimal spacecraft trajectory.

Significant modeling was demonstrated by McAdoo, Jezewski and Dawkins [39] to utilize impulsive maneuvers for optimizing spacecraft trajectories. The cornerstone of this work was is Primer Vector Theory highlighted in section 2.2.5.

2.2.5 Primer Vector Theory.

Vast research has been executed in the field of primer vector theory. Most notable to this application is its utilization of impulsive maneuvers. Jezewski [40] provides a very detailed history and derivation of primer vector theory. McAdoo, Jezewski and Dawkins [39] elaborate on the primer vector theory and demonstrate some utility of the algorithms with a geostationary transfer mission. Prussing [41] also derives the aspects of primer vector theory utilizing only impulsive maneuvers and applies his findings to a Hohmann transfer with the addition of mid-course burns and wait times.

2.2.6 The Traveling Salesman Problem.

Barbee, Alfano, Pinon, Gold and Gaylor present a means of efficiently executing a multiple rendezvous spacecraft trajectory problem, akin to the Traveling Salesman problem [42]. It is framed as a nonlinear programming, complete combinatorial optimization where the orbital debris pieces relate to the cities visited by the traveling salesman. Ultimately, their goal demonstrates the ability to choose the order of orbital debris so as to minimize the total path traveled to ultimately minimize the fuel required.

2.3 Orbital Model

There are many sources providing information regarding the selection of an orbital model for various applications. This section serves to demonstrate the necessary research required to hone in on the models selected for this research, as well as provide cause for their selection.

2.3.1 Drag Formulation.

Incorporating the drag acceleration into the system model is imperative. There are three main areas associated with the development of the drag force utilized in this research. They are the form of the acceleration term, the atmospheric model, and the constants related to the drag terms.

Based on work completed by Cowell [43], a very good model for the drag term is identified. Fichtl, Antar and Collins [44] highlight drag as a non-conservative force, ultimately draining energy from an orbit. They also provide a model for the drag force. Wiesel [45] describes the acceleration form of drag and highlights sources of error associated with estimating drag. He cites, atmospheric variations, shifts in the Earth's magnetic field, as well as imperfections in the satellites' attitude. Vallado [10] and Meirovitch [46] provide sufficient derivations for the drag acceleration term.

Ignoring the variational effects of the atmosphere, a constant atmospheric model will be pursued in this research. The model presented by Vallado [10] is sufficient for this application. The model is also utilized by Wertz [26].

Finally, acceptable constants for the Coefficient of Drag (C_D) and Ballistic Coefficient (BC) terms need to be identified. Sengupta, Vadali and Alfriend [47] describe multiple launch scenarios utilizing various values for C_D. Their values for C_D demonstrate the impact of variations in C_D on low altitude orbits. Humble [24] recommends a value for C_D. The BC value, a function of C_D, surface area and mass, is derived for many systems by Bowman [48]. Both, Wiesel [45] and Sidi [27] provide thoughts towards determining a suitable BC.

2.3.2 Third Body Effects.

Incorporating the perturbations introduced by third bodies is addressed by Roscoe, Vadali and Alfriend [49]. Excellent derivations of the acceleration effects of third bodies is also explained by Wiesel [45], Vallado [10], Boulet [14] and Prussing and Conway [11].

Vallado [10] points out that the effects caused by third bodies are not as dominant as the Earth's oblateness effects for Low Earth Orbiting (LEO) satellites. This is especially true for modeling scenarios on the order of one low earth orbital period. Therefore, for the purpose of this research, the third body effects will be ignored and will have no bearing on the system models.

2.3.3 Two-body Equations of Motion.

Two-body effects will dominate the system dynamics during this research. Ocampo [50] derives the Clohessy-Wiltshire equations for an intercept/target model assuming only two body motion of the satellites. Thorne and Hall [51] utilize two-body equations of motion to demonstrate minimum-time, continuous-thrust orbital transfers. Additional development for the two-body equations of motion are found in References [25, 45, 52].

2.3.4 Equations of Motion including Equatorial Bulge.

Significant development of the equations of motion including the effects of J_2 are found in [4, 13, 52–56]. Schaub and Alfriend [53, 55, 56] present a model capitalizing on the secular drifts in Ω and ω to control multiple spacecraft in formation. Schaub and Alfriend highlight the necessity of modeling the effects of the oblate Earth over single orbital period trajectories. While, Vadali, Vaddi and Alfriend [54] utilize equations of motion including the effects of J_2 to propagate multiple reference trajectories for error approximations.

2.3.5 State Transition Matrix for Two-body System.

In order to execute the proposed algorithm, the state transition matrix for the relay satellite is required. No further development in this particular research is required beyond the scope introduced by Wiesel [45] and Vallado [10] for the state transition matrix for the two body solution.

2.3.6 State Transition Matrix accounting for Equatorial Bulge.

Alfriend, Schaub and Gim [57] derive a form of state transition matrix for their formation flying application capitalizing on the effects of J_2. Vadali, Schaub and Alfriend [58] generate a unique form of the state transition matrix propagating the states of the satellite as the classical orbital elements. Their unique model also leverages the effects of J_2.

2.4 Tactics, Techniques and Procedures

2.4.1 Responsive Space.

Responsive space is quickly becoming a critical component of the United States' space strategy. It focuses on the ability for a system or series of systems to deliver a desired effect to a particular region or latitude / longitude on the surface of Earth in satisfaction of agreed to metrics [47]. France [59] identifies the necessity of harnessing the capability. Other applications include satellite servicing [60] and space superiority [4].

2.4.2 Micro-Satellites.

Significant attention has been placed on the development of micro-satellites. Wertz [26] analyzes the economics of developing micro-satellites. While, Boden [24] discusses the limitations of micro-sat scaled propulsion technology.

2.4.3 Communications Range for Collector Satellite.

Richharia [61] devotes a tremendous amount of attention towards the factors that influence the range of communications between a satellite and the ground station. Additional attention is focused on the capability for a satellite to communicate with another satellite. Vallado [10] provides a generic development and description of communication range issues.

2.4.4 Earth Limits for Communication.

Richharia [61], also develops considerations for analyzing the impact of the Earth 'shine' on satellite communications. Earth 'shine' is comprised of water attenuation in the

atmosphere, effects of the location of the sun relative to communications pointing, etc. An overall impact will be evaluated for the limits of communication which will have a bearing on solution space for effective satellite communication.

2.4.5 Communications Range for Ground Element.

Similarly developed to the communications range, significant literature exists covering the limits of the ground component for a satellite communications architecture. Boden[23], Richharia[61] and Vallado[10] provide examples and applications for consideration for the communications range of ground stations. Ippolito [62] provides a detailed calculation to effectively determine the range between a ground station and a satellite based on the latitude and longitude of the ground station on a non-spherical Earth. Ippolito [62] also provides an analysis concerning the level of noise existing between a ground station and satellite that would need to be overcome for effective communication.

2.5 T-Matrix Navigation

T-Matrix Navigation is an algorithm developed which ultimately delivers a differential correction control scheme leveraging the state transition matrix of a maneuverable satellite and the state information of a non-maneuvering satellite. The concept was developed and presented by Chioma [4] in 2007. He tailored the algorithm to demonstrate a repeated intercept, with zero miss distance, between two separate satellites. Chioma, presented and utilized the T-Matrix Navigation algorithm in a manner that required the state information for an interceptor and target satellite as well as the state transition matrix for the interceptor satellite. Combining this information and running it through his orbital model delivered a minimum fuel solution for a single impulsive maneuver of the interceptor satellite to rendezvous with the target satellite approximately one or 'n' target satellite orbit(s) later. Chioma provided an algorithm to deliver a longer orbital period interceptor satellite to a shorter orbital period target satellite from a zero miss distance starting point to a zero miss distance ending point approximately one target satellite orbit later. The T-Matrix

Navigation algorithm was further demonstrated and utilized by Geisel [12]. Geisel tailored the algorithm to demonstrate repeated intercept from a Highly Elliptical Orbit (HEO). A very similar technique for state transition matrix differential correction was demonstrated by Sears. Sears utilized a form of the non-linear least squares algorithm in Reference [63] to demonstrate optimal non-coplanar launch and rendezvous.

The T-Matrix Navigation Algorithm is summarized through the following steps. The development of the algorithm is credited to Chioma[4].

1. Establish initial Classic Orbital Elements (COEs) for satellites.
2. Convert COEs to initial position, $\vec{R}_0$, and velocity, $\vec{V}_0$ vectors.
3. Establish scaling parameters and scaling matrix, **S**.
4. Establish weight matrix, **Q**.
5. Determine initial guess for required fuel, ΔV, and transfer time, t.
6. Integrate Equations of Motion (EOM) for target satellite for duration of t.
7. Calculate final state, $\vec{R}$, $\vec{V}$, for target satellite at t.
8. Apply ΔV to interceptor satellite to yield $\vec{V}_{0+}$.
9. Integrate EOM for interceptor satellite for duration of t.
10. Calculate final state $\vec{R}$, $\vec{V}$, for interceptor satellite at t.
11. Calculate component by component separation distance between interceptor satellite and target satellite.
12. Integrate interceptor satellite's State Transition Matrix (STM) using Equations of Variation (EOV) for duration of t.

13. Declare ϕ matrix as upper right 3x3 portion of STM.

14. Calculate velocity difference vector, $\vec{V}_{DIFF}$, between interceptor satellite's and target satellite's velocity vectors.

15. Calculate ΔV for interceptor satellite: $\Delta V = \vec{V}_{0+} - \vec{V}_{0}$.

16. Compile error vector, $\bar{e}$, as the component by component separation distance and components of ΔV.

17. Build $\tilde{T}$ matrix: $\begin{bmatrix} \phi & \vec{V}_{DIFF} \\ 3\times 3 & 3\times 1 \\ \mathbf{I} & \mathbf{0} \\ 3\times 3 & 3\times 1 \end{bmatrix}$.

18. Calculate $\mathbf{T}$ matrix: $\mathbf{T} = \mathbf{S}^{-1}\tilde{T}$.

19. Declare convergence criteria.

20. Determine ∂u: $\partial u = -(\mathbf{T}'\mathbf{Q}^{-1}\mathbf{T})^{-1}\mathbf{T}'\mathbf{Q}^{-1}\bar{e}$.

21. Check ∂u components versus convergence criteria: $\partial u = \begin{bmatrix} \Delta V_X & \Delta V_Y & \Delta V_Z & \Delta t \end{bmatrix}$.

22. If convergence criteria are satisfied then the algorithm is complete.

    - Final ΔV = ΔV from error vector, $\bar{e}$
    - Final transfer time = current t

23. Add ΔV from ∂u to $\vec{V}_{0+}$ yielding new ΔV.

24. Add Δt from ∂u to transfer time, t, for updated time.

25. Return to #6.

2.6 Methodology

The final section of this review can be broken into a few different areas. They are least squares, linear algebra and general astrodynamics. They are mentioned for brevity on the overall topic.

2.6.1 Nonlinear Least Squares.

Bate, Mueller and White [3] have a complete derivation on the solution to the least squares iterative differential correction algorithm. The least squares differential correction algorithm provides a method of orbit determination. The algorithm provides insight to the necessity of deriving the state transition matrix and the impact of differential changes over time. Significant additional information is provided by Wiesel [64]. Wiesel provides the foundation for trajectory estimation utilizing the state matrix and the state covariance matrix. Prussing and Conway [11] provide an additional model and examples utilizing impulsive maneuvers to achieve rendezvous with a nonlinear least squares algorithm.

2.6.2 Matrix Mathematics.

Hoffman and Kunze [65] and Arora [21] provide complete analysis on the matrix condition and all matrix mathematics. Arora, provides a method to analyze matrices for optimization problems. Zill [66] provides numerous techniques to approximate solutions to nonlinear differential equations utilizing matrices as well as providing techniques to solve nonlinear boundary value problems.

2.6.3 General Astrodynamics.

There are several other methods utilized throughout this research that come from several sources. Hughes [67] provides a complete summary of the linear approximation for the system. Both Vallado [10] and Bate, Mueller and White [3] develop and provide examples for solving Kepler's problem. Additionally, they introduce the standard units of Distance Unit (DU) and Time Unit (TU). Wertz [26] discusses overall parameters of interest for designing spacecraft with potential trade-offs. While Meirovitch [46],

Wiesel [45], and Sidi [27] sufficiently develop and analyze the disturbing function form for determining the system's equations of motion.

2.7 Summary

The previous sections provide an outline for the direction necessary for the scope of this research. The literature has provided tools to implement the desired algorithms. However, the literature reveals a gap in the community's knowledge with regard to an enhanced utilization of the T-Matrix Navigation algorithm. Specifically, this research intends to expand on the nonlinear optimal control problem for determining impulsive orbital maneuvers for various geometric relationships between multiple satellites and ground locations utilizing the differential correction presented in the T-Matrix Navigation algorithm as a foundation.

III. System Dynamics

3.1 Two-body System Dynamics

The T-Matrix Navigation (TMN) algorithm requires the development of the maneuvering and non-maneuvering satellite's Equations of Motion (EOM) and Equations of Variation (EOV). The 2-body orbital motion solution for this model is straightforward and readily available. The position and velocity EOM for the satellites are in Eqs.(3.1) and (3.2) respectively. $\vec{R}$ is the position vector, $\vec{V}$ is the velocity vector, and μ is the Earth's gravitational parameter.

$$\dot{\vec{R}} = \vec{V} \tag{3.1}$$

$$\dot{\vec{V}} = -\frac{\mu \vec{R}}{|\vec{R}|^3} \tag{3.2}$$

The EOV for the 2-body model are straightforward as well. The general form for deriving the State Transition Matrix (STM), Φ, is shown in Eqs.(3.3) and (3.4) directly transfered from Reference[45]. $\vec{R}_n$ is the component of the position vector.

$$\Phi(t) = \begin{bmatrix} \mathbf{0} & \mathbf{I} \\ \mathbf{\Phi}_{21} & \mathbf{0} \end{bmatrix} \tag{3.3}$$

$$\mathbf{\Phi}_{21} = \begin{bmatrix} -\frac{\mu}{|\vec{R}|^3} + \frac{3\mu|\vec{R}_X|^2}{|\vec{R}|^5} & \frac{3\mu|\vec{R}_X||\vec{R}_Y|}{|\vec{R}|^5} & \frac{3\mu|\vec{R}_X||\vec{R}_Z|}{|\vec{R}|^5} \\ \frac{3\mu|\vec{R}_X||\vec{R}_Y|}{|\vec{R}|^5} & -\frac{\mu}{|\vec{R}|^3} + \frac{3\mu|\vec{R}_Y|^2}{|\vec{R}|^5} & \frac{3\mu|\vec{R}_Y||\vec{R}_Z|}{|\vec{R}|^5} \\ \frac{3\mu|\vec{R}_X||\vec{R}_Z|}{|\vec{R}|^5} & \frac{3\mu|\vec{R}_Y||\vec{R}_Z|}{|\vec{R}|^5} & -\frac{\mu}{|\vec{R}|^3} + \frac{3\mu|\vec{R}_Z|^2}{|\vec{R}|^5} \end{bmatrix} \tag{3.4}$$

3.2 System Dynamics Using Earth's 2nd Zonal Harmonic

The effect on the satellite's motion from the Earth's 2nd zonal harmonic, J_2, is captured in Eqs.(3.1) and (3.5)[4]. J_2 is the unit-less constant for the oblate Earth and $R_\oplus$ is the Earth's radius.

$$\dot{V} = \frac{\mu \vec{R}}{|\vec{R}|^3} - \frac{3}{2}\frac{J_2 \mu R_\oplus^2 \vec{R}}{|\vec{R}|^5}\left(1 - \frac{5|\vec{R}_Z|^2}{|\vec{R}|^2}\right) \tag{3.5}$$

The general form of the J_2 model's EOV is captured in Eq.(3.6). Each specific component of the lower left 3×3 matrix is expanded in Eqs.(3.7) through (3.15).

$$\Phi(t) = \begin{bmatrix} 0 & 0 & 0 & 1 & 0 & 0 \\ 0 & 0 & 0 & 0 & 1 & 0 \\ 0 & 0 & 0 & 0 & 0 & 1 \\ \Phi_{41} & \Phi_{42} & \Phi_{43} & 0 & 0 & 0 \\ \Phi_{51} & \Phi_{52} & \Phi_{53} & 0 & 0 & 0 \\ \Phi_{61} & \Phi_{62} & \Phi_{63} & 0 & 0 & 0 \end{bmatrix} \tag{3.6}$$

$$\Phi_{41} = \frac{\mu}{2|\vec{R}|^9}\Big(3J_2R_\oplus^2\left(4|\vec{R}_X|^4 + 3|\vec{R}_X|^2\left(|\vec{R}_Y|^2 - 9|\vec{R}_Z|^2\right) - |\vec{R}_Y|^4 + 3|\vec{R}_Y|^2|\vec{R}_Z|^2 + 4|\vec{R}_Z|^4\right) + 2\left(2|\vec{R}_X|^2 - |\vec{R}_Y|^2 - |\vec{R}_Z|^2\right)\left(|\vec{R}_X|^2 + |\vec{R}_Y|^2 + |\vec{R}_Z|^2\right)^2\Big) \tag{3.7}$$

$$\Phi_{42} = \frac{3\mu|\vec{R}_X||\vec{R}_Y|\left(5J_2R_\oplus^2\left(|\vec{R}_X|^2 + |\vec{R}_Y|^2 - 6|\vec{R}_Z|^2\right) + 2\left(|\vec{R}_X|^2 + |\vec{R}_Y|^2 + |\vec{R}_Z|^2\right)^2\right)}{2|\vec{R}|^9} \tag{3.8}$$

$$\Phi_{43} = \frac{3\mu|\vec{R}_X||\vec{R}_Z|\left(5J_2R_\oplus^2\left(3|\vec{R}_X|^2 + 3|\vec{R}_Y|^2 - 4|\vec{R}_Z|^2\right) + 2\left(|\vec{R}_X|^2 + |\vec{R}_Y|^2 + |\vec{R}_Z|^2\right)^2\right)}{2|\vec{R}|^9} \tag{3.9}$$

$$\Phi_{51} = \frac{3\mu|\vec{R}_X||\vec{R}_Y|\left(5J_2R_\oplus^2\left(|\vec{R}_X|^2 + |\vec{R}_Y|^2 - 6|\vec{R}_Z|^2\right) + 2\left(|\vec{R}_X|^2 + |\vec{R}_Y|^2 + |\vec{R}_Z|^2\right)^2\right)}{2|\vec{R}|^9} \tag{3.10}$$

$$\Phi_{52} = \mu\Big(\frac{-|\vec{R}_X|^2 + 2|\vec{R}_Y|^2 - |\vec{R}_Z|^2}{|\vec{R}|^5} - \frac{3J_2R_\oplus^2\left(|\vec{R}_X|^4 - 3|\vec{R}_X|^2\left(|\vec{R}_Y|^2 + |\vec{R}_Z|^2\right) - 4|\vec{R}_Y|^4 + 27|\vec{R}_Y|^2|\vec{R}_Z|^2 - 4|\vec{R}_Z|^4\right)}{2|\vec{R}|^9}\Big) \tag{3.11}$$

$$\Phi_{53} = \frac{3\mu|\vec{R}_Y||\vec{R}_Z|\left(5J_2R_\oplus^2\left(3|\vec{R}_X|^2+3|\vec{R}_Y|^2-4|\vec{R}_Z|^2\right)+2\left(|\vec{R}_X|^2+|\vec{R}_Y|^2+|\vec{R}_Z|^2\right)^2\right)}{2|\vec{R}|^9} \tag{3.12}$$

$$\Phi_{61} = \frac{3\mu|\vec{R}_X||\vec{R}_Z|\left(5J_2R_\oplus^2\left(3|\vec{R}_X|^2+3|\vec{R}_Y|^2-4|\vec{R}_Z|^2\right)+2\left(|\vec{R}_X|^2+|\vec{R}_Y|^2+|\vec{R}_Z|^2\right)^2\right)}{2|\vec{R}|^9} \tag{3.13}$$

$$\Phi_{62} = \frac{3\mu|\vec{R}_Y||\vec{R}_Z|\left(5J_2R_\oplus^2\left(3|\vec{R}_X|^2+3|\vec{R}_Y|^2-4|\vec{R}_Z|^2\right)+2\left(|\vec{R}_X|^2+|\vec{R}_Y|^2+|\vec{R}_Z|^2\right)^2\right)}{2|\vec{R}|^9} \tag{3.14}$$

$$\Phi_{63} = \mu\Bigg(\frac{-|\vec{R}_X|^2-|\vec{R}_Y|^2+2|\vec{R}_Z|^2}{|\vec{R}|^5} - \frac{3J_2R_\oplus^2\left(3|\vec{R}_X|^4+6|\vec{R}_X|^2\left(|\vec{R}_Y|^2-4|\vec{R}_Z|^2\right)+3|\vec{R}_Y|^4-24|\vec{R}_Y|^2|\vec{R}_Z|^2+8|\vec{R}_Z|^4\right)}{2|\vec{R}|^9}\Bigg) \tag{3.15}$$

3.3 System Dynamics Utilizing Earth's 2nd Zonal Harmonic and Air Drag

Using an atmospheric model derived from Vallado[10] and Wertz and Lawson[26], the force of air drag is added to the system model. The first consideration for the effect of air drag is to define the ballistic coefficient, B^*, defined by $B^* = \frac{C_D * A}{m}$.

The coefficient of drag is denoted by C_D, A is the cross-sectional area and m is the mass of the satellite. The values for A and m are case specific and, therefore, user-defined variables. For this study, a typical value for the coefficient of drag from [26] is used, $C_D = 2.2$.

According to [10] and [26], the atmospheric density, ρ, is determined by Eq.(3.16). The nominal atmospheric density (ρ_0), the base altitude (h_0), and the scale height (H) are pulled from a look-up table. The height above the elliptical, h_{ellp}, is simply the satellite's altitude.

$$\rho = \rho_0 * exp\left(-\frac{h_{ellp}-h_0}{H}\right) \tag{3.16}$$

According to [10] and [26], the atmospheric density is nearly 0 at 2,000 km altitude giving this model a relatively accurate range from altitudes of 150 km - 2,000 km.

Combining the ballistic coefficient and the atmospheric drag, a formula for the drag acceleration term is presented in Eq.(3.17). The relative velocity term, $\vec{V}_{REL}$, requires its own development.

$$\vec{a}_{DRAG} = -\frac{1}{2}B^*\rho|\vec{V}_{REL}|^2 \tag{3.17}$$

The relative velocity term is the difference between the satellite's velocity vector, and the cross product of the Earth's rotational vector and the satellite's position vector $\vec{V}_{REL} = \vec{V} - \vec{\omega} \times \vec{R}$. It is assumed that the atmosphere rotates at nearly the same rate as the rotation of the Earth.

The $\vec{\omega}$ vector is defined by Eq.(3.18). The rotation rate of the Earth, $\omega_\oplus$, is $7.2921158 \times 10^{-5} \frac{rad}{sec}$.

$$\vec{\omega} = \omega_\oplus \begin{bmatrix} 0 \\ 0 \\ 1 \end{bmatrix} \tag{3.18}$$

Expanding the cross product and executing the subtraction, the general form of the relative velocity vector is

$$\vec{V}_{REL} = \begin{bmatrix} \vec{V}_X + \omega_\oplus \vec{R}_Y \\ \vec{V}_Y - \omega_\oplus \vec{R}_X \\ \vec{V}_Z \end{bmatrix}. \tag{3.19}$$

Once the definition of the relative velocity vector is established, the EOM for the orbital model with the non-spherical effects due to J_2 and the atmospheric drag acceleration are captured in Eqs.(3.1) and (3.20).

$$\dot{V} = \frac{\mu\vec{R}}{|\vec{R}|^3} - \frac{3}{2}\frac{J_2\mu R_\oplus^2\vec{R}}{|\vec{R}|^5}(1 - \frac{5R_Z^2}{|\vec{R}|^2}) - \frac{1}{2}B^*\rho|\vec{V}_{REL}|^2 \tag{3.20}$$

Introducing the drag acceleration term in the EOM causes increased complexity in the variational equations. To help define the EOV, the relative velocity vector is expanded in

Eq.(3.21).

$$|\vec{V}_{REL}|^2 = |\vec{V}_X|^2 + 2\omega_\oplus|\vec{V}_X||\vec{R}_Y| + \omega_\oplus^2|\vec{R}_Y|^2 + |\vec{V}_Y|^2 - 2\omega_\oplus|\vec{V}_Y||\vec{R}_X| + \omega_\oplus^2|\vec{R}_X|^2 + |\vec{V}_Z|^2 \quad (3.21)$$

Noticing the introduction of the velocity terms in the $\dot{V}$ equation, the lower right 3×3 portion of the EOV are no longer '0's as previously seen. The general form of the model's EOV are in Eq.(3.22).

$$\Phi(t) = \begin{bmatrix} 0 & 0 & 0 & 1 & 0 & 0 \\ 0 & 0 & 0 & 0 & 1 & 0 \\ 0 & 0 & 0 & 0 & 0 & 1 \\ \Phi_{41} + \frac{\partial \vec{a}_{DRAG}}{\partial \vec{R}_X} & \Phi_{42} + \frac{\partial \vec{a}_{DRAG}}{\partial \vec{R}_Y} & \Phi_{43} + \frac{\partial \vec{a}_{DRAG}}{\partial \vec{R}_Z} & \frac{\partial \vec{a}_{DRAG}}{\partial \vec{V}_X} & \frac{\partial \vec{a}_{DRAG}}{\partial \vec{V}_Y} & \frac{\partial \vec{a}_{DRAG}}{\partial \vec{V}_Z} \\ \Phi_{51} + \frac{\partial \vec{a}_{DRAG}}{\partial \vec{R}_X} & \Phi_{52} + \frac{\partial \vec{a}_{DRAG}}{\partial \vec{R}_Y} & \Phi_{53} + \frac{\partial \vec{a}_{DRAG}}{\partial \vec{R}_Z} & \frac{\partial \vec{a}_{DRAG}}{\partial \vec{V}_X} & \frac{\partial \vec{a}_{DRAG}}{\partial \vec{V}_Y} & \frac{\partial \vec{a}_{DRAG}}{\partial \vec{V}_Z} \\ \Phi_{61} + \frac{\partial \vec{a}_{DRAG}}{\partial \vec{R}_X} & \Phi_{62} + \frac{\partial \vec{a}_{DRAG}}{\partial \vec{R}_Y} & \Phi_{63} + \frac{\partial \vec{a}_{DRAG}}{\partial \vec{R}_Z} & \frac{\partial \vec{a}_{DRAG}}{\partial \vec{V}_X} & \frac{\partial \vec{a}_{DRAG}}{\partial \vec{V}_Y} & \frac{\partial \vec{a}_{DRAG}}{\partial \vec{V}_Z} \end{bmatrix} \quad (3.22)$$

Recall that the EOV in Eq.(3.22) are established based on the same dynamics as the previous model, with the introduction of the air drag acceleration term. Therefore, the initial Φ matrix is the same as Eq.(3.6). The addition to the variational equations are the component associated with the drag acceleration vector, in Eq.(3.17), including the expanded relative velocity term. The additions are the partial derivatives of the drag acceleration vector with respect to the position and velocity vectors. Eqs. (3.23) through (3.28) highlight these components.

$$\frac{\partial \vec{a}_{DRAG}}{\partial \vec{R}_X} = B^* \rho \left(\omega_\oplus |\vec{V}_Y| - \omega_\oplus^2 |\vec{R}_X| \right) \quad (3.23)$$

$$\frac{\partial \vec{a}_{DRAG}}{\partial \vec{R}_Y} = B^* \rho \left(-\omega_\oplus |\vec{V}_X| - \omega_\oplus^2 |\vec{R}_Y| \right) \quad (3.24)$$

$$\frac{\partial \vec{a}_{DRAG}}{\partial \vec{R}_Z} = 0 \quad (3.25)$$

$$\frac{\partial \vec{a}_{DRAG}}{\partial \vec{V}_X} = B^* \rho \left(-|\vec{V}_X| - \omega_{\oplus} |\vec{R}_Y| \right) \tag{3.26}$$

$$\frac{\partial \vec{a}_{DRAG}}{\partial \vec{V}_Y} = B^* \rho \left(\omega_{\oplus} |\vec{R}_X| - |\vec{V}_Y| \right) \tag{3.27}$$

$$\frac{\partial \vec{a}_{DRAG}}{\partial \vec{V}_Z} = -B^* \rho |\vec{V}_Z| \tag{3.28}$$

While the development of the system models are not new, including them ensures the same baseline for implementing the model in the future. The development and presentation of the system models' EOM and EOV are the cornerstone for accurately executing the TMN differential correction algorithm.

3.4 Coordinate System

Throughout this research the coordinate system used is the Geocentric Inertial Coordinate System[3, 10, 25, 26]. The origin for this system is the center of the Earth. The fundamental plane is the equatorial plane. The perpendicular component, completing the right-hand-rule, is the North Pole. The principal direction of the coordinate system is the vernal equinox when the Earth is aligned with the Sun and the First Point of Aires. The principal direction is the $\hat{X}$ axis. The $\hat{Z}$ axis points through the North Pole and the $\hat{Y}$ axis is completed from the right-hand-rule.

3.5 Impulsive Maneuver

The duration of the thruster's firing is significantly shorter than the orbital period of the satellite. Therefore, the maneuver used throughout this research is considered instantaneous and impulsive.

IV. Navigation Solution to Solve Impulsive Tangential Orbital Maneuvers

4.1 Introduction

The development and execution of the Hohmann Transfer using various methods has been studied for years. Boden[23], Humble[24], Vallado[10], Sellers[25], Bate, Mueller and White[3], Wertz[26], Sidi[27], Curtis[13] and Kaplan[9] all give sufficient treatment to the minimum fuel development and construct of the Hohmann Transfer. Kaplan[9] analytically proves the Hohmann Transfer's optimality. Prussing and Chiu [22] highlight the limitations of declaring the Hohmann Transfer the minimum fuel solution. These limitations include the requirement that the initial and final orbits are coplanar and cocentric circular orbits with a final to initial orbital ratio of 11.94 [22]. This work will demonstrate an orbit estimation driven, state transition matrix based, differential correction algorithm to solve for the impulsive maneuver required for a tangential burn analogous to first burn of the Hohmann Transfer.

T-Matrix Navigation is an algorithm that delivers a control scheme, leveraging the state transition matrix of a maneuverable satellite and the state information of a non-maneuvering satellite. The most recent application concerning the T-Matrix Navigation approach was by Chioma and Titus [4, 68, 69]. The algorithm was further developed by Geisel[12] to be utilized for Highly Elliptical Orbits (HEO). The algorithm they presented was used to execute repeated intercept, between two separate satellites. Chioma, presented and used the TMN algorithm for an interceptor and target satellite. Executing the algorithm including the State Transition Matrix and the state information for the two satellites delivered a unique solution for a single impulsive maneuver of the interceptor satellite to rendezvous with the target satellite approximately one or 'N' target satellite orbit(s) later. Chioma provided an algorithm to deliver a longer orbital period interceptor satellite to a shorter orbital period target satellite approximately one target satellite orbit later. A very

similar technique for state transition matrix differential correction was demonstrated by Sears[63]. Sears, utilized a form of the nonlinear least squares algorithm to demonstrate optimal non-coplanar launch and rendezvous.

The foundation for Chioma, Geisel and Sears' work lies in the realm of nonlinear least squares. Bate, Mueller and White [3] have a complete derivation on the solution to the least squares iterative differential correction algorithm. The least squares differential correction algorithm provides a method of orbit determination. The algorithm provides insight to the necessity of deriving the state transition matrix and the impact of differential changes over time. Significant additional information is provided by Wiesel [64] with the foundation for trajectory estimation utilizing the state matrix and the state covariance matrix. Vallado[10] provides guidelines for tolerances and convergence criteria least squares techniques. Prussing and Conway [11] provide an additional model and examples utilizing impulsive maneuvers to achieve rendezvous with a nonlinear least squares algorithm.

Extensive literature exists in the development and implementation of solving Lambert's Problem. Lambert's Problem is to determine the trajectory connecting specified initial and terminal position vectors over a specified transfer time [5]. It is regarded as a significant problem in the field of astrodynamics [3]. Many sources exist highlighting means to solve Lambert's Problem. Lambert's Problem is recognized as a target/intercept astrodynamics problem. Engles and Junkins [6] utilize a Kustaanheimo-Stiefel Transformation to solve the first order J_2 perturbed solution to Lambert's Problem. Lawton and Martell [7] demonstrate their ability to solve Lambert's Problem in a ballistic missile boost phase targeting algorithm by reducing residual velocity errors to place the interceptor on a nearly exact intercept path. Lawton and Byrum [8] highlight the necessity of discerning between the two possible Lambert Solutions in their algorithm to intercept ballistic missiles. They address the possibility of achieving the "lofted or depressed" [8] solutions. Lawton and Byrum introduce the model in which Lambert's Problem is solved

by identifying moving targets and interceptors, versus fixed position vectors [8]. Lawton and Byrum [8] demonstrate one of the earliest applications of Lambert's Problem as a target intercept problem. Bate, Mueller and White [3], Kaplan [9], Vallado [10], Prussing and Conway [11] provide an excellent derivation of the traditional Lambert's Problem and highlight the most significant drawback.

Bate, Mueller and White [3] highlight that if the two position vectors are collinear, then a unique solution to Lambert's Problem does not exist. This limitation is also validated by Chioma [4]. This means that if the initial position vector is also the final position vector, representing one orbital revolution later with no perturbations or maneuvers, as designed, the Lambert algorithms will not converge to a viable solution. The algorithm would determine that it would need an infinite ΔV to accomplish the transfer [3, 10]. However, Vallado provides several algorithms to solve Lambert's Problem with examples in Reference[10]. Curtis [13] combines the challenge of solving Lambert's Problem with a Gauss method of preliminary orbit determination. Which is also addressed by Boulet [14] demonstrating numerical examples. Prussing and Conway [11] also demonstrate examples of solving Lambert's Problem utilizing a Gauss method for orbit determination.

The final idea, leveraging terminal guidance, delivers the backbone for the T-Matrix Navigation algorithm. The most relevant contribution for terminal guidance is regarded as certainty control. The concept of certainty control is introduced by Alfano [28]. He highlights a form of an optimal control problem based on controlling an interceptor to a reducing radius sphere target over each iteration to minimize the initial impulsive velocity change required for intercept. Alfano and Fasha [29] modify the methodology to a problem of constraining the final state of an intercept trajectory to a projected error target state. Alfano enhances the algorithm to replace the shrinking sphere with a shrinking ellipsoid [30]. An application of this control is demonstrated by Lawton, Martell and Jesionowski [31] to minimize terminal state error for ballistic missile intercept.

4.2 Problem Statement

Ultimately, this chapter aims to illustrate the robust optimality of the T-Matrix Navigation algorithm. Demonstrating optimality will be accomplished by determining the impulsive maneuver required to execute a tangential burn to transfer a satellite from an initial altitude towards a desired final altitude. The algorithm will be presented and configured in a manner which will apply to any general tangential impulsive maneuver from an elliptic orbit from varying inclinations. This represents a unique application of the TMN algorithm with results that are comparable to the first burn of the Hohmann Transfer, the widely recognized minimum fuel maneuver sequence. The algorithm presented here solves only for the first tangential burn, omitting the circularizing, second, burn to remain at the desired altitude. This assumption allows the results in this paper to summarize a 'fly-by' orbital dynamics problem. Provided an initial altitude and a desired final altitude, the algorithm will yield the impulsive maneuver required to achieve the desired orbital altitude. The solution's maneuver is applied tangentially, therefore it is defined as the most fuel efficient maneuver necessary. This chapter also aims to prove that the T-Matrix Navigation differential correction algorithm is not constrained to the previously identified limitations of a standard Hohmann Transfer. Specifically, the algorithm presented allows the user to declare the solution as the minimum fuel impulsive maneuver especially while considering the effects of the oblate Earth and air drag. A summary of the optimal control

problem being solved this this chapter is presented in (4.1).

$$
\begin{aligned}
&\text{Minimize: J} = \int_{t_0}^{t_f} |u(t)|\, dt \\
&\text{Subject to:} \\
&\quad \dot{\vec{R}}, \dot{\vec{V}} \\
&\quad u(t) = \Delta V \delta_0 (t - t_0) \\
&\text{Initial Conditions:} \\
&\quad \vec{R}_1(t_0) = \vec{R}_{1_{t_0}} \\
&\quad \vec{V}_1(t_0) = \vec{V}_{1_{t_0}} \\
&\quad \vec{R}_2(t_0) = \vec{R}_{2_{t_0}} \\
&\quad \vec{V}_2(t_0) = \vec{V}_{2_{t_0}} \\
&\quad t_0 = 0 \\
&\text{Terminal Conditions:} \\
&\quad \vec{R}_1(t_f) = \vec{R}_2(t_f)
\end{aligned}
\tag{4.1}
$$

Solving this problem is summarized through the following procedure. The contributions provided throughout this chapter are in **boldface**.

1. **Establish initial Classic Orbital Elements (COEs) for satellites.**
2. Convert COEs to initial position, $\vec{R}_0$, and velocity, $\vec{V}_0$ vectors.
3. Establish scaling parameters and scaling matrix, **S**[4].
4. Establish weight matrix, **Q**[4].
5. **Determine initial guess for required fuel, ΔV, and transfer time, *t*.**
6. Integrate Equations of Motion (EOM) for Satellite 2 for duration of *t*.
7. Calculate final state, $\vec{R}$, $\vec{V}$, for Satellite 2 at *t*.
8. Apply ΔV to Satellite 1 to yield $\vec{V}_{0+}$.

9. Integrate EOM for Satellite 1 for duration of t.

10. Calculate final state $\vec{R}, \vec{V}$, for Satellite 1 at t.

11. Calculate component by component separation distance between Satellite 1 and Satellite 2.

12. **Integrate Satellite 1's State Transition Matrix (STM) using Equations of Variation (EOV) for duration of *t*.**

13. Declare ϕ matrix as upper right 3x3 portion of STM[4].

14. Calculate velocity difference vector, $\vec{V}_{DIFF}$, between Satellite 1's and Satellite 2's velocity vectors[4].

15. Calculate ΔV for Satellite 1: $\Delta V = \vec{V}_{0+} - \vec{V}_0$.

16. Compile error vector, $\bar{e}$, as the component by component separation distance and components of ΔV[4].

17. Build $\tilde{T}$ matrix: $\begin{bmatrix} \phi & \vec{V}_{DIFF} \\ 3\times 3 & 3\times 1 \\ \mathbf{I} & \mathbf{0} \\ 3\times 3 & 3\times 1 \end{bmatrix}$[4].

18. Calculate $\mathbf{T}$ matrix: $\mathbf{T} = \mathbf{S}^{-1}\tilde{T}$[4].

19. Declare convergence criteria[4].

20. Determine ∂u: $\partial u = -(\mathbf{T}'\mathbf{Q}^{-1}\mathbf{T})^{-1}\mathbf{T}'\mathbf{Q}^{-1}\bar{e}$[4].

21. Check ∂u components versus convergence criteria: $\partial u = \begin{bmatrix} \Delta V_X & \Delta V_Y & \Delta V_Z & \Delta t \end{bmatrix}$[4].

22. If convergence criteria are satisfied then the algorithm is complete.

- Final ΔV = ΔV from error vector, $\bar{e}$
- Final transfer time = current t

23. Add ΔV from ∂u to $\vec{V}_{0+}$ yielding new ΔV.

24. Add Δt from ∂u to transfer time, t, for updated time.

25. Return to #6.

4.3 T-Matrix Navigation Differential Correction Algorithm

T-Matrix Navigation (TMN) has its roots in nonlinear least squares. Fundamentally, it is a method to reduce the amount of residual error in a system of complex nonlinear differential equations. In order to use this method in an optimization problem, an algorithm must be implemented to adequately bound the solution space of the nonlinear system of equations, while allowing the variational equations to be iterated towards a solution. Chioma presents the algorithm development [4].

In order to implement the TMN method, two orbits are needed. In this particular case, they are the maneuvering satellite (Sat 1) and non-maneuvering satellite (Sat 2). The maneuvering satellite will be the satellite to which the ΔV is applied. The non-maneuvering satellite will be in a circular and equatorial orbit at the desired altitude for the maneuvering vehicle. Assuming the maneuvering satellite is located directly in line with the $\hat{X}$ axis at the start time, the maneuvering satellite's initial position vector is shown in Eq.(4.2).

It is fundamental to identify that the position vector of the maneuvering satellite has one initial value, while the velocity vector has two. They are the velocity of the maneuvering vehicle just before the maneuver and just after a maneuver, while still at the original position. The state vectors for the maneuvering satellite are defined by equations

(4.3) and (4.4) [4].

$$\vec{R}_{Sat1} = R_{t_0} \begin{bmatrix} 1 \\ 0 \\ 0 \end{bmatrix} km \tag{4.2}$$

$$X_{Sat1}(t_0^-) = \begin{bmatrix} R_X(t_0) \\ R_Y(t_0) \\ R_Z(t_0) \\ V_X(t_0^-) \\ V_Y(t_0^-) \\ V_Z(t_0^-) \end{bmatrix} \tag{4.3}$$

$$X_{Sat1}(t_0^+) = \begin{bmatrix} R_X(t_0) \\ R_Y(t_0) \\ R_Z(t_0) \\ V_X(t_0^-) + \Delta V_X \\ V_Y(t_0^-) + \Delta V_Y \\ V_Z(t_0^-) + \Delta V_Z \end{bmatrix} \tag{4.4}$$

The applied ΔV is implemented and adjusted during each iteration through the algorithm. During each update the system is propagated through time to find each resulting end position for each applied ΔV from the starting point. Therefore, for each ΔV, new position and velocity vectors at t_f can be determined.

Sat 2 is in a circular and equatorial orbit at the desired altitude for the transfer. Therefore, utilizing 2-body dynamics, the initial position and velocity vectors can be calculated for Sat 2. Because the desired orbit is circular and equatorial, Table 4.1 provides the Classical Orbital Elements (COEs) necessary to determine the initial vectors.

The desired altitude is R_{t_f}. The angle β is derived from the relationship between the final orbital period and the expected transfer time knowing that the desired final location

Table 4.1: COEs for Sat 2 Initial Conditions.

Orbital Element	Symbol	Value	Units
Semi-Major Axis	a	R_{t_f}	km
Eccentricity	e	0	n/a
Inclination	i	0	Degrees
Right Ascension of Ascending Node	Ω	0	Degrees
Argument of Perigee	ω	0	Degrees
True Anomaly	ν	180°-β	Degrees

for Sat 1 is 180^0 from its starting position. This location is known as the final position for the maneuvering satellite provided a minimum fuel transfer utilizing an impulsive maneuver as demonstrated by the Hohmann Transfer. The relationship to calculate β is $\beta = \frac{360° \times TransferTime}{PeriodSat2}$.

Once the position vector in the future is determined for Sat 1, that same time is used to determine the position vector of Sat 2 and an error vector is calculated. The error vector is given by Eq.(4.5) [4].

$$\bar{e} = \begin{bmatrix} R_{SAT1_X} - R_{SAT2_X} \\ R_{SAT1_Y} - R_{SAT2_Y} \\ R_{SAT1_Z} - R_{SAT2_Z} \\ \Delta V_{SAT1_X} \\ \Delta V_{SAT1_Y} \\ \Delta V_{SAT1_Z} \end{bmatrix} \tag{4.5}$$

The error vector highlights the component by component miss distance between Sat 1 and Sat 2, as well as the applied ΔV on Sat 1.

It is necessary to identify that the integrated equations of motion for the solution will vary based on the desired model and required fidelity. Specifically, this study will demonstrate the versatility of the algorithm utilizing three separate models: (1) 2-body EOM, (2) EOM including J_2 and (3) EOM including both J_2 and an air drag model. Each system will require the appropriate variational equations according to the model that will be demonstrated.

The maneuvering satellite's State Transition Matrix (STM), Φ, needs to be determined based on the variational equations. The STM is determined by integrating the satellite's equations of motion, as well as the variational equations of motion, which are the partial derivatives of the EOM. This is the most computationally taxing calculation due to the fact that there are 36 variational equations combined with the 6 EOM that have to be integrated simultaneously. The general form of the EOV is Eq.(4.6) [4].

$$\Phi = \begin{bmatrix} \frac{\partial \vec{R}_X}{\partial \vec{R}_X} & \frac{\partial \vec{R}_X}{\partial \vec{R}_Y} & \frac{\partial \vec{R}_X}{\partial \vec{R}_Z} & \frac{\partial \vec{R}_X}{\partial \vec{V}_X} & \frac{\partial \vec{R}_X}{\partial \vec{V}_Y} & \frac{\partial \vec{R}_X}{\partial \vec{V}_Z} \\ \frac{\partial \vec{R}_Y}{\partial \vec{R}_X} & \frac{\partial \vec{R}_Y}{\partial \vec{R}_Y} & \frac{\partial \vec{R}_Y}{\partial \vec{R}_Z} & \frac{\partial \vec{R}_Y}{\partial \vec{V}_X} & \frac{\partial \vec{R}_Y}{\partial \vec{V}_Y} & \frac{\partial \vec{R}_Y}{\partial \vec{V}_Z} \\ \frac{\partial \vec{R}_Z}{\partial \vec{R}_X} & \frac{\partial \vec{R}_Z}{\partial \vec{R}_Y} & \frac{\partial \vec{R}_Z}{\partial \vec{R}_Z} & \frac{\partial \vec{R}_Z}{\partial \vec{V}_X} & \frac{\partial \vec{R}_Z}{\partial \vec{V}_Y} & \frac{\partial \vec{R}_Z}{\partial \vec{V}_Z} \\ \frac{\partial \vec{V}_X}{\partial \vec{R}_X} & \frac{\partial \vec{V}_X}{\partial \vec{R}_Y} & \frac{\partial \vec{V}_X}{\partial \vec{R}_Z} & \frac{\partial \vec{V}_X}{\partial \vec{V}_X} & \frac{\partial \vec{V}_X}{\partial \vec{V}_Y} & \frac{\partial \vec{V}_X}{\partial \vec{V}_Z} \\ \frac{\partial \vec{V}_Y}{\partial \vec{R}_X} & \frac{\partial \vec{V}_Y}{\partial \vec{R}_Y} & \frac{\partial \vec{V}_Y}{\partial \vec{R}_Z} & \frac{\partial \vec{V}_Y}{\partial \vec{V}_X} & \frac{\partial \vec{V}_Y}{\partial \vec{V}_Y} & \frac{\partial \vec{V}_Y}{\partial \vec{V}_Z} \\ \frac{\partial \vec{V}_Z}{\partial \vec{R}_X} & \frac{\partial \vec{V}_Z}{\partial \vec{R}_Y} & \frac{\partial \vec{V}_Z}{\partial \vec{R}_Z} & \frac{\partial \vec{V}_Z}{\partial \vec{V}_X} & \frac{\partial \vec{V}_Z}{\partial \vec{V}_Y} & \frac{\partial \vec{V}_Z}{\partial \vec{V}_Z} \end{bmatrix} \tag{4.6}$$

Even though the entire STM needs to be calculated, only the upper right 3×3 portion is needed in the algorithm. The upper right portion of the STM contains the information regarding the maneuvering satellite's differential position with respect to the applied ΔV. The components of the upper right portion of the STM, identified by ϕ, is shown in equation (4.7). Notice that the necessary piece of the STM is the component that relates Sat 1's final position vector components with the initial velocity vector components. This information ultimately provides for how the various ΔV's are integrated to find the best solution in the

algorithm.

$$\phi = \begin{bmatrix} \frac{\partial \vec{R}_X}{\partial \vec{V}_X} & \frac{\partial \vec{R}_X}{\partial \vec{V}_Y} & \frac{\partial \vec{R}_X}{\partial \vec{V}_Z} \\ \frac{\partial \vec{R}_Y}{\partial \vec{V}_X} & \frac{\partial \vec{R}_Y}{\partial \vec{V}_Y} & \frac{\partial \vec{R}_Y}{\partial \vec{V}_Z} \\ \frac{\partial \vec{R}_Z}{\partial \vec{V}_X} & \frac{\partial \vec{R}_Z}{\partial \vec{V}_Y} & \frac{\partial \vec{R}_Z}{\partial \vec{V}_Z} \end{bmatrix} \tag{4.7}$$

Another component necessary in the algorithm is the relationship between the satellite's final velocity vectors. Identifying this vector and combining this with ϕ, a form of the $\tilde{T}$ matrix is determined and shown in equation (4.8) [4]. The upper right portion of the STM, ϕ, is a 3×3 matrix. $\mathbf{I}$ is also a 3×3 matrix. While $\mathbf{0}$ is a 3×1 vector, yielding, $\tilde{T}$, a 6×4 matrix. The final $\mathbf{T}$ matrix is derived from scaling parameters combined with $\tilde{T}$.

$$\tilde{T} = \begin{bmatrix} \phi & \vec{V_{Sat1}} - \vec{V_{Sat2}} \\ \mathbf{I} & \mathbf{0} \end{bmatrix} \tag{4.8}$$

The final components of the TMN setup is the identification of a weight matrix, $\mathbf{Q}$ and a scale matrix, $\mathbf{S}$. The weight matrix allows for the user to shift convergence focus from final position to applied ΔV. In order to maintain a balanced focus on both minimizing miss distance and fuel used, an identity matrix, $\mathbf{I}$, should be used. For this study, $\mathbf{Q}$, is simply a 6×6 $\mathbf{I}$ matrix. The scale matrix, $\mathbf{S}$, is utilized to allow faster convergence within the algorithm. For this study, $\mathbf{S}$ is a constant 6×6 matrix transfered directly from Reference[4]. $\mathbf{S}$ is defined in (4.9) while $\mathbf{T}$ is calculated from $\tilde{T}$ and $\mathbf{S}$ in (4.10). $\mathbf{S}$ is an adjustable matrix to allow for better scaling of the nonlinear system of equations. Due to the placement of the upper right portion of the STM in kilometers (km) and the difference between final velocities in $\frac{km}{sec}$, within $\tilde{T}$, allows for a the possibility of a poorly scaled matrix. The poorly scaled matrix in some cases could result in a nearly singular matrix during the inversion in Eq.(4.10). For this study however, the scaling between the variables achieves desired

results using **S** in Eq.(4.9).

$$\mathbf{S} = \begin{bmatrix} 0.1 & 0 & 0 & 0 & 0 & 0 \\ 0 & 0.1 & 0 & 0 & 0 & 0 \\ 0 & 0 & 0.1 & 0 & 0 & 0 \\ 0 & 0 & 0 & 0.1 & 0 & 0 \\ 0 & 0 & 0 & 0 & 0.1 & 0 \\ 0 & 0 & 0 & 0 & 0 & 0.1 \end{bmatrix} \tag{4.9}$$

$$\mathbf{T} = \mathbf{S}^{-1}\tilde{T} \tag{4.10}$$

Ultimately, the variation of the control vector, $\vec{u}$, can be calculated. The variation of $\vec{u}$ is the core of TMN. Once the variation is within user defined tolerances, a unique solution is declared for the model. Based on matrix dimensions, $\vec{u}$, will have 4 components. Specifically, the components of $\vec{u}$ are

$$\vec{u} = \begin{bmatrix} \Delta V_{SAT1_X} \\ \Delta V_{SAT1_Y} \\ \Delta V_{SAT1_Z} \\ \Delta t \end{bmatrix}. \tag{4.11}$$

The ΔV terms are the changes in the initial impulsive maneuver applied to Sat 1 and the Δt term is the change in transfer time during each iteration. Summing the results for each component after each iteration yields the total ΔV for the impulsive manuever. Combining the sum of the Δt's with the initial transfer time, results in the final transfer time for the optimum ΔV.

The model iterates on Eq.(4.12) [4] until all the convergence criteria have been satisfied. Every iteration includes all of the previous steps for determining **T**. **Q** is the weight matrix and $\bar{e}$ is the error vector from Eq.(4.5).

$$\partial u = -(\mathbf{T}'\mathbf{Q}^{-1}\mathbf{T})^{-1}\mathbf{T}'\mathbf{Q}^{-1}\bar{e} \tag{4.12}$$

4.4 Results and Discussion

Recall in the derivation of the TMN differential correction algorithm that tolerance levels are needed to declare model convergence. Once the variation of the ΔV components is within 0.001 $\frac{meters}{sec}$ and the variation of the Δt component is within 0.01 sec on successive iterations, convergence is complete and a unique solution to the model can be declared. While there is no specific argument for these particular values, 'real life' factors weigh in. Considering at LEO velocity can be as high as 7500$\frac{m}{sec}$, 0.01 sec translates to approximately 75 meters of error. At Geostationary Orbit (GEO) this translates to about 30 meters of error. Balancing the desire to minimize computing time, while providing a viable solution, this margin of error is accepted throughout this chapter.

Solving for the impulsive tangential burn demonstrated in a Hohmann Transfer utilizing 2-Body dynamics is a basic exercise in the field of astrodynamics. Fortunately, that is why this type of problem was chosen for demonstration of optimality of the TMN differential correction algorithm. The same is not true for modeling the impulsive tangential transfer maneuvers utilizing J_2 system dynamics or the effects of air drag. However, the TMN differential correction algorithm can be used to determine accurate solutions, using these system dynamics, which represent a novel application of the previously developed algorithm.

4.4.1 Two-body Hohmann Transfer Impulsive Tangential Burn Analytical Solution.

Leveraging example problems from several different sources, the TMN differential correction algorithm was used to glean important information that can be expanded to user specific scenarios. Table 4.2 includes five specific scenarios executed during this study. In keeping with the guidance outlined by Kaplan [9], Prussing, and Chiu [22], the orbital ratios are also identified and are well under the threshold of 11.94 [22] cited as the ratio limit for the Hohmann Transfer being the optimum solution.

Table 4.2: Table-Top Solutions for Various 2-body Hohmann Transfer Problems.

Scenario	Initial Alt (km)	Final Alt (km)	Orbit Ratio	ΔV ($\frac{m}{sec}$)	Time (sec)
1	191.34411	35781.34857	6.417	2457	18924.2 [10]
2	6378.137	12756.3	1.5	533.565	10019.2 [3]
3	400	35785	6.22	2397	19048.6 [26]
4	300	35785	6.31	2425.8	18994.4 [13]
5	150	2000	1.283	470.708	3201.77

Recall that this study is focused on executing the algorithm to solve for the first of the two burns necessary in a minimum fuel orbital transfer. This unique application of the TMN algorithm is analogous to the first burn in a Hohmann Transfer maneuver sequence. This means that the algorithm will prove optimality for solving for the impulsive tangential burn intended to 'fly-by' the second satellite located at the desired orbit. It is not the intent of this algorithm to achieve the final orbit, but simply to intercept it. Therefore, the ΔV's cited are only those for the magnitude of the first tangential burn. The transfer time is the time to achieve fly-by with the second satellite at the desired orbit 180° from the starting location.

4.4.2 Two-body Hohmann Transfer Impulsive Tangential Burn TMN Solution.

Using the TMN algorithm to solve the previous scenarios yields the results identified in Tables 4.3 and 4.4.

The expected value is from the analytic solutions, while the actual values are determined directly from the algorithm. The percent (%) error terms are the difference between what the algorithm determined and the expected analytic solutions. As can be seen, the results determined by the algorithm are excellent. What slight differences exist

Table 4.3: Algorithm Solutions for Various 2-body Hohmann Transfer Problems.

Scenario	Expected ΔV ($\frac{m}{sec}$)	Actual ΔV ($\frac{m}{sec}$)	% Error
1	2457.00	2457.04	0.001
2	533.57	533.53	0.006
3	2397.00	2397.46	0.019
4	2425.80	2425.72	0.003
5	470.71	470.72	0.003

Table 4.4: Algorithm Solutions for Various 2-body Hohmann Transfer Problems.

Scenario	Expected Time (sec)	Actual Time (sec)	% Error
1	18924.20	18924.17	$1.58e^{-4}$
2	10019.20	10019.18	$1.99e^{-4}$
3	19048.60	19047.98	0.003
4	18994.40	18989.63	0.025
5	3201.77	3201.77	0

are due to order ϵ calculation differences throughout the actual implementation of solving for the analytical solutions and executing a numerical integrator on the necessary 42 EOM and EOV through the TMN algorithm.

These results demonstrate the optimality of the TMN differential correction algorithm. However, more information can be gleaned from these problems. Thus providing further evidence of the algorithm's robustness.

4.4.3 Two-body Varying Inclination Impulsive Tangential Burn TMN Solution.

Recall that the goal of the algorithm is to determine the minimum fuel maneuver required to execute a fly-by between a maneuvering satellite at a starting altitude and a non-maneuvering satellite located at the desired final altitude. Therefore, it is intuitive that the algorithm should deliver the same solution regardless of the starting inclination, utilizing 2-Body orbital dynamics. Figure 4.1 shows exaclty that result. The algorithm was repeated for several hundred random inclinations following a normal distribution, according to $i = Mod(Abs(Normal) \times \frac{\pi}{4}, \pi)$[70], and provided a fixed inclination for the non-maneuvering satellite.

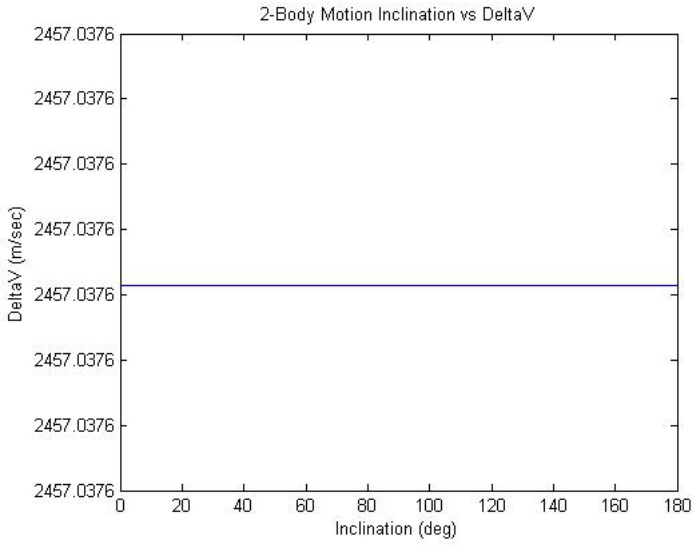

Figure 4.1: GTO Inclination vs. ΔV for Minimum Fuel Solution.

Recall that scenario 1 was a GTO from 191.34 km to 35781.35 km. This GTO was repeated to demonstrate the negligible effect of the maneuvering satellite's inclination in achieving a fly-by with the non-maneuvering satellite at the desired orbital altitude.

Keep in mind that for the purpose of the TMN differential correction algorithm, the non-maneuvering satellite, was in a circular, equatorial orbit.

Further analysis presented in Figure 4.2 demonstrates that the fly-by time, or transfer time, is also not effected by the change in inclination.

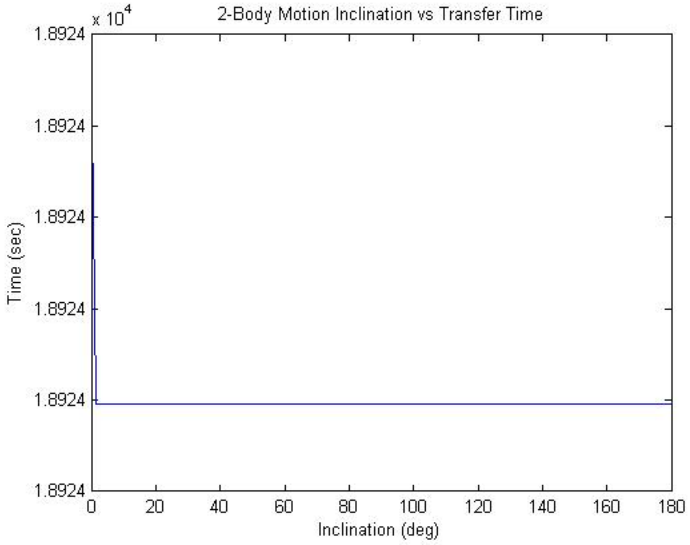

Figure 4.2: GTO Inclination vs. Rendezvous Time for Minimum Fuel Solution.

Overall, the effect of varying the inclination of the maneuvering vehicle does not have an impact on the calculated optimum result from the TMN differential correction algorithm.

4.4.4 Two-body Varying Eccentricity Impulsive Tangential Burn TMN Solution.

Further robustness of the algorithm is demonstrated by varying eccentricity for the maneuvering vehicle. The results in the previous section concluded what intuition suggested. The same is true for varying the eccentricity of the maneuvering satellite.

Executing the previous GTO from perigee at 191.34411 km altitude yields the following results from the TMN differential correction algorithm. Figure 4.3 shows a range of eccentricity values that yield a possible solution for the GTO transfer problem. Notice

the eccentricity ranges from 0 to 0.73. The value, 0.73, represents the eccentricity for an orbit with a fixed perigee at 191.34 km altitude and a fixed apogee at the desired altitude, 35781.35 km. Utilizing 2-Body astrodynamics equations, the eccentricities were varied within the differential correction algorithm to yield the final ΔVs.

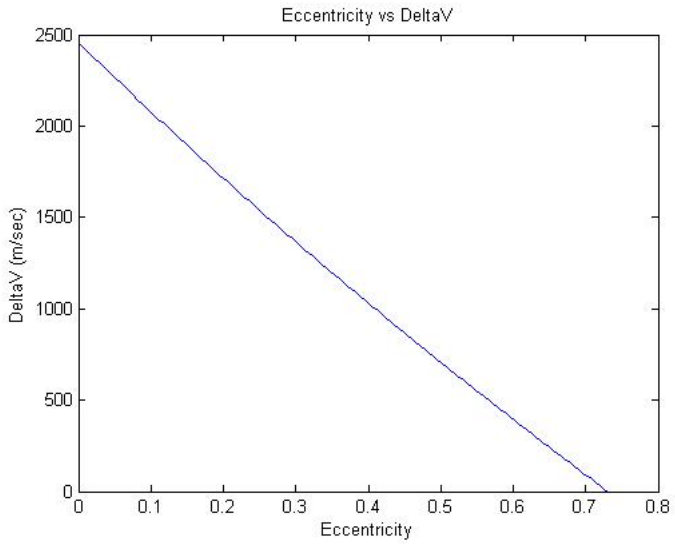

Figure 4.3: GTO Eccentricty vs. ΔV for Minimum Fuel Solution.

The results displayed in Figure 4.3 show the previously identified ΔV value of $2457.04\frac{m}{sec}$ at $e = 0$ and, as expected, $\Delta V = 0$ at the eccentricity that places apogee at the desired altitude, therefore achieving a successful fly-by for a minimum fuel cost. Further information from the TMN differential correction algorithm can be gleaned from Figure 4.4.

Figure 4.4 proves that the TMN differential correction algorithm is in fact finding a unique solution to each initial starting orbit. Even though the ΔV magnitudes are different, the resulting transfer time is identical. Therefore, considering the maneuvering vehicle is beginning at the same starting point and ending at the same point, with an identical transfer

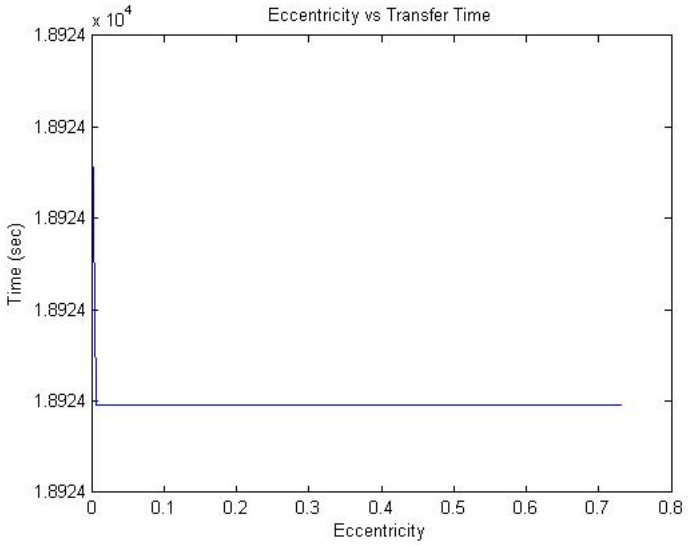

Figure 4.4: GTO Eccentricty vs. Transfer Time for Minimum Fuel Solution.

time, then the algorithm is solving for the minimum fuel, impulsive and tangential ΔV, to place the maneuvering satellite onto the optimum path to fly-by the non-maneuvering satellite at the desired altitude.

Utilizing the algorithm yields Figures 4.5 and 4.6 to illustrate the impact to ΔV of selecting an apogee height or the specific mechanical energy of the initial orbit with a fixed perigee of 191.34 km. These figures further demonstrate that increasing the initial apogee height and therefore increasing the specific mechanical energy, ultimately yields a lower necessary ΔV to achieve the desired orbital altitude.

Figures 4.5 and 4.6 provide a valuable view for selecting an initial orbit prior to applying an impulsive tangential maneuver determined by the algorithm.

4.4.5 Impulsive Tangential Burn TMN Solution Around Non-Spherical Earth.

The previous sections portray the capabilities of the TMN algorithm with 2-body dynamics. That is important because those are the solutions that are easily verified

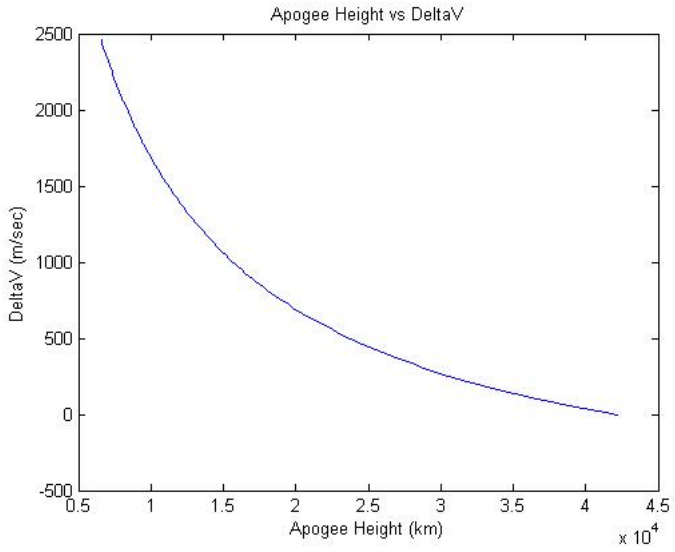

Figure 4.5: GTO Apogee Height vs. ΔV for Minimum Fuel Solution.

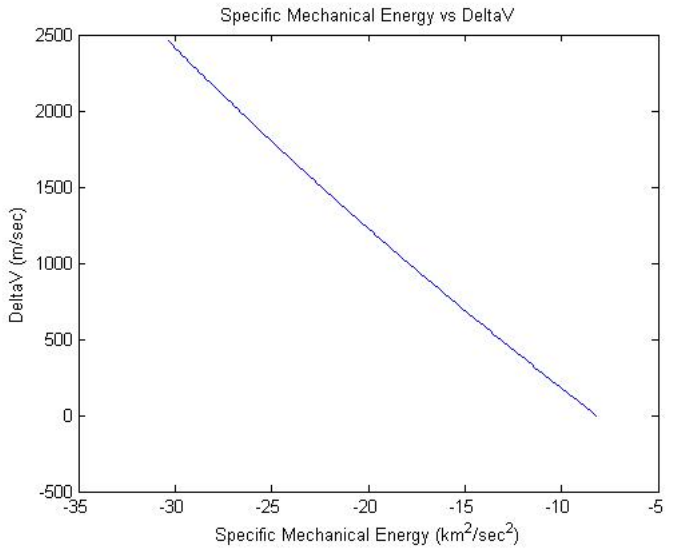

Figure 4.6: GTO Specific Mechanical Energy vs. ΔV for Minimum Fuel Solution.

analytically. However, 2-body dynamics do not yield the most accurate model for practical use. It provides an excellent starting point for introducing the results from the algorithm considering the effect on the orbits from J_2.

The 2-body system demonstrated no effect on the optimum fuel solution for transfer while varying the maneuvering satellite's inclination. This will not be the case while accounting for the Earth's equatorial bulge. Scenarios 1 and 5, identified in Table 4.5, will be re-executed using the TMN algorithm to demonstrate the changes and impact introduced by modeling the effect of J_2.

Table 4.5: Initial Conditions for Hohmann Transfer Problems.

Scenario	Initial Altitude (km)	Final Altitude (km)	Orbit Ratio
1	191.34	35781.35	6.42 [10]
5	150	2000	1.28

Figures 4.7 and 4.8 show the resulting impact from introducing the J_2 effect into the system model given by Eqs. (4.13) and (4.14).

$$\dot{R} = \vec{V} \tag{4.13}$$

$$\dot{V} = \frac{\mu\vec{R}}{|\vec{R}|^3} - \frac{3}{2} \times \frac{J_2 \mu R_\oplus^2 \vec{R}}{|\vec{R}|^5} \times (1 - \frac{5|\vec{R}_Z|^2}{|\vec{R}|^2}) \tag{4.14}$$

Figures 4.7 and 4.8 show that the minimum fuel condition is achieved at 90° and the maximum fuel maneuver is at an inclination of 0° and 180°. This produces the expected results for the effects due to the oblate Earth.

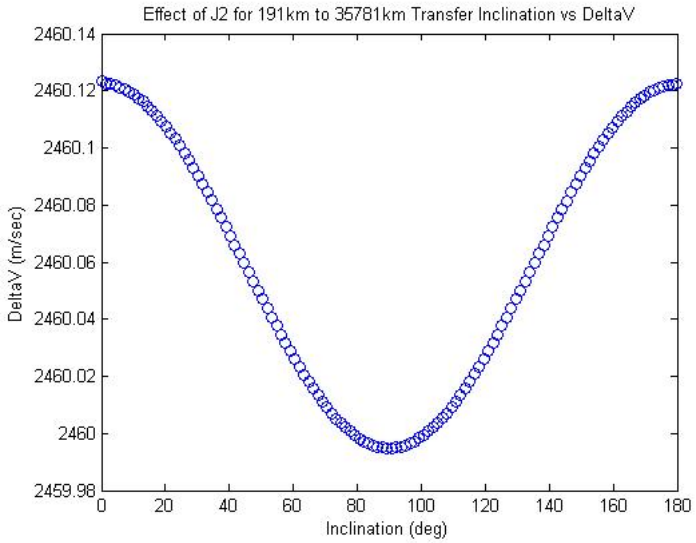

Figure 4.7: GTO Inclination vs. ΔV with J2 for Minimum Fuel Solution.

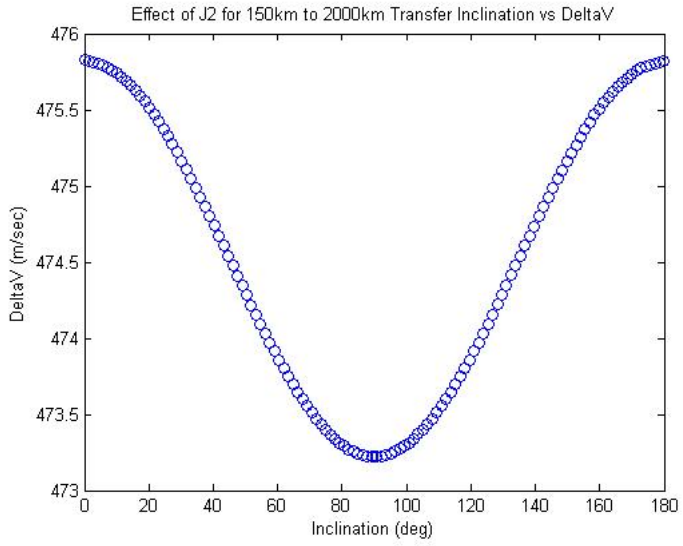

Figure 4.8: 150km to 2000km Transfer Inclination vs. ΔV with J2 for Minimum Fuel Solution.

Recall that this information has been gleaned from the TMN differential correction algorithm. The algorithm produced the minimum fuel, impulsive tangential burn, placing the maneuvering satellite onto the optimum trajectory to achieve a fly-by of the non-maneuvering satellite at the desired orbital altitude, provided a random sampling of initial inclinations. Figures 4.7 and 4.8 illustrate the versatility of the TMN algorithm to determine the impulsive tangential maneuver, provided the effects of the oblate Earth, analogous to the first burn of the Hohmann Transfer maneuver sequence.

4.4.6 Impulsive Tangential Burn TMN Solution Around Non-Spherical Earth with Air Drag.

The value of the TMN algorithm can be demonstrated by incorporating the air drag model into the system. Coupled with the J_2 effects of the non-spherical Earth, the impact of drag is significant. The same two scenarios are executed within the algorithm. This time, however, a ballistic coefficient, B^*, is added in order to illustrate the specific impacts of air drag on the minimum fuel solution. Table 4.6 summarizes the results of incorporating air drag into the model for the GTO from 191.34 km to 35781.35 km.

Table 4.6: Min ΔV Solutions for Varying Inclination GTO with J2 and Air Drag.

B^*	ΔV ($\frac{m}{sec}$)	Inclination (deg)
0	2459.99	90
0.044	2460.07	87.84
0.5	2460.88	67.68
1	2461.72	23.04

Figure 4.9 illustrates the impact of air drag on this maneuver. Based on the information in Table 4.6 and Figure 4.9, it is clear that there is a significant impact from the addition of

air drag into the model. The TMN differential correction algorithm still accounts for this and determines the necessary maneuver to place the vehicle onto the optimum trajectory to fly-by the non-maneuvering satellite located at the desired orbital altitude.

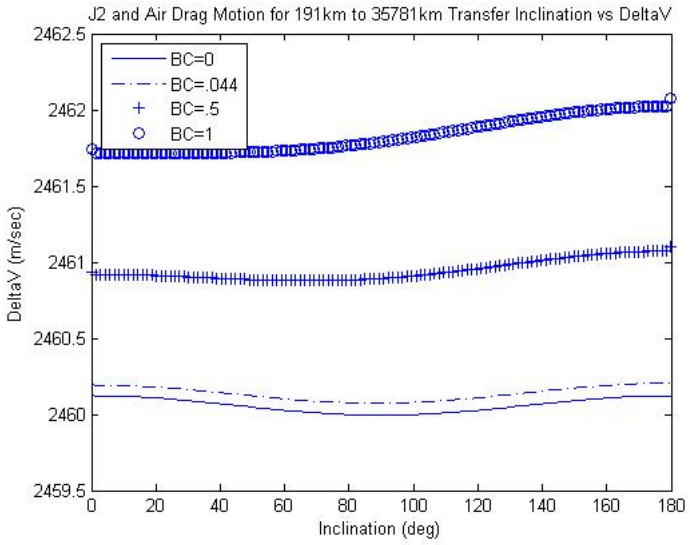

Figure 4.9: GTO Inclination vs. ΔV with J2 and Air Drag for Minimum Fuel Solution.

Further evaluation of Table 4.6 and Figure 4.9 illustrate that the more the satellite is orbiting against the rotation of the Earth ($i > 90°$), the larger magnitude ΔV is required to obtain the optimum trajectory. This is clear upon further understanding of the development of the relative velocity vector calculated in the air drag EOM and EOV. For further reference, the TMN differential correction algorithm also yields the maximum ΔV maneuvers for various inclinations for the GTO scenario in Table 4.7.

This coincides with earlier conclusions that the more the satellite is maneuvering against the rotation of the Earth, the larger the required maneuver is to obtain the optimum trajectory.

Table 4.7: Max ΔV Solutions for Varying Inclination GTO with J2 and Air Drag.

B^*	ΔV ($\frac{m}{sec}$)	Inclination (deg)
0	2460.12	0 and 180
0.044	2460.21	180
0.5	2461.1	180
1	2462.08	180

A similar analysis was completed with the transfer from 150 km to 2000 km. This scenario was selected because it would illustrate the biggest impact of air drag due to the entire flight regime residing within the atmospheric model (150 km to 2000 km)[10, 26].

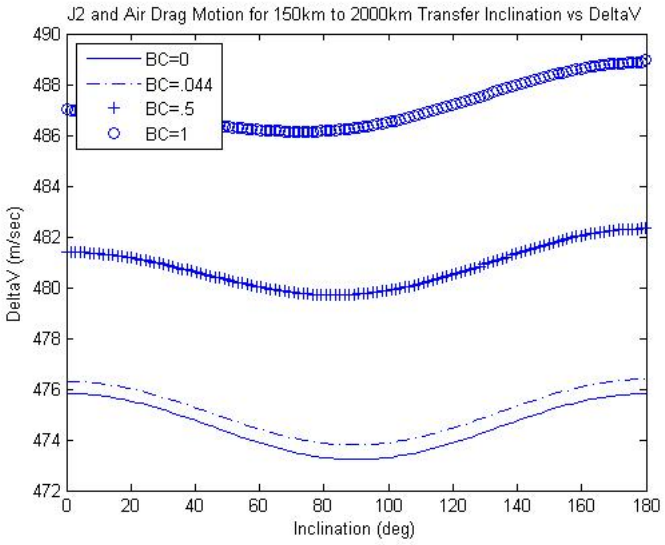

Figure 4.10: LEO Orbital Transfer Inclination vs. ΔV with J2 and Air Drag for Minimum Fuel Solution.

Figure 4.10 illustrates the impact of various ballistic coefficients over the range of possible inclinations. Tables 4.8 and 4.9 provide the minimum and maximum ΔV at their respective inclinations for the given ballistic coefficient.

Table 4.8: Min ΔV Solutions for Varying Inclination LEO Transfer with J2 and Air Drag.

B^*	ΔV ($\frac{m}{sec}$)	Inclination (deg)
0	473.22	90
0.044	473.79	89.28
0.5	479.71	83.52
1	486.14	72

Table 4.9: Max ΔV Solutions for Varying Inclination LEO Transfer with J2 and Air Drag.

B^*	ΔV ($\frac{m}{sec}$)	Inclination (deg)
0	475.83	0 and 180
0.044	476.40	180
0.5	482.33	180
1	489.00	180

4.5 Chapter Summary

Overall, this chapter has applied and adapted the TMN algorithm in a new way. This chapter has clearly shown the optimality of the T-Matrix Navigation differential correction algorithm to determine the single, minimum fuel, impulsive, tangential maneuver required

to achieve a fly-by with a non-maneuvering satellite. This study demonstrates and validates an extremely useful extension of the TMN differential correction algorithm. The extension of this study allows the TMN differential correction algorithm to be utilized as an additional tool for calculating generic orbital transfers utilizing a complex orbital model. This research also validates the algorithm's ability to determine the solution to a developed system of nonlinear equations, including the EOM and the EOV that make up the satellite's STM. The results within this chapter demonstrate the TMN algorithm's flexibility to determine the maneuver required to achieve a fly-by with a non-maneuvering satellite orbiting at a desired altitude. Specifically, this study accomplished these results by varying the initial eccentricity, as well portraying the impact of mission design considerations relating to the ballistic coefficient, initial orbital inclination, and initial apogee altitude with a fixed perigee altitude. Ultimately, the TMN algorithm was adapted and extended to this problem based on its previous utilization and success. Demonstrating the algorithm's ability to determine the impulsive tangential maneuver to fly-by a non-maneuvering satellite provides a more general and unique application for the algorithm. This study provides evidence that the TMN algorithm's solutions match those of the first tangential burn of a Hohmann Transfer, which validates the algorithm's solution as the minimum fuel maneuver.

V. Navigation Solution to Solve a Minimum Time, Fixed ΔV Optimal Trajectory

5.1 Introduction

Minimum time, impulsive tangential thrust spacecraft trajectory optimization problems are of interest, but somewhat rare in literature. Kluever, Kechichian, Martin and Conway [37, 38, 71] each develop optimal spacecraft transfer trajectories using non-impulsive, low-thrust models. Thorne [32] develops a minimum time optimal control problem utilizing continuous thrust. He also introduces the concept of deriving and propagating the variational equations of motion to accurately integrate reference trajectories. This chapter aims to develop and utilize a differential correction algorithm to ultimately solve for the minimum time trajectory that results from a fixed magnitude impulsive tangential thrust maneuver to deliver a satellite from an initial altitude to a desired altitude.

5.2 Problem Statement

Leveraging the work initiated by Chioma and Titus [4, 68, 69], Sears[63], Leigh and Black[1], this chapter aims to develop the case for the state transition matrix driven, differential correction algorithm solution to the fixed ΔV, minimum time spacecraft trajectory problem. The algorithm presented here solves for the rendezvous time and rendezvous angle, between an initial and desired final altitude, resulting from a fixed ΔV. The result of this algorithm is not intended to achieve orbit at the desired altitude, but to intercept it. This assumption turns the resulting solutions into a type of rendezvous/intercept orbital dynamics problem. Given an initial altitude and a desired final altitude, the differential correction algorithm will ultimately yield the minimum time trajectory, from a fixed magnitude impulsive tangential maneuver, to achieve the desired orbital altitude. This chapter will prove that the differential correction algorithm presented allows the user to declare the solution as the minimum time trajectory. The summary of the

optimal control problem that is being solved through this chapter is shown in Eq.(5.1).

$$
\begin{aligned}
&\text{Minimize: } \mathrm{J} = t_{t_f} - t_{t_0} \\
&\text{Subject to:} \\
&\quad \dot{\vec{R}}, \dot{\vec{V}} \\
&\quad u(t) = \Delta V \delta_0 (t - t_0) \\
&\text{Initial Conditions:} \\
&\quad \vec{R}_1(t_0) = \vec{R}_{1_{t_0}} \\
&\quad \vec{V}_1(t_0) = \vec{V}_{1_{t_0}} \\
&\quad \vec{R}_2(t_0) = \vec{R}_{2_{t_0}} \\
&\quad \vec{V}_2(t_0) = \vec{V}_{2_{t_0}} \\
&\quad t_0 = 0 \\
&\text{Terminal Conditions:} \\
&\quad \vec{R}_1(t_f) = \vec{R}_2(t_f)
\end{aligned}
\tag{5.1}
$$

The step-by-step procedure to solve this problem is provided. The items that represent a unique contribution from the original algorithm are highlighted in **boldface**.

1. **Establish initial Classic Orbital Elements (COEs) for satellites.**
2. Convert COEs to initial position, $\vec{R}_0$, and velocity, $\vec{V}_0$ vectors.
3. Establish scaling parameters and scaling matrix, **S**[4].
4. Establish weight matrix, **Q**[4].
5. **Determine initial guess for required fuel, ΔV, and transfer time, *t*.**
6. Integrate Equations of Motion (EOM) for Satellite 2 for duration of t.
7. Calculate final state, $\vec{R}, \vec{V}$, for Satellite 2 at t.
8. Apply ΔV to Satellite 1 to yield $\vec{V}_{0+}$.

9. Integrate EOM for Satellite 1 for duration of t.

10. Calculate final state $\vec{R}, \vec{V}$, for Satellite 1 at t.

11. Calculate component by component separation distance between maneuvering satellite and cooperative satellite(s)[4].

12. Integrate Satellite 1's State Transition Matrix (STM) using Equations of Variation (EOV) for duration of t.

13. Declare ϕ matrix as upper right 3x3 portion of STM[4].

14. Calculate velocity difference vector, $\vec{V}_{DIFF}$, between Satellite 1's and Satellite 2's velocity vectors.

15. Calculate ΔV for Satellite 1: $\Delta V = \vec{V}_{0+} - \vec{V}_0$.

16. **Compile error vector, $\bar{e}$, as the component by component separation distance and 0's for fixed fuel scenario.**

17. Build $\tilde{T}$ matrix: $\begin{bmatrix} \phi & \vec{V}_{DIFF} \\ 3\times 3 & 3\times 1 \\ \mathbf{I} & \mathbf{0} \\ 3\times 3 & 3\times 1 \end{bmatrix}$[4].

18. Calculate $\mathbf{T}$ matrix: $\mathbf{T} = \mathbf{S}^{-1}\tilde{T}$[4].

19. Declare convergence criteria[4].

20. Determine ∂u: $\partial u = -(\mathbf{T}'\mathbf{Q}^{-1}\mathbf{T})^{-1}\mathbf{T}'\mathbf{Q}^{-1}\bar{e}$[4].

21. **Check ∂u components versus convergence criteria:** $\partial u = \begin{bmatrix} 0 & 0 & 0 & \Delta t \end{bmatrix}$.

22. If convergence criteria are satisfied then the algorithm is complete.

- **Final ΔV = Fixed initial ΔV**
- Final transfer time = current t

23. ~~**Add ΔV from ∂u yielding new ΔV.**~~

24. Add Δt from ∂u to transfer time, t, for updated time.

25. Return to #6.

5.3 T-Matrix Navigation Differential Correction Algorithm

TMN has its roots in nonlinear least squares. Fundamentally, it is a method to reduce the amount of residual error in a system of complex nonlinear differential equations. In order to use this method in an optimization problem, an algorithm must be implemented to adequately bound the solution space of the nonlinear system of equations, while allowing the variational equations to be iterated towards a solution. Chioma presents the algorithm development [4].

In order to implement the TMN method within this chapter, two orbits are needed. In this particular case, they are the maneuvering satellite (Sat 1) and non-maneuvering satellite (Sat 2). For the minimum time fixed ΔV problem, the maneuvering satellite will be the satellite to which the ΔV is applied. The non-maneuvering satellite will be in a circular and equatorial orbit at the desired altitude for the maneuvering vehicle. Assuming the maneuvering satellite is located directly in line with the $\hat{X}$ axis at the start time, the maneuvering satellite's initial position vector is shown in Eq.(5.2).

It is fundamental to identify that the position vector of the maneuvering satellite has one initial value, while the velocity vector has two. They are the velocity of the maneuvering vehicle just before the maneuver and just after a maneuver, while still at the original position. The state vectors for the maneuvering satellite are given in equations

(5.3) and (5.4) [4].

$$\vec{R}_{Sat1} = R_{t_0} \begin{bmatrix} 1 \\ 0 \\ 0 \end{bmatrix} km \tag{5.2}$$

$$X_{Sat1}(t_0^-) = \begin{bmatrix} R_X(t_0) \\ R_Y(t_0) \\ R_Z(t_0) \\ V_X(t_0^-) \\ V_Y(t_0^-) \\ V_Z(t_0^-) \end{bmatrix} \tag{5.3}$$

$$X_{Sat1}(t_0^+) = \begin{bmatrix} R_X(t_0) \\ R_Y(t_0) \\ R_Z(t_0) \\ V_X(t_0^-) + \Delta V_X \\ V_Y(t_0^-) + \Delta V_Y \\ V_Z(t_0^-) + \Delta V_Z \end{bmatrix} \tag{5.4}$$

Normally, the applied ΔV is implemented and adjusted during each iteration through the algorithm. However, solving for the minimum time, fixed ΔV solution, the system is propagated through time to find each resulting end position for the varying time. The applied ΔV is not updated through each iteration. Therefore, for each iteration and updated time, only new position and velocity vectors at t_f will be determined.

Sat 2 is in a circular and equatorial orbit at the desired altitude for the transfer. Therefore, simply utilizing 2-body dynamics, the initial position and velocity vectors can be calculated for Sat 2. Because the desired orbit is circular and equatorial, Table 5.1 provides the COEs necessary to determine the initial vectors.

Table 5.1: COEs for Sat 2 Initial Conditions.

Orbital Element	Symbol	Value	Units
Semi-Major Axis	a	R_{t_f}	km
Eccentricity	e	0	n/a
Inclination	i	0	Degrees
Right Ascension of Ascending Node	Ω	0	Degrees
Argument of Perigee	ω	0	Degrees
True Anomaly	ν	β	Degrees

The desired altitude, R_{t_f}, for the transfer and β are derived from the final orbital period and the expected transfer time. The initial guess for the transfer time is derived from the 2-body dynamics relationship between the original velocity, the fixed ΔV, and the ratio between the initial orbital altitude and the final orbital altitude. Eqs. (5.5) through (5.11) provide the foundation for determining β in Eq. (5.12). The transfer ellipse velocity, $\vec{V}_T$, the eccentricity of the transfer ellipse, e_T, the semi-major axis of the transfer ellipse, a_T, and the eccentric anomaly of the transfer ellipse, E, are all intermediate values required to determine β.

$$|\vec{V}_T| = |\vec{V}_0| + |\Delta V| \tag{5.5}$$

$$a_T = -\mu/\left(|\vec{V}_T|^2 - \frac{2\mu}{|\vec{R}_{Sat1}|}\right) \tag{5.6}$$

$$e_T = 1 - \frac{|\vec{R}_{Sat1}|}{a_T} \tag{5.7}$$

$$R^{-1} = \frac{|\vec{R}_{Sat1}|}{|\vec{R}_{Sat2}|} \tag{5.8}$$

$$\nu_0 = \cos^{-1}\left(\frac{R^{-1} - 1}{e_T} + R^{-1}\right) \tag{5.9}$$

$$E = \cos^{-1}\left(\frac{e_T + \cos(\nu_0)}{1 + e_T * \cos(\nu_0)}\right) \tag{5.10}$$

$$TransferTimeGuess = \sqrt{\frac{a_T^3}{\mu}} * (E - e_T * \sin(E)) \tag{5.11}$$

$$\beta = 180^\circ - \nu_0 + (\frac{360^\circ * TransferTimeGuess}{PeriodSat2}) \tag{5.12}$$

Once the position vector in the future is determined for Sat 1, that same time is used to determine the position vector of Sat 2 and an error vector is calculated. The error vector is displayed in Eq.(5.13).

$$\bar{e} = \begin{bmatrix} R_{SAT1_X} - R_{SAT2_X} \\ R_{SAT1_Y} - R_{SAT2_Y} \\ R_{SAT1_Z} - R_{SAT2_Z} \\ 0 \\ 0 \\ 0 \end{bmatrix} \tag{5.13}$$

The error vector highlights the component by component miss distance between Sat 1 and Sat 2, as well as 0's as the applied ΔV on Sat 1. Since the ΔV is fixed, there is no change in the applied ΔV between iterations, therefore the 0's in the error vector.

Provided the direction for the algorithm to proceed, it is necessary to identify that the integrated equations for the solution will vary based on the desired model and required fidelity. Specifically, this study will demonstrate the versatility of the algorithm utilizing three separate models: (1) 2-body EOM, (2) EOM including J_2 and (3) EOM including both J_2 and an air drag model. Each system will require the appropriate variational equations according to the model that will be demonstrated.

The remaining development and implementation of the T-Matrix Navigation algorithm throughout this chapter follows directly with Section 4.3.

5.4 Results and Discussion

Recall in the derivation of the algorithm that tolerance levels are needed to declare model convergence. Once the variation of the Δt component is within 0.00001 sec on successive iterations, convergence is complete and a solution exists for the fixed ΔV. While there is no specific argument for this particular value, 'real life' factors weigh in. Considering that at LEO velocity can be as high as $7500\frac{m}{sec}$, thus 0.00001 sec translates to approximately 0.075 meters of error. At GEO this translates to about 0.03 meters of error. Balancing the desire to minimize computing time, while providing a viable solution, this margin of error is acceptable throughout this study.

It is also noteworthy that in order to efficiently complete the computations required through the algorithm, new units need to be introduced. According to Bate et al.[3] and Chioma[4], it is acceptable to define the constants DU and TU. The DU is simply the radius of the Earth (1 DU = 6378.137 km) and to simplify the system models, the Earth's Gravitational Parameter, μ, will equal 1 if TU = 806.811 seconds.

Solving for the transfer time and transfer angle, utilizing a fixed ΔV, is an intermediate astrodynamics exercise utilizing 2-body dynamics. However, it is still achievable by hand and with the assistance of a desktop calculator. This feature leads itself as a prime candidate for proving the optimality of the differential correction algorithm. Unfortunately, similar ease is not present for modeling the minimum time maneuver utilizing J_2 system dynamics or including the effects of air drag. However, the differential correction algorithm can be used to determine accurate solutions in these systems.

5.4.1 Two-body Minimum Time Tangential Burn Analytical Solution.

Leveraging example problems, the differential correction algorithm was utilized to glean important information that can be expanded to user specific scenarios. Table 5.2 includes two scenarios executed during this study.

Table 5.2: Table-Top Solutions for 2-body Minimum Time / Fixed ΔV Transfer Problems.

Scenario	t_0 Altitude (km)	t_f Altitude (km)	ΔV ($\frac{m}{sec}$)	Time (sec)	Angle (deg)
1	191.34	35781.35	2575.48	12446.02	160 Ref[10]
2	191.34	35781.35	3000	8690.87	139.74

Recall that this study is focused on executing the differential correction algorithm to solve for the minimum transfer time provided a fixed ΔV. This means that the algorithm will prove optimality for solving for the minimum time, assuming a tangential burn, necessary to 'fly-by' the second satellite at the desired orbital altitude. It is not the intent of this algorithm to achieve the final orbit, but simply to intercept it. Therefore, the ΔV's cited are only those for the magnitude of the tangential burn. The 'Time' column is the time to achieve intercept with the desired orbit. The 'Angle' column, represents the angle between the initial and final position vectors for Satellite 1.

5.4.2 Two-body Minimum Time Tangential Burn TMN Solution.

Using the fully developed differential correction algorithm to solve the previous scenarios yields the results identified in Tables 5.3 and 5.4.

Table 5.3: Algorithm Solutions for 2-body Minimum Time / Fixed ΔV Transfer Problems.

Scenario	ΔV ($\frac{m}{s}$)	Calc Time (s)	Actual Time (s)	% Error
1	2575.48	12446.02	12404.51	0.335
2	3000	8690.87	8680.61	0.118

Table 5.4: Algorithm Solutions for 2-body Minimum Time / Fixed ΔV Transfer Problems.

Scenario	ΔV ($\frac{m}{s}$)	Calc Angle (deg)	Actual Angle (deg)	% Error
1	2575.48	160	159.82	0.113
2	3000	139.74	139.70	0.029

The 'Calc Angle' value is actually the expected value from the analytic solutions, while the actual values are determined directly from the algorithm. The % error terms are the difference between what the algorithm determined and the expected analytic solutions. As can be seen, the results determined by the algorithm are excellent. What slight differences exist are due to order 'ϵ' calculation differences throughout the actual implementation of solving for the analytical solutions and executing an integrator on the necessary 42 EOM and EOV through the differential correction algorithm.

While these results demonstrate the optimality of the differential correction algorithm, more information can be gleaned from these problems, further proving the robustness of the algorithm.

5.4.3 GTO in Minimum Time with Fixed ΔV Using TMN Solution.

Keep in mind that the goal of the algorithm is to determine the minimum time maneuver required to execute a rendezvous between a starting altitude and a final altitude. Therefore, it is intuitive that the algorithm should deliver a solution that varies with the amount of fixed ΔV. Additionally, it is intuitive that the rendezvous angle, the angle between the initial and final position vectors for Satellite 1, should decrease as the amount of fixed ΔV applied is increased. In summary, both the amount of time and the rendezvous angle, for the maneuvering satellite to reach the desired altitude, should decrease as the amount of the applied ΔV increases. Figures 5.1 and 5.2 display these exact results utilizing

the aforementioned differential correction algorithm. These figures show the algorithm's results for a GTO from 191.34 km initial altitude to 35781.35 km final altitude.

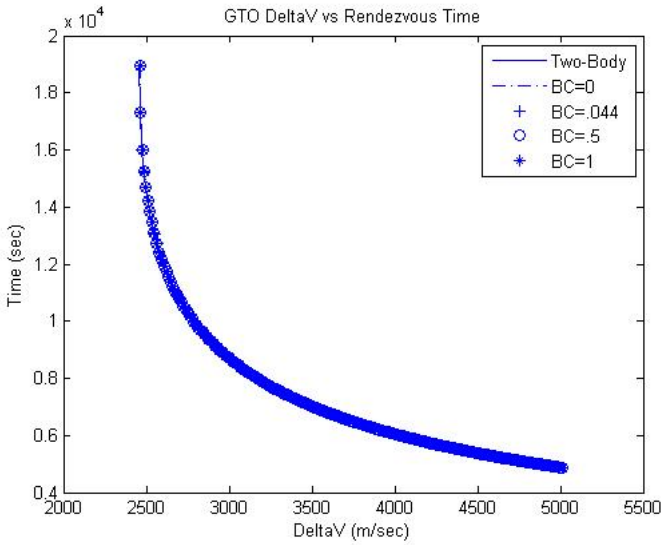

Figure 5.1: GTO ΔV vs. Rendezvous Time for Minimum Time Solution.

The results displayed in Figures 5.1 and 5.2 are for an initial eccentricity and inclination equal to zero. According to Reference [1] the minimum fuel tangential burn solutions for this problem are summarized in Table 5.5. B^*, or BC, is the ballistic coefficient while 'N/A' simply means that the results are for the 2-body solution. The results in Table 5.5 drive the lower range for the fixed ΔV while 5,000 $\frac{m}{sec}$ is arbitrarily selected as a very high value only for illustrative purposes on the impact of varying the ΔV on the minimum time solution utilizing the differential correction algorithm.

Recall that the results of the minimum fuel solutions match the Hohmann Transfer results. Therefore, the solution requires that the angle between the initial and final position vectors for the maneuvering satellite be equal to 180°. Table 5.5 also shows that regardless

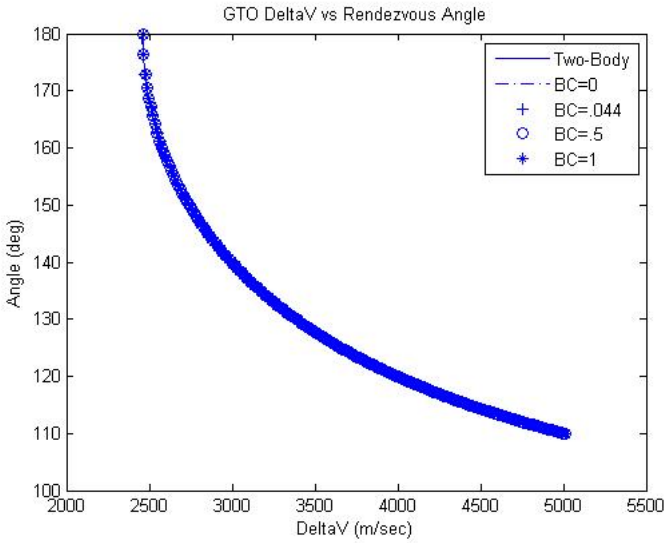

Figure 5.2: GTO ΔV vs. Rendezvous Angle for Minimum Time Solution.

Table 5.5: Hohmann Transfer Results for GTO at 0° Inclination [1].

B^*	ΔV ($\frac{m}{sec}$)	Rendezvous Time (s)	Rendezvous Angle (deg)
N/A	2457.04	18924.17	180
0	2460.12	18956.82	180
0.044	2460.19	18956.78	180
0.5	2460.93	18956.31	180
1	2461.74	18955.80	180

of the BC value, the ΔV variation is approximately 4.7 $\frac{m}{sec}$ between the 2-body solution and the highest BC value, 1, at 0° inclination.

Tight variation exists between the minimum fuel solutions, as well as the minimum time results. Figure 5.3 represents a closer range for ΔV. This zoomed in plot identifies the variation between the solutions, however slight.

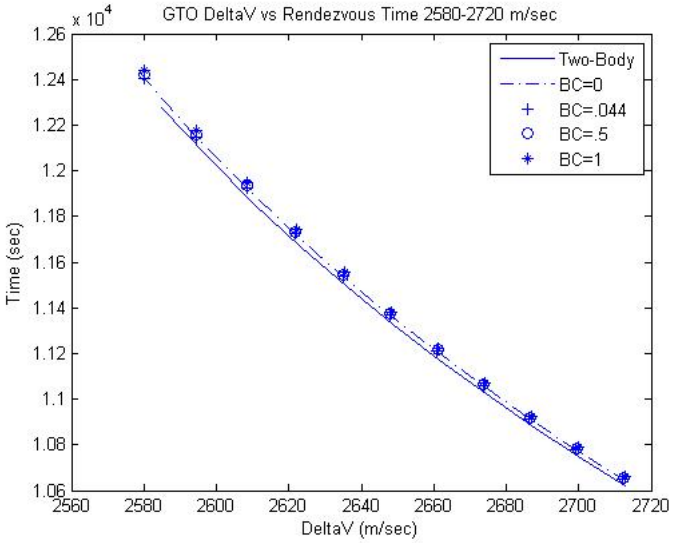

Figure 5.3: GTO ΔV vs. Rendezvous Time for Minimum Time Solution.

Figure 5.4 displays a zoomed in section of the high end of fixed ΔV's studied. Figure 5.4 simply shows that the higher the initial ΔV, the tighter the grouping between the models from the 2-body solution to the $B^* = 1$ solution. Table 5.6 summarizes these results for both ends of the ΔV range.

The results summarized in Table 5.6 validate what intuition conceives. To further validate this point, utilizing the differential correction algorithm, Figure 5.5 shows the percentage of time the maneuvering satellite remains in the atmosphere (150 km - 2000 km). Recall that the atmospheric model in this study is valid from 150 km to 2000 km altitude. Therefore, identifying within the algorithm's solution, the time that the satellite

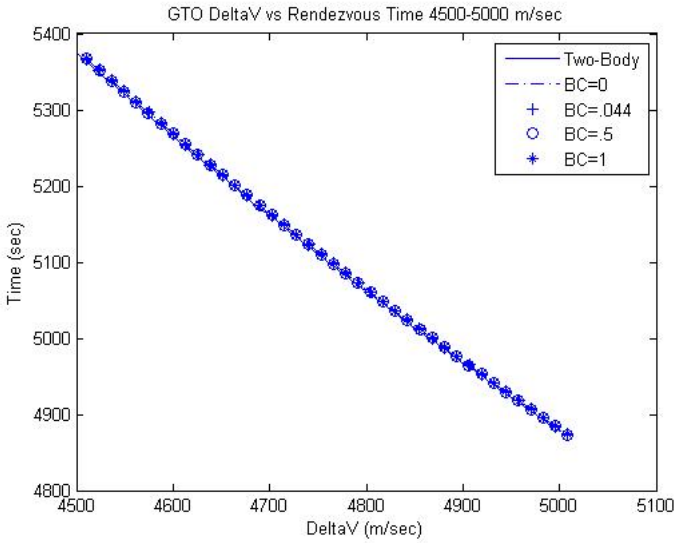

Figure 5.4: GTO ΔV vs. Rendezvous Time for Minimum Time Solution.

exceeds 2000 km altitude and dividing that time by the total transfer time results in the percentage of time the satellite traversed the valid atmosphere. Figure 5.5 validates this simply by illustrating the point that as the applied ΔV increases, the amount of time the vehicle remains in the atmosphere range decreases. This is also evident through the results in Table 5.6 showing how the solution's grouping gets closer due to less impact on the trajectory from the atmopshere.

Other mission design considerations can be gleaned from utilizing the differential correction algorithm to solve for the minimum time maneuver. According to Figure 5.6 the user can select a desired location, rendezvous angle, for his application and then determine the minimum time solution based on the 2-body solution, J_2 only or the design B^*.

It is also possible to utilize the differential correction algorithm to make further mission design decisions including the initial eccentricity for the maneuvering vehicle. Figures 5.7 and 5.8 display the results of varying the initial eccentricity for a given fixed

Table 5.6: Rendezvous Times and Differences from 2-body Solution for GTO at 0° Inclination.

B^*	ΔV ($\frac{m}{sec}$)	Rendezvous Time (s)	Time Difference (sec)
N/A	2520.94	13736.74	0
N/A	4910.80	4957.92	0
0	2520.94	13809.35	72.61
0	4910.80	4958.34	0.42
0.044	2520.94	13838.45	101.71
0.044	4910.80	4960.32	2.4
0.5	2520.94	13848.21	111.47
0.5	4910.80	4960.82	2.9
1	2520.94	13858.68	121.94
1	4910.80	4961.46	3.54

ΔV of 3000 $\frac{m}{sec}$ at 40° inclination. The results assume that perigee is located at 191.34 km altitude, while the desired altitude is 35781.35 km. The range of values for eccentricity are 0 to 0.73, which represents an apogee altitude equivalent to the desired altitude (35781.35 km).

Leveraging the differential correction algorithm to solve for the minimum time trajectory for the GTO example has proven to yield significant mission design utility. A further example of the algorithm's flexibility is evaluating the minimum time solutions for LEO transfer within the entirety of the referenced atmospheric altitude 150 km to 2000 km.

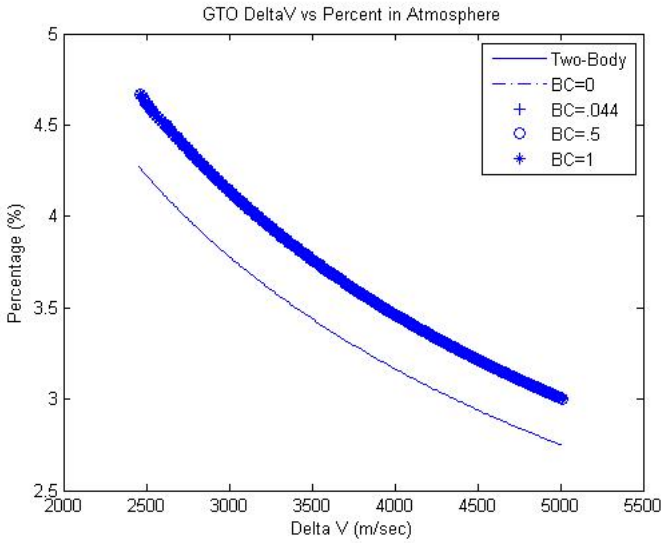

Figure 5.5: GTO ΔV vs. Percent of Time in Atmosphere for Minimum Time Solution.

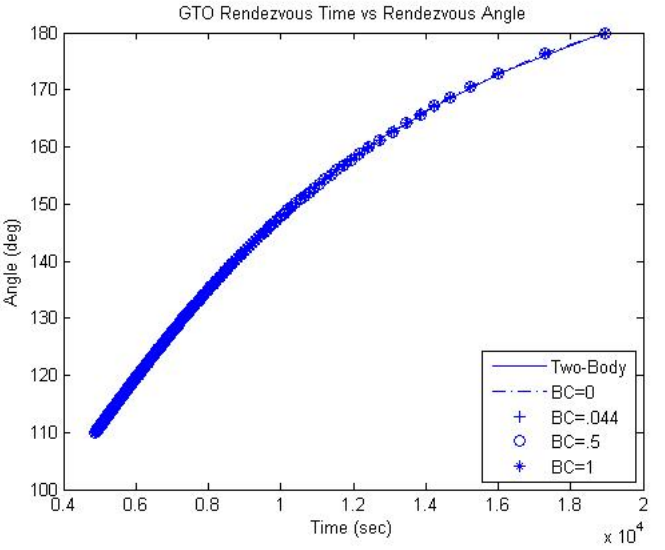

Figure 5.6: GTO Rendezvous Time vs. Rendezvous Angle for Minimum Time Solution.

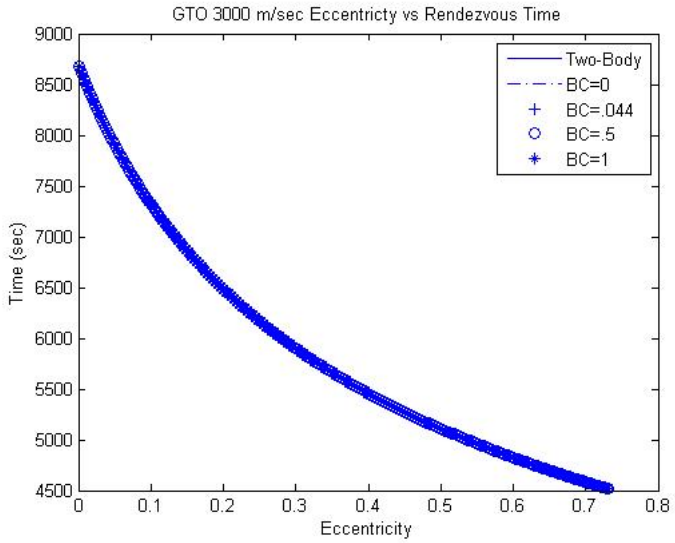

Figure 5.7: GTO Eccentricity vs. Rendezvous Time with Fixed ΔV=3000$\frac{m}{sec}$ for Minimum Time Solution.

5.4.4 LEO transfer in Minimum Time with Fixed ΔV Using TMN Solution.

Keep in mind that both the amount of time and the location, rendezvous angle, for the maneuvering satellite to reach the desired altitude should decrease as the amount of the applied ΔV increases. Figures 5.9 and 5.10 display these exact results utilizing the aforementioned differential correction algorithm. These figures show the algorithm's results for a LEO transfer from 150 km initial altitude to 2000 km final altitude.

The results displayed in Figures 5.9 and 5.10 are for an initial eccentricity and inclination equal to zero. According to Reference [1] the minimum fuel tangential burn solutions for this problem are summarized in Table 5.7. The results in Table 5.7 drive the lower range for the fixed ΔV, while 5,000 $\frac{m}{sec}$ is arbitrarily selected as a very high value only for illustrative purposes on the impact of varying the ΔV on the minimum time solution utilizing the differential correction algorithm.

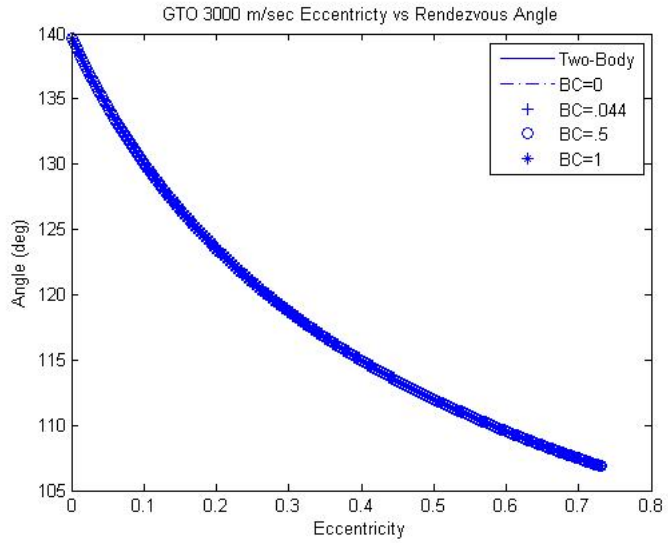

Figure 5.8: GTO Eccentricity vs. Rendezvous Angle with Fixed ΔV=3000$\frac{m}{sec}$ for Minimum Time Solution.

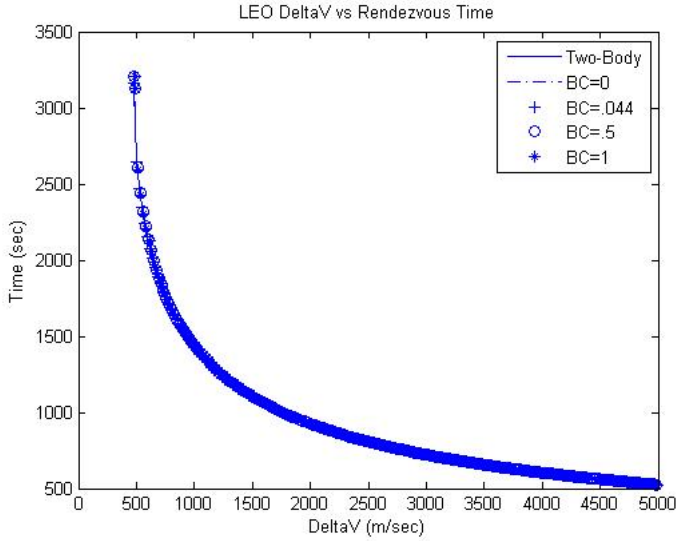

Figure 5.9: LEO Orbital Transfer ΔV vs. Rendezvous Time for Minimum Time Solution.

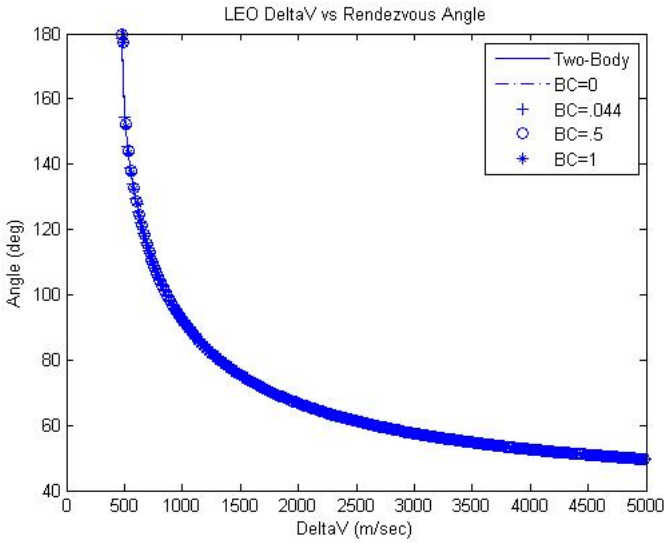

Figure 5.10: LEO Orbital Transfer ΔV vs. Rendezvous Angle for Minimum Time Solution.

Table 5.7: Hohmann Transfer Results for LEO Transfer at 0° Inclination [1].

B^*	ΔV ($\frac{m}{sec}$)	Rendezvous Time (s)	Rendezvous Angle (deg)
N/A	470.71	3201.77	180
0	475.83	3208.05	180
0.044	476.32	3207.02	180
0.5	481.42	3205	180
1	487.03	3202	180

Recall that the results of the minimum fuel solutions match the Hohmann Transfer results. Therefore, the solution requires that the angle between the initial and final position vectors for the maneuvering satellite be equal to 180°. Table 5.7 also shows that regardless of the BC value, the ΔV variation is approximately $17\frac{m}{sec}$ between the 2-body solution and

the highest BC value, 1, at 0° inclination. This value displays the significant impact the atmosphere plays on the trajectory in the LEO transfer example.

Further demonstration of this fact is captured in Figure 5.11. Figure 5.11 shows the significant difference between the algorithm's solutions for the 2-body solution and the solutions based on the various ballistic coefficients.

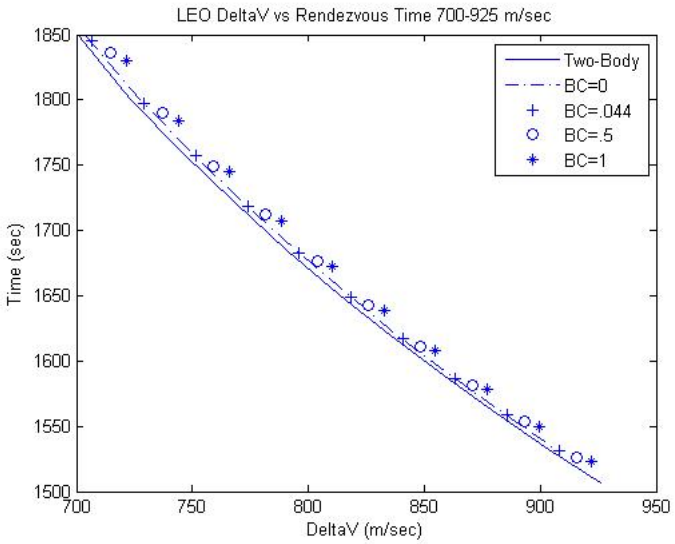

Figure 5.11: LEO Orbital Transfer ΔV vs. Rendezvous Time for Minimum Time Solution with Low Fixed ΔV.

Figure 5.12 portrays the tighter variation of the solutions between the 2-body solution and the various ballistic coefficients at much higher fixed ΔV.

The minimum time differential correction algorithm is also suited to aid in mission design through the selection of a desired rendezvous location to determine the resulting transfer time and therefore the required ΔV. For this example, Figure 5.13 shows this information for a LEO transfer between 150 km altitude to 2000 km altitude at 0° inclination and 0 eccentricity.

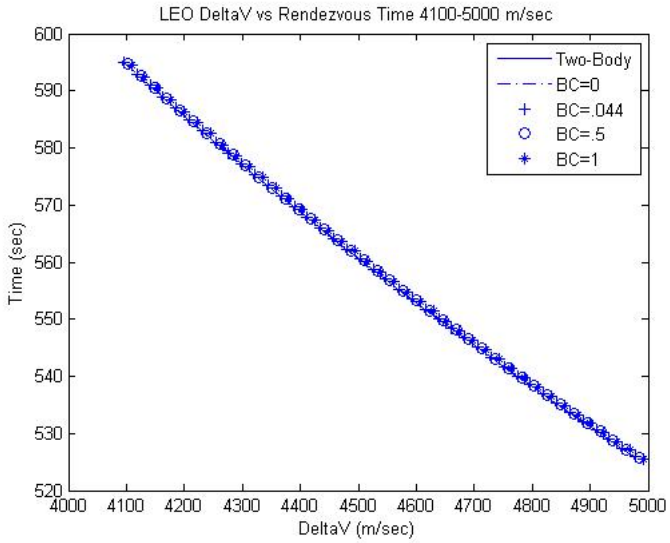

Figure 5.12: LEO Orbital Transfer ΔV vs. Rendezvous Time for Minimum Time Solution with High Fixed ΔV.

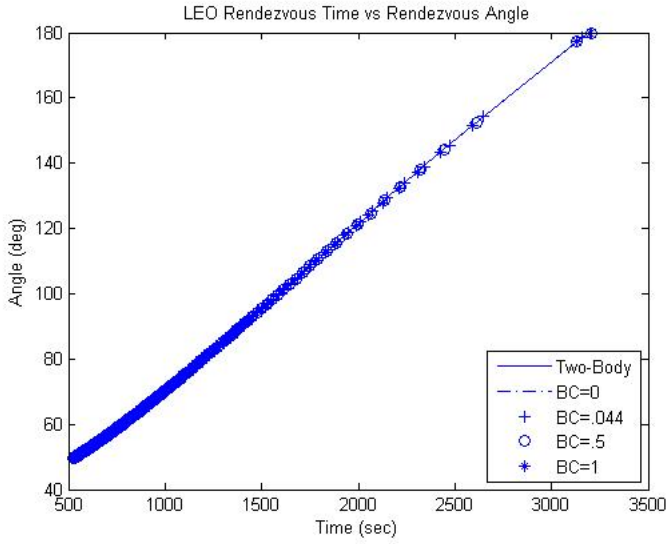

Figure 5.13: LEO Orbital Transfer Rendezvous Time vs. Rendezvous Angle for Minimum Time Solution.

5.5 Chapter Summary

Overall, this chapter has demonstrated the ability for the differential correction algorithm to determine the single minimum time, fixed ΔV, impulsive maneuver required to achieve a fly-by with a desired final orbital altitude. This study demonstrates and validates an extremely useful extension of the differential correction algorithm by utilizing the STM to allow the user to investigate individual design impacts on the minimum time trajectory. This research also validates the algorithm's ability to determine the minimum time solution to a developed system of nonlinear equations, including the EOM and the EOV that make up the satellite's STM. While determining the transfer time and rendezvous angle with a fixed ΔV can be easily verified utilizing only 2-body dynamics, the results within this chapter demonstrate the differential correction algorithm's flexibility to calculate this solution provided a more complex system model including both J_2 and atmospheric drag. Further, the presented algorithm, allows the user to specify mission design parameters in order to assess their impacts on the overall solution. These design parameters include the ballistic coefficient, initial orbital eccentricity with a fixed perigee altitude, and the selection of a final rendezvous angle at the desired altitude.

This chapter demonstrates that the differential correction algorithm can be expanded to solve for the minimum time trajectory provided a fixed maneuver magnitude within a complex system model and a non-circular initial orbit. The results from this study demonstrate the capability of the differential correction algorithm to determine the minimum time satellite transfer trajectory. These results also lead themselves to the possibility of utilizing the algorithm to determine more complex non-tangential maneuvers to achieve minimum time trajectories with a provided fixed magnitude maneuver.

VI. Navigation Solution to Maneuver a Spacecraft Relative to a Sphere Centered on a Cooperative Satellite

6.1 Introduction

This chapter seeks to extend the T-Matrix Navigation algorithm to allow for a varying geometric solution between the maneuvering satellite relative to a single non-maneuvering satellite. The concept of theater-based responsive relay satellite coverage is of interest in this study. Provided a vector for guiding this research, an algorithm is presented and then modified to introduce the orbit considerations for satisfying the potential mission requirement of ultimately optimizing the required ΔV.

6.2 Problem Statement

The purpose of this chapter is to demonstrate the ability for the modified TMN algorithm to deliver an impulsive maneuver to a satellite to place it within a sphere, with a user-defined radius, centered around a non-maneuvering satellite within a constrained time. Specifically, the proceeding results are generalized for the satellites' altitudes, but it is assumed throughout that the non-maneuvering satellite must complete one full orbit +/- 10%, based on orbital period, before the maneuvering satellite can successfully declare a solution within the radius with margin. The maneuvering satellite must only complete one orbit as well, in order to synchronize the orbital phase. This study only focuses on prograde orbits, therefore inclinations range between 0° and 90°. The focus of the results is based on the success of the modified TMN algorithm, while demonstrating unique aspects of this problem. Ultimately, this chapter will present generalized modifications to the TMN algorithm which allow for expanded utilization of the algorithm to be applied towards a user-defined scenario. Throughout this chapter the terms Satellite 1, Sat 1 and maneuvering satellite are one in the same, while Satellite 2, Sat 2 and the non-maneuvering satellite are

all the same. A summary of the optimal control problem being solved in this chapter is displayed in Eq.(6.1)

$$
\begin{aligned}
&\text{Minimize: J} = \int_{t_0}^{t_f} |u(t)|\, dt \\
&\text{Subject to:} \\
&\quad \dot{\vec{R}}, \dot{\vec{V}} \\
&\quad u(t) = \Delta V \delta_0(t - t_0) \\
&\quad t_f \in [0.9\text{P}_2, 1.1\text{P}_2] \\
&\text{Initial Conditions:} \\
&\quad \vec{R}_1(t_0) = \vec{R}_{1_{t_0}} \\
&\quad \vec{V}_1(t_0) = \vec{V}_{1_{t_0}} \\
&\quad \vec{R}_2(t_0) = \vec{R}_{2_{t_0}} \\
&\quad \vec{V}_2(t_0) = \vec{V}_{2_{t_0}} \\
&\quad t_0 = 0 \\
&\text{Terminal Conditions:} \\
&\quad \vec{R}_1(t_f) \in \mathbf{B}(\vec{R}_2(t_f), \eta) = \{\vec{R}_1(t_f) \in R^3 : |\vec{R}_1(t_f) - \vec{R}_2(t_f)| \leq \eta\}
\end{aligned}
\tag{6.1}
$$

A brief summary of the step-by-step procedure to solve this problem is provided. The unique contributions from this chapter are highlighted in **boldface**.

1. **Establish initial Classic Orbital Elements (COEs) for satellites.**
2. Convert COEs to initial position, $\vec{R}_0$, and velocity, $\vec{V}_0$ vectors.
3. Establish scaling parameters and scaling matrix, **S**[4].
4. Establish weight matrix, **Q**[4].
5. **Determine initial guess for required fuel, ΔV, and transfer time, *t*.**
6. Integrate Equations of Motion (EOM) for Satellite 2 for duration of t.

7. Calculate final state, $\vec{R}, \vec{V}$, for Satellite 2 at t.

8. Apply ΔV to Satellite 1 to yield $\vec{V}_{0+}$.

9. Integrate EOM for Satellite 1 for duration of t.

10. Calculate final state $\vec{R}, \vec{V}$, for Satellite 1 at t.

11. **Calculate spherical separation distance between Satellite 1 and Satellite 2.**

12. Integrate Satellite 1's State Transition Matrix (STM) using Equations of Variation (EOV) for duration of t.

13. Declare ϕ matrix as upper right 3x3 portion of STM[4].

14. Calculate velocity difference vector, $\vec{V}_{DIFF}$, between maneuvering satellite and cooperative satellite(s) velocity vectors.

15. Calculate ΔV for Satellite 1: $\Delta V = \vec{V}_{0+} - \vec{V}_0$.

16. **Compile error vector, $\bar{e}$, as the spherical separation distance and components of ΔV.**

17. Build $\tilde{T}$ matrix: $\begin{bmatrix} \phi & \vec{V}_{DIFF} \\ 3\times 3 & 3\times 1 \\ \mathbf{I} & \mathbf{0} \\ 3\times 3 & 3\times 1 \end{bmatrix}$[4].

18. Calculate $\mathbf{T}$ matrix: $\mathbf{T} = \mathbf{S}^{-1}\tilde{T}$[4].

19. Declare convergence criteria[4].

20. Determine ∂u: $\partial u = -(\mathbf{T}'\mathbf{Q}^{-1}\mathbf{T})^{-1}\mathbf{T}'\mathbf{Q}^{-1}\bar{e}$[4].

21. Check ∂u components versus convergence criteria: $\partial u = \begin{bmatrix} \Delta V_X & \Delta V_Y & \Delta V_Z & \Delta t \end{bmatrix}$[4].

22. If convergence criteria are satisfied then the algorithm is complete.

    - Final ΔV = ΔV from error vector, $\bar{e}$
    - Final transfer time = current t

23. Add ΔV from ∂u to $\vec{V}_{0+}$ yielding new ΔV.

24. Add Δt from ∂u to transfer time, t, for updated time.

25. Return to #6.

6.3 Establishing the Algorithm

The initial position for Satellite 2 is random. Even though the initial altitude is fixed, the orbital period is random, following a normal distribution. Specifically for this study, a fixed number of orbital periods could be randomly selected from for Satellite 2's orbital period. Once the orbital period was randomly selected, knowing the fixed initial altitude, the semi-major axis could be determined, as well as the eccentricity. The minimum and maximum periods allowed for this study were 90 and 1,440 minutes. This allowed for a range between a low eccentricity orbit, as well an extremely elliptical orbit. Provided Satellite 2 began at the fixed initial altitude of 150 km, this ensured that the initial true anomaly, ν, was at 0°. To complete the initial conditions for the non-maneuvering satellite, the remaining Classical Orbital Elements (COEs), were determined following a normal distribution according to Eqs.(6.2), (6.3) and (6.4) [70].

$$i = Mod(Abs(Normal) \times \frac{\pi}{4}, \frac{\pi}{2}) \tag{6.2}$$

$$\Omega = Mod(Abs(Normal) \times 2\pi, 2\pi) \tag{6.3}$$

$$\omega = Mod(Abs(Normal) \times 2\pi, 2\pi) \tag{6.4}$$

Once the initial COEs were determined for the non-maneuvering satellite, the original position and velocity vectors needed to be determined for the maneuvering satellite,

Satellite 1. The process to determine the initial conditions for Satellite 1 are much more involved.

The orbital period for Satellite 1 is randomized with the same range of values as the non-maneuvering satellite, between 90 and 1,440 minutes. Provided the orbital period and a fixed initial altitude, the semi-major axis and eccentricity of Satellite 1 is calculated. Then the initial specific mechanical energy, ϵ, of the orbit is determined from Eq.(6.5). Further, assuming the maneuvering satellite begins at perigee along the same unit position vector as the non-maneuvering satellite, the position vector, $\vec{R}$, is known. The magnitude of $\vec{R}$ is $R_{\oplus}$ + 250 km. The magnitude of the initial velocity of Satellite 1 is calculated by Eq.(6.6). Therefore, the magnitude of the specific angular momentum can also be calculated using Eq.(6.7).

$$\epsilon = \frac{-\mu}{2a_{Sat1}} \tag{6.5}$$

$$|\vec{V}| = \sqrt{2(\frac{\mu}{|\vec{R}|} + \epsilon)} \tag{6.6}$$

$$|\vec{h}| = |\vec{R}||\vec{V}| \tag{6.7}$$

Provided all three components of the position vector, the magnitude of the velocity vector, and the magnitude of the specific angular momentum vector, a nonlinear system of six equations will need to be solved for the remaining six unknowns. The unknowns are the three components of both the velocity vector, as well as the specific angular momentum vector. The first of the six equations, Eq.(6.8), comes from the dot product relationship between two vectors. Therefore, knowing that the maneuvering satellite is beginning at perigee, the angle between the position vector, $\vec{R}$, and the velocity vector, $\vec{V}$, is 90°. The second and third equations, Eqs.(6.9) and (6.10), come from the magnitude equations for a vector of three dimensions. While the final equations, Eqs.(6.11) through (6.13), come from the cross product relationship between the position and velocity vectors to yield the

specific angular momentum vector.

$$0 = R_X(t_0)V_X(t_0) + R_Y(t_0)V_Y(t_0) + R_Z(t_0)V_Z(t_0) \tag{6.8}$$

$$|\vec{V}_{t_0}| = \sqrt{V_X(t_0)^2 + V_Y(t_0)^2 + V_Z(t_0)^2} \tag{6.9}$$

$$|\vec{h}_{t_0}| = \sqrt{h_X(t_0)^2 + h_Y(t_0)^2 + h_Z(t_0)^2} \tag{6.10}$$

$$h_X(t_0) = R_Y(t_0)V_Z(t_0) - R_Z(t_0)V_Y(t_0) \tag{6.11}$$

$$h_Y(t_0) = -(R_X(t_0)V_Z(t_0) - R_Z(t_0)V_X(t_0)) \tag{6.12}$$

$$h_Z(t_0) = R_X(t_0)V_Y(t_0) - R_Y(t_0)V_X(t_0) \tag{6.13}$$

While the specific angular momentum vector is not needed for this algorithm, it is a by-product necessary to determine the maneuvering satellite's initial velocity vector. A straightforward conversion to COEs is now possible for the maneuvering satellite.

In order for the algorithm to proceed, the future state, both the position and velocity vectors, needs to be determined for the maneuvering satellite. Once the position vector in the future is determined for Sat 1, that same time is used to determine the position vector of Sat 2, and an error vector is calculated. The original error vector within the TMN algorithm is represented by Eq.(6.14)[4]. The updated error vector for this chapter is displayed in Eq.(6.15).

$$\bar{e} = \begin{bmatrix} R_{SAT1_X} - R_{SAT2_X} \\ R_{SAT1_Y} - R_{SAT2_Y} \\ R_{SAT1_Z} - R_{SAT2_Z} \\ \Delta V_{SAT1_X} \\ \Delta V_{SAT1_Y} \\ \Delta V_{SAT1_Z} \end{bmatrix} \tag{6.14}$$

$$\bar{e} = \begin{bmatrix} \Lambda_X \\ \Lambda_Y \\ \Lambda_Z \\ \Delta V_{SAT1_X} \\ \Delta V_{SAT1_Y} \\ \Delta V_{SAT1_Z} \end{bmatrix} \tag{6.15}$$

Recall that this particular problem is establishing an algorithm to yield a solution that maneuvers a satellite within a sphere, with a user-defined radius, from the non-maneuvering satellite. Therefore, the introduction of the vector, $\vec{\Lambda}$, represents a relationship between the maneuvering and non-maneuvering satellites according to the radius of the user-defined sphere. The components of the $\vec{\Lambda}$ vector are presented in Eqs.(6.16) through (6.18).

$$\Lambda_X = R_{SAT1_X} - \left(\frac{R_{SAT1_X} - R_{SAT2_X}}{|\vec{R}_{SAT1} - \vec{R}_{SAT2}|} \times \eta + R_{SAT2_X} \right) \tag{6.16}$$

$$\Lambda_Y = R_{SAT1_Y} - \left(\frac{R_{SAT1_Y} - R_{SAT2_Y}}{|\vec{R}_{SAT1} - \vec{R}_{SAT2}|} \times \eta + R_{SAT2_Y} \right) \tag{6.17}$$

$$\Lambda_Z = R_{SAT1_Z} - \left(\frac{R_{SAT1_Z} - R_{SAT2_Z}}{|\vec{R}_{SAT1} - \vec{R}_{SAT2}|} \times \eta + R_{SAT2_Z} \right) \tag{6.18}$$

Eqs.(6.16) through (6.18) displays the components of the unit vector of the component by component miss distance vector between Sat 1 and Sat 2. The unit vector components are multiplied by η, the radius of the sphere, and added to the component of the non-maneuvering satellite. Interestingly, this technique makes the solution dynamic. Meaning, that the solution to the sphere edge changes with each iteration because the solution itself is based on the position of both the maneuvering and non-maneuvering satellites.

Overall, the error vector, Eq.(6.15), represents the dynamic solution for the position and the applied ΔV on the maneuvering satellite, Sat 1.

The remaining development and implementation of the algorithm proceeds according to Section 4.3.

6.4 Results and Discussion

Recall in the derivation of the dynamic TMN differential correction algorithm that tolerance levels are needed to declare model convergence. Once the variation of the applied ΔV components are within 0.001 $\frac{meters}{sec}$ and the variation of the Δt component is within 0.01 sec on successive iterations, convergence is complete and a unique solution to the model can be declared. While there is no specific argument for these particular values, 'real life' factors weigh in. Considering at LEO velocity can be as high as 7500$\frac{m}{sec}$, a Δt of 0.01 sec translates to approximately 75 meters of error. At GEO Δt of 0.01 sec, translates to about 30 meters of error. Balancing the desire to minimize computing time and providing a viable solution, this margin of error is acceptable throughout this study.

It is also noteworthy that in order to efficiently complete the computations required through the algorithm, new units need to be introduced. According to References [3] and [4], it is acceptable to define the constants DU and TU. The DU is simply the radius of the Earth (1 DU = 6378.137 km) and to simplify the system models, the Earth's Gravitational Parameter, μ, will equal 1 if TU = 806.811 seconds.

Throughout the results of this study, the range, η, utilized was 100 km. The margin for error was 1%, allowing for a maximum sphere radius of 101 km, or 0.016 DU. Provided the solution sphere radius, solving for the impulsive tangential phasing maneuver required utilizing standard 2-body dynamics. Fortunately, that is why this type of problem is used to demonstrate the versatility of the dynamic TMN differential correction algorithm. Additionally, the dynamic algorithm is able to provide the required impulsive maneuver for Sat 1, to meet the specified sphere radius utilizing complex system dynamics including the effects of J_2 and air drag.

Additionally, the following results are illustrated for various values of ballistic coefficient regarding design decision impacts. The ballistic coefficient is identical for both the maneuvering and non-maneuvering satellite, for each specific value, throughout these

results. It is also important to keep in mind that the goal of this study is to deliver the maneuvering satellite within the solution sphere of the non-maneuvering satellite at the time that the non-maneuvering satellite has completed one single orbit.

6.4.1 Results Based on Initial Maneuvering Vehicle Inclination.

Figure 6.1 illustrates the impact of the miss distance between the maneuvering and non-maneuvering satellites, Sat 1 and Sat 2, based on the initial inclination of the maneuvering satellite. The normalized value represents the maximum sphere radius. Overall, Figure 6.1 shows that there is little impact on the miss distance due to the initial inclination of Sat 1, regardless of the ballistic coefficient. Keep in mind that the desired value is to be at or within the user defined sphere, 0.99, with 1% margin representing a normalized value of 1. Also, the algorithm begins with Sat 1 located at the 0.99 sphere range.

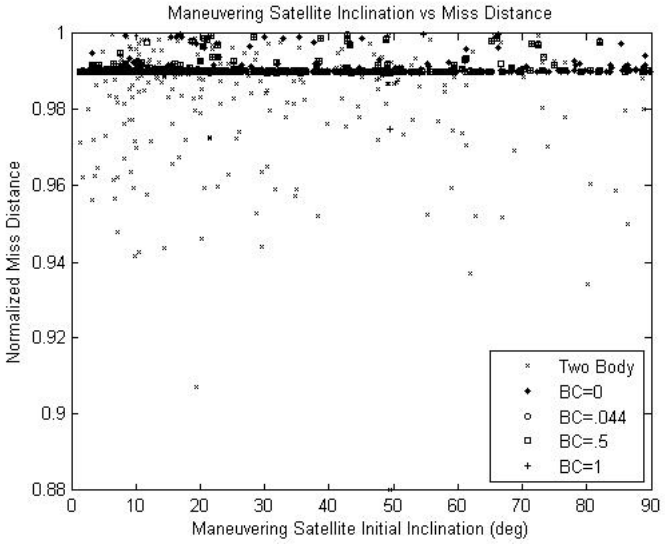

Figure 6.1: Maneuvering Satellite's Inclination vs. Normalized Miss Distance.

Not surprisingly, the 2-body solutions in Figure 6.2 show a normalized transfer time very near 1. This normalized transfer time is the algorithm's time solution for the maneuver divided by the orbital period of the non-maneuvering satellite. Therefore, a normalized transfer time of 1 is equal to Sat 2's orbital period. Values less than 1 are times shorter than the non-maneuvering satellite's orbital period, while values greater than 1 represent times greater than Sat 2's orbital period. Figure 6.2 shows that there is a slight increase in time relative to the non-maneuvering satellite's orbital period as the maneuvering satellite's initial inclination is increased. Recall, that the initial position for the maneuvering satellite is based on the initial position of the non-maneuvering satellite and that the maneuvering satellite begins at the edge of the solution sphere of the non-maneuvering satellite along its unit position vector. Therefore, a lower maneuvering satellite inclination will deliver Sat 1 to the solution sphere sooner than a higher initial inclination ultimately due to the differences between the satellite's initial inclinations. Also recall that the range of normalized time values is dependent on the orbital period, an integer value from 90 to 1440 minutes. Therefore, the range which represents the majority of the simulations, in Figure 6.2, of $\approx$0.99 to $\approx$1.01 represents +/- 0.9 to +/- 14.4 minutes depending on the non-maneuvering satellite's orbital period.

Figure 6.3 demonstrates that there is no specific correlation between only the maneuvering satellite's initial inclination and the required ΔV.

6.4.2 Results Based on Non-maneuvering Vehicle Inclination.

There is no specific impact on the normalized miss distance or required ΔV resulting from the non-maneuvering satellite's initial inclination. However for reference the plots are included in this chapter's Appendix as Figures 6.1 and 6.2.

Similarly to the maneuvering satellite results, Figure 6.4 also shows a slight upward trend in transfer time as the non-maneuvering satellite's initial inclination is increased.

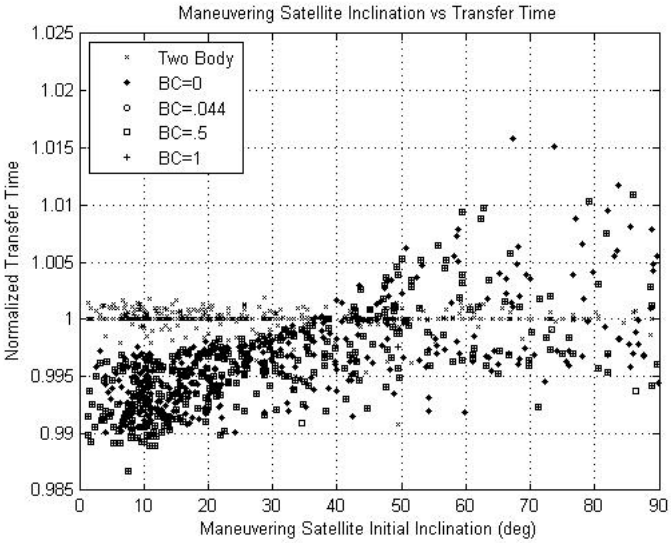

Figure 6.2: Maneuvering Satellite's Inclination vs. Normalized Transfer Time.

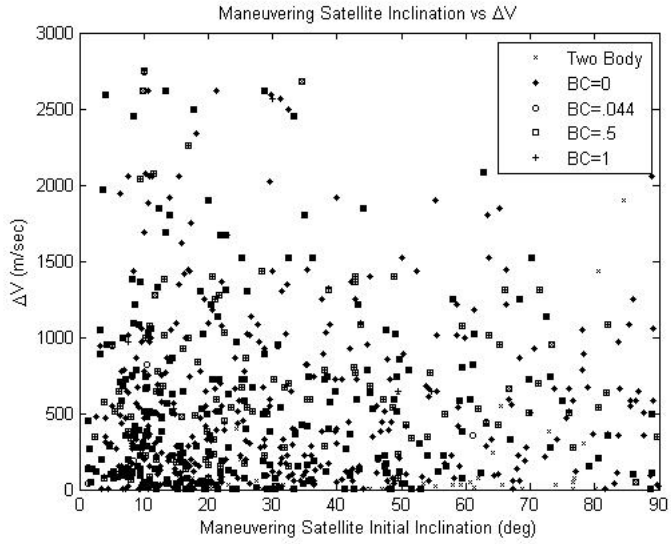

Figure 6.3: Maneuvering Satellite's Inclination vs. ΔV.

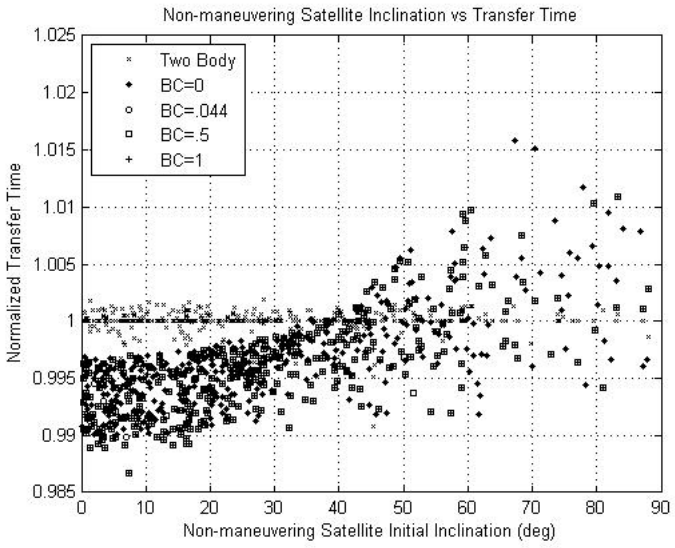

Figure 6.4: Non-maneuvering Satellite's Inclination vs. Normalized Transfer Time.

6.4.3 Results Based on Initial Maneuvering Vehicle Semi-major Axis.

Now considering the results for the semi-major axis, recall how the study was executed. The semi-major axis will only have certain values based on the random integer selection for the orbital period. Therefore, an orbital period ranging from 90 to 1440 minutes and a fixed initial altitude of 250 km yields semi-major axis values of 6652.56 km to 42241.1 km for the maneuvering satellite.

Figures 6.5 and 6.6 illustrate that varying the maneuvering satellite's initial semi-major axis does not impact the normalized miss distance or transfer time.

Much more interesting information can be gleaned from analyzing Figure 6.7. It is clear a pattern is trying to emerge from the information. However, at this point, based only on the initial semi-major axis of the maneuvering satellite, it can be seen that a larger range for ΔV exists with the lowest initial semi-major axis value, 6652.56 km. The range in this case is $\approx$0 to $\approx$2750 $\frac{m}{sec}$. The opposite is illustrated for an initial semi-major axis value

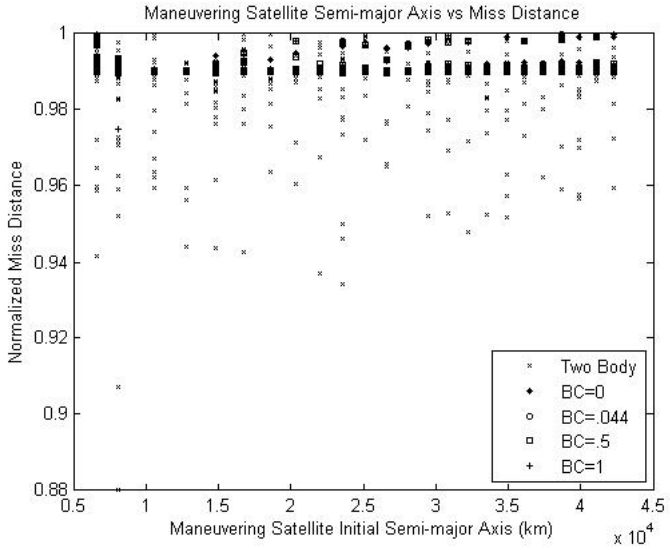

Figure 6.5: Maneuvering Satellite's Semi-major Axis vs. Normalized Miss Distance.

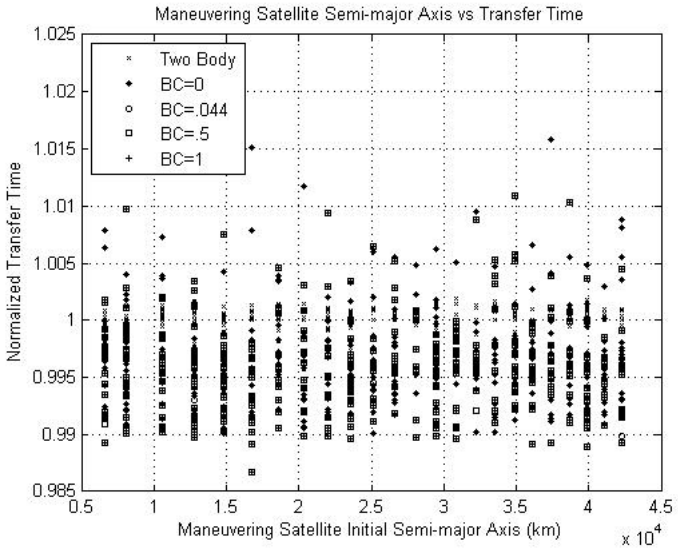

Figure 6.6: Maneuvering Satellite's Semi-major Axis vs. Normalized Transfer Time.

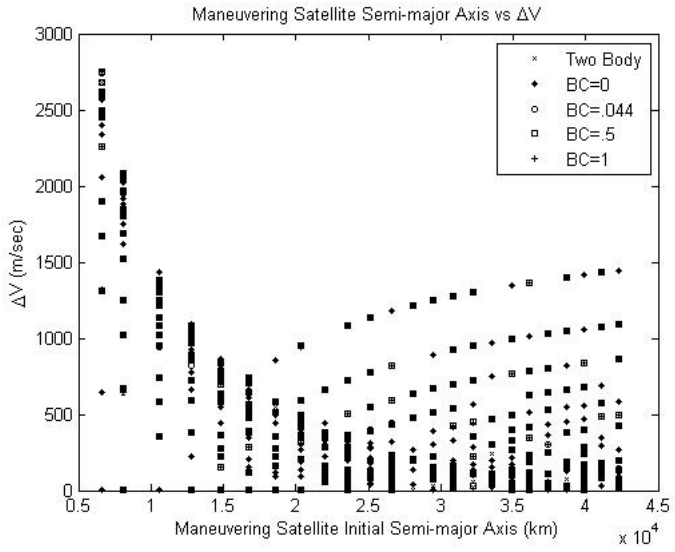

Figure 6.7: Maneuvering Satellite's Semi-major Axis vs. ΔV.

of 16763.39 km. The range in this case is only ≈0 to ≈800 $\frac{m}{sec}$. Keep in mind that these particular results are based solely on the randomness of the initial conditions. Meaning, that the specific values ultimately are random. They are provided to illustrate the value of the contribution of the dynamic TMN algorithm. These results again, appear to be independent of the dynamics model used or the ballistic coefficient.

6.4.4 Results Based on Initial Non-maneuvering Vehicle Semi-major Axis.

Similar to the maneuvering satellite's semi-major axis results, there are only fixed values for the non-maneuvering satellite's semi-major axis. Therefore, Satellite 2, also has a semi-major axis range of 6652.56 km to 42241.1 km, however, with an initial altitude of 150 km.

The impact on the normalized miss distance, based solely on the non-maneuvering satellite's initial semi-major axis, is negligible. For reference, Figure 6.3 in this chapter's Appendix illustrates this relationship.

Figure 6.8 shows that a tighter range of transfer times exists at the lower values of initial semi-major axis, with a larger range of times at the higher initial semi-major axis values. While this information is not directly applicable in a mission design, it can demonstrate that a generally lower non-maneuvering satellite initial semi-major axis leads to a higher probability for Satellite 1's maneuver solution to drive it to the sphere with a transfer time closer to Satellite 2's orbital period. However, these results by themselves are inconclusive due to the lack of visual knowledge of the maneuvering satellite's initial semi-major axis at these points.

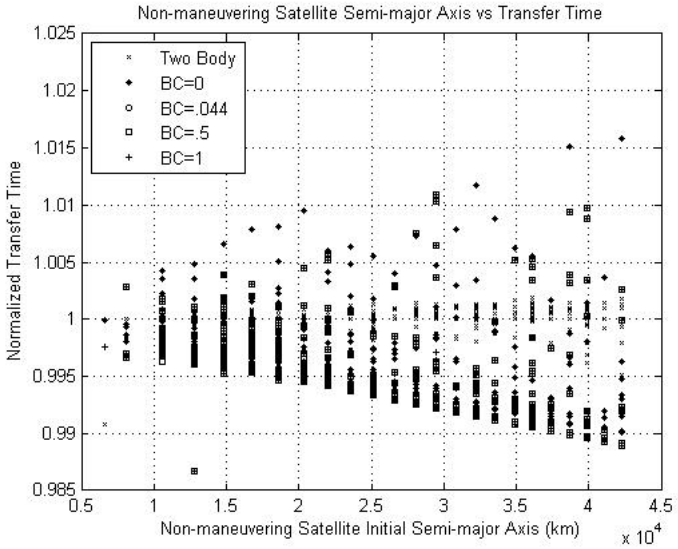

Figure 6.8: Non-maneuvering Satellite's Semi-major Axis vs. Normalized Transfer Time.

The results presented in Figure 6.9 begin to display more useful design information. It can be clearly seen that the lower the initial non-maneuvering satellite's initial semi-major axis, the lower the range of required ΔV. Specifically, the range at the lowest values for semi-major axis is from $\approx$0 to $\approx$650 $\frac{m}{sec}$, while the higher values of initial semi-major axis yield the largest range from $\approx$0 to $\approx$2750 $\frac{m}{sec}$. This makes sense considering the fixed initial

altitudes for both the maneuvering and non-maneuvering satellites. Meaning, the lower non-maneuvering satellite's semi-major axis, has a higher chance of requiring a lower ΔV. While interesting, these results are still not independent of the initial maneuvering satellite's semi-major axis.

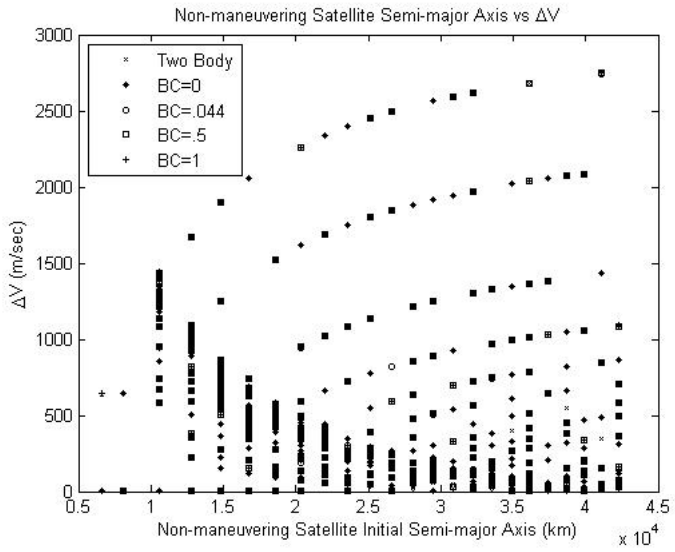

Figure 6.9: Non-maneuvering Satellite's Semi-major Axis vs. ΔV.

6.4.5 Results Based on Initial Semi-major Axis Ratio.

Since there were design implications gleaned from analyzing the individual impacts of the initial semi-major axes for both the maneuvering and non-maneuvering satellites, more information can be gained by comparing the values together. This is accomplished by determining the ratio between the non-maneuvering satellite's semi-major axis vs. the maneuvering satellite's semi-major axis.

Figure 6.10 shows the range of semi-major axis ratios and illustrates the majority of data points exist with a ratio less than 5.

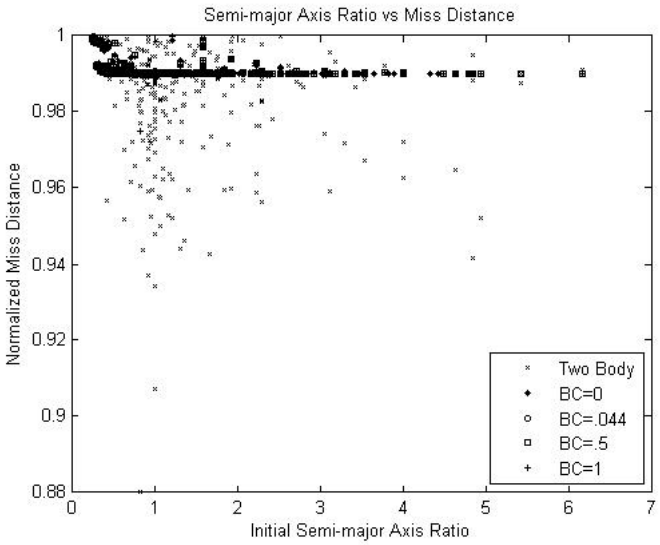

Figure 6.10: Satellites' Semi-major Axis Ratio vs. Normalized Miss Distance.

The results in Figure 6.11 illustrate that based on the relationship between the semi-major axes, the majority of transfers occurs within +/- 0.01, or 0.9 to 14.4 minutes, of the non-maneuvering satellite's orbital period.

Significant information can be gleaned from the semi-major axis ratio relationship versus the required ΔV. Figure 6.12 presents these results for the range of system dynamics and ballistic coefficients. Clearly, the lowest ΔV occurs when the size of Satellite 2's orbit is the same as Satellite 1's orbit, i.e. the ratio is equal to 1. It is more interesting, however, when the non-maneuvering satellite's semi-major axis is smaller than the maneuvering satellite's semi-major axis, making the ratio less than 1. The grouping of results in this range is very tight, leading to a very accurate model to then predict a ΔV for any provided values for Satellite 1 and Satellite 2's semi-major axes. For a non-maneuvering semi-major axis, to a maneuvering semi-major axis ratio range of 0.25 to 0.97, Eq.(6.19) provides a very accurate approximation of the required ΔV to solve this mission, regardless of system

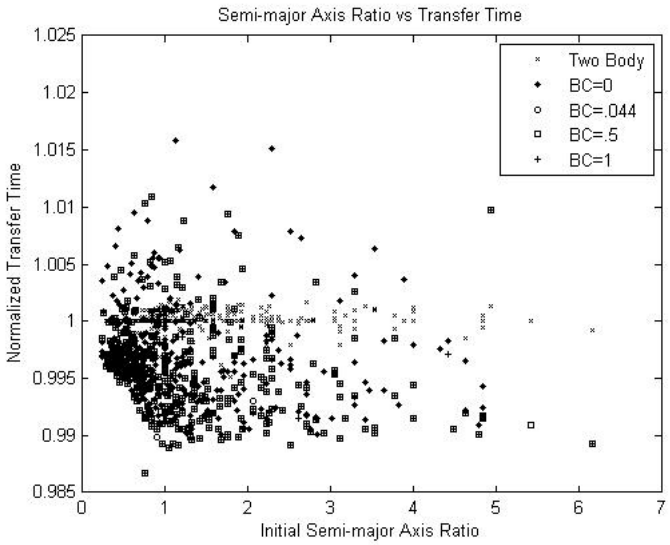

Figure 6.11: Satellites' Semi-major Axis Ratio vs. Normalized Transfer Time.

model and ballistic coefficient. ΔV is in $\frac{m}{sec}$ and a_R is $\frac{a_{Sat2}}{a_{Sat1}}$.

$$\Delta V = 1639 \times a_R^{-0.4745} - 1658 \tag{6.19}$$

While not nearly as accurate, Rough-Order-of-Magnitude (ROM) values for ratio values greater than 1 can be approximated based on the system model and ballistic coefficient. These values represent starting points for further evaluation during mission design. Following the template in Eq.(6.20), Table 6.1 summarizes the values for these ROM approximations. These approximations are valid for a ratio value of 1.03 to 6.5.

$$\Delta V = A \times a_R^B - C \tag{6.20}$$

In summary, Figure 6.13 is a plot of the approximations in Eqs. (6.19) and (6.20). For ratio values between 0.97 and 1.03, the ΔV is $\approx 0 \frac{m}{sec}$.

Valid solutions to complex nonlinear differential equations require excellent knowledge of the system's dynamics and initial conditions. Initiating the dynamic TMN algo-

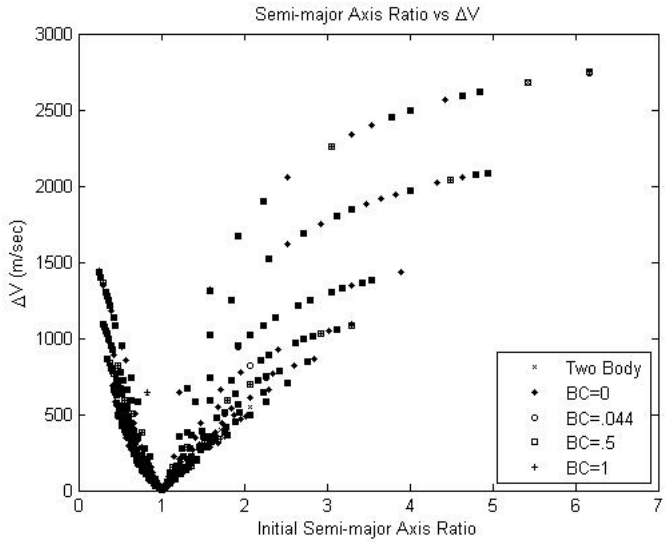

Figure 6.12: Actual Satellites' Semi-major Axis Ratio vs. ΔV.

Table 6.1: Coefficients for ΔV ROM Estimations for Semi-major Axis Ratio.

Dynamics	A	B	C
2-body	1979	0.5174	2015
J_2	1840	0.5367	1866
BC=0.044	2099	0.4792	2112
BC=0.5	1948	0.5079	1958
BC=1	1848	0.5253	1848

rithm is no exception. Specifically, the algorithm is much more efficient provided a valid input for the required ΔV. Previous to the development of the results in Figure 6.13, the initial guess at the required ΔV for the dynamic TMN algorithm followed five steps:

1. Calculate specific mechanical energy of the non-maneuvering satellite at the specified semi-major axis.
2. Calculate velocity magnitude, assuming 150 km starting altitude.
3. Calculate specific mechanical energy of the maneuvering satellite at the specified semi-major axis.
4. Calculate velocity magnitude, assuming 250 km starting altitude.
5. Calculate initial ΔV, $|\vec{V}_{SAT2}| - |\vec{V}_{SAT1}|$.

While the five step method is not extremely laborious, the relationships highlighted in Table 6.1 using Eq.(6.20) requires only one step and its accuracy is highlighted in Table 6.2. The TMN ΔV is the simulation result from the initial semi-major axes. The column marked 'Eq.(6.20) ΔV $\frac{m}{sec}$' are the results from said equation utilizing the values from Table 6.1. The, '5 Step ΔV $\frac{m}{sec}$', is calculated following the previously identified steps. The percent error columns are for the empirical results compared to the simulated results from the dynamic TMN differential correction algorithm.

The 'Better' column in Table 6.2 shows which method delivers a more accurate prediction to the actual results found through the TMN algorithm. Out of the eight examples, it is a draw, four and four, on which method is better, however a closer evaluation highlighted in Table 6.3 tells a different story.

Overall, as evidenced by the results in Table 6.3, the equation presented by Eq.(6.20) and the results in Table 6.1, provide a better estimate of the required ΔV to execute the prescribed mission.

Figure 6.13 provides a very good starting point for conducting mission design trade-offs. Ultimately, keep in mind that these results are possible due to the implementation of the dynamic TMN differential correction algorithm.

Table 6.2: Summary of Results for Semi-major Axis Ratio Initial ΔV Guess for TMN Algorithm Using 2-body System Dynamics

Ratio	TMN ΔV $\frac{m}{sec}$	Eq.(6.20) ΔV $\frac{m}{sec}$	% Error	5 Step ΔV $\frac{m}{sec}$	% Error	Better ΔV
0.303	1087.80	1230.7	13.1	990.73	8.9	5 Step
0.816	119.82	147.02	22.7	31.01	74.1	Eq.(6.20)
1.498	394.36	424.25	7.5	484.17	22.8	Eq.(6.20)
2.378	1132.90	1083.12	4.4	1222.9	7.9	Eq.(6.20)
3.302	1846.20	1656.65	10.3	1935.6	4.8	5 Step
4.642	2591.60	2364.24	8.8	2681.2	3.5	5 Step
5.429	2683.83	2734.32	1.9	2770.9	3.2	Eq.(6.20)
6.172	2745.40	3059.72	11.4	2833.3	3.2	5 Step

Table 6.3: Average % Error for Empirical Method.

Eq.(6.20) ΔV	5 Step ΔV
10.01%	16.05%

6.4.6 Results Based on Initial Inclination Ratio.

The following results are presented by defining the initial inclination ratio as the non-maneuvering satellite inclination versus the maneuvering satellite inclination. Therefore, an inclination ratio value less than one means that the non-maneuvering satellite is at a lower inclination than the maneuvering satellite and vice versa for a ratio value greater than one. Recall that the non-maneuvering satellite's inclination is selected first, following a random normal distribution according to Eq.(6.2). The maneuvering satellite's inclination

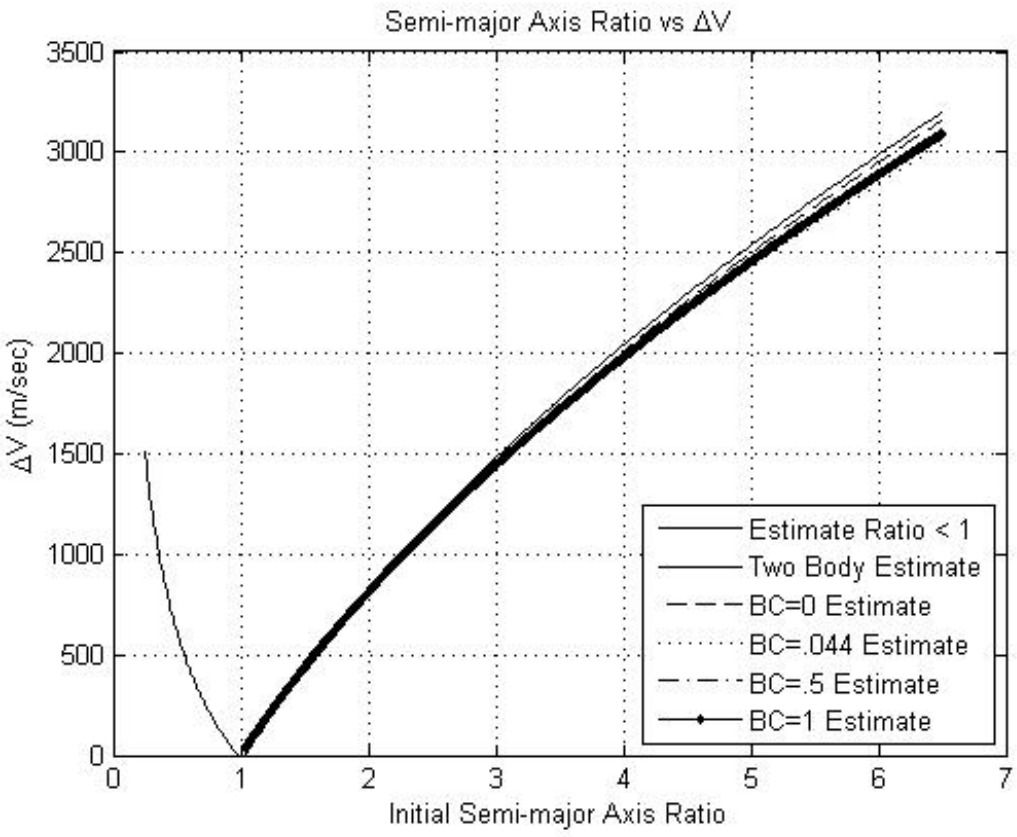

Figure 6.13: Estimated Satellites' Semi-major Axis Ratio vs. ΔV.

is determined as a result of the conversion to COEs of Satellite 1's initial position and velocity vectors following from the algorithm development in Section 6.3.

Figure 6.14 highlights that all of the simulations still achieve the desired sphere radius of 100 km, with a 1% margin for 101 km regardless of inclination ratio. The majority of simulations result in an inclination ratio less than six.

No additional significant design considerations can be gleaned from the results illustrated in Figure 6.15, except that the largest range of transfer time values occurs at

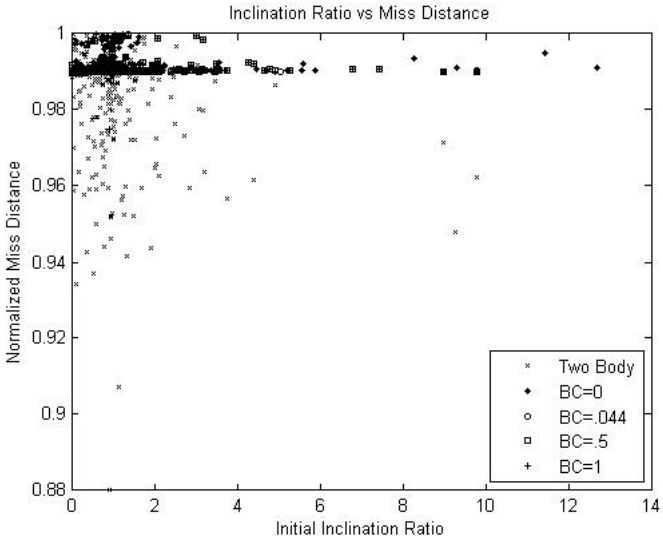

Figure 6.14: Satellites' Inclination Ratio vs. Normalized Miss Distance.

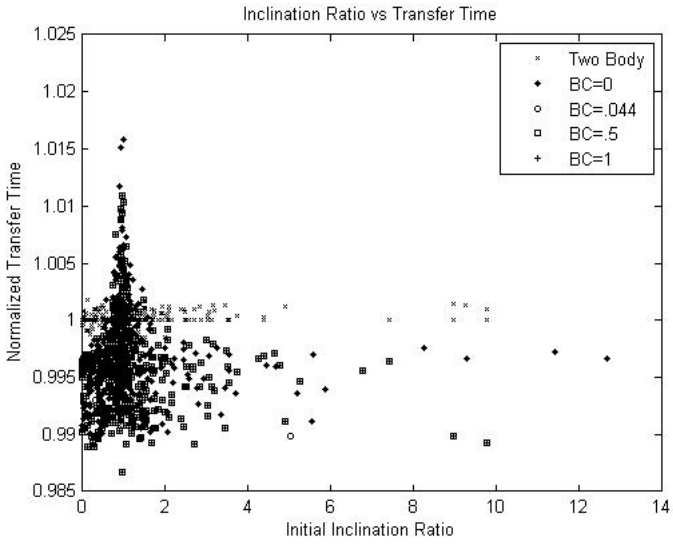

Figure 6.15: Satellites' Inclination Ratio vs. Normalized Transfer Time.

a ratio value ≈1. Based solely on the ratio value at this point does not provide helpful orbit design information.

Figure 6.16 illustrates that overall, the lower values for inclination ratio, yield the higher required ΔVs with the largest range of values, even though no specific pattern emerges.

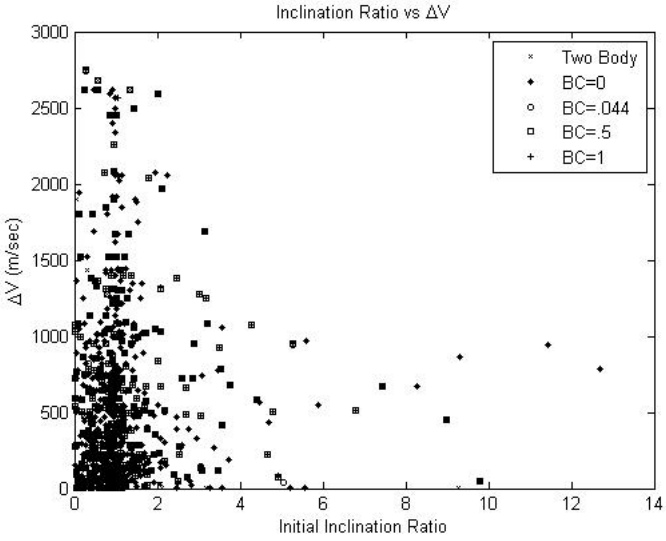

Figure 6.16: Satellites' Inclination Ratio vs. ΔV.

6.4.7 Results Based on Initial Semi-major Axis and Initial Inclination Ratio.

The preceding analysis has demonstrated that the most significant impact on the required ΔV to complete the mission has been based ultimately on the ratio between the non-maneuvering satellite's semi-major axis and the maneuvering satellite's semi-major axis. However, [3, 10, 25–27, 45] all cite the perturbation modeling as a function of inclination. Note, these sources also cite eccentricity, but how this problem was framed, with a fixed initial altitude, impacts due to eccentricity are the same as the semi-major axis impacts. Therefore, the most complete analysis of mission design impacts can be

attributed to the relationship between Satellite 1 and Satellite 2's semi-major axes and inclinations. This information has already been presented independently, but is better illustrated combined in Figures 6.17 through 6.19.

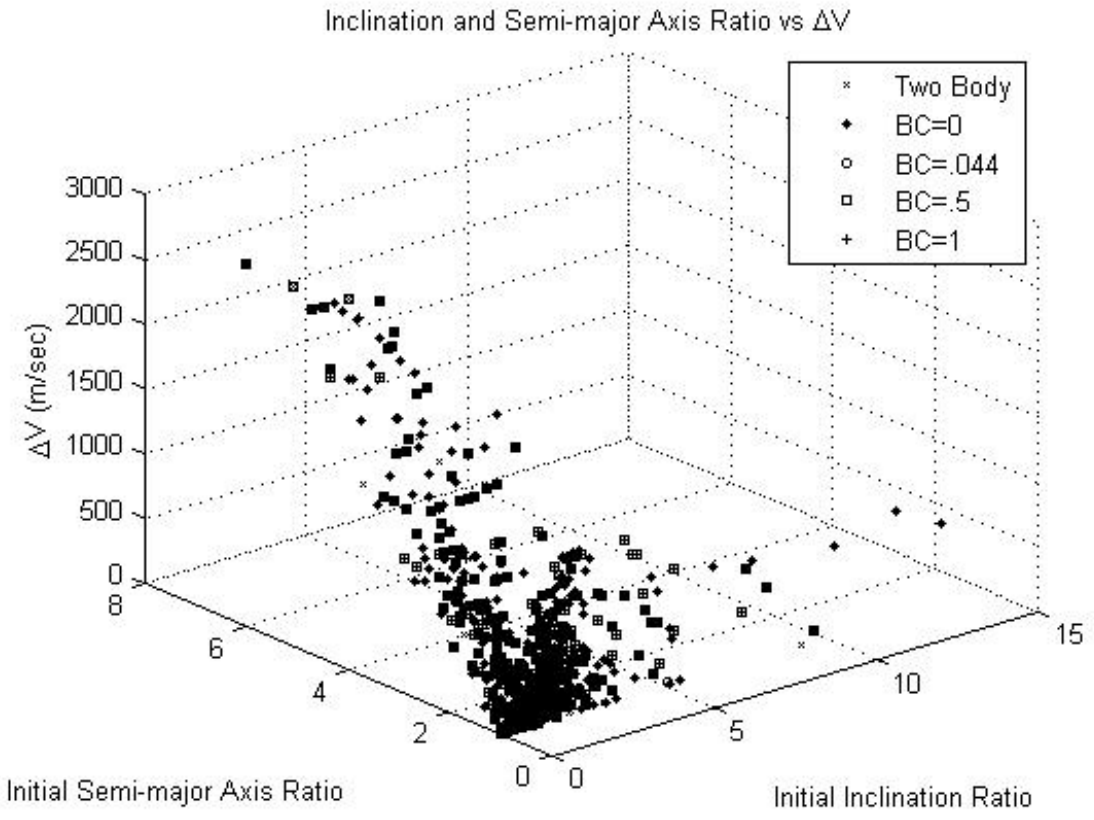

Figure 6.17: Satellites' Inclination Ratio vs. Semi-major Axis Ratio vs. ΔV.

Figure 6.17 represents a 3-Dimensional view illustrating the impacts of the orbit design parameters of the semi-major axis, as well as the inclination. Presenting the information in this form ultimately allows the user to define four variables and picture their impact on the resulting required ΔV. The four variables are the maneuvering satellite's semi-major axis and inclination, as well as the non-maneuvering satellite's semi-major axis and inclination.

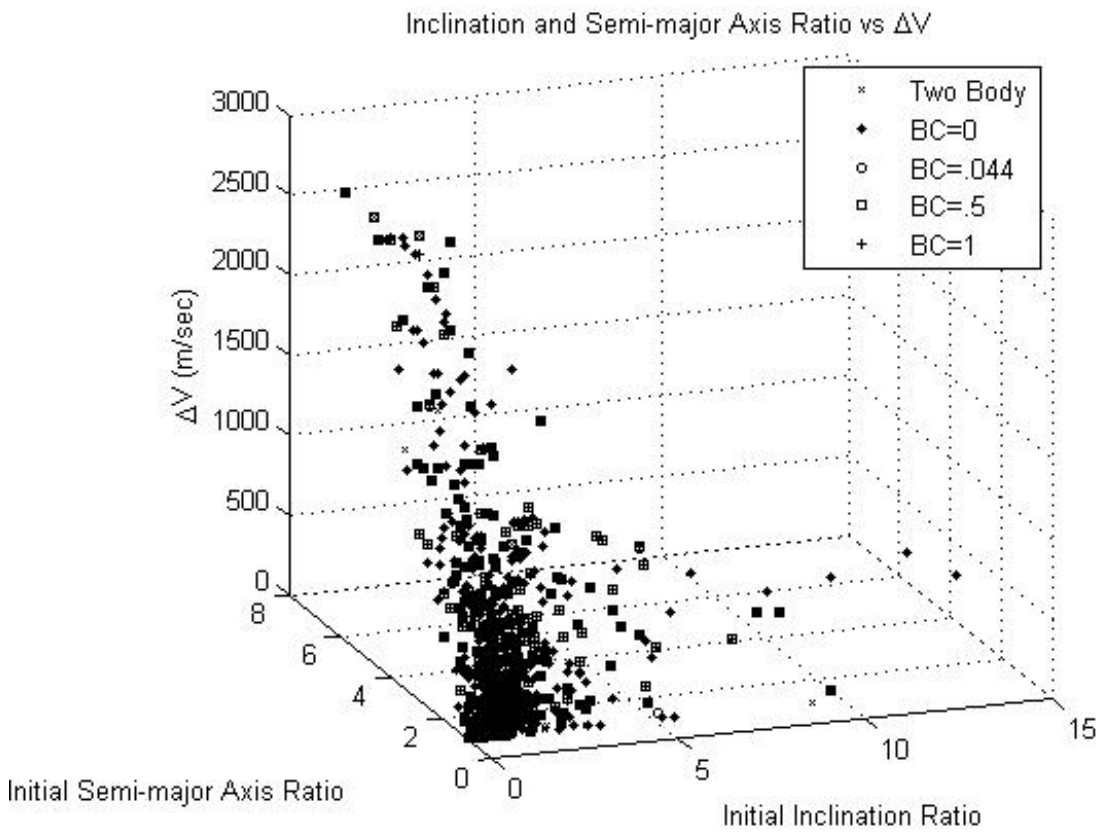

Figure 6.18: Satellites' Inclination Ratio vs. Semi-major Axis Ratio vs. ΔV.

A view that is partial towards the inclination ratio's impact on overall ΔV is presented in Figure 6.18. A biased view towards the semi-major axis ratio impact is provided in Figure 6.19.

6.4.8 Results Based on Combined Initial Vehicle Semi-major Axes.

Ultimately, the most significant ΔV mission design consideration can be gleaned from a comparison of the actual semi-major axis values for the maneuvering and non-maneuvering satellites. Figure 6.20 provides that information. It follows intuition that the higher required ΔV values occur when the largest difference exists between the size of the non-maneuvering satellite's orbit compared to the size of the maneuvering satellite's orbit.

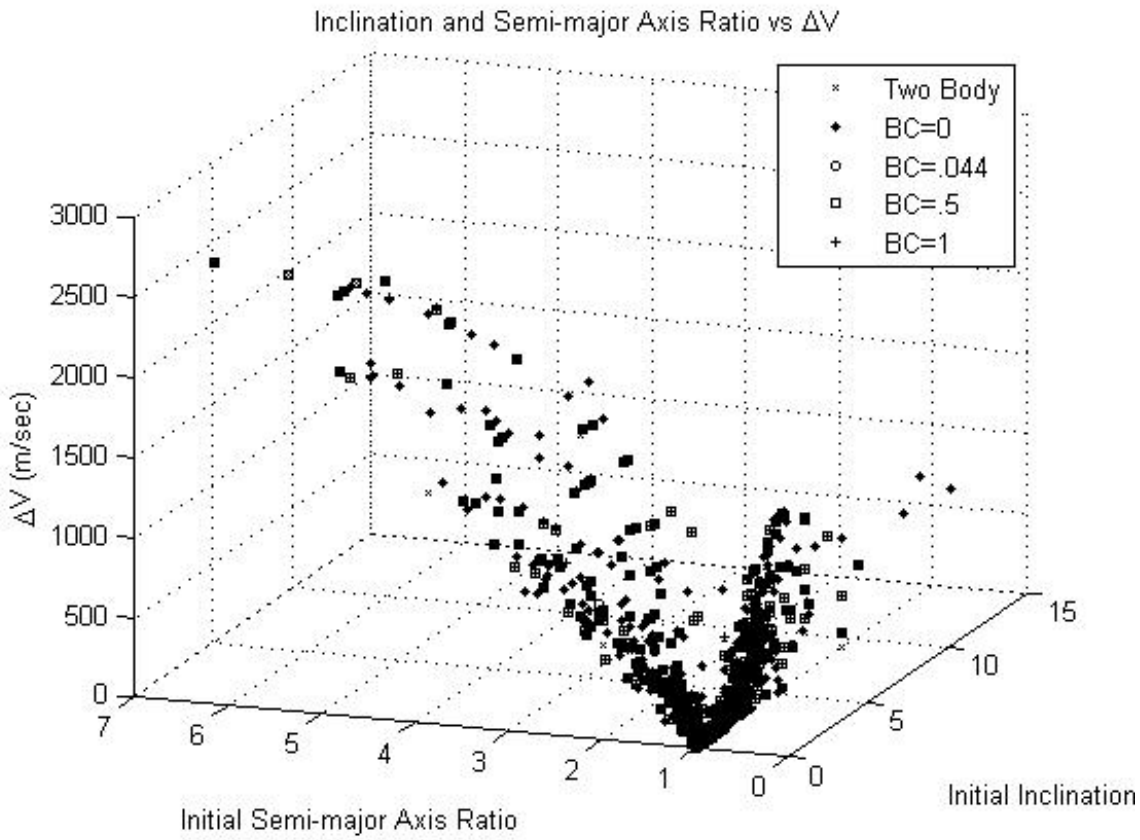

Figure 6.19: Satellites' Inclination Ratio vs. Semi-major Axis Ratio vs. ΔV.

Figure 6.20 also highlights the line titled '1/1 Ratio Line' as the series of points in the solution space where the values of both, Satellite 1 and Satellite 2's semi-major axes are equivalent, resulting in the minimum fuel expenditure.

6.5 Chapter Summary

Overall, this chapter presented the Dynamic T-Matrix Navigation algorithm to deliver an impulsive maneuver to place a satellite within a sphere of user defined radius, centered around a non-maneuvering satellite within a constrained time. The methodology and results were presented for a non-maneuvering satellite, beginning at a perigee altitude of 150 km

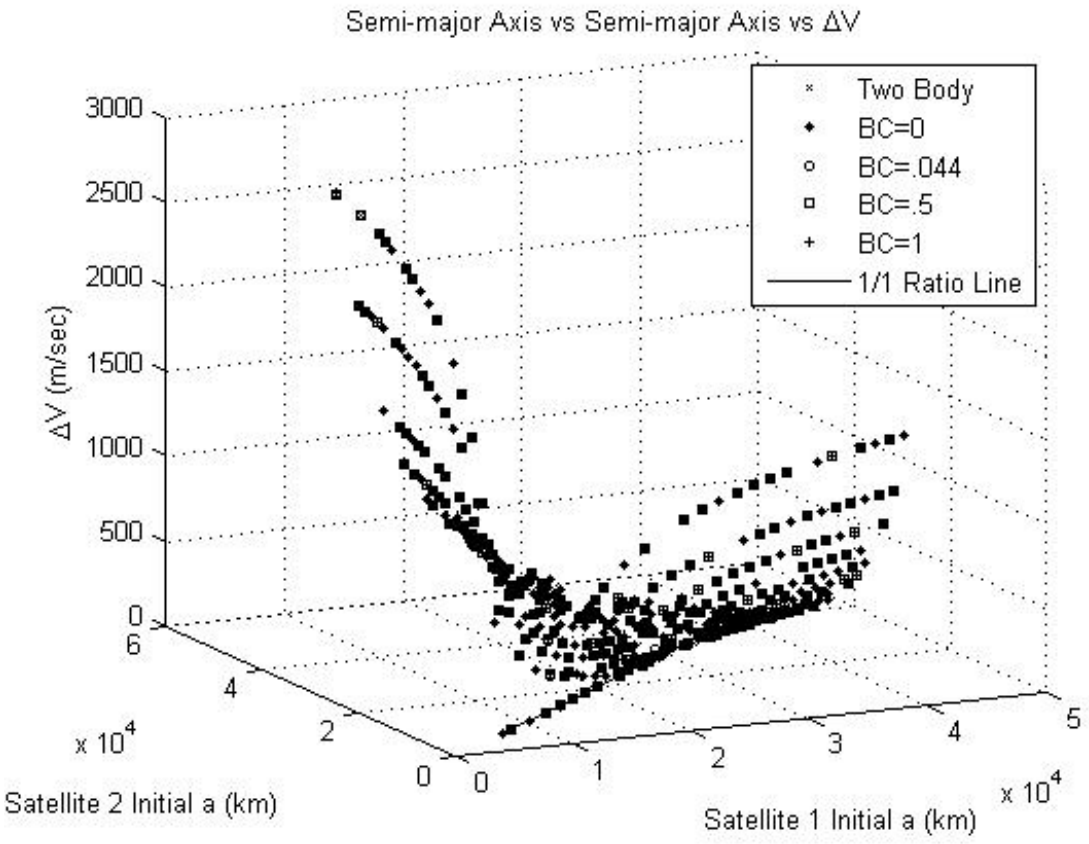

Figure 6.20: Satellite 1 Semi-major Axis vs. Satellite 2 Semi-major Axis vs. ΔV.

and a maneuvering satellite, beginning along the same unit position vector at an altitude of 250 km. The sphere radius was 100 km with a 1% margin allowing for a solution when the maneuvering satellite returns to within 101 km of the non-maneuvering satellite at a time +/- 10% of the non-maneuvering satellite's orbital period. The presented results were constrained to prograde orbits. In the end, the focus of the results was based on the success of the modified Dynamic T-Matrix Navigation algorithm, while demonstrating unique information about this problem. Several orbit design considerations were studied, including the selection of the satellites' initial inclinations, semi-major axes, as well as the ballistic coefficients. The capstone of the study is the ability for the user to empirically

predict the necessary ΔV for a desired combination of semi-major axes. Ultimately, the successful modification to the original T-Matrix Navigation algorithm further demonstrates the algorithm's flexibility, especially while laying the groundwork for a theater based responsive relay satellite coverage or responsive cooperative collection capability.

6.6 Chapter Appendix

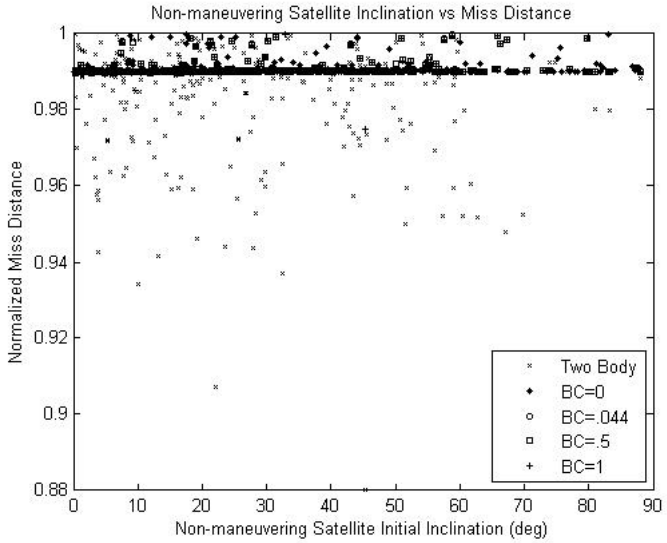

Figure 6.1: Non-maneuvering Satellite's Inclination vs. Normalized Miss Distance.

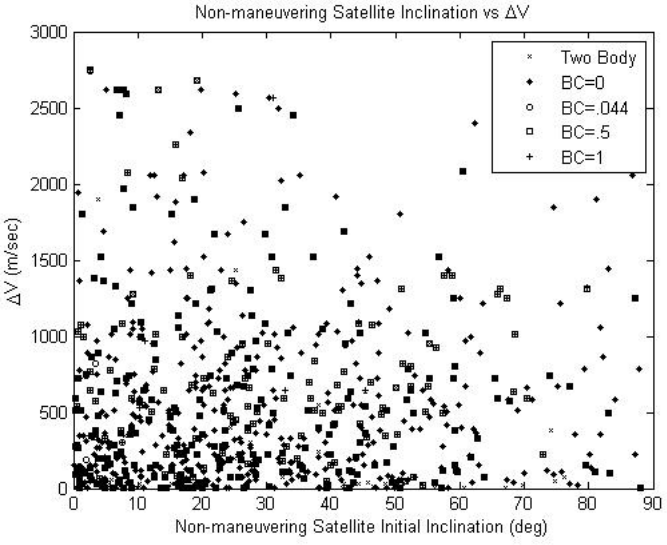

Figure 6.2: Non-maneuvering Satellite's Inclination vs. ΔV.

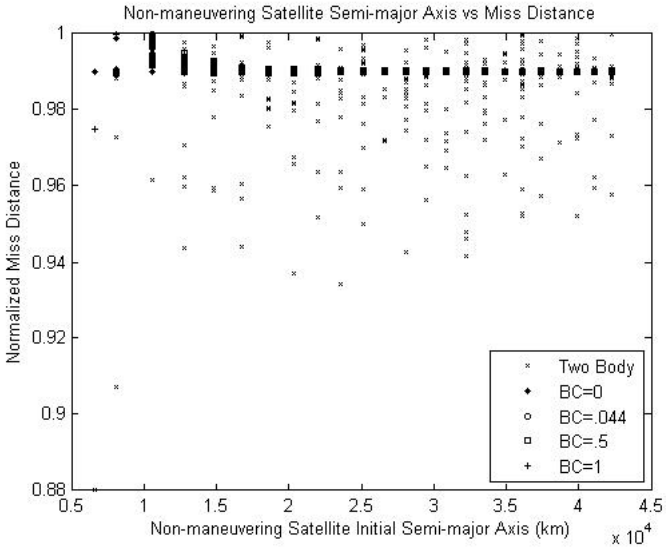

Figure 6.3: Non-maneuvering Satellite's Semi-major Axis vs. Normalized Miss Distance.

VII. Navigation Solution to Maneuver a Spacecraft Relative to Spheres Centered on Multiple Cooperative Satellites

7.1 Introduction

This chapter will continue to expand on the development of the Dynamic T-Matrix Navigation algorithm presented in the previous chapter, leveraging the T-Matrix Navigation algorithm. Specifically, this chapter will present the algorithm for varying the geometric solution between the maneuvering satellite relative to multiple non-maneuvering satellites.

7.2 Problem Statement

The purpose of this study is to demonstrate the ability for the Dynamic TMN algorithm to deliver an impulsive maneuver to a satellite to place it within the overlapping 3-Dimensional space of multiple spheres, with a user-defined radius, centered around multiple non-maneuvering satellites within a constrained time. Figure 7.1, illustrates the problem.

Specifically, the proceeding methodology and results are based on multiple non-maneuvering satellites beginning at a perigee altitude of 274.41 km and a maneuvering satellite beginning along the same unit position vector at an altitude of 1406.4 km. The radius within this study is 1500 km with a 5% margin, allowing for a viable solution to be achieved when the maneuvering satellite returns to within 1575 km of the non-maneuvering satellites. Further, it is assumed throughout that the non-maneuvering satellites must return to their original inertial positions in space relative to the Earth +/- 10% before the maneuvering satellite can successfully declare a solution within the overlapping spheres. This study only focuses on prograde orbits, therefore inclinations range between 0° and 90°. The focus of the results is based on the success of the Dynamic TMN algorithm, while demonstrating unique information about this problem. Throughout the development and

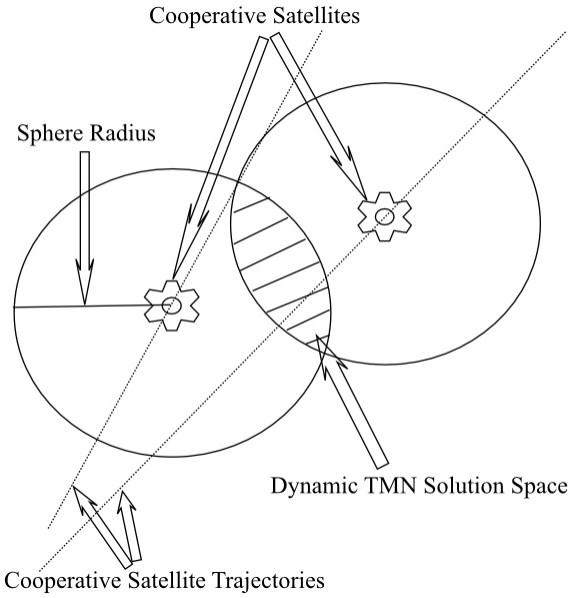

Figure 7.1: Illustration of Problem Statement.

results, the terms ‘Satellite 1’, ‘Sat 1’ and ‘maneuvering satellite’ are one in the same, while ‘cooperative satellites’ and ‘non-maneuvering satellites’ are both the same. A summary of

the optimal control problem solved in this chapter is in Eq.(7.1)

$$
\begin{aligned}
&\text{Minimize: } \mathrm{J} = \int_{t_0}^{t_f} |u(t)|\, dt \\
&\text{Subject to:} \\
&\quad \dot{\vec{R}}, \dot{\vec{V}} \\
&\quad u(t) = \Delta V \delta_0(t - t_0) \\
&\quad t_f \in [0.9\mathrm{LCM}(\mathrm{P}_{COOP_1}, \ldots, \mathrm{P}_{COOP_N}), 1.1\mathrm{LCM}(\mathrm{P}_{COOP_1}, \ldots, \mathrm{P}_{COOP_N})] \\
&\text{Initial Conditions:} \\
&\quad \vec{R}_1(t_0) = \vec{R}_{1_{t_0}} \\
&\quad \vec{V}_1(t_0) = \vec{V}_{1_{t_0}} \\
&\quad \vec{R}_{COOP_1}(t_0) = \vec{R}_{COOP_{1t_0}} \\
&\quad \vec{V}_{COOP_1}(t_0) = \vec{V}_{COOP_{1t_0}} \\
&\quad \vdots \\
&\quad \vec{R}_{COOP_N}(t_0) = \vec{R}_{COOP_{Nt_0}} \\
&\quad \vec{V}_{COOP_N}(t_0) = \vec{V}_{COOP_{Nt_0}} \\
&\quad t_0 = 0 \\
&\text{Terminal Conditions:} \\
&\quad \vec{R}_1(t_f) \in \mathbf{B}(\vec{R}_{COOP_1}(t_f), \eta) \bigcap \ldots \bigcap \mathbf{B}(\vec{R}_{COOP_N}(t_f), \eta)
\end{aligned}
\tag{7.1}
$$

A summary of the step-by-step procedure to solve the problem is shown. The unique contributions in this chapter are highlighted by **boldface**.

1. **Establish initial Classic Orbital Elements (COEs) for satellites.**
2. Convert COEs to initial position, $\vec{R}_0$, and velocity, $\vec{V}_0$ vectors.
3. Establish scaling parameters and scaling matrix, **S**[4].
4. Establish weight matrix, **Q**[4].
5. **Determine initial guess for required fuel, ΔV, and transfer time, *t*.**

6. **Integrate Equations of Motion (EOM) for cooperative satellites for duration of *t*.**

7. **Calculate final state, $\vec{R}, \vec{V}$, for cooperative satellites at *t*.**

8. Apply ΔV to maneuvering satellite to yield $\vec{V}_{0+}$.

9. Integrate EOM for maneuvering satellite for duration of t.

10. Calculate final state $\vec{R}, \vec{V}$, for maneuvering satellite at t.

11. **Calculate spherical separation distance between maneuvering satellite and cooperative satellites.**

12. Integrate maneuvering satellite's State Transition Matrix (STM) using Equations of Variation (EOV) for duration of t.

13. Declare ϕ matrix as upper right 3x3 portion of STM[4].

14. **Calculate velocity difference vector, $\vec{V}_{DIFF}$, between maneuvering satellite and cooperative satellites velocity vectors.**

15. Calculate ΔV for maneuvering satellite: $\Delta V = \vec{V}_{0+} - \vec{V}_0$.

16. **Compile error vector, $\bar{e}$, as the spherical separation distance between the maneuvering satellite and each cooperative satellite and components of ΔV.**

17. **Build $\tilde{T}$ matrix:** $\begin{bmatrix} \phi_1\phi_2...\phi_N & \vec{V}_{Diff} \\ \mathbf{I} & \mathbf{0} \end{bmatrix}$.

18. Calculate **T** matrix: $\mathbf{T} = \mathbf{S}^{-1}\tilde{T}$[4].

19. **Declare convergence criteria when all control contributions to ΔV are 0.**

20. Determine ∂u: $\partial u = -(\mathbf{T}'\mathbf{Q}^{-1}\mathbf{T})^{-1}\mathbf{T}'\mathbf{Q}^{-1}\bar{e}$[4].

21. Check ∂u components versus convergence criteria.

22. If convergence criteria are satisfied then the algorithm is complete.

    - Final ΔV = ΔV from error vector, $\bar{e}$
    - Final transfer time = current t

23. **Add $\sum\Delta$V from ∂u to $\vec{V}_{0+}$ yielding new ΔV.**

24. Add Δt from ∂u to transfer time, t, for updated time.

25. Return to #6.

7.3 Establishing the Algorithm

In order to implement the Dynamic TMN algorithm, the initial orbits are needed. Depending on how the problem is framed there can be a variable number of non-maneuvering satellites within the scenario. This number will simply be referred to as 'N' cooperative satellites. Regardless of the number of cooperative satellites, there will only be one maneuvering satellite (Sat 1). The maneuvering satellite will be the satellite to which the ΔV is applied. For this particular problem, all satellites will begin along the same unit position vector. Specifically, the 'N' cooperative satellites will begin at the same point, therefore the position vector is identical for each. They will begin at an altitude of 274.41 km. The maneuvering satellite, along the same initial unit vector is at 1406.4 km altitude. An additional assumption for establishing this problem places all satellites along the $\hat{X}$ axis at the starting time, providing for the initial position vectors in Eqs.(7.2) and (7.3).

$$\vec{R}_{Sat1} = |\vec{R}_{Sat1}| \begin{bmatrix} 1 \\ 0 \\ 0 \end{bmatrix} km \tag{7.2}$$

$$\vec{R}_N = |\vec{R}_N| \begin{bmatrix} 1 \\ 0 \\ 0 \end{bmatrix} km \tag{7.3}$$

The initial positions for the cooperative satellites are fixed, as are their orbital periods. Specifically for this chapter, the fixed orbital periods are different for each cooperative satellite, therefore resulting in differing final positions after each orbital period. However, the lowest value for the orbital period is 90 minutes, resulting in a circular orbit at 274.41 km altitude. Considering 90 minutes as the fastest orbital period, this ensures that the initial position vectors for the cooperative satellites are at perigee. Because the cooperative satellites are beginning along the $\hat{X}$ unit vector, the Right Ascension of the Ascending Node (RAAN) and the argument of perigee are 0°. Also, provided a fixed initial position and orbital period, the semi-major axis and eccentricity are determined. That simply means that the initial COEs are nearly complete.

To complete the initial conditions for the cooperative satellites, the only remaining COE, inclination, is determined following a normal distribution according to Eq.(7.4) [70]. Each cooperative satellite has a random value for inclination between 0° and 90°. A straightforward conversion from COEs is now possible for the cooperative satellites.

$$i = Mod\left(Abs(NormalDistribution) \times \frac{\pi}{4}, \frac{\pi}{2}\right) \tag{7.4}$$

Once the initial COEs were determined for the cooperative satellites, the original position and velocity vectors needed to be determined for the maneuvering satellite, Satellite 1. Provided the fixed altitude, Satellite 1 is in a circular orbit, therefore, semi-major axis and eccentricity are known. Understanding the initial position vector for Satellite 1, at the fixed altitude of 1406.4 km in Eq.(7.2) leads to a RAAN and argument of perigee of 0°. The inclination for Satellite 1 is also randomized according to Eq.(7.4) and has a range of 0° and 90°. Converting to $\vec{R}$ and $\vec{V}$ is possible with the COEs for the maneuvering satellite.

In order for the algorithm to proceed, the future state, both the position and velocity vectors need to be determined for the maneuvering satellite. Once the position vector in the future is determined for Sat 1, that same time is used to determine the position vectors for the cooperative satellites, and an error vector is calculated. The error vector for this study is displayed in Eq.(7.5). Because the error is in vector form, it is a function of the number of relationships between the maneuvering satellite and the 'N' cooperative satellites. Therefore, the error vector in Eq.(7.5) is representative of any number of cooperative satellites and has dimensions, $(3N + 3) \times 1$.

$$\bar{e}^T = \begin{bmatrix} \Lambda_{1_X} & \Lambda_{1_Y} & \Lambda_{1_Z} & \Lambda_{2_X} & \Lambda_{2_Y} & \Lambda_{2_Z} & \cdots & \Lambda_{N_X} & \Lambda_{N_Y} & \Lambda_{N_Z} & \Delta V_X & \Delta V_Y & \Delta V_Z \end{bmatrix} \quad (7.5)$$

The vector $\vec{\Lambda}$ represents a relationship between the maneuvering and non-maneuvering satellites, according to the radius of the user-defined sphere. The components of the $\vec{\Lambda}$ vector relationships are described in Eqs.(7.6) through (7.8).

$$\Lambda_{N_X} = R_{SAT1_X} - \left(\frac{R_{SAT1_X} - R_{N_X}}{|\vec{R}_{SAT1} - \vec{R}_N|} * \eta + R_{N_X} \right) \quad (7.6)$$

$$\Lambda_{N_Y} = R_{SAT1_Y} - \left(\frac{R_{SAT1_Y} - R_{N_Y}}{|\vec{R}_{SAT1} - \vec{R}_N|} * \eta + R_{N_Y} \right) \quad (7.7)$$

$$\Lambda_{N_Z} = R_{SAT1_Z} - \left(\frac{R_{SAT1_Z} - R_{N_Z}}{|\vec{R}_{SAT1} - \vec{R}_N|} * \eta + R_{N_Z} \right) \quad (7.8)$$

Eqs.(7.6) through (7.8) display the elements of the unit vector of the component by component miss distance vector between Sat 1 and the cooperative satellites. The unit vector components are multiplied by η, the radius of the sphere, and added to the component of the non-maneuvering satellites. Interestingly, the solution is dynamic. Meaning that the solution to the sphere edge changes with each iteration because the solution itself is based on the position of the maneuvering and each of the non-maneuvering satellites.

It is necessary to identify that the integrated equations for the solution will follow two separate models. The first is for the maneuvering satellite and the second is for the cooperative satellites. The maneuvering satellite will be subject to EOM including both J_2

and an air drag model. While, the cooperative satellites will simply follow 2-body EOM. The cooperative satellites will be simulating active orbit control needing to return over to the same inertial position in space.

The development and derivation of the maneuvering satellite's State Transition Matrix follows from Section 4.3.

Another component necessary in the algorithm is the relationship between the satellites' final velocity vectors. Identifying this vector and combining this with ϕ, a form of the $\tilde{T}$ matrix is determined and shown in equation (7.9). Noticing that the $\tilde{T}$ matrix is adjustable based on the number of cooperative satellites yields the dimensions, $(3N + 3) \times (3N + 1)$.

$$\tilde{T} = \begin{bmatrix} \phi_1\phi_2...\phi_N & \vec{V}_{Diff} \\ \mathbf{I} & \mathbf{0} \end{bmatrix} \tag{7.9}$$

$$\vec{V}_{Diff} = \sum \vec{V}_{SAT1} - \vec{V}_N \tag{7.10}$$

The ϕ_N, terms come directly from Eq.(4.7). It is required to insert an additional ϕ for each of the 'N' cooperative satellites. Eq.(7.10) represents the sum of the differences between the maneuvering satellite's final velocity vector and each cooperative satellite and has dimensions, 3×1. Therefore, the **I** matrix requires dimensions $(3N\times3N)$ and **0** requires dimesions $(3N \times 1)$. The final **T** matrix is derived from scaling parameters combined with $\tilde{T}$.

The final components of the Dynamic TMN setup is the identification of a weight matrix, **Q** and a scale matrix, **S**. The weight matrix allows for the user to shift convergence focus from final position to applied ΔV. In order to maintain a balanced focus on both, minimizing miss distance and fuel used, an identity matrix, **I**, should be used. For this study, **Q**, is simply a $(3N + 3) \times (3N + 3)$ **I** matrix. The scale matrix, **S**, is utilized to allow faster convergence within the algorithm. For this study, **S** is a constant $(3N + 3) \times (3N + 3)$ matrix. **S** is defined in (7.11) while **T** is calculated from $\tilde{T}$ and **S** in (7.12). **S** is an adjustable

matrix to allow for better scaling of the nonlinear system of equations.

$$\mathbf{S} = 0.1 \times \mathbf{I} \tag{7.11}$$

$$\mathbf{T} = \mathbf{S}^{-1}\tilde{T} \tag{7.12}$$

Ultimately, combining all of this information, the variation of the control vector, $\vec{u}$, can be calculated. The variation of $\vec{u}$ is the core of the Dynamic TMN algorithm. Once the maneuvering satellite is within the overlapping space of the 'N' cooperative satellite spheres, the minimum fuel solution is declared for the model within the constrained time. It is important to note that based on units and matrix dimensions, $\vec{u}$, will have $(3N + 1) \times 1$ components. Specifically, the components of $\vec{u}$ are shown below in Eq.(7.13).

$$\vec{u}^T = \begin{bmatrix} \Delta V_{1_X} & \Delta V_{1_Y} & \Delta V_{1_Z} & \Delta V_{2_X} & \Delta V_{2_Y} & \Delta V_{2_Z} & \cdots & \Delta V_{N_X} & \Delta V_{N_Y} & \Delta V_{N_Z} & \Delta t \end{bmatrix} \tag{7.13}$$

The ΔV terms are the changes in the initial impulsive maneuver applied to Sat 1 and the Δt term is the change in transfer time during each iteration. Summing the results for each component after each iteration, and then dividing by 'N', yields the total ΔV for the impulsive manuever. Combining the sum of the Δt's with the initial transfer time results in the final transfer time for the optimum ΔV. However, the Dynamic TMN algorithm is designed so that once the maneuvering satellite is within a sphere, the contribution to the solution from that cooperative satellite is zeroed out for that iteration. If the next iteration's solution forces the maneuvering satellite outside of the sphere, it is reconsidered towards the solution again. For example, Eqs.(7.5) and (7.13) have been updated in Eqs.(7.14) and (7.15), considering that the maneuvering satellite is within the sphere of cooperative satellite 2.

$$\bar{e}^T = \begin{bmatrix} \Lambda_{1_X} & \Lambda_{1_Y} & \Lambda_{1_Z} & 0 & 0 & 0 & \cdots & \Lambda_{N_X} & \Lambda_{N_Y} & \Lambda_{N_Z} & \Delta V_X & \Delta V_Y & \Delta V_Z \end{bmatrix} \tag{7.14}$$

The $\tilde{T}$ and therefore the **T** matrices are not adjusted as derived in Eqs.(7.9) and (7.12) because the final velocity difference towards solution is still viable since it will never equal

$\vec{0}$ for a non-rendezvous mission. Considering this change, the resulting $\vec{u}$ is demonstrated in Eq.(7.15) for a satisfying solution for cooperative satellite 2.

$$\vec{u}^T = \begin{bmatrix} \Delta V_{1_X} & \Delta V_{1_Y} & \Delta V_{1_Z} & 0 & 0 & 0 & \cdots & \Delta V_{N_X} & \Delta V_{N_Y} & \Delta V_{N_Z} & \Delta t \end{bmatrix} \tag{7.15}$$

Ultimately, once the net ΔV contribution is 0 in any given iteration, the algorithm declares a solution. The algorithm iterates on Eq.(7.16) [4]. Every iteration includes all of the previous steps for determining **T**. The weight matrix is **Q** and $\bar{e}$ is the error vector from Eq.(7.5).

$$\partial u = -(\mathbf{T}'\mathbf{Q}^{-1}\mathbf{T})^{-1}\mathbf{T}'\mathbf{Q}^{-1}\bar{e} \tag{7.16}$$

7.4 Background for Results

Throughout the results of this study, the range, η, utilized was 1500 km. The margin for error was 5%, allowing for a maximum sphere radius of 1575 km, or 0.25 DU. Provided the sphere radius, solving for the impulsive tangential phasing maneuver required utilizing 2-body dynamics, which is a basic astrodynamics exercise. Fortunately, that is why this type of problem is used to demonstrate the versatility of the Dynamic TMN differential correction algorithm. Additionally, the dynamic algorithm is able to provide the required impulsive maneuver to be applied to Sat 1, to meet the specified sphere radius utilizing complex system dynamics including the effects of J_2 and air drag.

It is also of note that this study focused only on prograde orbits, therefore inclination, i, is between 0° and 90° for both the maneuvering and non-maneuvering satellites. Additionally, the following results are illustrated for one single value of ballistic coefficient for the maneuvering satellite. That value is 0.044, which is a reasonable value from Reference [48]. The cooperative satellites, however will follow only 2-body dynamics in satisfaction of the assumption that their mission requirements are to maintain the same inertial position in space relative to the Earth. It is also important to keep in mind that the goal of this study is to deliver the maneuvering satellite within the overlapping region of the

spheres of the non-maneuvering satellites at the time that the non-maneuvering satellites are nearly at their beginning positions, as soon as possible. Due to the differing orbital periods of the cooperative satellites, this time is the time that is the Least Common Multiple (LCM) of the orbital periods.

Overall, there are two viable solutions for solving this problem within the provided time constraints of being near the same inertial position in space relative to the Earth. One is the solution that executes a maneuver to allow Satellite 1 to become in phase with the combination of cooperative satellites' orbital periods. The second, is to execute a maneuver only to offset the perturbations in order for Satellite 1 to be in the correct inertial position in space relative to the Earth at the time when the cooperative satellites' orbital periods line up. Either solution requires the LCM for the orbital periods, however the phasing solution only requires the LCM for the cooperative satellites, while the non-phasing maneuver solution requires the LCM of the cooperative satellites with Satellite 1.

In order to facilitate the best comparison, the orbital periods used throughout the results allow for the same time solution for both the phasing and non-phasing scenarios. Specifically, the transfer time is the LCM for the scenario with and without the orbital period of the maneuvering satellite included. That orbital period is 108,000 seconds, or 30 hours, or 133.86 TU.

Demonstrating the effectiveness of the algorithm throughout these results is paramount. Some interesting characteristics of the problem design are also realized. These results are presented for 3 separate scenarios. All scenarios have one maneuvering satellite. The first is a scenario with two cooperative satellites, for a total of three satellites. The second is a scenario with three cooperative satellites, while the third has four cooperative satellites to make four and five total satellites respectively. Because of the identical LCM for the orbital periods, Tables 7.1 through 7.3 displays the initial conditions for the satellites.

Table 7.1: Initial Orbits for Maneuvering and Cooperative Satellites 3 Total Sats Scenario.

	Man. Sat	Coop. Sat 1	Coop. Sat 2
Semi-major Axis, a (DU)	1.264	1.043	3.695
Eccentricity, e	0	0	0.718
Period (TU)	8.924	6.693	44.620

Table 7.2: Initial Orbits for Maneuvering and Cooperative Satellites 4 Total Sats Scenario.

	Man. Sat	Coop. Sat 1	Coop. Sat 2	Coop. Sat 3
a (DU)	1.264	1.043	1.264	1.466
e	0	0	0.175	0.289
Period (TU)	8.924	6.693	8.924	11.155

7.5 Results and Discussion with Phasing Maneuver

Recall that the phasing maneuver results highlight the maneuver required to deliver the maneuvering satellite on a trajectory that has an orbital period in phase with

Table 7.3: Initial Orbits for Maneuvering and Cooperative Satellites 5 Total Sats Scenario.

	Man. Sat	Coop. Sat 1	Coop. Sat 2	Coop. Sat 3	Coop. Sat 4
a (DU)	1.264	1.043	1.264	1.466	1.657
e	0	0	0.175	0.289	0.370
Period (TU)	8.924	6.693	8.924	11.155	13.386

cooperative satellites' orbital periods. The period is 108,000 seconds or 30 hours. The phasing maneuver was analyzed for the maneuvering satellite to cooperative satellite miss distance, transfer time, and required ΔV. These three quantities were evaluated versus the maneuvering satellite's initial inclination, the cooperative satellite's inclination, the ratio of the cooperative satellites' semi-major axis versus the maneuvering satellite's semi-major axis and the ratio of the cooperative satellites' inclination versus Satellite 1's inclination. Unfortunately, the majority of the analysis was inconclusive. Figures 7.14 through 7.23 in this chapter's Appendix, provide the analysis for the maneuvering satellite inclination, cooperative satellite inclination and semi-major axis ratio versus the miss distance, transfer time and required ΔV.

Significant orbit design information was learned from the Dynamic TMN algorithm's results for the initial satellite inclination ratio analysis. The inclination ratio is defined as the average cooperative satellite inclination divided by the maneuvering satellite inclination.

To begin, Figure 7.2 illustrates the range of values between the maneuvering satellite's initial inclination and the average cooperative satellites' initial inclination. A good random range in this plot is what is expected and what is displayed.

The actual range of inclination ratio values is from $\approx$0 to $\approx$41. Over 93% of the Dynamic TMN algorithm's solutions have an inclination ratio less than 2.5. For illustrative purposes the following figures are only displayed from 0 to 2.5 to show the emerging patterns.

Figure 7.3 shows the beginning of a pattern with the expected normalized miss distance and the ratio of the initial inclinations of all of the satellites within the scenario. The normalized average miss distance is the average distance of the difference between the maneuvering satellite and each of the cooperative satellites. Keep in mind that the maximum sphere radius was 1575 km with a 5% margin, therefore the '1' value represents 1575 km.

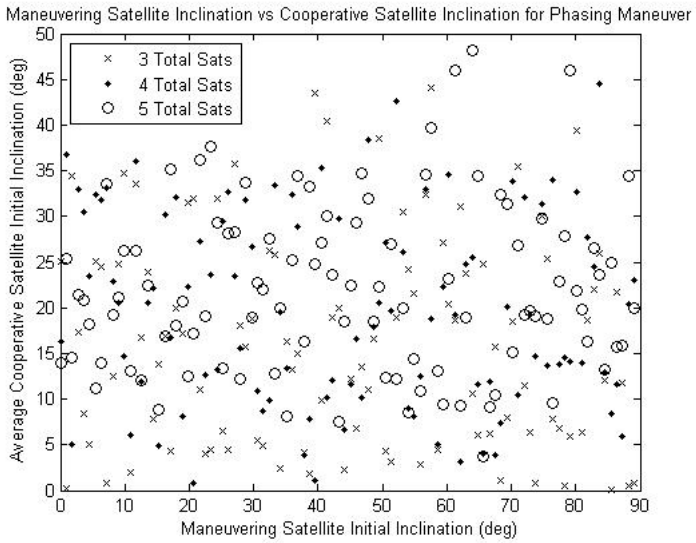

Figure 7.2: Maneuvering Satellite Inclination vs. Average Cooperative Satellites' Inclination.

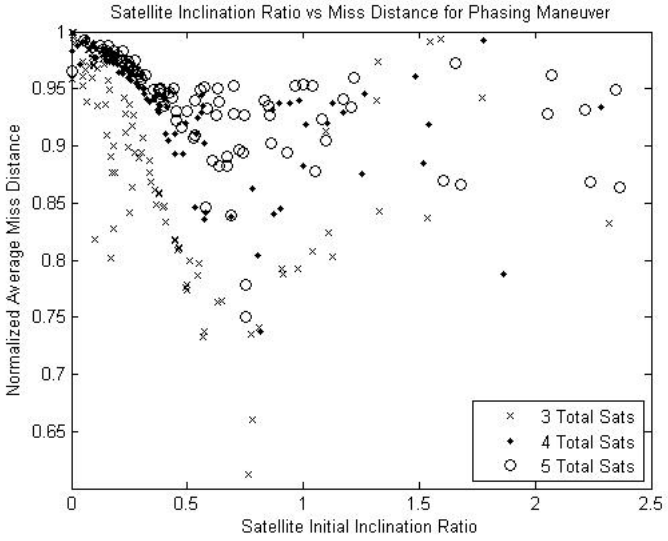

Figure 7.3: Satellites' Initial Inclination Ratio vs. Normalized Miss Distance.

Figure 7.4 represents the normalized ΔV required to send the maneuvering vehicle within the overlapping spheres of the cooperative satellites. The ΔV is normalized by the transfer time in TUs.

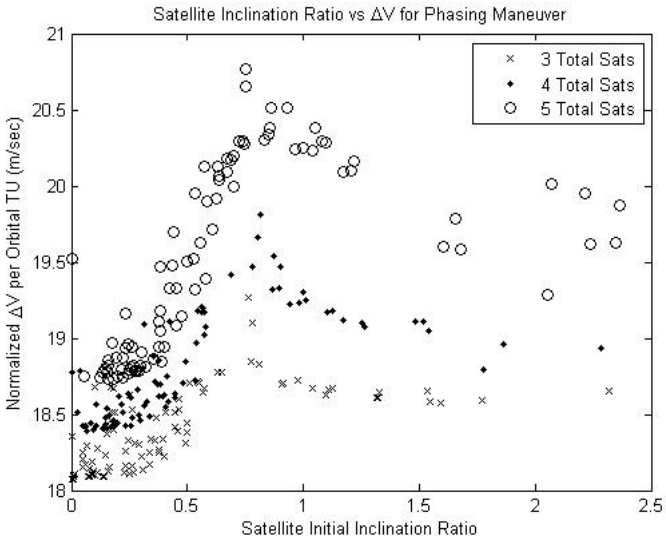

Figure 7.4: Satellites' Initial Inclination Ratio vs. Normalized ΔV.

These results, based on the inclination ratio, have all presented emerging patterns. Polynomial expressions were derived to estimate the behavior of any given inclination ratio from 0 to 2.5 with reasonable accuracy.

Eq.(7.17) shows the a polynomial approximation model for predicting the expected normalized miss distance provided an inclination ratio, i_R. The coefficients for the approximation model are in Table 7.4 for each of the 3, 4, and 5 satellite scenarios.

$$Miss = Ai_R^7 + Bi_R^6 + Ci_R^5 + Di_R^4 + Ei_R^3 + Fi_R^2 + Gi_R + H \tag{7.17}$$

Provided the coefficients for the normalized miss distance, Figure 7.5 shows the results for inclination ratios from ≈0 to 2.5. While the results are not as good as simulated results,

Table 7.4: Coefficients for Empirical Solution for Normalized Miss Distance.

Scenario	A	B	C	D	E	F	G	H
3 Total Sats	-0.1386	1.177	-3.631	4.794	-2.325	0.2704	-0.351	0.9866
4 Total Sats	0	-0.1325	1.094	-3.363	4.689	-2.807	0.4479	0.9669
5 Total Sats	0	-0.08954	0.7439	-2.32	3.311	-2.053	0.3511	0.9686

they are a ROM approximation of the system output. Tables 7.6 through 7.11 provide more detailed illustration of the values of the analytical solutions.

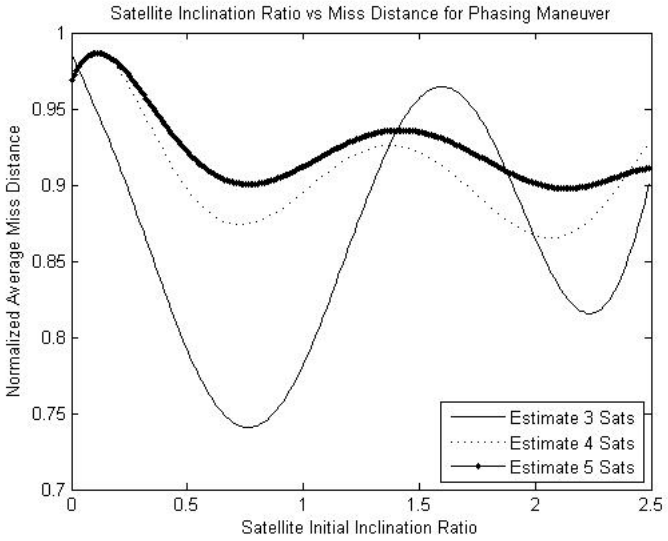

Figure 7.5: Satellites' Initial Inclination Ratio vs. Analytical Normalized Miss Distance.

Eq.(7.18) is presented as the polynomial expression for the required ΔV based on the inclination ratio. Table 7.5 highlights the coefficients necessary to accurately estimate the

normalized ΔV for each scenario.

$$\Delta V = Ai_R^5 + Bi_R^4 + Ci_R^3 + Di_R^2 + Ei_R + F \tag{7.18}$$

Table 7.5: Coefficients for Empirical Solution for Normalized ΔV.

Scenario	A	B	C	D	E	F
3 Total Sats	0	-0.01224	0.1724	-0.7858	1.245	18.09
4 Total Sats	-0.001438	0.003057	0.1526	-1.011	1.838	18.24
5 Total Sats	-0.006143	0.03691	0.2417	-2.08	3.874	18.15

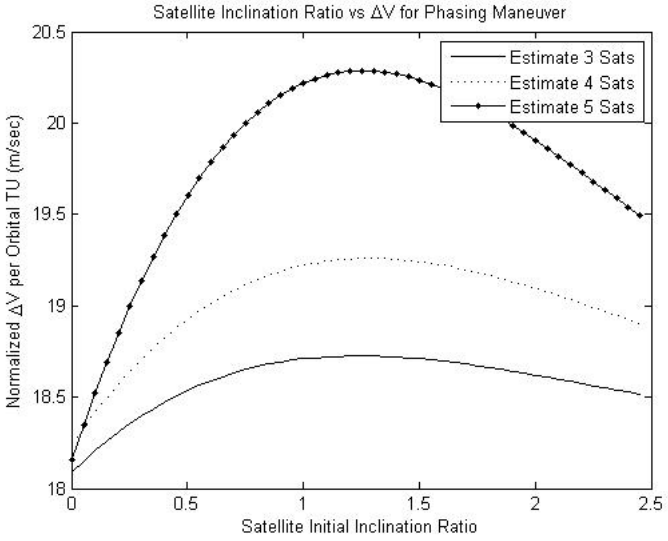

Figure 7.6: Satellites' Initial Inclination Ratio vs. Analytical Normalized ΔV.

The overall accuracy of the required ΔV polynomial approximation model is also highlighted in Tables 7.6 through 7.11.

Table 7.6: Empirical vs. Dynamic TMN Results for 3 Satellite Scenario.

Ratio Value	Actual Miss	Estimate Miss	Actual ΔV	Estimate ΔV
0.0500	0.9740	0.9695	18.152	18.1503
0.1419	0.9717	0.9373	18.0936	18.2513
0.2640	0.9178	0.8890	18.1604	18.3670
0.4630	0.8110	0.8053	18.5984	18.5145
1.1108	0.8245	0.8236	18.6598	18.7210
2.3211	0.8316	0.8251	18.6564	18.5469

Table 7.7: % Error for Empirical vs. Dynamic TMN Results for 3 Satellite Scenario.

Ratio Value	Miss %	Miss Value (km)	ΔV %	ΔV Value $\frac{m}{sec}$
0.0500	0.4657	7.3346	0.0093	0.2266
0.1419	3.5362	55.6949	0.8717	21.1139
0.2640	3.1359	49.3897	1.1378	27.6590
0.4630	0.7028	11.0695	0.4509	11.2265
1.1108	0.1045	1.6467	0.3281	8.1950
2.3211	0.7807	12.2961	0.5872	14.6643

Within Tables 7.6 to 7.11, the actual and estimated values are the normalized values presented throughout the figures. It is very promising to note that the largest percentage of error of all the simulations is 5.2593% in the 4 satellite scenario for miss distance. The 5.2593% is just slightly higher than the the 5% margin of error allowed for the miss distance. Overall, this highlights that the polynomial approximation solutions and the

Table 7.8: Empirical vs. Dynamic TMN Results for 4 Satellite Scenario.

Ratio Value	Actual Miss	Estimate Miss	Actual ΔV	Estimate ΔV
0.0511	0.9911	0.9831	18.4280	18.3313
0.1468	0.9763	0.9855	18.4811	18.4885
0.2632	0.9633	0.9610	18.4743	18.6565
0.4462	0.9104	0.9094	18.634	18.8725
1.1059	0.9201	0.9083	19.1695	19.2448
2.2848	0.9338	0.8847	18.9346	18.9756

Table 7.9: % Error for Empirical vs. Dynamic TMN Results for 4 Satellite Scenario.

Ratio Value	Miss %	Miss Value (km)	ΔV %	ΔV Value $\frac{m}{sec}$
0.0511	0.8111	12.7749	0.5247	12.944
0.1468	0.9429	14.8508	0.0401	0.9926
0.2632	0.2359	3.7149	0.9863	24.3921
0.4462	0.1048	1.6511	1.2798	31.9234
1.1059	1.2863	20.2588	0.3926	10.0752
2.2848	5.2593	82.8335	0.2166	5.4904

coefficients presented do a very good job at providing a ROM for the miss distance and required ΔV, to deliver a maneuvering satellite within the overlapping spheres of multiple non-maneuvering satellites.

Table 7.10: Empirical vs. Dynamic TMN Results for 5 Satellite Scenario.

Ratio Value	Actual Miss	Estimate Miss	Actual ΔV	Estimate ΔV
0.0564	0.9926	0.9824	18.7469	18.3619
0.1487	0.9824	0.9852	18.7994	18.6809
0.2636	0.9656	0.9689	18.9387	19.0313
0.4740	0.9162	0.9260	19.146	19.5464
1.0954	0.9047	0.9200	20.2815	20.2589
2.3461	0.9497	0.9049	19.6273	19.5928

Table 7.11: % Error for Empirical vs.Dynamic TMN Results for 5 Satellite Scenario.

Ratio Value	Miss %	Miss Value (km)	ΔV %	ΔV Value $\frac{m}{sec}$
0.0564	1.0233	16.1173	2.0536	51.5334
0.1487	0.2869	4.5189	0.6304	15.8646
0.2636	0.3374	5.3138	0.4887	12.3895
0.4740	1.0743	16.921	2.0913	53.5985
1.0954	1.6871	26.5711	0.1113	3.0223
2.3461	4.7176	74.3023	0.1755	4.6121

7.6 Results and Discussion without Phasing Maneuver

The solution without the phasing maneuver, highlights the maneuver required to overcome perturbations and ultimately deliver the maneuvering satellite on a trajectory that has an orbital period very similar to its initial orbital period. The following scenario is similarly constrained to deliver the maneuvering satellite within the overlapping spheres

of the non-maneuvering satellites within 108000 seconds or 30 hours. The 'phase-less' maneuver results are presented for miss distance, transfer time and required ΔV versus the maneuvering satellite's initial inclination, the cooperative satellite's inclination, the ratio of the cooperative satellites' semi-major axis versus the maneuvering satellite's semi-major axis, and the ratio of the cooperative satellites' inclination versus Satellite 1's inclination.

Similar to the phasing maneuver analysis, only certain information is significant for the 'phase-less' maneuver. Results for the average cooperative satellite inclination, initial semi-major axis ratio, and initial inclination ratio can be found in this chapter's Appendix, Figures 7.24 through 7.34. However, considerable mission design information is gleaned from the initial maneuvering satellite's orbital inclination. The results illustrated in Figures 7.7 through 7.13 highlight these impacts.

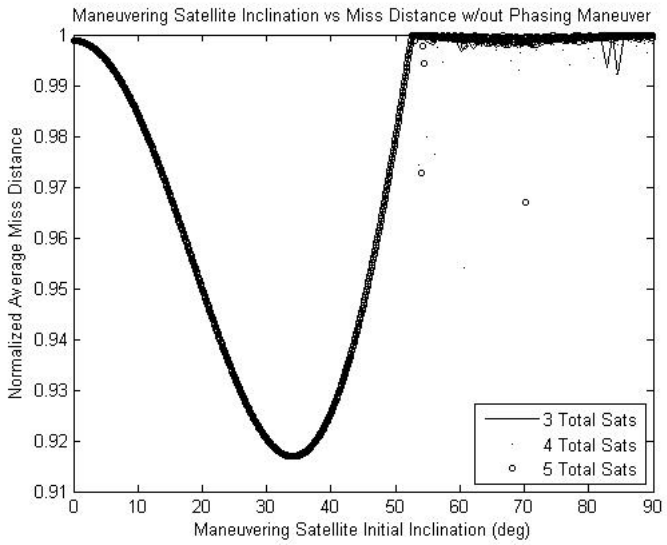

Figure 7.7: Maneuvering Satellite's Inclination vs. Normalized Miss Distance.

Clearly there is a relationship between the maneuvering satellite's initial inclination and the Dynamic TMN algorithm's miss distance between the maneuvering satellite and

the overlapping spheres of the non-maneuvering satellites. This is evidenced in Figure 7.7. There is little difference between the results achieved with the 3, 4 or 5 satellite scenarios. Between 0° and ≈52.5° there is a clear pattern and any inclination greater than 52.5° yields the maximum value of the range, 1575 km. Figures 7.8 and 7.9 show the lower inclinations, $0° - 52.5°$, and the higher inclinations, $52.5° - 90°$. respectively.

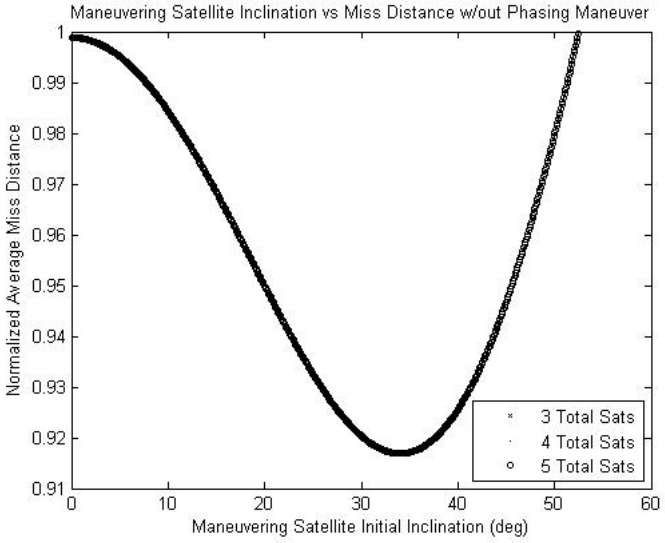

Figure 7.8: Maneuvering Satellite's Inclination vs. Normalized Miss Distance.

Provided the obvious relationship, an analytical solution for estimating the miss distance based on the maneuvering satellite's initial inclination is possible. Eq. (7.19) provides the polynomial approximation model that represents a very good representation of the Dynamic TMN algorithm's results. The inclination, i, is simply represented in Eq. (7.19).

$$Miss(i) = -1.628x10^{-9}i^5 + 1.817x10^{-7}i^4 - 2.666x10^{-6}i^3 - 1.224x10^{-4}i^2 - 1.365x10^{-4}i + 9.99x10^{-1} \quad (7.19)$$

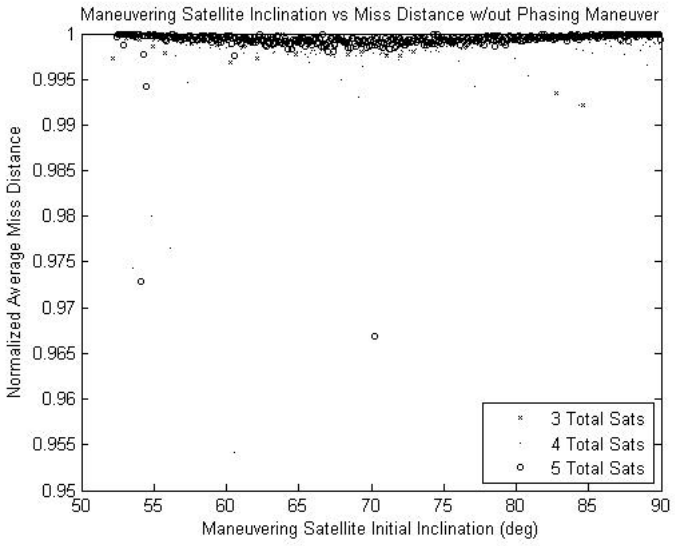

Figure 7.9: Maneuvering Satellite's Inclination vs. Normalized Miss Distance.

The results for the analytical representation are summarized in Tables 7.12 through 7.14. Clearly, the empirical model is an excellent fit for the expected value for normalized miss distance regardless of the 3, 4 or 5 satellite scenario.

Tables 7.12 through 7.14 display the miss distance as the normalized value unless noted otherwise. Figure 7.10 represents the full range of polynomial approximation solutions between 0° and ≈52.5°. For initial inclinations greater than 52.5°, a normalized value of 1 is used.

More orbit design information can be gleaned from the results of the Dynamic TMN algorithm. The maneuvering satellite's inclination versus the required ΔV is portrayed in Figure 7.11. Figure 7.11 also displays an impact at ≈52.5°. Table 7.15 shows the minimum values and the associated inclinations. Keep in mind, however, even at 48°, the actual required ΔV is still only 1.205 $\frac{m}{sec}$.

Table 7.12: Empirical vs. Dynamic TMN Results for 3 Satellite Scenario.

Inclination (deg)	Actual Miss	Estimate Miss	Miss % Error	Miss Value (km)
0	0.9989	0.9990	0.0100	0.1577
10	0.9846	0.9643	2.0618	32.4726
30	0.9209	0.9204	0.0543	0.8551
45	0.9468	0.9468	0.0000	0.0000
60	0.9978	1	0.2205	3.4726
75	0.9998	1	0.0200	0.3151
90	0.9999	1	0.0100	0.1575

Table 7.13: Empirical vs. Dynamic TMN Results for 4 Satellite Scenario.

Inclination (deg)	Actual Miss	Estimate Miss	Miss % Error	Miss Value (km)
0	0.9989	0.9990	0.0100	0.1577
10	0.9844	0.9643	2.0419	32.1592
30	0.9204	0.9204	0.0000	0.0000
45	0.9468	0.9468	0.0000	0.0000
60	0.9985	1	0.1502	2.3660
75	0.9990	1	0.1001	1.5766
90	0.9983	1	0.1703	2.6821

Figure 7.12 illustrates the Dynamic TMN algorithm's solutions provided maneuvering satellite inclinations greater than 54°.

Table 7.14: Empirical vs. Dynamic TMN Results for 5 Satellite Scenario.

Inclination (deg)	Actual Miss	Estimate Miss	Miss % Error	Miss Value (km)
0	0.9989	0.9990	0.0100	0.1577
10	0.9844	0.9643	2.0419	32.1592
30	0.9204	0.9204	0.0000	0.0000
45	0.9468	0.9468	0.0000	0.0000
60	0.9997	1	0.0300	0.4726
75	0.9994	1	0.0600	0.9456
90	0.9994	1	0.0600	0.9456

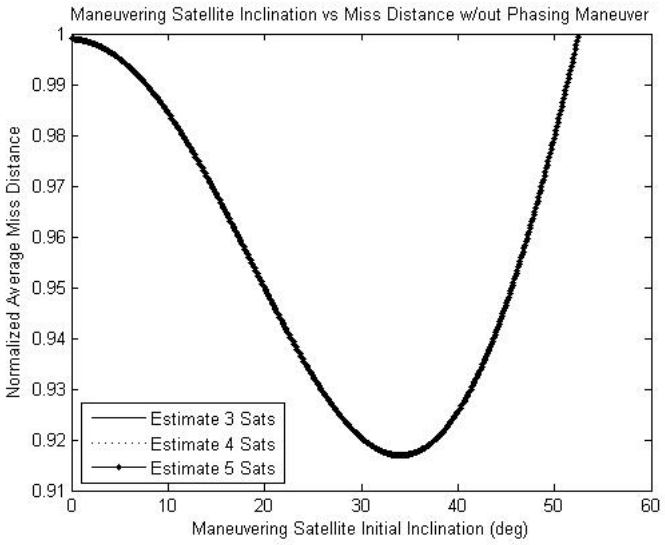

Figure 7.10: Maneuvering Satellite's Inclination vs. Empirical Normalized Miss Distance.

With such a clear representation of the algorithm's results, developing a polynomial approximation expression to predict the expected ΔV, based on the maneuvering satellite's

Table 7.15: Minimum Required ΔV and Associated Maneuvering Satellite Inclinations.

Scenario	Inclination (deg)	ΔV $\frac{m}{sec}$
3 Total Sats	53.1	0.2627
4 Total Sats	53.46	0.295
5 Total Sats	53.46	0.00797

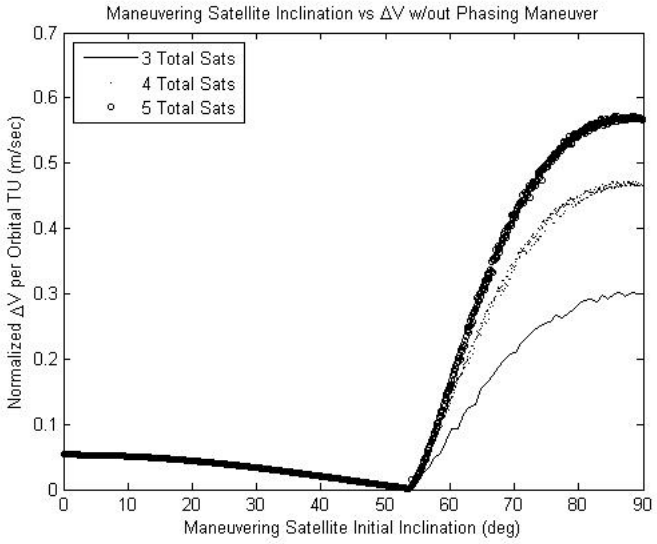

Figure 7.11: Maneuvering Satellite's Inclination vs. Normalized ΔV.

inclination, is desired. For a ROM value, a piecewise function is necessary. There is a function for representing inclinations less than 47° and a function for inclinations greater than 55°. Between 47° and 55°, it is expected that the required ΔV is simply less than $1\frac{m}{sec}$. The lower inclinations can be empirically modeled by Eq.(7.20). The higher inclinations follow a form of the equation highlighted by Eq.(7.21), with the coefficients in Tables 7.16

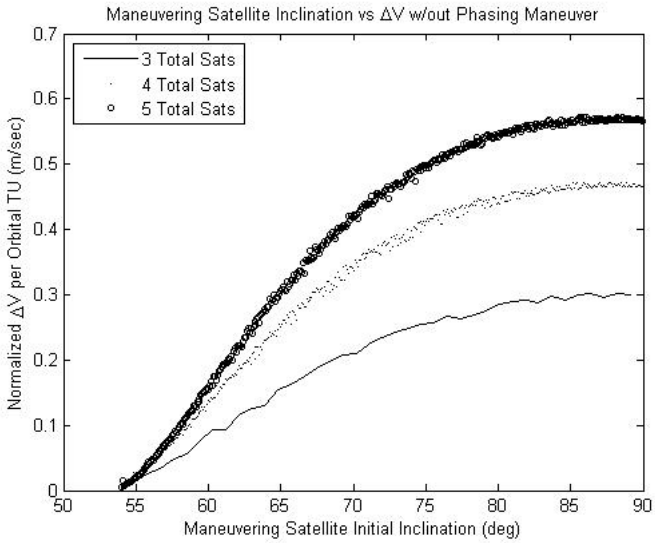

Figure 7.12: Maneuvering Satellite's Inclination vs. Normalized ΔV.

and 7.17 depending on the scenario.

$$\Delta V = 2.006x10^{-7}i^3 - 3x10^{-5}i^2 + 5.801x10^{-5}i + 5.323x10^{-2} \tag{7.20}$$

$$\Delta V = A_1 sin(B_1 i + C_1) + A_2 sin(B_2 i + C_2) + A_3 sin(B_3 i + C_3) + A_4 sin(B_4 i + C_4) + A_5 sin(B_5 i + C_5) + A_6 sin(B_6 i + C_6) + A_7 sin(B_7 i + C_7) + A_8 sin(B_8 i + C_8) \tag{7.21}$$

For the complete range of maneuvering satellite initial inclinations, Figure 7.13 illustrates the empirical solutions using Eqs.(7.20) and (7.21) with the appropriate coefficients in Tables 7.16 and 7.17.

Tables 7.18 through 7.20 provide more detailed results for the empirical solution for the required ΔV versus the Dynamic TMN algorithm's solutions. Keep in mind that the actual and estimated ΔV values are normalized per the orbital time unit.

Table 7.16: Coefficients for Empirical Solution for Required ΔV Without Phasing Maneuver.

Coefficient	3 Total Sats	4 Total Sats	5 Total Sats
A_1	0.3003	0.3189	0.4488
B_1	0.06866	0.02912	0.04559
C_1	2.495	5.367	4.39
A_2	0.05227	0.1589	0.2661
B_2	0.1498	0.1015	0.1042
C_2	0.5295	5.751	5
A_3	0.01592	0.02461	0.1006
B_3	0.3215	0.2534	0.1572
C_3	4.44	9.828	16.66
A_4	0.007044	0.006606	0
B_4	0.4761	0.4135	0
C_4	2.985	7.602	0

The results highlighted in Tables 7.18 through 7.20 are very positive for the empirical model. The highest value of concern however, is the % error value of 10.4235 in the 3 satellite scenario. While the percentage is relatively high, the absolute value of the error margin is only 1.2851($\frac{m}{sec}$).

Table 7.17: Coefficients for Empirical Solution for Required ΔV Without Phasing Maneuver.

Coefficient	3 Total Sats	4 Total Sats	5 Total Sats
A_5	0.004551	0.001546	0
B_5	0.6336	0.5841	0
C_5	1.025	5.209	0
A_6	0.003777	0	0
B_6	0.7896	0	0
C_6	5.815	0	0
A_7	-0.002605	0	0
B_7	1.084	0	0
C_7	-6.636	0	0
A_8	0.001644	0	0
B_8	1.103	0	0
C_8	10.84	0	0

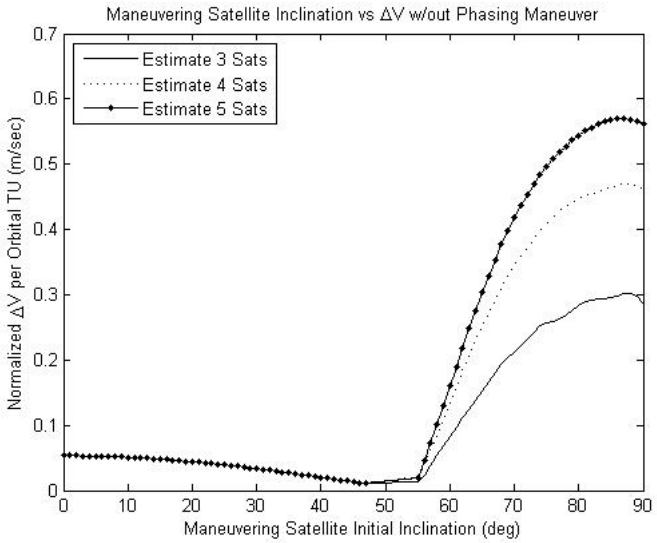

Figure 7.13: Maneuvering Satellite's Inclination vs. Empirical Normalized ΔV.

Table 7.18: Empirical vs. Dynamic TMN Results for 3 Satellite Scenario.

Inclination (deg)	Actual ΔV	Estimate ΔV	ΔV % Error	ΔV Value ($\frac{m}{sec}$)
0	0.0534	0.0532	0.3745	0.0268
10	0.0510	0.0510	0.0000	0.0000
30	0.0338	0.0334	1.1834	0.0535
45	0.0134	0.0134	0.0000	0.0000
60	0.0921	0.0825	10.4235	1.2851
75	0.2554	0.2570	0.6265	0.2142
90	0.2992	0.2857	4.5120	1.8071

Table 7.19: Empirical vs. Dynamic TMN Results for 4 Satellite Scenario.

Inclination (deg)	Actual ΔV	Estimate ΔV	ΔV % Error	ΔV Value ($\frac{m}{sec}$)
0	0.0534	0.0532	0.3745	0.0268
10	0.0510	0.0510	0.0000	0.0000
30	0.0334	0.0334	0.0000	0.0000
45	0.0134	0.0134	0.0000	0.0000
60	0.1389	0.1341	3.4557	0.6425
75	0.4067	0.4088	0.5164	0.2811
90	0.4661	0.4619	0.9011	0.5622

Table 7.20: Empirical vs. Dynamic TMN Results for 5 Satellite Scenario.

Inclination (deg)	Actual ΔV	Estimate ΔV	ΔV % Error	ΔV Value ($\frac{m}{sec}$)
0	0.0534	0.0532	0.3745	0.0268
10	0.0510	0.0510	0.0000	0.0000
30	0.0334	0.0334	0.0000	0.0000
45	0.0134	0.0134	0.0000	0.0000
60	0.1552	0.1598	2.9639	0.6158
75	0.4975	0.4963	0.2412	0.1606
90	0.5666	0.5612	0.9531	0.7228

7.7 Chapter Summary

Overall, this chapter presented the Dynamic TMN algorithm to deliver an impulsive maneuver to a satellite to be within overlapping spheres, with user-defined radii, centered around multiple non-maneuvering satellites at a specific time, as illustrated in Figure 7.1. The methodology and results were presented for non-maneuvering satellites, beginning at a perigee altitude of 274.41 km and a maneuvering satellite, beginning along the same unit position vector at an altitude of 1406.4 km. The sphere radius was 1500 km with a 5% margin, allowing for a solution when the maneuvering satellite returns to within 1575 km of the non-maneuvering satellites at a time +/- 10% of the least common multiple of the non-maneuvering satellites' orbital periods. The presented results were constrained to prograde orbits. In the end, the focus of the results was based on the success of the Dynamic TMN algorithm, while demonstrating unique information about this problem. A critical mission design consideration was presented through the selection of the satellites' initial inclinations. A significant result from this study is the ability for the user to empirically predict the necessary ΔV, for a desired combination of inclinations for the phasing orbit solution. Another result is the ability to empirically predict the average miss distance and required ΔV based on the maneuvering satellite's initial inclination for the solution without the phasing orbit. Ultimately, the successful presentation of the Dynamic TMN algorithm lays the groundwork for continued development of theater based responsive space capabilities.

7.8 Chapter Appendix

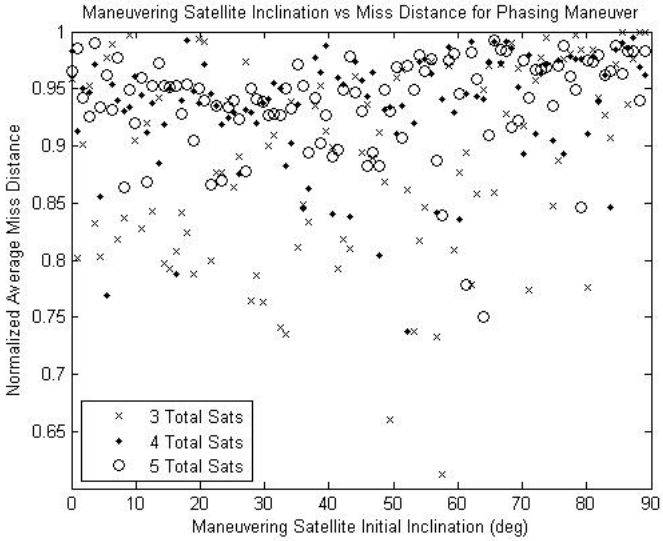

Figure 7.14: Maneuvering Satellite's Inclination vs. Normalized Miss Distance.

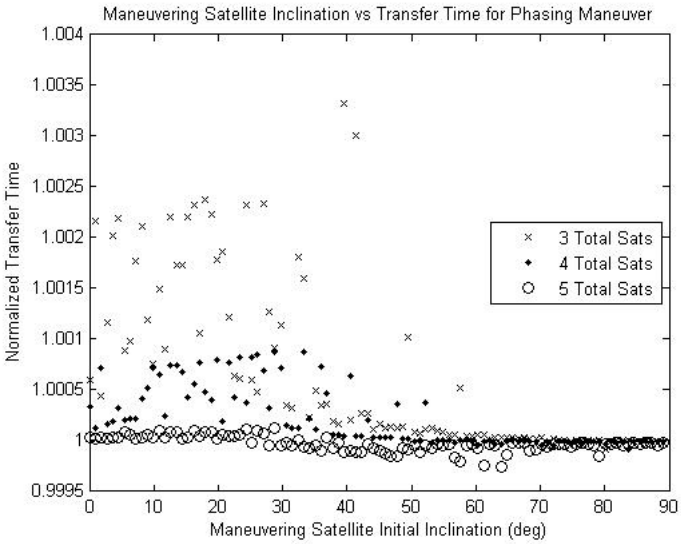

Figure 7.15: Maneuvering Satellite's Inclination vs. Normalized Transfer Time.

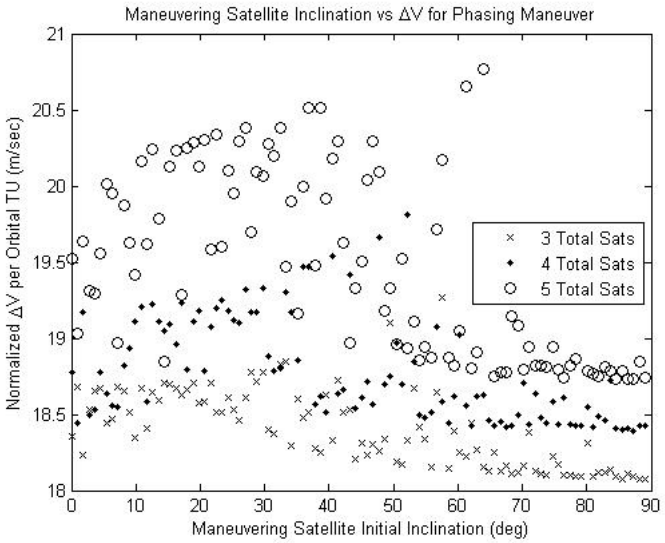

Figure 7.16: Maneuvering Satellite's Inclination vs. Normalized ΔV.

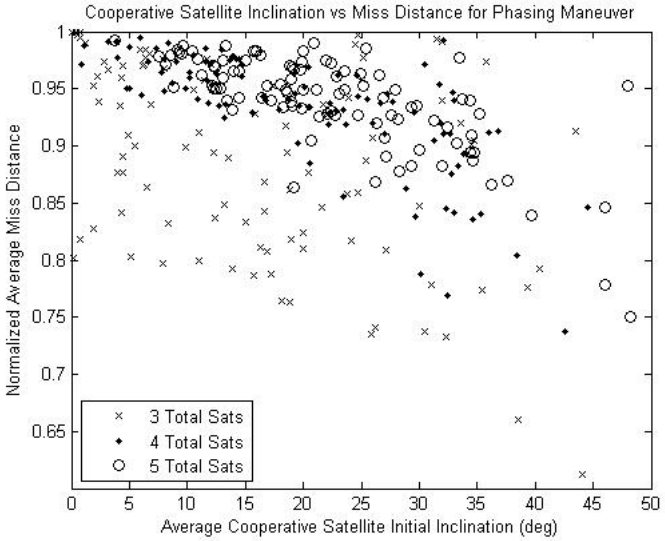

Figure 7.17: Cooperative Satellites' Inclination vs. Normalized Miss Distance.

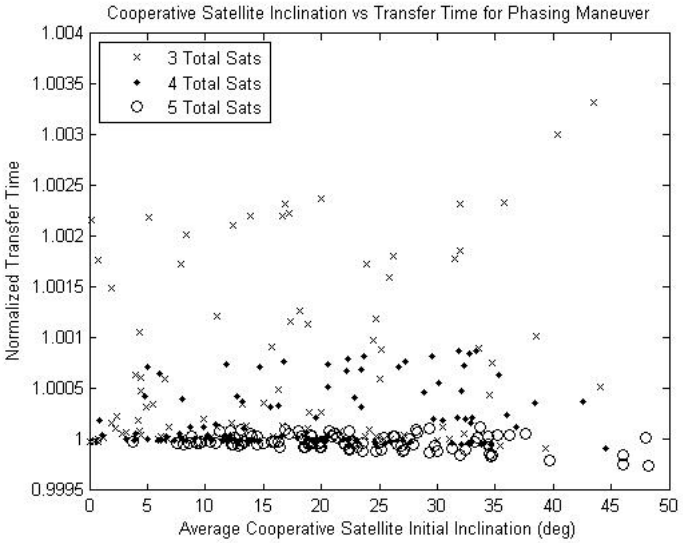

Figure 7.18: Cooperative Satellites' Inclination vs. Normalized Transfer Time.

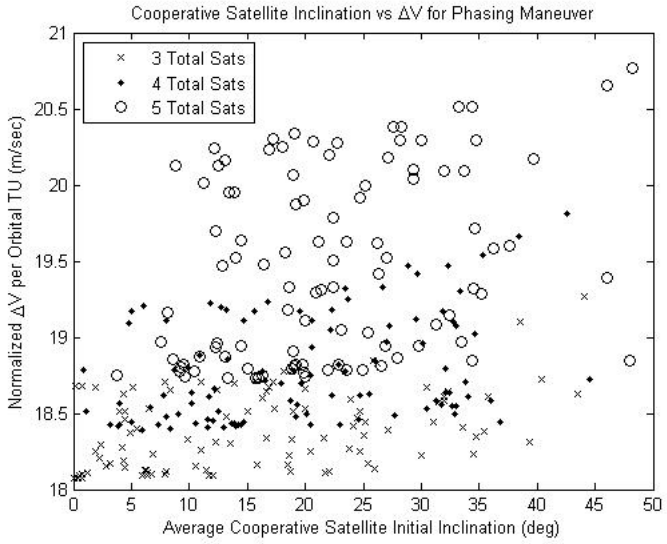

Figure 7.19: Cooperative Satellites' Inclination vs. Normalized ΔV.

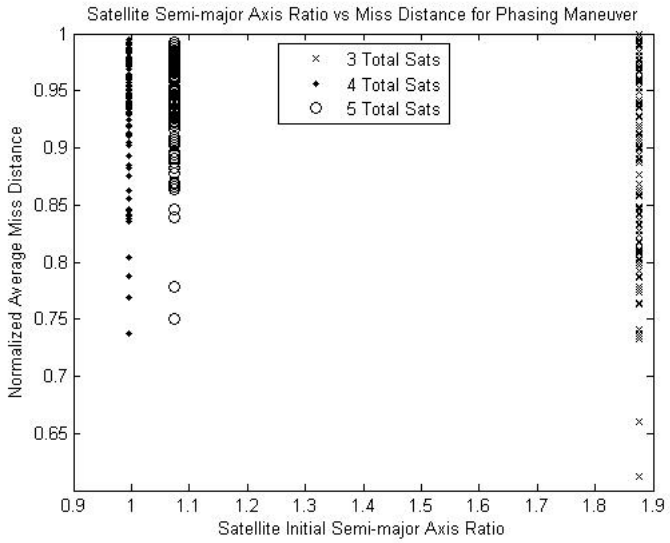

Figure 7.20: Satellites' Initial Semi-major Axis Ratio vs. Normalized Miss Distance.

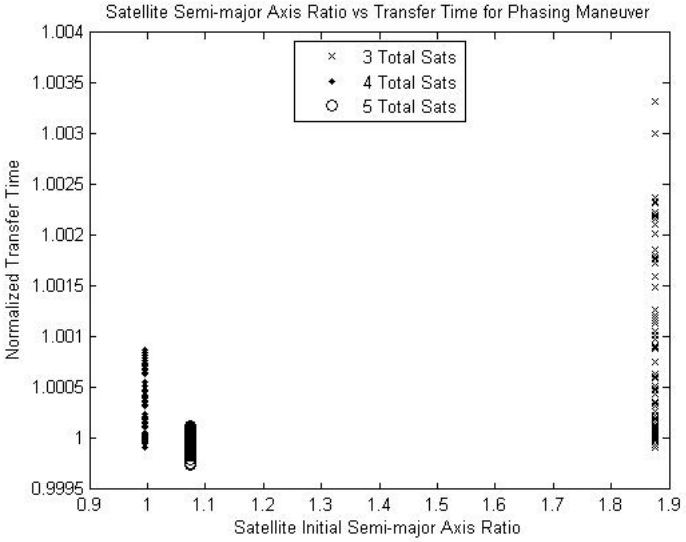

Figure 7.21: Satellites' Initial Semi-major Axis Ratio vs. Normalized Transfer Time.

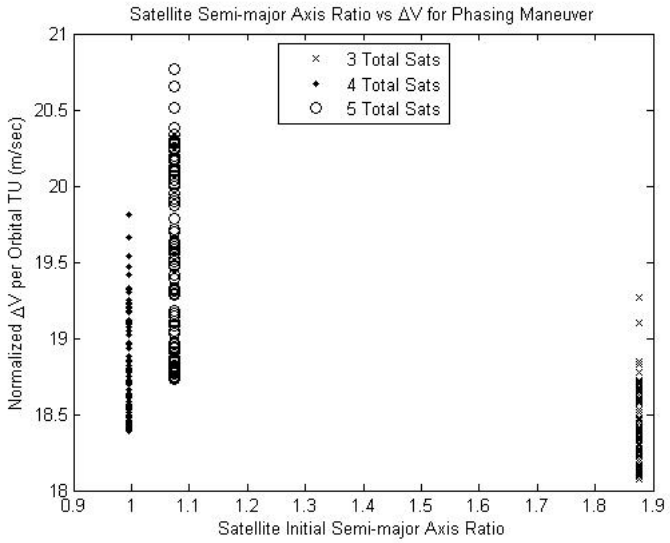

Figure 7.22: Satellites' Initial Semi-major Axis Ratio vs. Normalized ΔV.

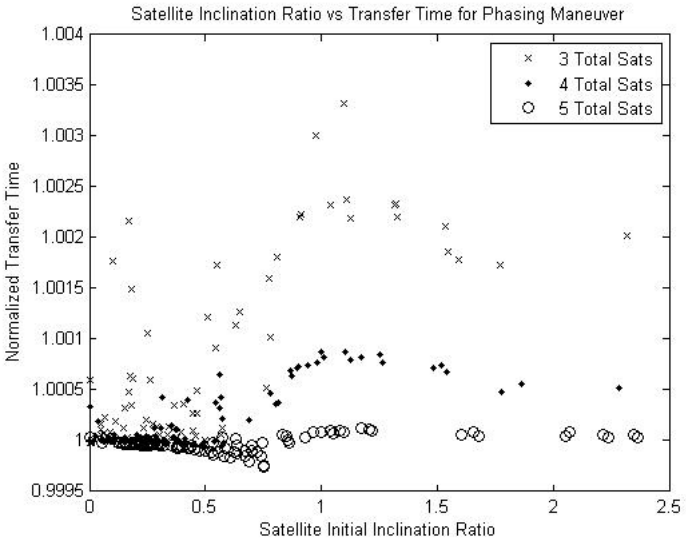

Figure 7.23: Satellites' Initial Inclination Ratio vs. Normalized Transfer Time.

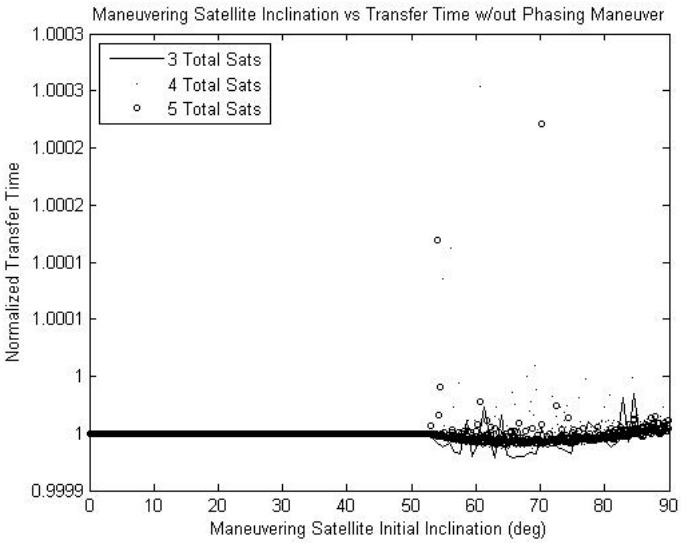

Figure 7.24: Maneuvering Satellite's Inclination vs. Normalized Transfer Time.

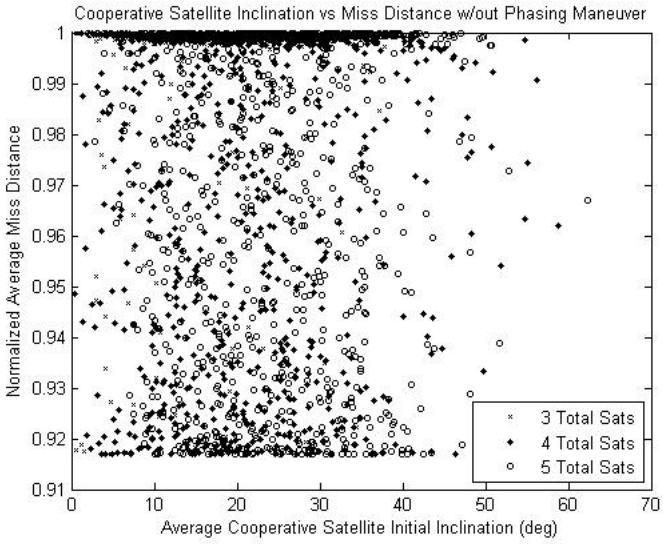

Figure 7.25: Cooperative Satellite's Inclination vs. Normalized Miss Distance.

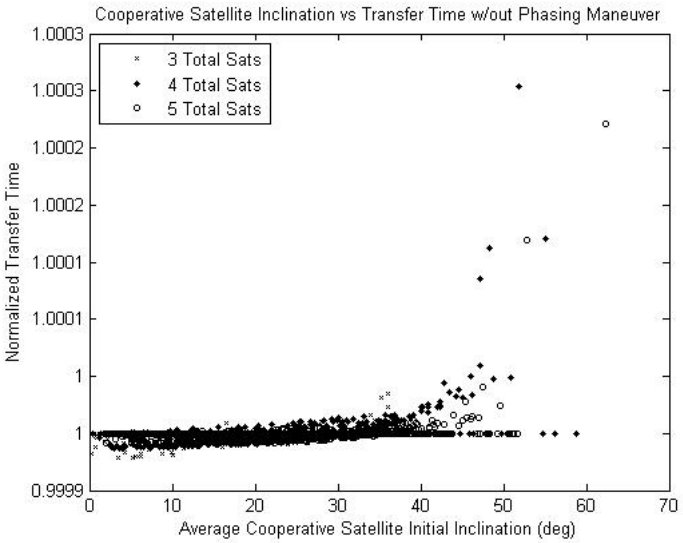

Figure 7.26: Cooperative Satellite's Inclination vs. Normalized Transfer Time.

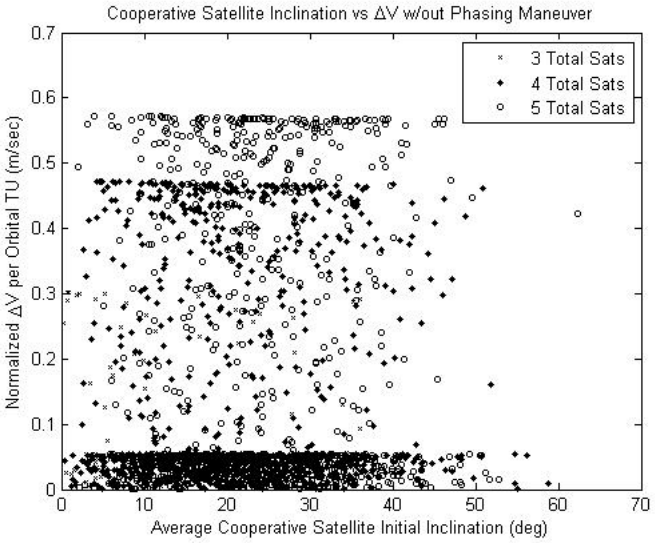

Figure 7.27: Cooperative Satellite's Inclination vs. Normalized ΔV.

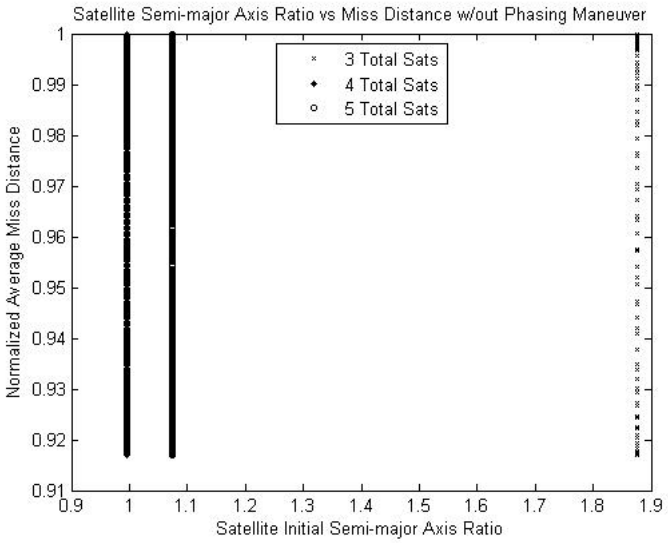

Figure 7.28: Satellites' Initial Semi-major Axis Ratio vs. Normalized Miss Distance.

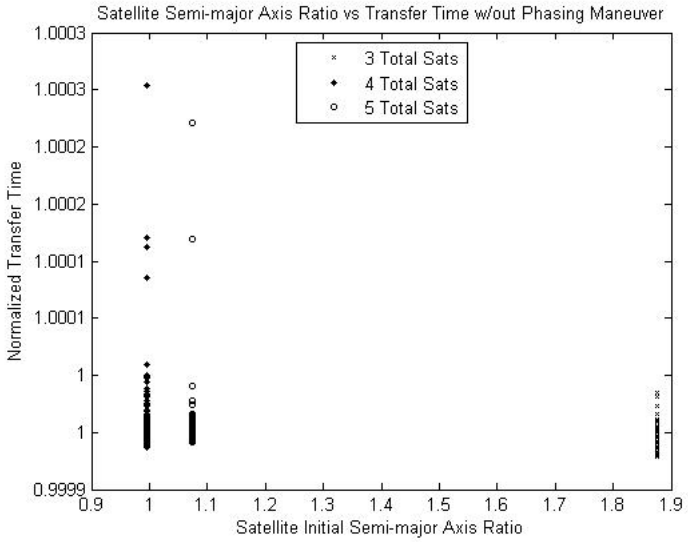

Figure 7.29: Satellites' Initial Semi-major Axis Ratio vs. Normalized Transfer Time.

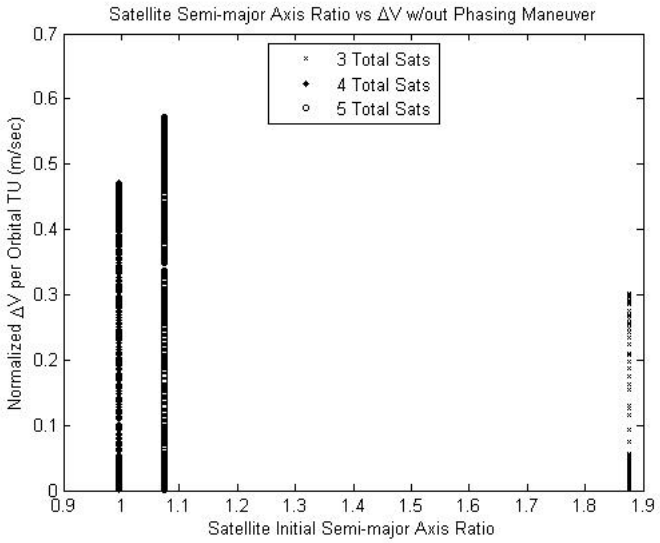

Figure 7.30: Satellites' Initial Semi-major Axis Ratio vs. Normalized ΔV.

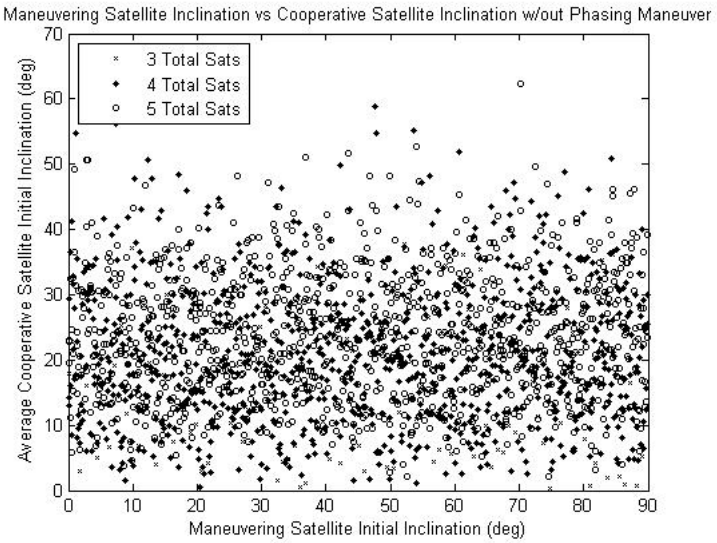

Figure 7.31: Maneuvering Satellite Inclination vs. Average Cooperative Satellites' Inclination.

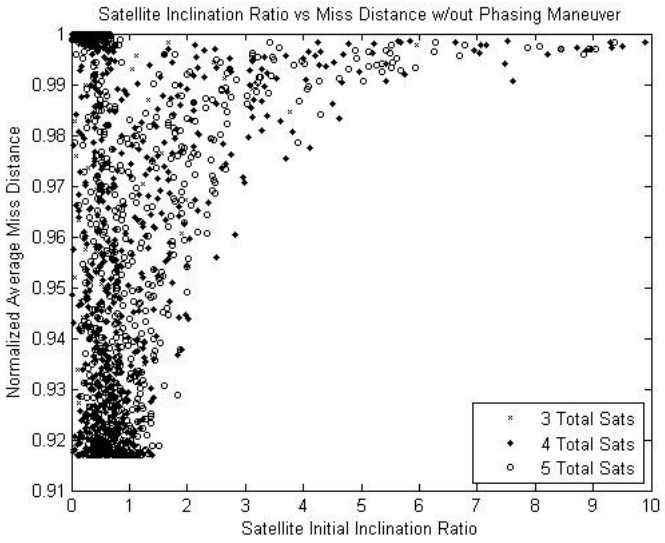

Figure 7.32: Satellites' Initial Inclination Ratio vs. Normalized Miss Distance.

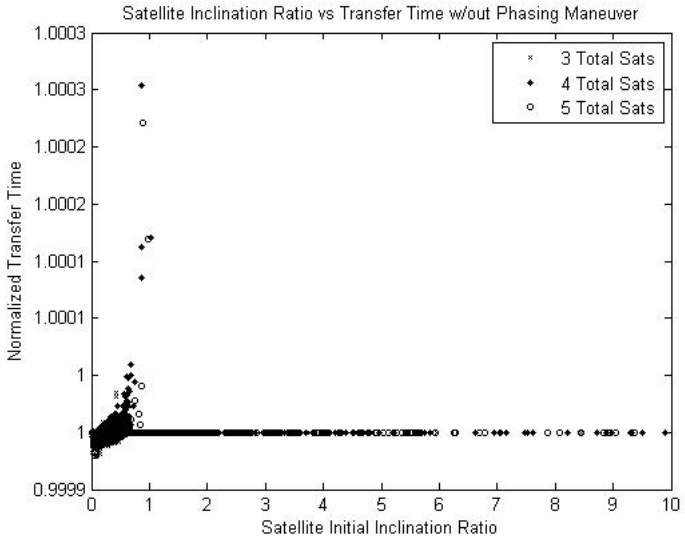

Figure 7.33: Satellites' Initial Inclination Ratio vs. Normalized Transfer Time.

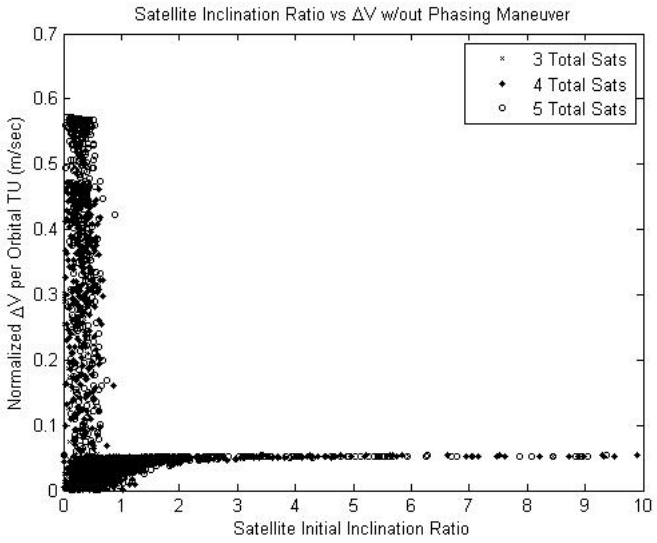

Figure 7.34: Satellites' Initial Inclination Ratio vs. Normalized ΔV.

VIII. Navigation Solution to Maneuver a Spacecraft Relative to Multiple Satellites and Ground Locations

8.1 Introduction

The following chapter will extend the presentation of the Dynamic T-Matrix Navigation algorithm to allow for varying geometry between the maneuvering satellite relative to both multiple non-maneuvering satellites as well as multiple ground locations.

8.2 Problem Statement

The purpose of this chapter is to demonstrate the ability for the Dynamic TMN algorithm to deliver an impulsive maneuver to a satellite and place it within overlapping spheres, with user-defined radii, centered around multiple non-maneuvering satellites within a constrained time. The algorithm will also account for user-specified range and elevation constraints for multiple ground locations. The algorithm will ultimately deliver a solution within the overlap of the cooperative satellites and ground locations ranges. Figure 8.1 illustrates the problem.

Specifically, the proceeding results are generalized for the satellites' altitudes, but it is assumed throughout that the Earth must complete one full rotation, 24 hours, before the maneuvering satellite can successfully declare a solution within the overlapping spheres. This study only focuses on prograde orbits, therefore inclinations range between 0° and 90°. The focus of the results is based on the success of the Dynamic TMN algorithm, while demonstrating unique aspects of this problem. Ultimately, this study will present a generalized algorithm that allows for expanded utilization to be applied towards any user's scenario. The description of the optimal control problem being addressed by this chapter

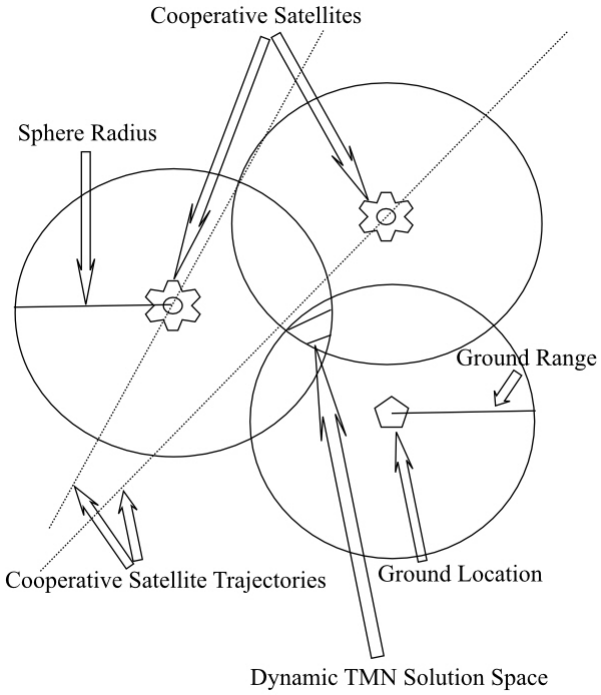

Figure 8.1: Illustration of Problem Statement

is in Eqs.(8.1) and (8.2).

$$
\begin{aligned}
&\text{Minimize: } \mathrm{J} = \int_{t_0}^{t_f} |u(t)|\, dt \\
&\text{Subject to:} \\
&\quad \dot{\vec{R}}, \dot{\vec{V}}, \vec{V}_{GND} \\
&\quad u(t) = \Delta V \delta_0(t - t_0) \\
&\quad t_f \in [0.9\mathrm{LCM}(\mathrm{P}_{COOP_1}, \ldots, \mathrm{P}_{COOP_N}, \omega_\oplus), 1.1\mathrm{LCM}(\mathrm{P}_{COOP_1}, \ldots, \mathrm{P}_{COOP_N}, \omega_\oplus)] \\
&\quad \mathrm{el} \geq 10^\circ
\end{aligned}
\tag{8.1}
$$

Initial Conditions:

$$
\begin{aligned}
&\vec{R}_1(t_0) = \vec{R}_{1_{t_0}} \\
&\vec{V}_1(t_0) = \vec{V}_{1_{t_0}} \\
&\vec{R}_{COOP_1}(t_0) = \vec{R}_{COOP_{1_{t_0}}} \\
&\vec{V}_{COOP_1}(t_0) = \vec{V}_{COOP_{1_{t_0}}} \\
&\vdots \\
&\vec{R}_{COOP_N}(t_0) = \vec{R}_{COOP_{N_{t_0}}} \\
&\vec{V}_{COOP_N}(t_0) = \vec{V}_{COOP_{N_{t_0}}} \\
&\phi_{GS_1}(t_0) = \phi_{GS_{1_{t_0}}} \\
&\lambda_1(t_0) = \lambda_{1_{t_0}} \\
&\vdots \\
&\phi_{GS_p}(t_0) = \phi_{GS_{p_{t_0}}} \\
&\lambda_p(t_0) = \lambda_{p_{t_0}}
\end{aligned}
\tag{8.2}
$$

Terminal Conditions:

$$
\begin{aligned}
\vec{R}_1(t_f) \in \mathbf{B}(\vec{R}_{COOP_1}(t_f), \eta) \bigcap \ldots \bigcap \mathbf{B}(\vec{R}_{COOP_N}(t_f), \eta) \\
\bigcap \mathbf{B}(\vec{R}_{GS_1}(t_f), \gamma) \bigcap \ldots \bigcap \mathbf{B}(\vec{R}_{GS_p}(t_f), \gamma)
\end{aligned}
$$

A brief summary of the procedure to solve this problem is provided below. The unique contributions to this chapter are highlighted in **boldface**.

1. **Establish initial Classic Orbital Elements (COEs) for satellites.**
2. **Establish initial conditions for the ground locations.**
3. Convert COEs to initial position, $\vec{R}_0$, and velocity, $\vec{V}_0$ vectors.
4. Establish scaling parameters and scaling matrix, **S**[4].
5. Establish weight matrix, **Q**[4].
6. **Determine initial guess for required fuel, ΔV, and transfer time, *t*.**

7. **Integrate Equations of Motion (EOM) for cooperative satellites for duration of *t*.**

8. **Calculate final state, $\vec{R}, \vec{V}$, for cooperative satellites at *t*.**

9. **Integrate EOM for ground locations for duration of *t*.**

10. **Calculate final state for ground locations at *t*.**

11. Apply ΔV to maneuvering satellite to yield $\vec{V}_{0+}$.

12. Integrate EOM for maneuvering satellite for duration of *t*.

13. Calculate final state $\vec{R}, \vec{V}$, for maneuvering satellite at *t*.

14. **Calculate spherical separation distance between maneuvering satellite and cooperative satellites.**

15. **Calculate range separation distance between maneuvering satellite and ground locations.**

16. Integrate maneuvering satellite's State Transition Matrix (STM) using Equations of Variation (EOV) for duration of *t*.

17. Declare ϕ matrix as upper right 3x3 portion of STM[4].

18. **Calculate velocity difference vector, $\vec{V}_{DIFF}$, between maneuvering satellite's and cooperative satellites' velocity vectors.**

19. **Calculate velocity difference vector between maneuvering satellite's and ground locations' velocity vectors.**

20. Calculate ΔV for maneuvering satellite: $\Delta V = \vec{V}_{0+} - \vec{V}_0$.

21. Compile error vector, $\bar{e}$, as the component by component separation distance and components of ΔV.

22. **Build $\tilde{T}$ matrix:** $\begin{bmatrix} \phi_1\phi_2...\phi_{N+p} & \vec{V}_{Diff} \\ \mathbf{I} & \mathbf{0} \end{bmatrix}$.

23. Calculate **T** matrix: $\mathbf{T} = \mathbf{S}^{-1}\tilde{T}$[4].

24. **Declare convergence criteria when all control contributions to ΔV are 0.**

25. Determine ∂u: $\partial u = -(\mathbf{T}'\mathbf{Q}^{-1}\mathbf{T})^{-1}\mathbf{T}'\mathbf{Q}^{-1}\bar{e}$[4].

26. **Check ∂u components versus convergence criteria.**

27. If convergence criteria are satisfied then the algorithm is complete.

    - Final ΔV = ΔV from error vector, $\bar{e}$
    - Final transfer time = current t

28. **Add $\sum\Delta$V from ∂u to $\vec{V}_{0+}$ yielding new ΔV.**

29. Add Δt from ∂u to transfer time, t, for updated time.

30. Return to #7.

8.3 Establishing the Algorithm

In order to implement the Dynamic TMN algorithm, the initial orbits and ground locations are required. Depending on how the problem is framed, there can be a variable number of non-maneuvering satellites within the scenario, as well as ground locations. This number will simply be referred to as 'N' cooperative satellites and 'p' ground locations. Regardless of the number of cooperative satellites and ground locations, there will only be one maneuvering satellite (Sat 1). The maneuvering satellite will be the satellite to which the ΔV is applied. To simplify the illustration of the algorithm within this particular

problem, all satellites will begin along the same unit position vector. Specifically, the 'N' cooperative satellites will begin at the same point, therefore the position vector is identical for each. An additional assumption for establishing illustrating this problem places all satellites along the $\hat{X}$ axis at the starting time, providing for the initial position vectors in Eqs.(8.3) and (8.4).

$$\vec{R}_{Sat1} = |\vec{R}_{Sat1}| \begin{bmatrix} 1 \\ 0 \\ 0 \end{bmatrix} km \tag{8.3}$$

$$\vec{R}_{N} = |\vec{R}_{N}| \begin{bmatrix} 1 \\ 0 \\ 0 \end{bmatrix} km \tag{8.4}$$

The initial positions for the cooperative satellites are fixed, as are their orbital periods. Specifically for this study, the orbital periods are different for each cooperative satellite, therefore resulting in differing final positions after a certain amount of time. The lowest value for the orbital period is 90 minutes, resulting in a circular orbit at 274.41 km altitude. Considering 90 minutes as the fastest orbital period ensures that the initial position vectors for the cooperative satellites are at perigee. Because the cooperative satellites are beginning along the $\hat{X}$ unit vector, the RAAN and the argument of perigee are 0°. Also, provided a fixed initial position and orbital period, the semi-major axis and eccentricity are determined. The initial COEs are nearly complete.

To complete the initial conditions for the cooperative satellites the only remaining COEs, inclination, is explored over a range of values following a normal distribution according to Eq.(8.5) [70]. Each cooperative satellite has a random value for inclination between 0° and 90°. A straightforward conversion from COEs is now possible for the cooperative satellites.

$$i = Mod(Abs(Normal) \times \frac{\pi}{4}, \frac{\pi}{2}) \tag{8.5}$$

Once the initial COEs were determined for the cooperative satellites, the original position and velocity vectors needed to be determined for the maneuvering satellite, Satellite 1. Provided a fixed altitude, Satellite 1 is in a circular orbit, therefore, semi-major axis and eccentricity are known. Understanding the initial position vector for Satellite 1, at a fixed altitude in Eq.(8.3) leads to a RAAN and argument of perigee of 0°. The inclination for Satellite 1 is also randomized according to Eq.(8.5) and has a range of 0° and 90°. Converting to $\vec{R}$ and $\vec{V}$ is possible with the COEs for the maneuvering satellite.

For this particular problem the initial position of the ground locations is randomized. However, they must satisfy the user defined range and elevation constraints relative to the cooperative satellites. Also note, the ground locations are on the surface of a spherical Earth.

In order for the algorithm to proceed, the future state, both the position and velocity vectors need to be determined for the maneuvering satellite. Once the position vector in the future is determined for Sat 1, that same time is used to determine the position vectors for the cooperative satellites and the ground locations, and an error vector is calculated. The error vector for this chapter is displayed in Eq.(8.8). Because the error is in vector form, it is a function of the number of relationships between the maneuvering satellite and the 'N' cooperative satellites and the 'p' ground locations. Therefore, the error vector in Eq.(8.8) is representative of any number of cooperative satellites and ground locations. The dimensions of the error vector are, $(3(N + p) + 3) \times 1$.

$$\bar{e}_{\Lambda}^{T} = \begin{bmatrix} \Lambda_{1_X} & \Lambda_{1_Y} & \Lambda_{1_Z} & \cdots & \Lambda_{N_X} & \Lambda_{N_Y} & \Lambda_{N_Z} \end{bmatrix} \tag{8.6}$$

$$\bar{e}_{\Upsilon}^{T} = \begin{bmatrix} \Upsilon_{1_X} & \Upsilon_{1_Y} & \Upsilon_{1_Z} & \cdots & \Upsilon_{p_X} & \Upsilon_{p_Y} & \Upsilon_{p_Z} \end{bmatrix} \tag{8.7}$$

$$\bar{e}^{T} = \begin{bmatrix} \bar{e}_{\Lambda}^{T} & \bar{e}_{\Upsilon}^{T} & \Delta V_{SAT1_X} & \Delta V_{SAT1_Y} & \Delta V_{SAT1_Z} \end{bmatrix} \tag{8.8}$$

Recall that this particular problem is establishing an algorithm to yield a solution that maneuvers a satellite within the combined spheres, with a user-defined radius, from the

non-maneuvering cooperative satellites constrained by the range and elevation of multiple ground locations. Therefore, the introduction of the vector, $\vec{\Lambda}$, represents a relationship between the maneuvering and non-maneuvering satellites, according to the radius of the user defined sphere. $\vec{\Upsilon}$, represents a relationship between the maneuvering satellite and the ground locations. The components of the $\vec{\Lambda}$ and $\vec{\Upsilon}$ vectors are defined in Eqs.(8.9) through (8.14).

$$\Lambda_{N_X} = R_{SAT1_X} - \left(\frac{R_{SAT1_X} - R_{N_X}}{|\vec{R}_{SAT1} - \vec{R}_N|} * \eta + R_{N_X} \right) \tag{8.9}$$

$$\Lambda_{N_Y} = R_{SAT1_Y} - \left(\frac{R_{SAT1_Y} - R_{N_Y}}{|\vec{R}_{SAT1} - \vec{R}_N|} * \eta + R_{N_Y} \right) \tag{8.10}$$

$$\Lambda_{N_Z} = R_{SAT1_Z} - \left(\frac{R_{SAT1_Z} - R_{N_Z}}{|\vec{R}_{SAT1} - \vec{R}_N|} * \eta + R_{N_Z} \right) \tag{8.11}$$

$$\Upsilon_{p_X} = R_{SAT1_X} - \left(\frac{R_{SAT1_X} - R_{p_X}}{|\vec{R}_{SAT1} - \vec{R}_p|} * \gamma + R_{p_X} \right) \tag{8.12}$$

$$\Upsilon_{p_Y} = R_{SAT1_Y} - \left(\frac{R_{SAT1_Y} - R_{p_Y}}{|\vec{R}_{SAT1} - \vec{R}_p|} * \gamma + R_{p_Y} \right) \tag{8.13}$$

$$\Upsilon_{p_Z} = R_{SAT1_Z} - \left(\frac{R_{SAT1_Z} - R_{p_Z}}{|\vec{R}_{SAT1} - \vec{R}_p|} * \gamma + R_{p_Z} \right) \tag{8.14}$$

Eqs.(8.9) through (8.11) display the elements of the unit vector of the component by component miss distance vector between Sat 1 and the cooperative satellites. The unit vector components are multiplied by η, the radius of the sphere, and added to the componenent of the non-maneuvering satellites. Eqs.(8.12) through (8.14) display the elements of the unit vector of the component by component miss distance vector between Sat 1 and the ground locations. The unit vector components are multiplied by γ, the range of the ground location, and added to the componenent of the non-maneuvering satellites. Interestingly, this makes the solution dynamic. This means that the solution to the sphere edge changes with each iteration because the solution itself is based on the position of the maneuvering and non-maneuvering satellites and ground locations.

Overall, the error vector, Eq.(8.8), represents the dynamic solution for the position and the applied ΔV on the maneuvering satellite, Sat 1.

Provided the direction for the algorithm to proceed, it is necessary to identify that the integrated equations for the solution will follow three separate models. The first is for the maneuvering satellite and the second is for the cooperative satellites, while the third is the rotation of the ground location on the surface of the Earth. The maneuvering satellite will be subject to EOM including both J_2 and an air drag model. For simplicity, the cooperative satellites will follow 2-body EOM simulating active orbit control with the desire to return over the same inertial position in space over the Earth. The model for the maneuvering satellite will require the appropriate variational equations.

The development and derivation of the maneuvering satellite's State Transition Matrix follows from Section 4.3.

Another necessary component in the algorithm is the relationship between the satellites' final velocity vectors. Identifying this vector and combining this with ϕ, a form of the $\tilde{T}$ matrix is determined and shown in equation (8.15). Even though the solution to this algorithm will be within the radius of the sphere, the relationship between the maneuvering satellite's velocity and the non-maneuvering satellites' velocity and ground location velocity vectors is important. Recall that the solution space, the spheres, will be moving identically to the movement of the non-maneuvering satellites and ground locations. This means that the solution for the maneuvering satellite will most likely be at higher altitude than the non-maneuvering satellites. The sphere at that higher altitude is still moving at the velocity of the non-maneuvering satellites. Noticing that the $\tilde{T}$ matrix is adjustable based on the number of cooperative satellites and ground locations yields the dimensions, $(3(N+p)+3) \times (3(N+p)+1)$.

$$\tilde{T} = \begin{bmatrix} \phi_1\phi_2...\phi_{N+p} & \vec{V}_{Diff} \\ \mathbf{I} & \mathbf{0} \end{bmatrix} \tag{8.15}$$

$$\vec{V}_{Diff} = \sum \vec{V}_{SAT1} - \vec{V}_N - \vec{V}_p \tag{8.16}$$

The ϕ_{N+p}, terms come directly from Eq.(4.7). It is required to add an additional ϕ for each of the 'N' cooperative satellites and each of the 'p' ground locations. Eq.(8.16) represents the sum of the differences between the maneuvering satellite's final velocity vector and each cooperative satellite's velocity vector and ground location velocity vector and has dimensions, 3×1. Therefore, the **I** matrix requires dimensions $(3(N + p) \times 3(N + p))$ and **0** requires dimesions $(3(N + p) \times 1)$. The final **T** matrix is derived from scaling parameters combined with $\tilde{T}$.

The final components of the Dynamic TMN setup are the identification of a weight matrix, **Q** and a scale matrix, **S**. The weight matrix allows for the user to shift convergence focus from final position to applied ΔV. In order to maintain a balanced focus on both, minimizing miss distance and fuel used, an identity matrix, **I**, should be used. For this study, **Q**, is simply a $(3(N + p) + 3) \times (3(N + p) + 3)$ **I** matrix. The scale matrix, **S**, is utilized to allow faster convergence within the algorithm. For this study, **S** is a constant $(3(N + p) + 3) \times (3(N + p) + 3)$ matrix. **S** is defined in (8.17) while **T** is calculated from $\tilde{T}$ and **S** in (8.18). **S** is an adjustable matrix to allow for better scaling of the nonlinear system of equations.

$$\mathbf{S} = 0.1\mathbf{I} \tag{8.17}$$

$$\mathbf{T} = \mathbf{S}^{-1}\tilde{T} \tag{8.18}$$

Ultimately, combining all of this information, the variation of the control vector, $\vec{u}$, can be calculated. The variation of $\vec{u}$ is the core of the Dynamic TMN. Once the maneuvering satellite is within the overlapping area of the 'N' cooperative satellite spheres and with range and elevation constraints of 'p' ground locations, a unique solution is declared for the model. It is important to note that based on units and matrix dimensions, $\vec{u}$, will have $(3(N + p) + 1) \times 1$ components. Specifically, the components of $\vec{u}$ are shown below in

Eq.(8.19).

$$\vec{u}^T = \Big[\Delta V_{1_X}, \Delta V_{1_Y}, \Delta V_{1_Z}, \cdots, \Delta V_{N_X}, \Delta V_{N_Y}, \Delta V_{N_Z}, \Delta V_{1_X}, \Delta V_{1_Y}, \Delta V_{1_Z}, \cdots, \Delta V_{p_X}, \Delta V_{p_Y}, \Delta V_{p_Z}, \Delta t\Big] \quad (8.19)$$

The ΔV terms are the changes in the initial impulsive maneuver applied to Sat 1 and the Δt term is the change in transfer time during each iteration. Summing the results for each component, after each iteration, and then dividing by 'N+p', yields the total ΔV for the impulsive maneuver. Notice that there are three contributions to the ΔV from each of the 'N' cooperative satellites and each of the 'p' ground locations. Combining the sum of the Δt's with the initial transfer time results in the final transfer time for the optimum ΔV. However, the Dynamic TMN algorithm is designed so that once the maneuvering satellite is within a sphere, the contribution to the solution from that cooperative satellite is zeroed out for that iteration. The same is true for the ground locations, including the constraint from the elevation angle. If the next iteration's solution forces the maneuvering satellite outside of the sphere, it is reconsidered towards the solution again. For example, Eqs.(8.8) and (8.19) have been updated in Eqs.(8.20) and (8.21), considering that the maneuvering satellite is within the sphere of cooperative satellite 2 and in range and elevation of one ground location.

$$\vec{e}^T = \Big[\Lambda_{1_X}, \Lambda_{1_Y}, \Lambda_{1_Z}, 0, 0, 0, \cdots, \Lambda_{N_X}, \Lambda_{N_Y}, \Lambda_{N_Z}, 0, 0, 0, \Delta V_X, \Delta V_Y, \Delta V_Z\Big] \quad (8.20)$$

The $\tilde{T}$ and therefore the **T** matrices are not adjusted as derived in Eqs.(8.15) and (8.18) because the final velocity difference towards solution is still viable since it will never equal $\vec{0}$ for a non-rendezvous mission. Considering this change, the resulting $\vec{u}$ is demonstrated in Eq.(8.21) for a satisfying solution for cooperative satellite 2 and one ground location.

$$\vec{u}^T = \Big[\Delta V_{1_X} \;\; \Delta V_{1_Y} \;\; \Delta V_{1_Z} \;\; 0 \;\; 0 \;\; 0 \;\; \cdots \;\; \Delta V_{N_X} \;\; \Delta V_{N_Y} \;\; \Delta V_{N_Z} \;\; 0 \;\; 0 \;\; 0 \;\; \Delta t\Big] \quad (8.21)$$

Ultimately, once the net ΔV contribution is 0 in any given iteration, the algorithm declares a solution. The algorithm iterates on Eq.(8.22) [4]. Every iteration includes all of

the previous steps for determining **T**. The weight matrix is **Q** and $\bar{e}$ is the error vector from Eq.(8.8).

$$\partial u = -(\mathbf{T}'\mathbf{Q}^{-1}\mathbf{T})^{-1}\mathbf{T}'\mathbf{Q}^{-1}\bar{e} \tag{8.22}$$

8.4 System Dynamics for Rotating Ground Location

In order to sufficiently model the motion of the ground station as the Earth rotates through time, the latitude angle, λ and initial ϕ_{GS} angle need to be determined. These are calculated through some simple algebraic manipulations of the dot product of the ground station's position unit vector, with the $\hat{Z}$ unit vector for λ and the $\hat{Y}$ unit vector for ϕ_{GS}.

The initial velocity of the ground station is a little bit more challenging. The full representation for the initial velocity for the ground station is in Eq.(8.23). $R_\oplus$ is the radius of the Earth and $\omega_\oplus$ represents the rotation rate of the Earth.

$$\vec{V}_{GND_0} = \begin{bmatrix} R_\oplus \times cos(\lambda) \times \omega_\oplus \times sin(\phi_{GS_0}) \\ R_\oplus \times cos(\lambda) \times \omega_\oplus \times cos(\phi_{GS_0}) \\ 0 \end{bmatrix} \tag{8.23}$$

The final position and velocity vectors of the ground locations are determined by executing Eq.(8.24) for the final angle, ϕ_{GS}, at the determined transfer time, t. The position vector is updated according to the dot product relationships between the final ϕ_{GS} angle and Eq.(8.25). Eq. (8.25) represents the final velocity vector for the ground locations.

$$\phi_{GS_{tf}} = \phi_{GS_0} + (cos(\lambda) \times t \times \omega_\oplus) \tag{8.24}$$

$$\vec{V}_{GND_{tf}} = \begin{bmatrix} R_\oplus \times cos(\lambda) \times \omega_\oplus \times sin(\phi_{GS_{tf}}) \\ R_\oplus \times cos(\lambda) \times \omega_\oplus \times cos(\phi_{GS_{tf}}) \\ 0 \end{bmatrix} \tag{8.25}$$

8.5 Background for Results

Recall in the derivation of the Dynamic TMN differential correction algorithm that due to all of the variational equations, new units need to be introduced in order to efficiently

complete the computations required through the algorithm. According to [3] and [4], it is acceptable to define the constants DU and TU. The DU is simply the radius of the Earth (1 DU = 6378.137 km) and to simplify the system models, the Earth's Gravitational Parameter, μ, will equal 1 if TU = 806.811 seconds.

Throughout the results of this study, the satellite range, η, used was 1800 km. The margin for error was 5%, allowing for a maximum sphere radius of 1890 km, or 0.2963 DU. The range for the ground station, γ, was 35000 km, or 5.4875 DU with no margin. The required elevation angle between the ground locations and the maneuvering satellite was $> 10°$.

It is also of note that this study focused only on prograde orbits, therefore inclination, i, is between 0° and 90° for both the maneuvering and non-maneuvering satellites. Additionally, the following results are illustrated for one single value of ballistic coefficient for the maneuvering satellite. That value is 0.044, which is a reasonable value from Reference [48]. The cooperative satellites, however, will follow only 2-body dynamics. It is also important to keep in mind that the goal of this study is to deliver the maneuvering satellite within the overlapping region of the spheres of the non-maneuvering satellites, within the range and elevation constraints of the ground locations within one day, 86400 seconds. For this particular demonstration, there are only 2 cooperative satellites and for illustration purposes their orbits are multiples of 86400 seconds, therefore they will be at the same location over the Earth every 86400 seconds.

Overall, there are two viable solutions for solving this problem within the provided time constraints. One is the solution that executes a maneuver to allow Satellite 1 to achieve a 24 hour period and become in phase with the combination of cooperative satellites' orbital periods. The second, is to execute a maneuver only to offset the perturbations in order for Satellite 1 to satisfy the constraints when the cooperative satellites' orbital periods are aligned.

Demonstrating the effectiveness of the algorithm throughout these results is paramount. Some interesting characteristics of the problem design are also realized. These results are presented for two separate scenarios. Each scenario has one maneuvering satellite. The first is a scenario with two cooperative satellites, for a total of three satellites with one ground location. The second is a scenario with two cooperative satellites, for a total of three satellites with two ground locations. Because of the constrained transfer time of 86400 seconds, Table 8.1 displays the initial conditions for the satellites.

Table 8.1: Initial Orbit Information for Maneuvering and Cooperative Satellites.

	Maneuvering Sat	Coop Sat 1	Coop Sat 2
Semi-major Axis, a (DU)	1.264	1.043	1.264
Eccentricity, e	0	0	0.175
Period (TU)	8.924	6.693	8.924

8.6 Results and Discussion

8.6.1 Results for Phasing Maneuver.

The phasing maneuver solution for this problem is simply allowing the algorithm to find the solution that applies the tangential ΔV required to place the maneuvering satellite in phase with the cooperative satellites. In this particular problem, the phasing maneuver is the maneuver that places the maneuvering satellite in a 24 hour period, in order to demonstrate the Dynamic TMN algorithm's ability to incorporate the ground locations into the solution. A thorough analysis was completed to determine orbit design trade-offs for this problem.

Since the thrust of this problem was to incorporate the ground location impact into the Dynamic TMN algorithm's solution, the phasing maneuver analysis will look at the

contributions from the ground locations first. Recall that the the ground locations were initially placed randomly while satisfying the range and elevation constraints for the cooperative satellites. Interestingly, patterns emerge from the algorithm's solution based on the maneuvering satellite's initial inclination and the elevation angle from the ground locations to the maneuvering satellite. Figure 8.2 illustrates this relationship. Keep in mind that the elevation angle is an average for the number of ground locations.

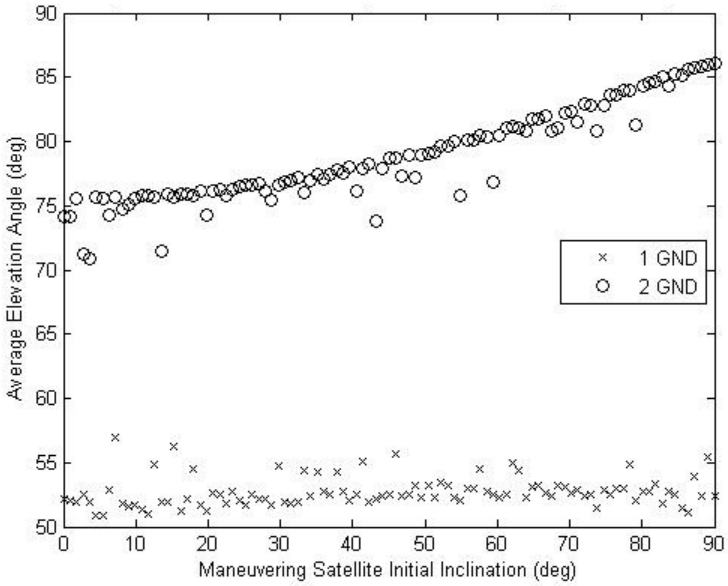

Figure 8.2: Maneuvering Satellite Inclination vs. Final Ground Elevation Angle.

The minimum elevation angle that was allowed for this scenario was 10°, therefore every solution satisfies the elevation constraint. Figure 8.3 illustrates the relationship between the maneuvering satellite and the initial elevation angle from the ground locations. Comparing the results between Figures 8.2 and 8.3 clearly portrays that there exists an impact from the ground locations on the Dynamic TMN algorithm's solution.

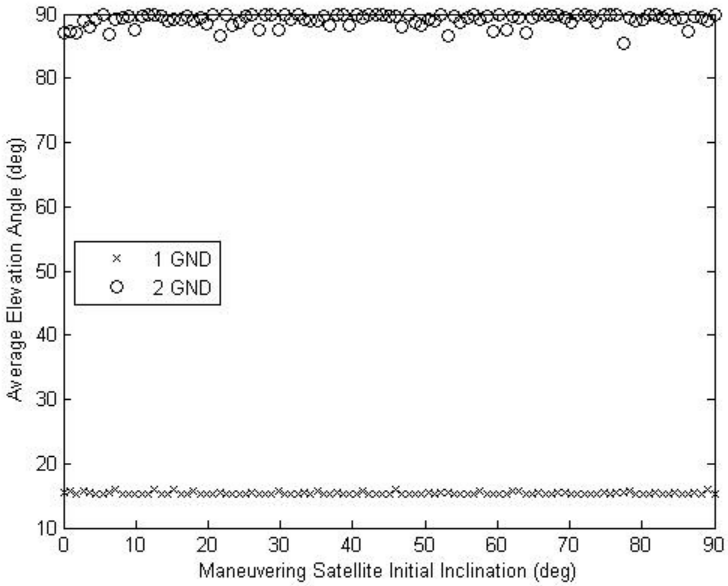

Figure 8.3: Maneuvering Satellite Inclination vs. Initial Ground Elevation Angle.

The second constraint of the ground location was the range. The range limit for these results was large and according to the results in Figure 8.4, the range constraint was satisfied. Again, keep in mind that the miss distance, is an average based on the number of ground locations. Considering that the maneuvering satellite is beginning at an altitude of ≈1680 km, it is clear there is an impact on the final distance between the ground location and the maneuvering satellite after the phasing maneuver.

Figure 8.5 illustrates how the Dynamic TMN algorithm also incorporates the cooperative satellites into the solution to meet the constraints. Recall, that the sphere range for the cooperative satellites was 1800 km, with a 5% margin for a maximum range of 1890 km. Fortunately, the results portrayed in Figure 8.5 illustrate that this constraint was satisfied. Further, the results highlight that the cooperative satellites have an impact on the solution due to the initial separation distance of ≈1406 km.

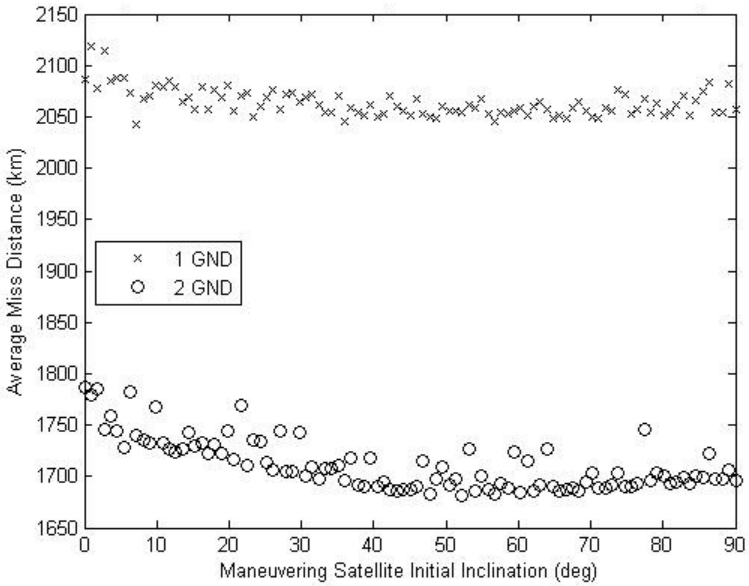

Figure 8.4: Maneuvering Satellite Inclination vs. Average Ground to Maneuvering Satellite Range.

The most significant information gleaned from the Dynamic TMN algorithm is presented in Figure 8.6. The required ΔV is normalized based on the transfer time in TUs. Therefore, the difference between the normalized value of 22.677 and 22.68 is a realized value of 0.325 $\frac{m}{sec}$. Even though the difference between the highest and lowest required ΔV is less than 0.325$\frac{m}{sec}$, a clear predictable pattern is seen based on the maneuvering satellite's initial inclination.

Specifically, a 4^{th} degree polynomial provides an approximation for the required ΔV, based on the maneuvering satellite's initial inclination, i. The frame of the equation is in Eq.(8.26) with the values for the coefficients in Table 8.2 for the empirical solution.

$$\Delta V = Ai^4 + Bi^3 + Ci^2 + Di + E \tag{8.26}$$

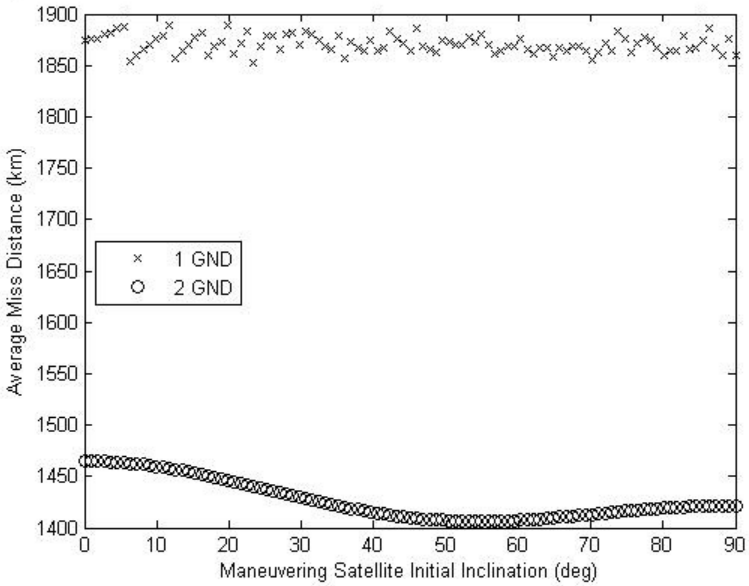

Figure 8.5: Maneuvering Satellite Inclination vs. Average Satellite Miss Distance.

Table 8.2: Coefficients for Empirical Solution for Required ΔV for Phasing Maneuver.

Coefficients	1 Ground Location	2 Ground Locations
A	-7.794×10^{-12}	1.444×10^{-15}
B	1.321×10^{-9}	7.854×10^{-9}
C	-1.321×10^{-7}	-1.06×10^{-6}
D	6.806×10^{-6}	3.675×10^{-6}
E	22.67	22.68

For the prograde inclinations for the maneuvering satellite, Figure 8.7, captures the empirical solution for the required ΔV, demonstrating the impact of multiple cooperative satellites and ground locations on the solution from the Dynamic TMN algorithm.

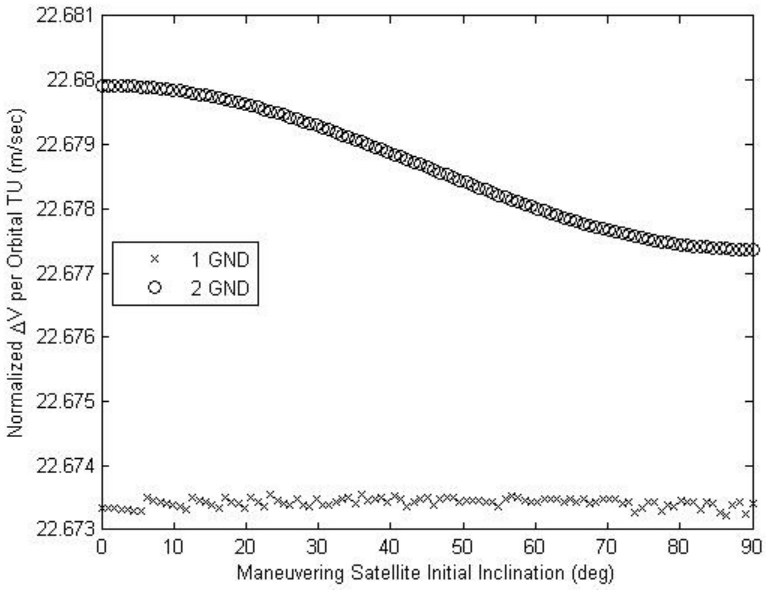

Figure 8.6: Maneuvering Satellite Inclination vs. Normalized ΔV.

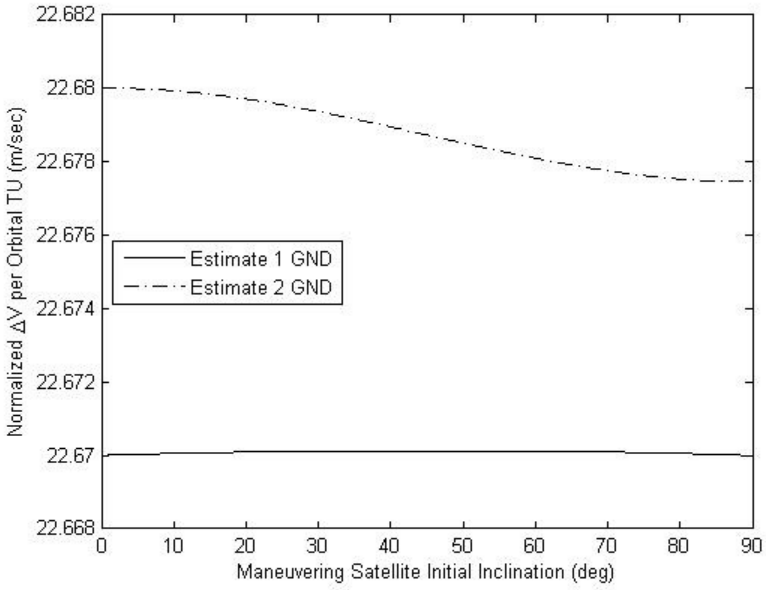

Figure 8.7: Maneuvering Satellite Inclination vs. Normalized ΔV.

Figures 8.14 through 8.21 in the this chapter's Appendix complete the analysis performed for the phasing maneuver solution for this problem.

8.6.2 Results without Phasing Maneuver.

Recall that the solution without the phasing maneuver is the impulsive burn that offsets the perturbations over the duration of the scenario. Specifically, for this scenario, the time was 86400 seconds. Since the initial maneuvering satellite and cooperative satellites' orbits share 86400 seconds as a common multiple, it is possible to view the results of the Dynamic TMN algorithm with the ground locations.

Keep in mind that the ground locations were initially placed randomly, while satisfying the range and elevation constraints for the cooperative satellites. The maneuvering satellite's inclination versus the initial elevation angle is displayed in Figure 8.8. The ground locations' impact on the Dynamic TMN algorithm is apparent in Figure 8.9.

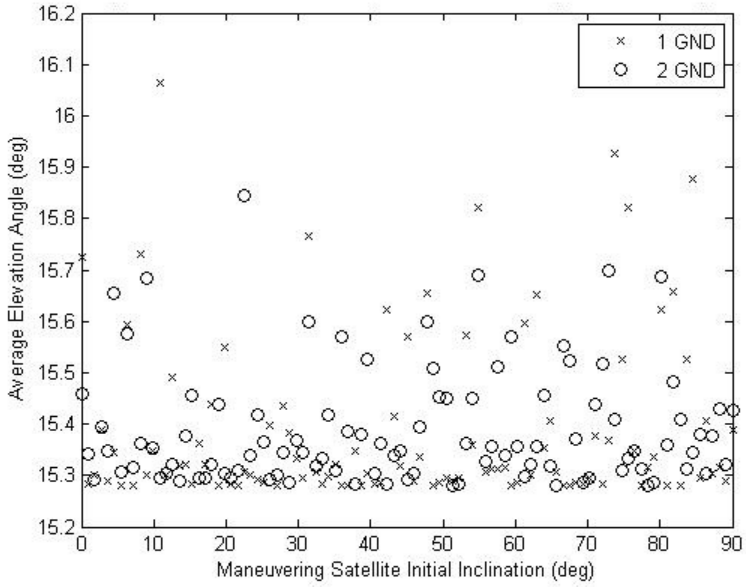

Figure 8.8: Maneuvering Satellite Inclination vs. Ground Elevation Angle.

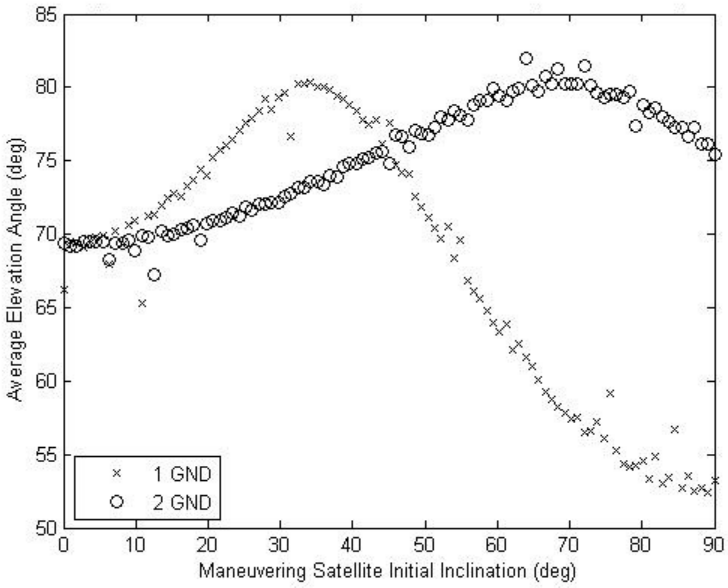

Figure 8.9: Maneuvering Satellite Inclination vs. Ground Elevation Angle.

Notice that the elevation angle is an average for the number of ground locations. The minimum value that was allowed for this scenario was 10°. Therefore, every solution satisfies the elevation constraint. Based on the initial conditions these results clearly portray the impact of the ground locations on the Dynamic TMN algorithm's solution.

The additional constraint regarding the ground locations was the range. Figure 8.10 clearly demonstrates that the range requirement is satisfied. The figure also illustrates that the ground locations have a clear impact on the Dynamic TMN algorithm's results simply from the fact that the initial maneuvering satellite altitude was ≈1680 km. Every value of maneuvering satellite inclination yields an average miss distance from the ground location that is greater than the maneuvering satellite's initial altitude.

The cooperative satellites still have an impact on the Dynamic TMN algorithm's solution. Figure 8.11 displays the relationship between the maneuvering satellite's initial

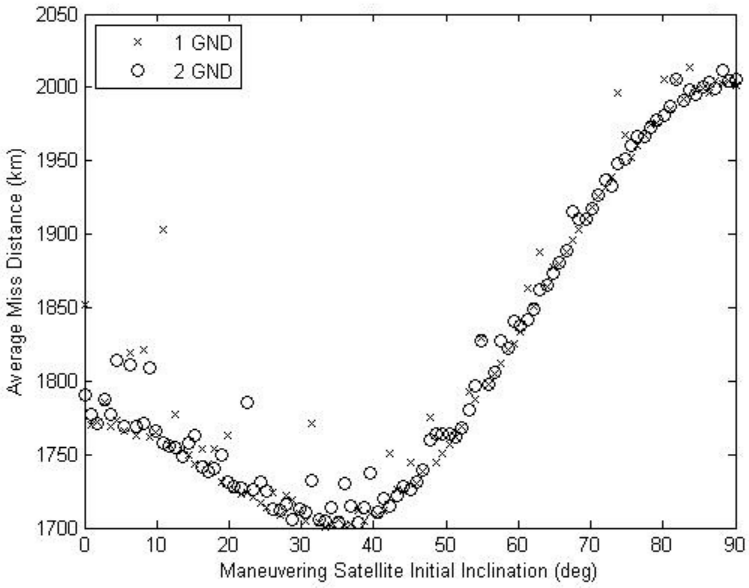

Figure 8.10: Maneuvering Satellite Inclination vs. Average Ground Miss Distance.

inclination and final average separation distance between the maneuvering satellite and the cooperative satellites. The results in Figure 8.11 are promising for showing the contribution of the cooperative satellites on the Dynamic TMN algorithm's solution since the initial separation distance between the maneuvering and cooperative satellites is ≈1406 km, with a limit of 1890 km. Clearly the constraints imposed by the cooperative satellites on the solution are satisfied.

Again, the most significant information gleaned from the Dynamic TMN algorithm for the maneuver without phasing is presented in Figure 8.12. The required ΔV is normalized based on the transfer time in TUs. Therefore, the difference between the normalized value of 0.07 and 0 is a realized value of 7.496 $\frac{m}{sec}$. A clear predictable solution for the required ΔV is evident based on the maneuvering satellite's initial inclination.

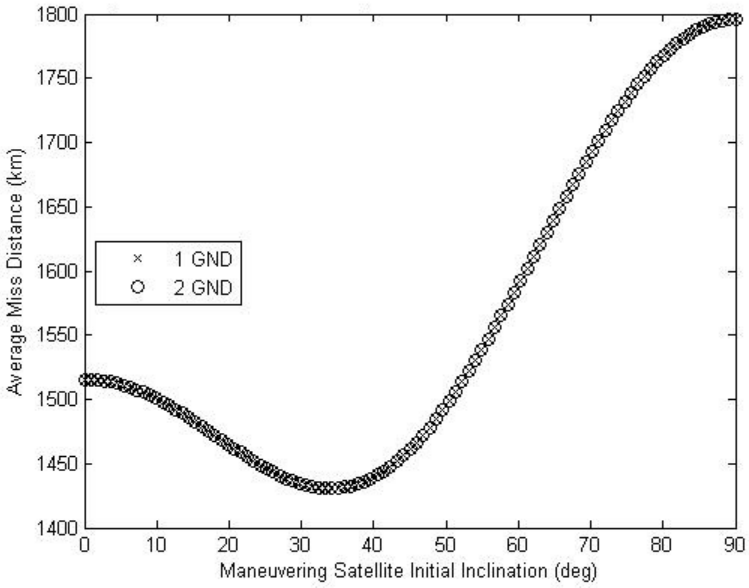

Figure 8.11: Maneuvering Satellite Inclination vs. Average Satellite Miss Distance.

A 3^{rd} degree polynomial provides an approximation of the required ΔV based on the maneuvering satellite's initial inclination, i. The frame of the equation is in Eq.(8.27) with the values for the coefficients in Table 8.3 for the empirical solution. The empirical expression is broken into two parts to account for the minimum at 54.9°. The second column of Table 8.3 show the values from 0° to 54.9°, while the third column is for inclinations from 55° to 90°.

$$\Delta V = Ai^3 + Bi^2 + Ci + D \tag{8.27}$$

For the prograde inclinations for the maneuvering satellite, Figure 8.13 captures the empirical solution for the required ΔV. These results demonstrate the impact of multiple cooperative satellites and ground locations on the solution from the Dynamic TMN algorithm.

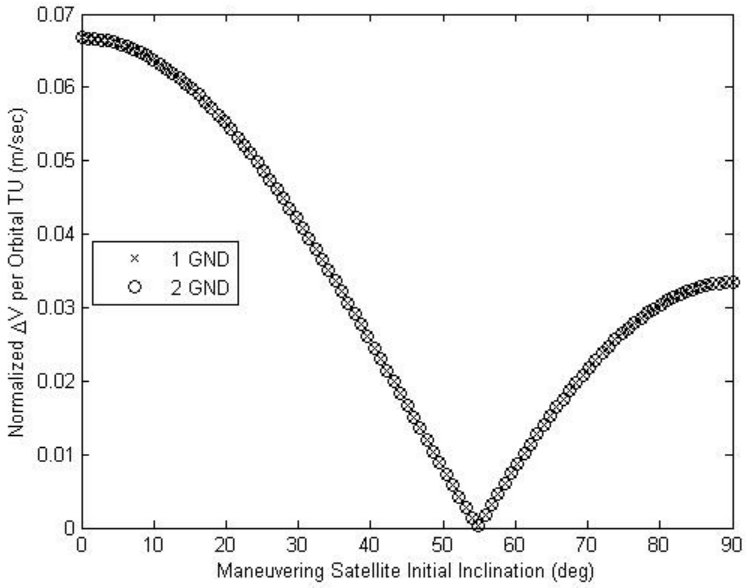

Figure 8.12: Maneuvering Satellite Inclination vs. Normalized ΔV.

Table 8.3: Coefficients for Empirical Solution for Required ΔV Without Phasing Maneuver.

Coefficients	$0° \leq i \leq 54.9°$	$55° \leq i \leq 90°$
A	2.803×10^{-7}	-1.951×10^{-7}
B	-3.943×10^{-5}	1.808×10^{-5}
C	1.032×10^{-4}	1.457×10^{-3}
D	0.0665	−0.102

Figures 8.22 through 8.28 in the Appendix complete the analysis performed for the Dynamic TMN algorithm's solution without the phasing maneuver for this problem.

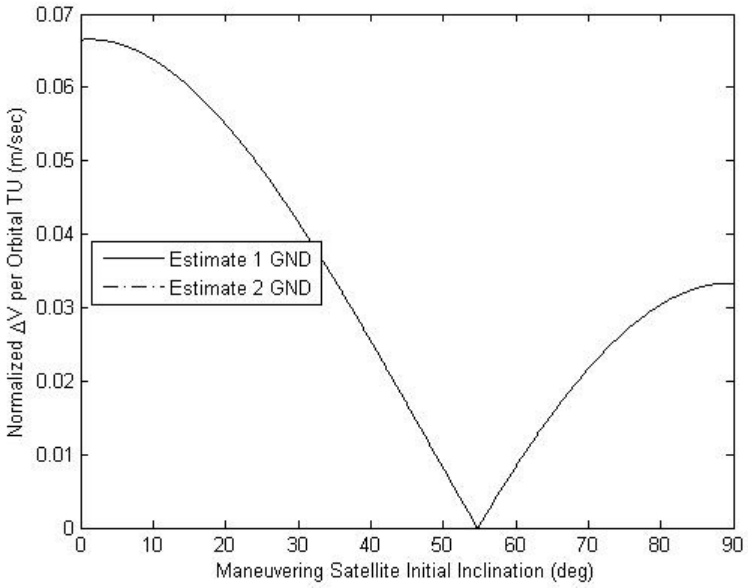

Figure 8.13: Maneuvering Satellite Inclination vs. Normalized ΔV.

8.7 Chapter Summary

This chapter presented the Dynamic T-Matrix Navigation algorithm to deliver an impulsive maneuver to place a satellite within the overlapping spheres of user-defined radius, centered around multiple non-maneuvering satellites, within a constrained time. The solution was also required to satisfy range and elevation constraints of multiple ground locations. The methodology and results were presented for the non-maneuvering satellites, beginning at a perigee altitude of 274 km and a maneuvering satellite, beginning along the same unit position vector at an altitude of 1680 km. The sphere radius for the cooperative satellites was 1800 km, with a 5% margin, allowing for a solution when the maneuvering satellite returns to within 1890 km of the non-maneuvering satellites. The range between the ground locations and the maneuvering satellite was constrained to 35000 km with an elevation $\geq 10^{\circ}$. The presented results were constrained to prograde orbits. In the end, the focus of the results was based on the success of the Dynamic T-Matrix Navigation algorithm, while demonstrating unique information about this problem. The most significant orbit design consideration studied was the maneuvering satellite's initial inclination. The capstone of the study is the ability for the user to empirically predict the necessary ΔV for a desired maneuvering satellite's initial inclination for both a phasing orbit solution and a solution without a phasing orbit. Specifically, a prediction of the required ΔV for the phasing orbit solution provides a nearly constant result of $2{,}428.12\frac{m}{sec}$ with a margin of $\pm 0.5\frac{m}{sec}$ regardless of initial maneuvering satellite inclination. The non-phasing maneuver results obviously yielded a significantly lower required ΔV. The results also demonstrated that a minimum fuel inclination exists at 54.9°. The maximum fuel initial inclination is 0°. The maximum fuel solution was $7.23\frac{m}{sec}$ with the minimum being $\approx 0\frac{m}{sec}$.

8.8 Chapter Appendix

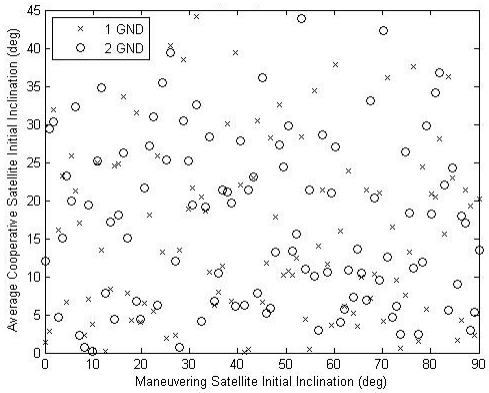

Figure 8.14: Maneuvering Satellite Inclination vs. Average Cooperative Satellite Inclination.

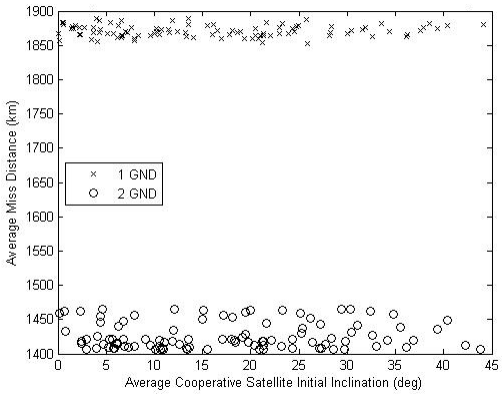

Figure 8.15: Average Cooperative Satellite Inclination vs. Satellite Miss Distance.

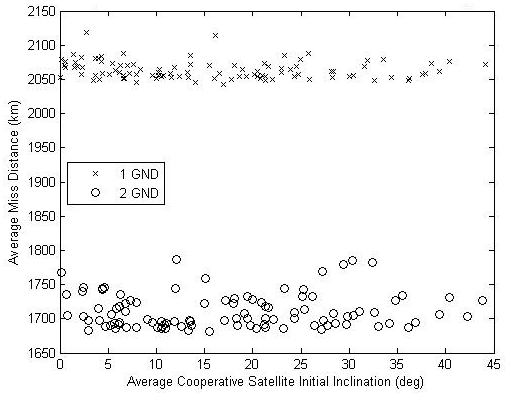

Figure 8.16: Average Cooperative Satellite Inclination vs. Ground Miss Distance.

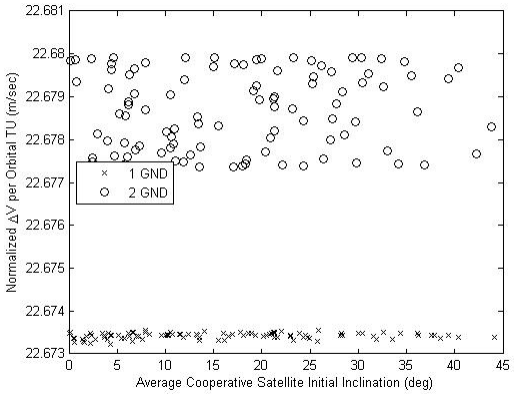

Figure 8.17: Average Cooperative Satellite Inclination vs. Normalized ΔV.

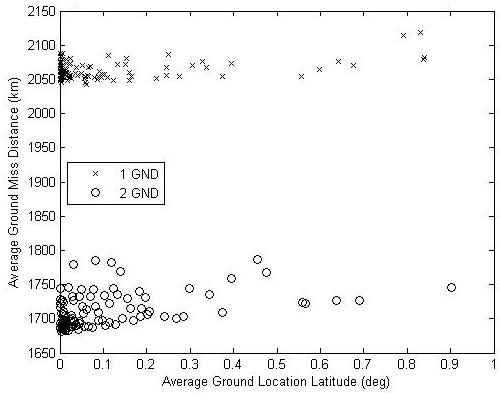

Figure 8.18: Ground Latitude vs. Ground Miss Distance.

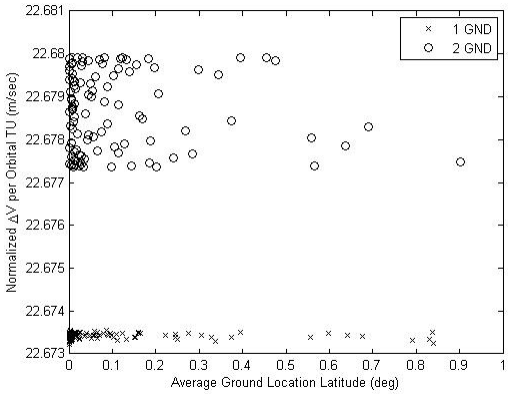

Figure 8.19: Ground Latitude vs. Normalized ΔV.

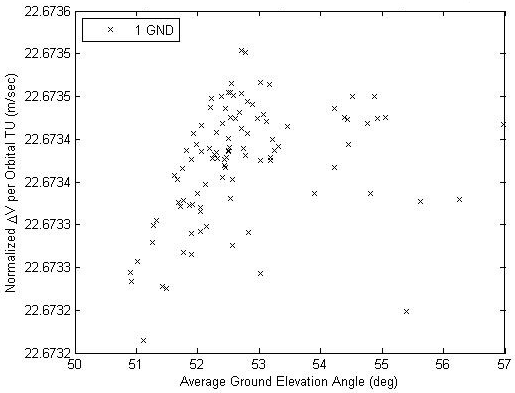

Figure 8.20: Ground Elevation Angle vs. Normalized ΔV.

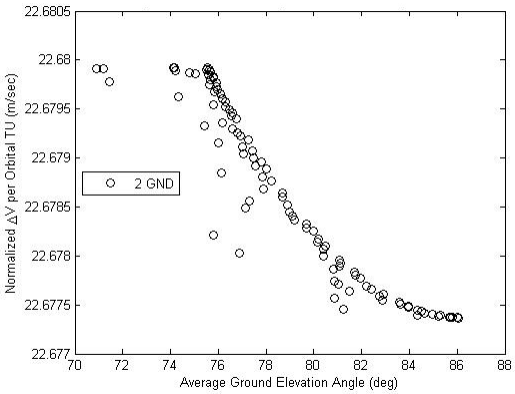

Figure 8.21: Ground Elevation Angle vs. Normalized ΔV.

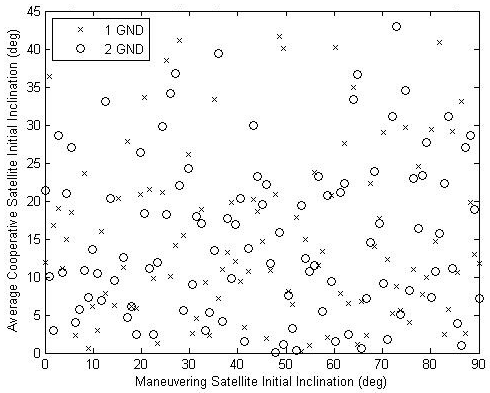

Figure 8.22: Maneuvering Satellite Inclination vs. Average Cooperative Satellite Inclination.

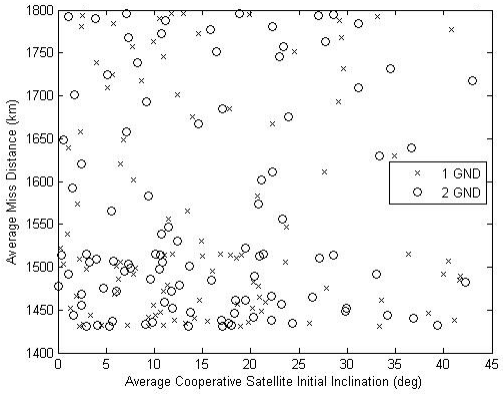

Figure 8.23: Average Cooperative Satellite Inclination vs. Satellite Miss Distance.

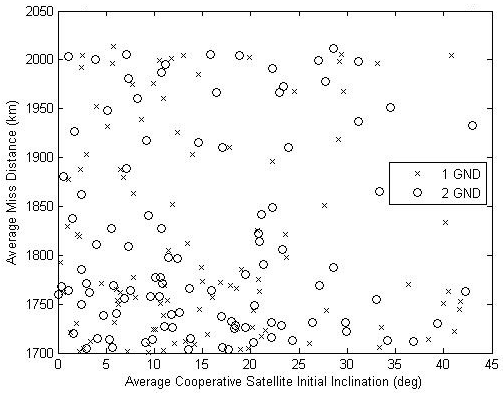

Figure 8.24: Average Cooperative Satellite Inclination vs. Ground Miss Distance.

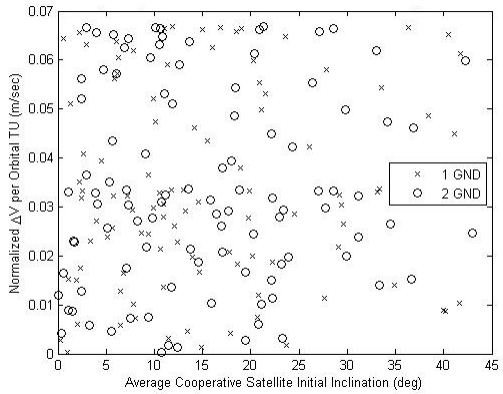

Figure 8.25: Average Cooperative Satellite Inclination vs. Normalized ΔV.

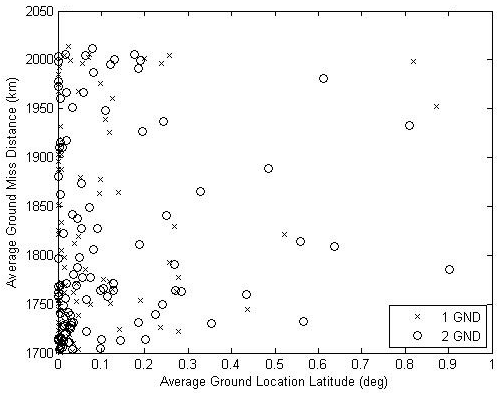

Figure 8.26: Ground Latitude vs. Ground Miss Distance.

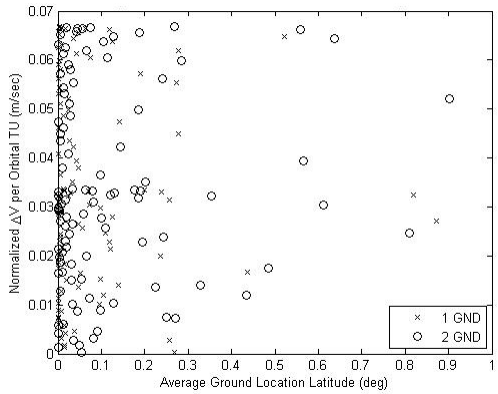

Figure 8.27: Ground Latitude vs. Normalized ΔV.

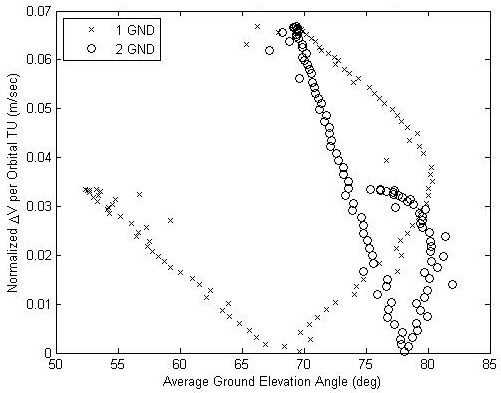

Figure 8.28: Final Ground Elevation Angle vs. Normalized ΔV.

IX. Conclusions and Contributions

Throughout this research many conclusions and contributions were drawn. This chapter presents the major findings.

9.1 T-Matrix Navigation for Tangential Burns

The first significant contribution of this research was the demonstration of the TMN algorithm to solve for the first burn of a Hohmann Transfer. This is significant because it has been clearly documented and demonstrated that, provided the limitations (Chapter 5), the Hohmann Transfer is the minimum fuel maneuver to execute satellite transfer. Therefore by extension, demonstrating the ability for the TMN algorithm to determine the magnitude and transfer time identical to the first burn of the Hohmann Transfer also proves optimality which is provided by the TMN algorithm. Further limitations of the Hohmann Transfer claim to maneuver only from a circular orbit. This research demonstrated that the TMN algorithm can deliver the minimum fuel, impulsive maneuver to transfer a satellite from perigee of an elliptical orbit to a circular orbit, 180° from the maneuver point. So, regardless of the initial orbit's eccentricity, the TMN algorithm was shown to solve for the minimum fuel, impulsive tangential maneuver to execute a satellite transfer 180° from the maneuver point.

Provided the foundation for the minimum fuel maneuver, this research also delivered the ability to analyze mission design trade-offs utilizing the TMN algorithm. The trade-offs include the satellite's ballistic coefficient, initial orbit's apogee height, initial orbit's specific mechanical energy, initial orbit's eccentricity and the initial orbit's inclination. This analysis was presented for the impact on the required ΔV.

9.2 T-Matrix Navigation for Minimum Time Trajectories

The second major contribution of this research was the development of the TMN algorithm to execute fixed ΔV minimum time maneuvers. Through a straightforward modification of the error vector development within the TMN algorithm the user can specify the ΔV and the algorithm will proceed to determine the transfer time. Provided that there is a unique time solution for each ΔV from a unique starting point to a unique ending point allows for the declaration of the minimum time trajectory. A comparison to literature results proves that the TMN algorithm delivers accurate solutions for the final angle and transfer time for these trajectories.

Further conclusions can be drawn for mission design parameters. These include the relationship between the rendezvous angle and transfer time, the required ΔV versus the transfer time and the ΔV versus the rendezvous angle. All of the aforementioned conclusions are drawn for various values for the satellite's ballistic coefficient.

9.3 T-Matrix Navigation for Relative Satellite Motion

The next major contribution of this research was the development of the TMN algorithm to provide the required impulsive maneuver to place a satellite within a user-defined geometry relative to another satellite. Specifically, modifications to the TMN algorithm allowed for a user-defined radius around a non-maneuvering satellite to define the valid solution space for the TMN algorithm. The definition of the spherical miss distance vectors is a unique development contributing to the results of this research.

Another unique development within this research was the identification of a polynomial approximation to model the required ΔV based on the semi-major axis ratio of the maneuvering and non-maneuver satellite's initial orbits. While the results are not perfect, a ROM solution is provided with the empirical models based on the maneuvering satellite's ballistic coefficient. Significant orbit design information can be gleaned from

this analysis at the onset of mission development. However, more refinement would still be required based on more mission specifics.

9.4 Dynamic T-Matrix Navigation for Relative Multiple Satellite Motion

The development of the Dynamic TMN algorithm is the next significant contribution through this research. The Dynamic TMN algorithm incorporates the relative geometry solution for the single non-maneuvering satellite and applies it towards multiple non-maneuvering satellites. Specifically, the algorithm allows for the user-defined radii for multiple satellites to define the valid solution space where the spheres overlap. The algorithm becomes dynamic from the elimination of each non-maneuvering satellite's impact on the overall solution once the sphere has been satisfied for that specific non-maneuvering satellite. If on successive iterations, the sphere is not satisfied it is then again considered for impact on the final solution for the maneuvering satellite's impulsive maneuver.

Interestingly more mission design information is leveraged from this phase of the research. The results were summarized for two possible solutions. The first solution required a phasing maneuver to align all orbital periods of the maneuvering satellite to the non-maneuvering satellites. The second solution only offset the impacts of the perturbations on the maneuvering satellite's orbit.

The phasing maneuver contributions from this research included an empirical expression for predicting the separation distance between the maneuvering satellite and the average of each non-maneuvering satellite. Also, an empirical solution for the required ΔV is derived. These results only depend on the inclination ratio between the satellites.

The contributions resulting from the solution without the phasing maneuver may be more substantial in that they also allow for predicting the separation distance as well as the required ΔV but they are only dependent on the initial maneuvering satellite's inclination. The most significant result from a mission design perspective, based on this phase of the

research, is that the minimum fuel solution for the described orbital geometry exists at a maneuvering satellite initial inclination of $\approx 53°$. Regardless of the non-maneuvering satellite's inclination, cost savings is demonstrated and achieved with these results.

9.5 Dynamic T-Matrix Navigation for Relative Multiple Satellite and Multiple Ground Location Motion

The final significant contribution from this research was the development and refinement of the Dynamic TMN algorithm to include the addition of multiple ground locations to the multiple satellite scenario. Specifically, in addition to the 'N' multiple satellites, there were introduced 'p' multiple ground locations. The algorithm allows for each to have user-defined radii and elevation constraints. The solution is where all of the spheres overlap. The algorithm is similarly dynamic to omit contributions to the solution once the solution satisfies that specific satellite's or ground location's user defined criteria. Significant results also include both the phasing maneuver and non-phasing maneuver solutions.

The phasing maneuver contributions ultimately include an empirical solution for the required ΔV to meet the mission requirements based only on the maneuvering satellite's initial inclination. While the non-phasing maneuver solution also yields a solution for the required ΔV based on the maneuvering satellite's initial inclination. Regardless of multiple satellites or multiple ground locations, the minimum fuel solution exists at an inclination of 54.9°. This result is a very important starting point for the mission design of responsive space capabilities.

9.6 Overall Conclusion

Throughout this research the ability to conceptualize and consider responsive space superiority scenarios and architectures was realized. Specifically, the algorithm presented could be leveraged to address these types of capabilities. One such capability of the

necessary architecture is to provide the ability to relay both satellite telemetry and payload communications between a ground station and the collection satellite during a responsive space scenario. Another capability is the ability to analytically predict satellite separation distances between multiple satellites. As well as develop maneuver sequences in complex dynamic scenarios. Overall, the intent of this research was to develop algorithms for determining the optimal maneuvers between a single satellite and a number of cooperative satellites including ground locations while satisfying user-defined criteria. The Dynamic T-Matrix Navigation algorithm leverages the work previously accomplished by Chioma[4] and Geisel[12]. However, the work presented in this research moves well beyond their contributions by providing to the literature proof that the algorithm can be further expanded to yield favorable results in user-defined scenarios. Moreover, the literature now has a single tool available to determine the impulsive maneuver required for satisfying the geometric criteria of multiple non-maneuvering satellites while simultaneously adhering to the range and elevation constraints of multiple ground locations. The community is also provided the ability to further expand the empirical solutions to estimate the fuel and separation distance requirements based on clear mission design criteria. Ultimately, this research yielded the ability for the reader to hone a new set of tools in order to support and execute responsive space superiority scenarios.

9.7 Areas for Continued Research

1. Multiple maneuvering satellites: Expand the Dynamic TMN algorithm to include the calculation of single impulsive maneuvers to be applied to multiple satellites based on the relative geometries.

2. Continuous thrust models: Explore the possibility of incorporating low magnitude, continuous thrust capabilities into algorithm development.

3. Various geometry solutions: Explore various geometry relationships for the solutions with multiple satellites and/or ground locations. Include sun location, moving ground locations (ships), and enhanced air drag modeling with ballistic coefficients and seasonal variations.

4. Range of limits for single relative solutions: Identify the range of valid TMN solutions for the analytical expressions for the relative single satellite scenario.

5. Range of limits for multiple relative solutions: Identify the range of valid Dynamic TMN solutions for the analytical expressions for the relative multiple satellites scenario.

6. Range of limits for multiple relative solutions including ground locations: Identify the range of valid Dynamic TMN solutions for the analytical expressions for the relative multiple satellites and multiple ground locations scenario.

Appendix: Initial Model Results

This endeavor requires establishing credibility towards the model and methodology in order to be effective. Specifically, an indepedent study was conducted in order to achieve and prove the desired level of accuracy for the system being proposed. This study pursued results to ultimately drive the system model to achieve a near zero miss distance between an interceptor and target satellite. The summary and conclusions of this study are found throughout the following sections. The goal of this study is to match the published results from Reference[4].

A.1 T-Matrix Navigation Background

T-Matrix Navigation (TMN) has its roots in nonlinear least squares. Fundamentally, it is a method to reduce the amount of residual error in a system of complex nonlinear differential equations. In order to use this method in an optimization problem, an algorithm must be implemented to adequately bound the solution space of the nonlinear system of equations while allowing the variational equations to be iterated towards a solution. Chioma presents the algorithm necessary to accomplish this [4]. Highlights from his work are presented.

In order to implement the TMN method, two orbits are needed. In this particular case, they are the target and interceptor orbits. Determining the position and velocity vectors from the provided COEs is the first step. Second, it is fundamental to identify that the position vector of the interceptor has one initial value, while the velocity vector has two. They are the velocity of the interceptor just before a manuever and just after a manuever, while still at the original position. This is highlighted in (A.1) [4] and (A.2) [4].

$$X_{int}(t_0^-) = \begin{bmatrix} R_x(t_0) \\ R_y(t_0) \\ R_z(t_0) \\ V_x(t_0^-) \\ V_y(t_0^-) \\ V_z(t_0^-) \end{bmatrix} \tag{A.1}$$

$$X_{int}(t_0^+) = \begin{bmatrix} R_x(t_0) \\ R_y(t_0) \\ R_z(t_0) \\ V_x(t_0^-) + \Delta V_x \\ V_y(t_0^-) + \Delta V_y \\ V_z(t_0^-) + \Delta V_z \end{bmatrix} \tag{A.2}$$

Understanding how the ΔV's are implemented and adjusted during each iteration through the algorithm allows the system to propogate through time to find each updated end position for each updated starting point. Therefore, for each ΔV , new position and velocity vectors at t_f can be determined.

Once the position vector in the future is determined for the interceptor that same time is used to determine the position vector of the target and an error vector is calculated. The error vector is displayed in (A.3) [4].

$$\bar{e} = \begin{bmatrix} R_{int_x} - R_{tgt_x} \\ R_{int_y} - R_{tgt_y} \\ R_{int_z} - R_{tgt_z} \\ \Delta V_{int_x} \\ \Delta V_{int_y} \\ \Delta V_{int_z} \end{bmatrix} \tag{A.3}$$

The error vector highlights the component by component miss distance between the interceptor and the target satellites as well as the applied ΔV on the interceptor.

The second major piece that needs to be determined is the interceptor's STM, Φ. The STM is determined by integrating the satellite's equations of motion as well as the variational equations of motion. This is the most computationally taxing calculation due to the fact that there are 36 variational equations combined with the 6 EOM which have to be integrated simultaneously. Even though the entire STM needs to be calculated only the upper right 3X3 portion is necessary in the TMN algorithm. The upper right portion of the STM contains the information regarding the interceptor satelite's differential position with respect to the applied ΔV. The components of the upper right portion of the STM, identifed by ϕ, is shown in equation (A.4). Notice that the necessary piece of the STM is the component that relates the interceptor's final position vector components with the initial velocity vector components. This information ultimately provides for how the various ΔV's are integrated to find the best final position in the algorithm.

$$\phi = \begin{bmatrix} \frac{\partial R_x(t_f)}{\partial V_x(t_0)} & \frac{\partial R_x(t_f)}{\partial V_y(t_0)} & \frac{\partial R_x(t_f)}{\partial V_z(t_0)} \\ \frac{\partial R_y(t_f)}{\partial V_x(t_0)} & \frac{\partial R_y(t_f)}{\partial V_y(t_0)} & \frac{\partial R_y(t_f)}{\partial V_z(t_0)} \\ \frac{\partial R_z(t_f)}{\partial V_x(t_0)} & \frac{\partial R_z(t_f)}{\partial V_y(t_0)} & \frac{\partial R_z(t_f)}{\partial V_z(t_0)} \end{bmatrix} \tag{A.4}$$

Another component necessary in the TMN algorithm is the relationship between the interceptor and target's final velocity vectors. Identifying this vector and combining this with ϕ, a form of the $\tilde{T}$ matrix is determined and shown in equation (A.5) [4]. The final **T** matrix is derived from scaling paramters combined with $\tilde{T}$.

$$\tilde{T} = \begin{bmatrix} \phi & \vec{V_{int}} - \vec{V_{tgt}} \\ 3 \times 3 & 3 \times 1 \\ \mathbf{I} & \mathbf{0} \\ 3 \times 3 & 3 \times 1 \end{bmatrix} \tag{A.5}$$

The final components of the TMN setup is the identification of a weight matrix, **Q** and a scale matrix, **S**. The weight matrix allows for the user to shift convergene focus from final position to applied ΔV. In order to maintain a balanced focus on both minimizing miss distance and fuel used, an identity matrix, **I**, should be used. For this study, **Q**, is simply a 6x6 **I** matrix. The scale matrix, **S**, is utilized to allow faster convergence within the TMN algorithm. For this study, **S** is a constant 6x6 matrix transfered directly from Reference[4]. **S** is defined in (A.6) while **T** is calculated from $\tilde{T}$ and **S** in (A.7).

$$\mathbf{S} = \begin{bmatrix} 0.1 & 0 & 0 & 0 & 0 & 0 \\ 0 & 0.1 & 0 & 0 & 0 & 0 \\ 0 & 0 & 0.1 & 0 & 0 & 0 \\ 0 & 0 & 0 & 0.1 & 0 & 0 \\ 0 & 0 & 0 & 0 & 0.1 & 0 \\ 0 & 0 & 0 & 0 & 0 & 0.1 \end{bmatrix} \tag{A.6}$$

$$\mathbf{T} = \mathbf{S}^{-1}\tilde{T} \tag{A.7}$$

Ultimately, combining all of this information, the variation of the control vector, $\vec{u}$, can be calculated. The variation of $\vec{u}$ is the core of TMN. Once the variation is within user defined tolerances, a unique solution is declared for the model. It is important to note that based on units and matrix dimensions, $\vec{u}$, will have 4 components. Specifically, the components of $\vec{u}$ are shown below in (A.8).

$$\vec{u} = \begin{bmatrix} \Delta V_{int_x} \\ \Delta V_{int_y} \\ \Delta V_{int_z} \\ \Delta t \end{bmatrix} \tag{A.8}$$

Where the ΔV terms are the changes in the initial impulsive maneuver applied to the interceptor, and the Δt term is the change in rendezvous time during each iteration. Summing the results for each component after each iteration yields the total ΔV for the impulsive manuever. Combining the sum of the Δt's with the initial orbital period, results in the final rendezvous time for the optimum ΔV.

Once the variation of the ΔV components is within 0.001 $\frac{meters}{sec}$ [4] and the variation of the Δt component is within 0.01 sec [4] on successive iterations, convergence is complete and a unique solution to the model can be declared. The development of the convergence criteria comes directly from Chioma[4]. The model iterates on equation (A.9) [4] until all the convergence criteria have been satisfied. Every iteration includes all of the previous steps for determining **T**. **Q** is the weight matrix and $\bar{e}$ is the error vector from Equation (A.3).

$$\partial u = -(\mathbf{T}'\mathbf{Q}^{-1}\mathbf{T})^{-1}\mathbf{T}\mathbf{Q}^{-1}\bar{e} \tag{A.9}$$

A.2 System Dynamics

The utility of the system model leads itself ultimately to its reliability and accuracy. For the single orbital rendezvous model, this is no different. Because of how this study was implemented, there are two separate models for the target and interceptor satellites. The first model is a numerical integration model and the second uses an analytical approach.

The numerical integration model takes into account the bulge around the equator of the Earth, J_2. It also takes into consideration the atmospheric drag on both the target and

interceptor satellites. In order to validate the atmospheric drag model, a BC for both the target and interceptor satellites has to be assumed. In this model, the target satellite's ballistic coefficient is 5x's larger than the interceptor's, which implies that the relative size to weight ratio of the target satellite to the interceptor satellite is about 5 times larger assuming the satellites have roughly the same shape and therefore the same coefficient of drag, C_D. This assumption is necessary to effectively model the atmospheric drag effects on both satellite's orbital motion. Specifically, the assumption is in line with Wertz's[26] calculations for micro-satellite technology for the interceptor satellite versus traditional technology for the target satellite.

The atmospheric model used in this model is derived from Vallado's *Fundamentals of Astrodynamics and Applications*[10]. The model looks up the atmospheric density, ρ, at each iteration of the orbital altitude and determines the impact of that density as the drag component of the satellite's acceleration represented in (A.10)[43] where $\vec{V_{REL}}$ is the satellite's relative velocity with respect to the rotating Earth.

$$\vec{a_{Drag}} = -.5 \times B^* \times \rho \times |\vec{V_{REL}}|^2 \tag{A.10}$$

With the addition of the drag term, the EOM for each satellite is captured in (A.11) and (A.12).

$$\dot{R} = \vec{V} \tag{A.11}$$

$$\dot{V} = \frac{\mu \times \vec{R}}{|\vec{R}|^3} - \frac{3}{2} \times \frac{J_2 \times \mu \times R_{EARTH}^2 \times \vec{R}}{|\vec{R}|^5} \times (1 - \frac{5 \times R_z^2}{|\vec{R}|^2}) + \vec{a_{Drag}} \tag{A.12}$$

The second system model is based on the analytical solution for the COEs at a future instant in time. In order to proceed, the Lagrange Planetary Equations in the disturbing function form are utilized[45]. The disturbing function that is utilized is accurate to J_2 and establishes the foundation for the analytical solution. Key assumptions required for the

analytical solutions include the fact that based only on J_2, the satellite's eccentricity and inclination do not change over the course of one orbital period[45]. Therefore, $e_{t_0} = e_{t_f}$ and $i_{t_0} = i_{t_f}$. The RAAN angle, Ω, is determined from (A.13).

$$\Omega = \Omega_0 + -\frac{(3 \times n \times J_2 \times R_{EARTH}^2)}{(2 \times a_0^2 \times (1 - e_0^2)^2)} \times cos(i_0) \times t \tag{A.13}$$

Knowledge of the orbital mean motion, n, and eccentric anomaly, E, are necessary to determine the initial mean anomaly, M_0. Once obtaining the expression for M_0 the future value for the semi-major axis, a, can be calculated from (A.14) [4]. Knowledge of the initial semi-major axis, a_0, the Earth's gravitation parameter, μ, Earth's second zonal harmonic constant, J_2, radius of the Earth, R_{EARTH}, mean motion, n, initial eccentricity, e_0, initial inclination, i_0, inital mean anomaly, M_0, perigee drift rate, $\dot{\omega}$ and initial argument of perigee ω_0 are required.

$$\begin{aligned} a = a_0 + ((2 \times \mu \times J_2 \times R_{EARTH}^2)/(n \times a_0^4)) \times (((3 \times e_0/n) \times (-.25 + .75 \times cos(i_0)^2) \times cos(M_0 + n \times t) \\ + (.75 - .75 \times cos(i_0)^2) \times ((-3 \times e_0)/(2 \times (n + 2 \times \dot{\omega})) \times cos((M_0 + n \times t) \\ + 2 \times (\omega_0 + \dot{\omega} \times t)) + (1/(n + \dot{\omega})) \times cos(2 \times (M_0 + n \times t) + 2 \times (\omega_0 + \dot{\omega} \times t)) \\ + ((21 \times e_0)/(2 \times (3 \times n + 2 \times \dot{\omega}))) \times cos(3 \times (M_0 + n \times t) + 2 \times (\omega_0 + \dot{\omega} \times t))) \\ -(((3 \times e_0)/n) \times (-.25 + .75 \times cos(i_0)^2) \times cos(M_0) + (.75 - .75 \times cos(i_0)^2) \times (((-3 \times e_0)/(2 \times (3 \times n + 2 \times \dot{\omega}))) \\ \times cos(M_0 + 2 \times \omega_0) + (1/(n + \dot{\omega})) \times cos(2 \times M_0 + 2 \times \omega_0) + ((21 \times e_0)/(2 \times (3 \times n + 2 \times \dot{\omega}))) \\ \times cos(3 \times M_0 + 2 \times \omega_0))))) \end{aligned} \tag{A.14}$$

The next step is to determine the partial derivatives of the disturbing function, **R** with respect to the eccentricity, inclination and semi-major axis. Wiesel[45] fully describes their derivation. It is also required to determine the partial derivative of the mean motion with respect to the semi-major axis[45].

Knowing the various partial derivatives leads to the determination of the argument of

perigee, ω, and mean anomaly at the future time. Determining the future mean anomaly then solving Kepler's problem[10] for the eccentric anomaly results in an expression for the true anomaly at the future time expressed in equation (A.15).

$$\nu = cos^{-1}(\frac{cos(E) - e}{1 - (e \times cos(E))}) \tag{A.15}$$

Ultimately, the numerical model is determined to a fidelity including J_2 and atmospheric drag, while the analytical model only accounts for J_2. Remember however, the selection of the model is not used in the determination of Φ. The method is the same in both the numerical and analytical models and requires the numerical integration of the interceptor satellite's equations of motion and the variational equations. The variational equations are the partial derivatives of the EOMs with respect to the position and velocity vector components.

A.3 Initial Conditions

Assuming the interceptor and target satellites are beginning at the same starting position, rendezvous will occur approximately one target satellite revolution later. The initial conditions for both the interceptor and target satellites are in tabular form in Table A.1. These initial conditions were directly transfered from Chioma[4]. The initial conditions are identified through each satellite's COEs.

A function was developed to convert the initial COEs to position and velocity vectors for the target and interceptor satellites. A function was also implemented to convert the initial COEs into radians, then calculate the semi-paramter value for the orbits and convert the COEs into the Perifocal Coordinate System (PQW), then rotate into the Geocentric Equatorial System. The intial position and velocity vectors for the target are represented below in (A.16).

Table A.1: Initial COEs for Target and Interceptor Satellites for Initial Model Validation

Orbital Element	Target Sat	Interceptor Sat
Semi-Major Axis, a, Earth radii	1.06	1.0709
Eccentricity, e	.005	.0152
Inclination, i, Degrees	15	40.0519
Right Ascension of Ascending Node, Ω , Degrees	45	106.3808
Argument of Perigee, ω , Degrees	70	13.3168
True Anomaly at Epoch, ν, Degrees	10	10.0182

$$\begin{aligned} \vec{R_{tgt}} &= [-3699.4, 5351.7, 1714.9]\, km \\ \vec{V_{tgt}} &= [-6.2922, -4.4529, .3485]\, \tfrac{km}{sec} \end{aligned} \tag{A.16}$$

The intial position and velocity for the interceptor are in (A.17).

$$\begin{aligned} \vec{R_{int}} &= [-3699.4, 5351.7, 1714.9]\, km \\ \vec{V_{int}} &= [-4.3738, -4.4679, 4.5868]\, \tfrac{km}{sec} \end{aligned} \tag{A.17}$$

Notice the difference in the velocity vector of the interceptor, representing an initial velocity of 7.75 $\frac{km}{sec}$ vs. 7.71 $\frac{km}{sec}$ for the target satellite. The slight difference in the initial orbits also yeilds a orbital period of 5,532 sec for the target while the interceptor has an initial orbital period of 5,618 sec. Therefore, after one revolution of both the target and interceptor satellites, they will not achieve rendezvous. In order for the interceptor satellite to meet the target satellite, a maneuver is necessary.

A.4 No Maneuver

Since it is only intuitively obvious that a maneuver is necessary to achieve rendezvous, Figure A.1 displays the position of the interceptor satellite after just one orbital period

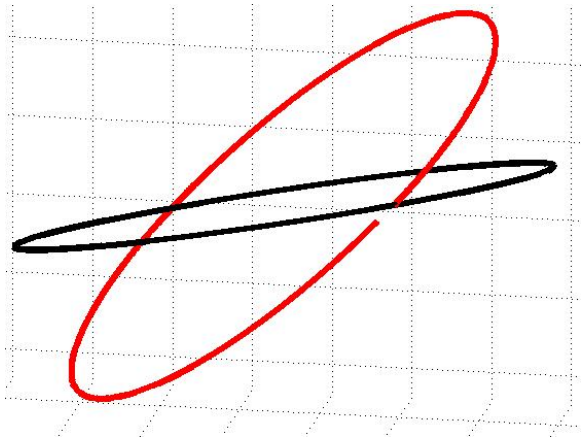

Figure A.1: Initial Miss Distance After One Target Satellite Revolution

of the target satellite. Remember, the satellites began at the same position with different velocities. Therefore, after one orbit, the miss distance between the interceptor and target satellite is 681.77 km. This demonstrates the necessity of executing a maneuver to achieve rendezvous.

A.5 Collinear Burn

A.5.1 Initial Conditions.

The collinear burn is executed using the same initial conditions highlighted in Table A.1. Therefore, the position of the interceptor and target satellites are identical at t=0 with different initial velocities. However, in order to initiate the algorithm, initial conditions must be assumed to search for the minimum fuel maneuver to achieve the closest possible intercept approximately one orbit later. A fundamental understanding of the initial orbits is necessary to drive the observation that to achieve the intercept one orbit later, the interceptor's orbital period must be nearly identical to the target's orbital period. Therefore the initial guess for the time of closest intercept is the original orbital period of the target satellite, 5,532 sec. In order to achieve this specific time an initial ΔV is required, -38.6 $\frac{m}{sec}$.

A.5.2 Collinear Methodology.

The T-Matrix Navigation algorithm is previously highlighted in sections A.1 and A.2. However, a few modifications are necessary in order to implement the algorithm in the collinear case. The collinear model for achieving intercept of the target satellite assumes that the only direction that the velocity can be changed is along the initial velocity direction. Therefore, the ΔV can only be in the + or - original velocity's direction. This requires that the algorithm be adjusted to accomodate this limitation. Specifically, the $\tilde{T}$ matrix is adjusted to include a sensitivity portion based on the the STM sub matrix, ϕ shown in equation (A.18)[4].

$$\tilde{T} = \begin{bmatrix} \phi \times \frac{\vec{V_0}}{|\vec{V_0}|} & \vec{V_{int}} - \vec{V_{tgt}} \\ 3 \times 1 & 3 \times 1 \end{bmatrix} \tag{A.18}$$

$\tilde{T}$ is a 3x2 matrix. Utilizing a 3x3 **S** matrix, converting $\tilde{T}$ into **T** yields different dimensions than the full 3-D case. This is necessary since the maneuver is only allowed to happen in the +/- original velocity direction for the interceptor. Noticing this change in dimension of **T** requires a slight modification to the error vector, $\bar{e}$ shown in (A.19).

$$\bar{e} = \begin{bmatrix} R_{int_x} - R_{tgt_x} \\ R_{int_y} - R_{tgt_y} \\ R_{int_z} - R_{tgt_z} \end{bmatrix} \tag{A.19}$$

Other than the updated matrix dimensions, the TMN algorithm will proceed as described in Section A.1 with a 3x3 **I** for **Q**.

A.5.3 Collinear Integration.

Utilizing the system dynamics described in Section A.2, a 4th order Runge-Kutta numerical integrator was implemented. Provided the overall initial conditions and the initial conditions specific to the collinear burn case, the target and interceptor satellites are propogated via numerical integration. Table A.2 summarizes the performance of the

TMN algorithm on finding the minimum fuel expended solution for this model. These results are validated as the minimum from an analysis completed in Reference[4].

Table A.2: Results for Collinear Burn via Numerical Integration for Initial Model Validation

Miss Distance, meters	440.0933
ΔV, $\frac{meters}{sec}$	-41.2701
Rendezvous Time, seconds	5512.9
Number of Algorithm Iterations	4

Of note is the relatively high miss distance of 440 m. Keep in mind that with no maneuver the miss distance was 681 km. Knowing that the maneuver is constrained to only occur in the + or - velocity direction directly impacts this value.

A.5.4 Collinear Analytical.

The only change in the analytical approach over the collinear numerical integration is using the analytic method highlighted in Section A.2. The analytic method determines the future value of both the target and interceptor satellite's COEs at a specified future time. Table A.3 displays the results of TMN limited to a collinear burn using the analytical method.

Interestingly, the analytical method yields a lower possible ΔV, but it converges to a further miss distance of 492 meters. It is also of interest that the analytical method, in the TMN algorithm, computes a rendezvous time that is about 4.5 seconds later than the numerical integration method.

Table A.3: Results for Collinear Burn via Analytic Approach for Initial Model Validation

Miss Distance, meters	492.4583
ΔV, $\frac{meters}{sec}$	-41.0111
Rendezvous Time, seconds	5517.3
Number of Algorithm Iterations	3

A.6 Coplanar Burn

A.6.1 Initial Conditions.

The coplanar burn is executed using the same initial conditions highlighted in Table A.1. Therefore, the position of the interceptor and target satellites are identical at t=0 with different initial velocities. Similar to the collinear cases, in order to initiate the algorithm, initial conditions must be tailored to the coplanar assumptions. These assumptions allow the algorithm to search for the minimum fuel expended maneuver in order to achieve the closest possible intercept approximately one orbit later. As above, the initial guess for the time of closest intercept is the original orbital period of the target satellite, 5,532 sec. In order to achieve this specific time an initial ΔV is required in the amount of -38.6 $\frac{m}{sec}$.

A.6.2 Coplanar Methodology.

The coplanar maneuver removes the constraint that the impulsive burn must be exectuted only in the + or - velocity direction. It also allows for the maneuver to occur in the radial direction of the satellite in its orbit. Combining the velocity and radial componenents obviously leads to an overall 3-D manuever, but the algorithm is constrained to apply the velocity changes along the unit vectors of the original position vector and the original velocity vectors. The initial ΔV is applied only in the velocity direction. While the initial ΔV in the radial direction is 0.

Additional modifications are necessary to the TMN method described in Section A.1.

For the coplanar case the $\tilde{T}$ matrix is modified from the collinear version to include an additional sensitivity matrix based on the original position and velocity vectors of the interceptor. The sensitivity matrix is a combination of the upper right portion, ϕ, of the interceptor's state transition matrix and the unit vectors for the interceptor satellite's original position and velocity vectors. The modified $\tilde{T}$ matrix is identified in equation (A.20)[4].

$$\tilde{T} = \begin{bmatrix} \phi \times \frac{\vec{V_0}}{|\vec{V_0}|} & \phi \times \frac{\vec{R_0}}{|\vec{R_0}|} & \vec{V_{int}} - \vec{V_{tgt}} \\ 3 \times 1 & 3 \times 1 & 3 \times 1 \end{bmatrix} \tag{A.20}$$

Even though the sensitivity portion to the original position vector was added, the **T** matrix is similarly derived. Since the dimensions are consistent, the same error vector, $\bar{e}$ shown in (A.19), will be used in the coplanar case as in the collinear case. Other than the noted changes the algorithm proceeds as outlined in section A.1.

A.6.3 Coplanar Integration.

Utilizing the system dynamics described in Section A.2, a 4th order Runge-Kutta numerical integrator was implemented. Provided the overall initial conditions and the initial conditions specific to the coplanar burn case, the target and interceptor satellites are propogated via numerical integration. Table A.4 summarizes the performance of the TMN algorithm on finding the minimum fuel expended solution for this model.

An immediate observation is that the overall miss distance of the model has been reduced to a mere 3.2 meters while expending .01 $\frac{m}{sec}$ less fuel than the collinear numerical integration method. This is a reasonable result due to the model's ability to apply the ΔV along both the +/- radial and velocity directions of the original interceptor's position and velocity vectors respectively. Similar to the collinear numerical integration method, the coplanar numerical integration method yields an optimum rendezvous time of 5,512.9 seconds.

Table A.4: Results for Coplanar Burn via Numerical Integration for Initial Model Validation

Miss Distance, meters	3.2241
ΔV, $\frac{meters}{sec}$	-41.2644
Rendezvous Time, seconds	5512.9
Number of Algorithm Iterations	5

A.6.4 Coplanar Analytical.

The only change in the analytical approach over the coplanar numerical integration is using the analytic method highlighted in Section A.2. Table A.5 displays the results of TMN limited to the coplanar maneuver described using the analytical method.

Table A.5: Results for Coplanar Burn via Analytic Approach for Initial Model Validation

Miss Distance, meters	.0103
ΔV, $\frac{meters}{sec}$	-41.0524
Rendezvous Time, seconds	5517.3
Number of Algorithm Iterations	28

A significant improvement in miss distance is achieved using the analytical method for the coplanar maneuver. A miss distance of 0.0103 meters is achieved with a ΔV savings of approximately 0.21 $\frac{m}{sec}$ over the numerically integrated approach. Also note, the analytic rendezvous time is identical to the collinear analytical rendezvous time.

A.7 3-Dimensional Burn

A.7.1 Initial Conditions.

The 3-Dimensional burn is executed using the same initial conditions highlighted in Table A.1. Therefore, the position of the interceptor and target satellites are identical at t=0 with different initial velocities. Previously identified assumptions for the initial guess for the time of closest intercept is the original orbital period of the target satellite, 5,532 sec and an initial ΔV of -38.6 $\frac{m}{sec}$.

A.7.2 3-D Methodology.

The 3-D manuever removes the constraint that the impulsive burn must be exectuted only in the velocity or radial directions. It ultimately allows for a maneuver within the full 3-D space. The algorithm is no longer constrained to executing the maneuver in any particular direction allowing a full use of the search space. The initial ΔV is applied along all three dimensions of the original velocity vector according to the unit vector of the interceptor's initial velocity.

No modifications are necessary to the TMN method described in Section A.1. Specifically, the scale matrix, **S**, is as defined in (A.6). Therefore, **T** is a 6x4 matrix, **Q** is a 6x6 **I** matrix and $\bar{e}$ is a 6x1 vector highlighted in (A.3).

A.7.3 3-D Integration.

Utilizing the system dynamics described in Section A.2, a 4th order Runge-Kutta numerical integrator was implemented. Provided the overall initial conditions and the initial conditions specific to the 3-D burn case, the target and interceptor satellites are propogated via numerical integration. Table A.6 summarizes the performance of the TMN algorithm on finding the minimum fuel expended solution for this model.

Noteworthy, is the fact that the miss distance of the 3-D numerical integration method increases to 0.7215 meters over the coplanar analytic method. While this is still a very good result it highlights the discrepancy introduced into the model with the modified error

Table A.6: Results for 3-Dimensional Burn via Numerical Integration for Initial Model Validation

Miss Distance, meters	.7215
ΔV, $\frac{meters}{sec}$	-41.2634
Rendezvous Time, seconds	5512.9
Number of Algorithm Iterations	27

vector in equation (A.3). The full 3-D case requires the introduction of the applied ΔV's, therefore a different solution is expected. However, as anticipated, for all of the numerically integrated approaches it ultimately yields the best result for overall miss distance.

A.7.4 3-D Analytical.

The only change in the analytical approach over the 3-D numerical integration is using the analytic method in section A.2. Table A.7 displays the results of the unconstrained TMN.

Table A.7: Results for 3-Dimensional Burn via Analytic Approach for Initial Model Validation

Miss Distance, meters	1.718
ΔV, $\frac{meters}{sec}$	-41.0505
Rendezvous Time, seconds	5517.3
Number of Algorithm Iterations	46

Executing the 3-D analytical approach yields a favorable miss distance of 1.718 meters, but it is not an improvement over the coplanar analytical solution. Most likely this is due to the increased value of $\bar{e}$ including adjustments for each ΔV.

A.8 Conclusions

The overall results of the study are summarized in Table A.8. As you can see, there are a few patterns that emerge. First, based on the dynamics of the system, regardless of which method of maneuver is utilized, the rendezvous times are the same for all numerical integration methods and the same for all analytic methods. It is also important to note, with the exception of the coplanar method, the analytic approach is significantly faster in the computational time over the numerical integration. This is a very important metric for long time interval simulations. The numerical integration methods require significant computing time, while the analytical approach is much faster albeit slightly less accurate, again with exception to the coplanar case.

Table A.8: Summary of Results for Initial Model Validation

	Miss Dist, m	ΔV, $\frac{meters}{sec}$	Time, sec	Iterations	Comp time, sec
Collinear Integration	440.0933	-41.2701	5512.9	4	61.85
Collinear Analytic	492.4583	-41.0111	5517.3	3	16.95
Coplanar Integration	3.2241	-41.2644	5512.9	5	60.09
Coplanar Analytic	.0103	-41.0524	5517.3	28	99.48
3-D Integration	.7215	-41.2634	5512.9	27	248.78
3-D Analytic	1.718	-41.0505	5517.3	46	158.84

It is extremely important to note that throughout the model validation, the ΔV's that are identified are the result of the magnitude of the new velocity minus the magnitude of the original velocity. The resulting value is very different from the component by component ΔV that would be required to actually execute the maneuver. This is a result of the triangle inequality for the subtraction of the vectors in 3-D space.

A final note should be provided that the difference between the results of the numerical integration methods versus the analytical methods cannot be easily compared. They are compared throughout this study from a summary view point, but they are drastically different models. Having only utilized the effects of J_2 in the analytic approach can and will yield a significantly different result from the numerical method using J_2 and atmospheric drag. Remember however, that the state transition matrix, Φ, of TMN for either method requires numerical integration accurate to J_2 and atmospheric drag making their comparrison applicable, as demonstrated.

Overall, the initial model validation proved to be successful by achieving a near zero miss distance of 0.7215 meters in the 3-D case with an achievable ΔV of -41.2634 $\frac{m}{sec}$.

A.9 Appendix Summary

The previous chapter was completed as an effort to replicate the published results of previous work. The methods and results of the chapter provide the basis for establishing credibility for the system model that will be the foundation for this research. The final results state that the model and algorithm being utilized in this research provided for a final miss distance accuracy of 0.7215 meters. For the proposed application that this research is aiming for, those results are tremendous. Considering, the impact from various altitudes on both the interceptor and target satellites, to yield results to within 2.5 feet over the course of an orbit are valid.

Appendix: Introduction to Relay and Collector Model with Preliminary Results

Utilizing the TMN methodology highlighted in Section A.1, modifications are introduced and ultimately, a new algorithm is demonstrated to maneuver a relay satellite in order to achieve a specified geometry between itself and one collector satellite. In the following material, the terminology has been changed from the previous chapter. Specifically, the interceptor satellite is now considered the relay satellite and the target satellite is called the collector satellite. From a theoretical view, there is no change in their concept, just a change in their application. The goal of the following chapter is to present to the reader the ability to establish an algorithm, based upon TMN, which allows for a relay satellite maneuver that satisfies user defined criteria utilizing the differential correction convergence from TMN. The initial approach and conclusions are summarized throughout the following sections.

B.1 Models for Relay and Collector Satellites

The system dynamics of this model are relatively straightforward. In order to execute the higher altitude orbit maneuver modeling the collector and relay satellites are propagated using numerical integration. The numerical integrator model takes into account the bulge around the equator of the Earth, J_2. The EOM for each satellite are captured in (B.1) and (B.2) [4] They are the same EOM highlighted in the previous chapter without the effect of atmoshperic drag.

$$\dot{R} = \vec{V} \tag{B.1}$$

$$\dot{V} = \frac{\mu \times \vec{R}}{|\vec{R}|^3} - \frac{3}{2} \times \frac{J_2 \times \mu \times R_{EARTH}^2 \times \vec{R}}{|\vec{R}|^5} \times (1 - \frac{5 \times R_z^2}{|\vec{R}|^2}) \tag{B.2}$$

Ultimately, the numerical model is determined to a fidelity including J_2. Remember however, calculating the STM, Φ, requires numerically integrating the relay satellite's equations of motion and the relay satellite's variational equations of motion. The variational equations are the partial derivatives of the EOM with respect to the position and velocity vector components.

B.2 Model Assumptions for Relay and Collector Satellites' Mission

The baseline assumption for this model is that the high altitude relay satellite and the collector satellite lie along the same radial vector from the center of the Earth, at the initial time. Fundamentally, the velocity vectors will be significantly different because of the differing orbital altitudes, which will be demonstrated. Therefore, this assumption ultimately results in two orbital planes that are significantly off-set from each other. The goal throughout the analysis is to maintain disparate orbits resulting in achieving end state altitudes as near to the initial conditions as possible. Fully understanding the dynamics within the TMN algorithm, yields a possible solution. Therefore, this can be achieved through the modifications of the error vector, $\vec{e}$, and the **T** matrix. In order to make the necessary modification, the initial magnitude of the separation distance between the relay and collector satellites is needed, as well as the initial difference between the relay and collector satellite's velocity vectors. Equations (B.3) and (B.4) highlight these resulting vectors, $\vec{\Lambda}$ and $\vec{\Gamma}$ respectively.

$$\vec{\Lambda} = Miss_{RELAY_{t0}-COLLECTOR_{t0}} = \vec{R}_{RELAY_{t0}} - \vec{R}_{COLLECTOR_{t0}} \tag{B.3}$$

$$\vec{\Gamma} = Vel_{RELAY_{t0}-COLLECTOR_{t0}} = \vec{V}_{RELAY_{t0}} - \vec{V}_{COLLECTOR_{t0}} \tag{B.4}$$

Once these values are determined, they are appropriately placed within the framework of the algorithm. Specifically, a form of $|\vec{\Lambda}|$ will be input into the error vector while $\vec{\Gamma}$ will have influence within the **T** matrix.

From the onset, there are two variables that can be adjusted to begin iteration. The first is the guess at the required ΔV, and the second essentially works out to be the rendezvous time. Recall, the rendezvous time in this scenario equates to the arrival of the relay satellite at the determined end state. Differing from the intercept mission, the initial guess at the rendezvous time will be the initial orbital period of the relay satellite. This initial guess allows for the algorithm to most appropriately begin searching for a solution, which would ultimately minimize fuel expenditure by the relay satellite. Still, the initial period of the collector satellite should also be explored. The guess at the ΔV is self explanatory and later proven to be somewhat arbitrary.

Inputing the initial guesses drives the algorithm to compute the resulting position and velocity vectors for both the collector and relay satellites at the future time. This results in the second calculation of the miss distance between the relay and collector satellites, as well as the second calculation of the velocity difference between the integrated orbits. These values contribute to the first iteration of the algorithm. Recall from Section A.1, how to calculate the error vector for the intercept mission. The intercept mission's error vector is shown in (B.5). This is where the value for the error vector is modified for the high altitude communications relay mission. Instead of driving the miss distance to zero as in equation (B.5), the miss distance is iterated towards a value related to $|\vec{\Lambda}|$. The new error vector is shown in equation (B.6).

$$\bar{e} = \begin{bmatrix} R_{int_x} - R_{tgt_x} \\ R_{int_y} - R_{tgt_y} \\ R_{int_z} - R_{tgt_z} \\ \Delta V_{int_x} \\ \Delta V_{int_y} \\ \Delta V_{int_z} \end{bmatrix} \tag{B.5}$$

$$\bar{e} = \begin{bmatrix} (R_{RELAY_x} - R_{COLLECTOR_x}) + \eta|\vec{\Lambda}| \\ (R_{RELAY_y} - R_{COLLECTOR_y}) + \eta|\vec{\Lambda}| \\ (R_{RELAY_z} - R_{COLLECTOR_z}) + \eta|\vec{\Lambda}| \\ \Delta V_{RELAY_x} \\ \Delta V_{RELAY_y} \\ \Delta V_{RELAY_z} \end{bmatrix} \tag{B.6}$$

η is an adjustable variable to account for the various conditions of the optimal solution that ultimately maintains the integrity of the higher altitude relay orbit referenced to the lower collector orbit.

Also from Section A.1, the $\tilde{T}$ matrix calculated in (A.5) has a component in the upper right that is equal to the difference in the relay and collector velocity vectors at the final time. This is the location for $\vec{\Gamma}$. Integrating the relay's STM, Φ, and extracting the upper right portion, ϕ, which relates the relay satellite's final position with respect to initial velocity, results in the modified $\tilde{T}$ matrix given by (B.7). These modifications are necessary for the high altitude solution.

$$\tilde{T} = \begin{bmatrix} \phi & \vec{V_{RELAY}} - \vec{V_{COLLECTOR}} + \vec{\Gamma} \\ 3 \times 3 & 3 \times 1 \\ \mathbf{I} & \mathbf{0} \\ 3 \times 3 & 3 \times 1 \end{bmatrix} \tag{B.7}$$

The addition of $\vec{\Gamma}$ ensures the integrity of the solution to maintain the initial reference between the relay and collector satellites.

Introducing these modifications, the improved algorithm can proceed as described in Section A.1 towards a viable solution.

B.3 Initial Conditions and Methodology for Relay and Collector Satellites' Mission

Throughout the high altitude study, there is one set of initial conditions that is universal regardless of the relay's initial altitude, the guess at the ΔV and the initial guess at the rendezvous time. Specifically, the initial COEs for the collector satellite remain the same throughout the study. They are shown below in Table B.1[4]. The COEs that define the position and velocity of the collector satellite in this model are identical to those used for the target satellite in the previous chapter.

Table B.1: Initial COEs for the Collector Satellite in 1 Relay + 1 Collector Scenario

Orbital Element	Collector Sat
Semi-Major Axis, a, km	6760.8
Eccentricity, e	.005
Inclination, i, Degrees	15
Right Ascension of Ascending Node, Ω , Degrees	45
Argument of Perigee, ω , Degrees	70
True Anomaly at Epoch, ν, Degrees	10

As a result of the fixed initial conditions for the collector satellite, the orbital period for the collector satellite is also fixed at 5532.4 sec.

For this phase, there are two specific relay satellite orbits being investigated. The first represents an orbital altitude of approximately 2000 km. The second is an orbital altitude of approximately 4000 km, which represents a relay satellite in an orbit with an orbital period nearly 2x's the collector's orbital period. To further simplify the scenarios, the relay satellite will begin on the same unit position vector as the collector satellite. This results in the COEs in Table B.2.

Table B.2: Initial COEs for the Relay Satellites in 1 Relay + 1 Collector Scenario

Orbital Element	Relay Sat 1	Relay Sat 2
Semi-Major Axis, a, km	8378.1	10732.2
Eccentricity, e	.0152	.0152
Inclination, i, Degrees	40.0519	40.0519
Right Ascension of Ascending Node, Ω , Degrees	106.3808	106.3808
Argument of Perigee, ω , Degrees	13.3168	13.3168
True Anomaly at Epoch, ν, Degrees	10.0182	10.0182

Provided the COEs, this study was conducted using three different initial ΔV's and the two guesses at the rendezvous time including the collector satellite's orbital period and the relay's orbital period. The test summary is outlined in Table B.3.

B.4 Relay Satellite 1 Results

Figure B.1 provides a view of the initial orbits without a maneuver for the first scenario.

In Figure B.1, notice that the original position vectors are collinear. The relay's position vector is longer, representing a higher altitude. This image of the original orbits is to provide some context for the results using Relay Satellite 1. Utilizing the aforementioned adjutments within the TMN algorithm, test cases 1 through 6 were executed. The results from the various tests are in Table B.4 keeping in mind that the semi-major axis for the collector satellite remains fixed at 6760.8 km. Test cases 1-6 utilized $\eta = .5$.

In Table B.4, t_0 Distance and t_f Distance represent the initial and final separation distance between the relay and collector satellites, respectively. Notice upfront that the

Table B.3: Test Methodology for High Altitude Relay Satellite Control using TMN

Test Case #	Relay Satellite	Guess ΔV $\frac{m}{sec}$	Time Guess
1	Relay Sat 1	-50	Collector Sat Period
2	Relay Sat 1	0	Collector Sat Period
3	Relay Sat 1	+50	Collector Sat Period
4	Relay Sat 1	-50	Relay Sat 1 Period
5	Relay Sat 1	0	Relay Sat 1 Period
6	Relay Sat 1	+50	Relay Sat 1 Period
7	Relay Sat 2	-50	Collector Sat Period
8	Relay Sat 2	0	Collector Sat Period
9	Relay Sat 2	+50	Collector Sat Period
10	Relay Sat 2	-50	Relay Sat 2 Period
11	Relay Sat 2	0	Relay Sat 2 Period
12	Relay Sat 2	+50	Relay Sat 2 Period

final separation distance between the relay and collector satellites is the same at the end of the algorithm regardless of the intial guess at the ΔV or the initial guess for the time. It is very important to note though, that differences do exist between the cases depending on the initial guess for the time. Specifically, when the orbital period of the collector satellite is used as the initial guess, it yields the same acutal ΔV and actual time regardless of the initial ΔV guess. The same is the case for the orbital period of the relay satellite. This shows the sensitivity to of the algorithm towards the guess at the initial time. The final ΔVs achieved all lie within 2% of each other, while the final time is within 0.07%.

Figure B.2 shows the results from one of the above cases. The inner circle represents the collector orbit, while the semi-circle represents the relay orbit. The top solid line is the

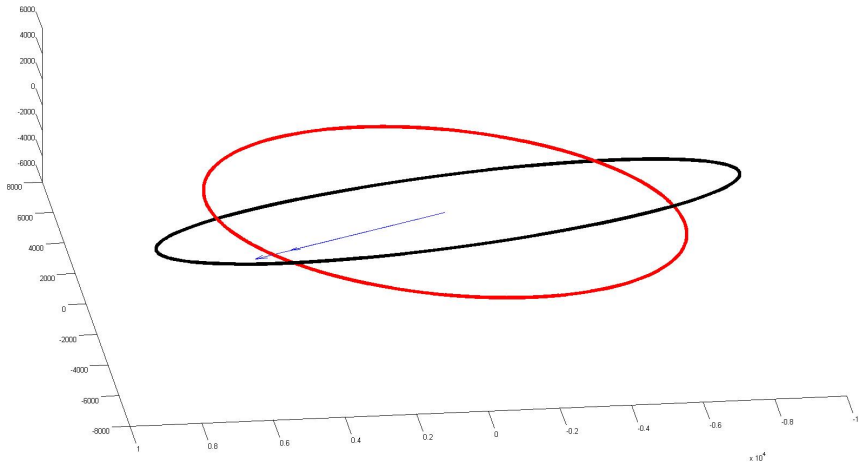

Figure B.1: Relay 1 and Collector Satellite after One Orbital Period

Table B.4: Results for Relay Satellite 1: Semi-Major Axis = 8378.1 km

Case #	t_0 Sep (km)	t_f Sep (km)	ΔV Guess $\frac{m}{sec}$	Actual ΔV $\frac{m}{sec}$	Guess t	Actual t (sec)
1	1525.1	1320.8	-50	-281.9	Col Period	6915.7
2	1525.1	1320.8	0	-281.9	Col Period	6915.7
3	1525.1	1320.8	+50	-281.9	Col Period	6915.7
4	1525.1	1320.8	-50	-289.79	Relay 1 Period	6910.6
5	1525.1	1320.8	0	-289.79	Relay 1 Period	6910.6
6	1525.1	1320.8	+50	-289.79	Relay 1 Period	6910.6

initial separation distance between the collector and relay satellites, while the lower solid line is the final separation distance. The shorter arrows represent the collector satellite's

position vector at its initial and final time, while the longer arrows are the relay's position vector at its initial and final time.

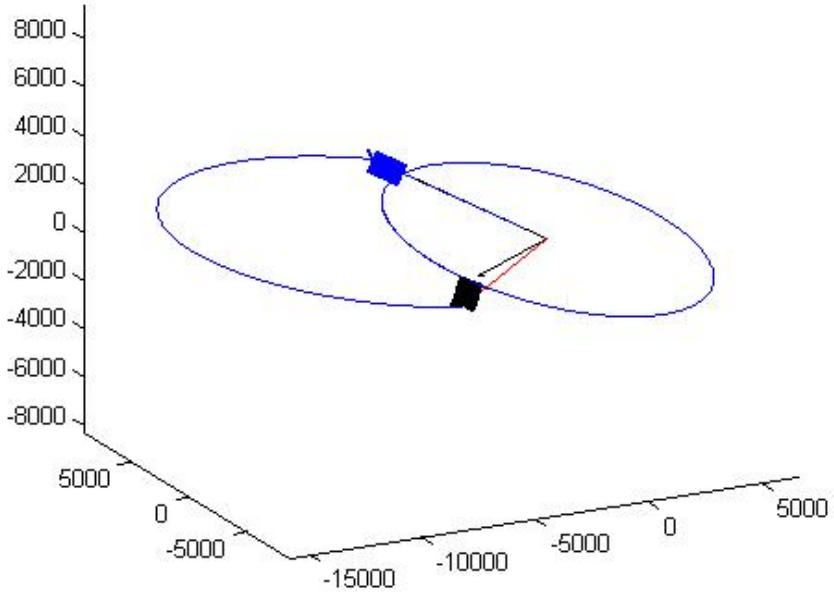

Figure B.2: Solution for Relay 1 and Collector Satellites' Orbits

The evolution of the satellite's miss distance through the algorithm's iterations is captured in Figure B.3. This simply shows that throughout the algorithm, various solutions are explored, while it shows a gradual convergence towards the final solution.

B.5 Relay Satellite 2 Results

Figure B.4 provides a view of the initial orbits without a maneuver for the first scenario.

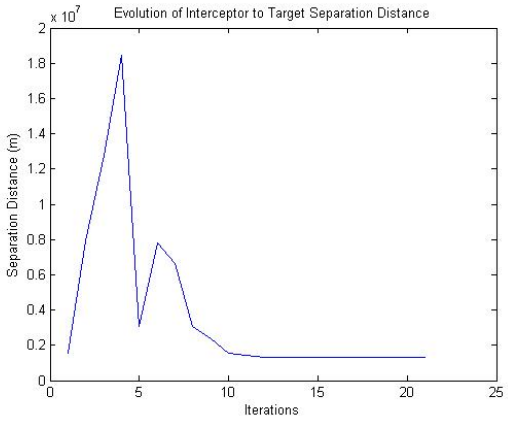

Figure B.3: Miss Distance per Iteration

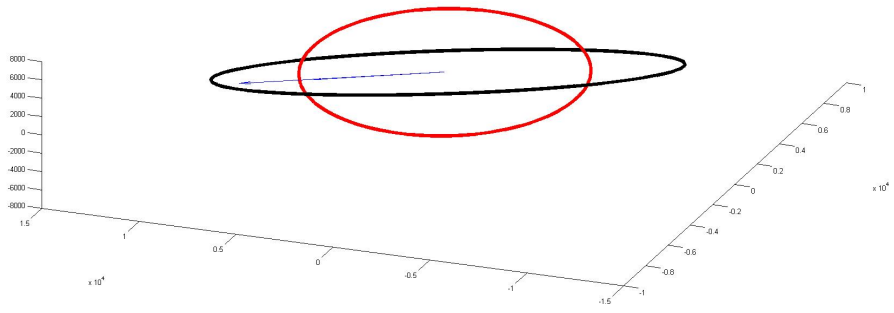

Figure B.4: Relay 2 and Collector Satellite after One Orbital Period

In Figure B.4 notice that the original position vectors are again, collinear. Utilizing the aforementioned adjutments within the TMN algorithm, test cases 7 through 12 were executed. The results from the various tests are in Table B.5, keeping in mind that the

semi-major axis for the collector satellite remains fixed at 6760.8 km. Test cases, 7-12 also utilized $\eta = .5$.

Table B.5: Results for Relay Satellite 2: Semi-Major Axis = 10732.2 km

Case #	t_0 Sep (km)	t_f Sep (km)	ΔV Guess $\frac{m}{sec}$	Actual ΔV $\frac{m}{sec}$	Guess t	Actual t (sec)
7	3844.0	3329.0	-50	-307.28	Col Period	6724.7
8	3844.0	3329.0	0	-307.28	Col Period	6724.7
9	3844.0	3329.0	+50	-307.28	Col Period	6724.7
10	3844.0	3329.0	-50	-315.7	Relay 2 Period	6767.0
11	3844.0	3329.0	0	-315.7	Relay 2 Period	6767.0
12	3844.0	3329.0	+50	-315.7	Relay 2 Period	6767.0

Similar to the 8,378 km orbit, the final separation distance between the relay and collector satellites is the same at the end of the algorithm regardless of the initial guess at the ΔV or the initial guess for the time. Similarly, differences do exist between the cases depending on the initial guess for the time. Specifically, when the orbital period of the collector satellite is used as the initial guess, it yields the same acutal ΔV and actual time regardless of the initial ΔV guess. The final ΔVs achieved all lie within 3% of each other, while the final time is within 0.7%.

Figure B.5 shows the results from one of the above cases. The inner ellipse represents the collector orbit, while the semi-circle represents the relay orbit. The top solid line is the initial separation distance between the collector and relay satellites, while the lower solid line is the final separation distance. The shorter arrows represent the collector satellite's position vector at its initial and final time, while the longer arrows are the relay's position vector at its initial and final time.

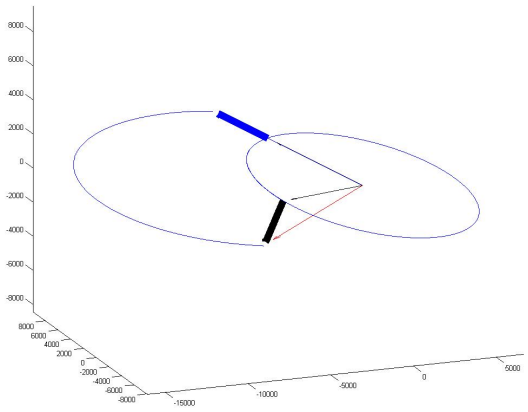

Figure B.5: Solution for Relay 2 and Collector Satellites' Orbits

The evolution of the satellite's miss distance through the algorithm's iterations is captured in Figure B.6. Similar to the first scenario, this demonstrates that throughout the algorithm, various solutions are explored while it shows a gradual convergence towards the final solution.

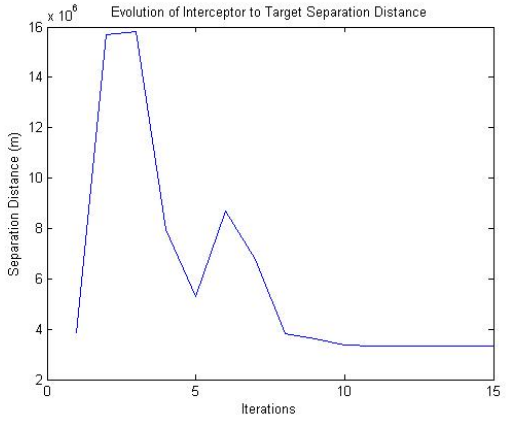

Figure B.6: Miss Distance per Iteration

B.6 Introduction to Relay and Collector Model: Preliminary Conclusions and Way Forward

Throughout this section it has been sufficiently demonstrated that an algorithm can be produced to initiate a maneuver that aims to optimize the ΔV required to achieve a desired end state based on the dynamics of a relay and collector satellite. However, the initial results still demonstrate that revisions are necessary in order to prove a design that is sustainable, the ΔV's identified through these results are too large.

That being said, since the modified algorithm works and demonstrates convergence, the work that needs to be completed hovers around the use of the η variable. More importantly, the path forward is to better understand and modify the system's geometry to demonstrate an ability to implement a strategy to optimize the fuel consumed over the course of a responsive space scenario. While a minimum distance end state separation is achieved throughout these scenarios, it is not the primary goal. The primary goal was to demonstrate the ability to modify the TMN algorithm into a new algorithm, which succeeded in converging towards a maneuver to a point in space based on the user defined geometry between the relay and collector satellites.

Appendix: Introduction to Relay, Collector and Ground Model with Preliminary Results

Utilizing the methodology highlighted in Section A.1 modifications are introduced and a new algorithm is demonstrated to achieve the desired effect of maneuvering a relay satellite in order to achieve a specified geometry between itself, one collector satellite and one fixed ground station. The initial approach and conclusions are summarized throughout the following sections.

C.1 Models for Relay and Collector Satellites and Ground Station

The satellite system dynamics are relatively straightforward. Numerical integration is utilized to propogate the the collector and relay satellites. The model accounts for the bulge around the equator of the Earth, J_2. The equations of motion for each satellite are captured in (B.1) and (B.2)[4].

The position and velocity components of the ground station are required as well. These vectors are represented in the same frame as the collector and relay satellites. The EOM for the ground station are ultimately a function of the ground station's latitude and the rotation rate of the Earth. Details regarding the derivation of the initial position and velocity vectors for the ground station are found in a later section.

C.2 Model Assumptions for Relay and Collector Satellite's Mission with Ground Station

The baseline assumption for this model is that the relay satellite, the collector satellite, and the ground station lie along the same radial vector from the center of the Earth at the beginning time. Fundamentally, the velocity vectors will be significanlty different because of the differing orbital altitudes and the rotation of the Earth. Therefore, this assumption ultimately results in three planes that are significantly off-set from each other. This requires

the analysis of the ground station as a point subject to its own EOM within its plane, the surface of the rotating Earth. The goal throughout the analysis is to maintain disparate satellite orbits, resulting in achieving end state altitudes as near to the initial conditions as possible. This is achieved through significant modifications to the TMN construct. In order to make the necessary modifications, the initial magnitude of the separation distance between the relay and collector satellites is needed, as well as the initial difference between the relay and collector satellite's velocity vectors. This information is also required for the difference between the relay satellite and the ground station at the initial time. Equations (C.1), (C.2), (C.3) and (C.4) highlight these resulting vectors, $\vec{\Lambda}$, $\vec{\Gamma}$, $\vec{\Upsilon}$ and $\vec{\Psi}$ respectively.

$$\vec{\Lambda} = Miss_{RELAY_{t0}-COLLECTOR_{t0}} = \vec{R}_{RELAY_{t0}} - \vec{R}_{COLLECTOR_{t0}} \tag{C.1}$$

$$\vec{\Gamma} = Vel_{RELAY_{t0}-COLLECTOR_{t0}} = \vec{V}_{RELAY_{t0}} - \vec{V}_{COLLECTOR_{t0}} \tag{C.2}$$

$$\vec{\Upsilon} = Miss_{RELAY_{t0}-GND_{t0}} = \vec{R}_{RELAY_{t0}} - \vec{R}_{GND_{t0}} \tag{C.3}$$

$$\vec{\Psi} = Vel_{RELAY_{t0}-GND_{t0}} = \vec{V}_{RELAY_{t0}} - \vec{V}_{GND_{t0}} \tag{C.4}$$

In order to appropriately place the ground station at the initial time, the unit vector of the collector satellite's position is acquired. Multiplying by the radius of the Earth, assuming a perfect sphere, yields the position vector for the ground station in the same coordinate frame as both the collector and relay satellites. In order to sufficiently model the motion of the ground station as the Earth rotates through time, the latitude angle, λ and initial ϕ_{GS} angle need to be determined. These are calculated through some simple algebraic manipulations of the dot product of the ground station's position unit vector with the $\hat{z}$ unit vector for λ and the $\hat{y}$ unit vector for ϕ_{GS}.

The initial velocity of the ground station is a little bit more challenging. The full

representation for the initial velocity for the ground station is in equation (C.5). R_{EARTH} is the radius of the Earth and ω_{EARTH} represents the rotation rate of the Earth.

$$\vec{V}_{GND_0} = \begin{bmatrix} R_{EARTH} \times cos(\lambda) \times \omega_{EARTH} \times sin(\phi_{GS_0}) \\ R_{EARTH} \times cos(\lambda) \times \omega_{EARTH} \times cos(\phi_{GS_0}) \\ 0 \end{bmatrix} \tag{C.5}$$

The EOM for the collector and relay satellites and the relay's Φ matrix are integrated as previously identified. The change in the ground station is determined from the amount of time surpased $\times\ \omega_{EARTH}$ and the $\cos(\lambda)$. This determines the change in the angle, ϕ_{GS}. Knowing that the position of the ground station cannot change in the $\hat{z}$ direction, a simple manipulation of the original magnitude of the ground station in the x and y directions, multiplied by the $\cos(\phi_{GS})$ and the $\sin(\phi_{GS})$ in the $\hat{x}$ and $\hat{y}$ directions, respectively yields the final ground station position. Utilizing the current value of ϕ and (C.5) determines the ground station's final velocity.

Now a form of $|\vec{\Lambda}|$ and $|\vec{\Upsilon}|$ will be input into the error vector, while $\vec{\Gamma}$ and $\vec{\Psi}$ will have influence within the **T** matrix.

The first major modification to the algorithm is with the error vector. Now, considering the role and influence of the ground station over the optimum solution, the modified error vector is in equation (C.6).

$$\bar{e} = \begin{bmatrix} (R_{RELAY_x} - R_{COLLECTOR_x}) + \eta|\vec{\Lambda}| \\ (R_{RELAY_y} - R_{COLLECTOR_y}) + \eta|\vec{\Lambda}| \\ (R_{RELAY_z} - R_{COLLECTOR_z}) + \eta|\vec{\Lambda}| \\ (R_{RELAY_x} - R_{GROUND_x}) + \sigma|\vec{\Upsilon}| \\ (R_{RELAY_y} - R_{GROUND_y}) + \sigma|\vec{\Upsilon}| \\ (R_{RELAY_z} - R_{GROUND_z}) + \sigma|\vec{\Upsilon}| \\ \Delta V_{RELAY_x} \\ \Delta V_{RELAY_y} \\ \Delta V_{RELAY_z} \end{bmatrix} \tag{C.6}$$

η is an adjustable variable to account for the various conditions of the optimal solution that ultimately maintains the integrity of the higher altitude relay orbit referenced to the lower collector orbit. And σ serves that function for the refrence between the relay satellite and the ground station.

Obviously, this is a significant modification to the TMN algorithm. Not only does it increase the dimension of the error vector, but it also demonstrates that the solution of the algorithm must satisfy both the initial reference between the relay and collector orbits, as well as between the relay orbit and the ground station. These will be competing interests throughout each iteration while implementing the algorithm. So much so, that the resulting output of each iteration is the variation of the control vector, $\vec{u}$, which is modfied to reflect this competition. It is important to note that based on matrix dimensions, $\vec{u}$, will now have seven components. Specifically, the components of $\vec{u}$ are shown below in (C.7).

$$\vec{u} = \begin{bmatrix} \Delta V_{col_x} \\ \Delta V_{col_y} \\ \Delta V_{col_z} \\ \Delta V_{gnd_x} \\ \Delta V_{gnd_y} \\ \Delta V_{gnd_z} \\ \Delta t \end{bmatrix} \tag{C.7}$$

The ultimate result after each iteration is to prove balance in both the collector satellite's and ground station's influence over the solution. Therefore, a mean average of the ΔV's for each component is fed back into the algorithm for successive iterations.

In order to adjust for the change in matrix dimension of the error vector, a ripple effect changes the weight matrix, **Q**. The addition of the ground station requires **Q** to change to a 9x9 **I** matrix and the **T** matrix will adjust to a 9x7 matrix.

Previously identifying the simple change to the $\tilde{T}$ matrix to maintain the reference between the relay and collector satellite in Section B.2 in equation (B.7), a more robust change is necessary to capture the ground component. The relay's Φ matrix is fixed and therefore ϕ is fixed. Since the dimension of the $\tilde{T}$ matrix has to be adjusted, the adjustments must come in another form. To maintain the intent of the **T** matrix would be to follow the same form as before. Therefore, the upper left corner is the ϕ matrix, the lower left corner is a 6x6 **I** matrix, the lower right corner is a column of zeros, leaving the upper right corner as a 3x4 matrix. It is also known from before that some form of the velocity difference between the relay and collector satellite must go here. Additionally, some form of the difference between the relay satellite and the ground station must be captured here as well. Therefore, new matrices are formed using the previously calculated Γ and Ψ vectors and the ϕ matrix. Equations (C.8) and (C.9) describe these matrices, resulting in two 3x2 matrices to fill the upper right corner of $\tilde{T}$.

$$\bar{\Xi}_1 = \phi \times \begin{bmatrix} & V_{rel_x} - V_{col_x} \\ \vec{\Gamma} & V_{rel_y} - V_{col_y} \\ & V_{rel_z} - V_{col_z} \end{bmatrix} \tag{C.8}$$

$$\bar{\Xi}_2 = \phi \times \begin{bmatrix} & V_{rel_x} - V_{gnd_x} \\ \vec{\Psi} & V_{rel_y} - V_{gnd_y} \\ & V_{rel_z} - V_{gnd_z} \end{bmatrix} \tag{C.9}$$

Now the new **T** matrix can be calculated from the modified $\tilde{T}$ matrix. This update is provided in equation (C.10) and is necessary for the relay and collector satellites with the ground station solution.

$$\tilde{T} = \begin{bmatrix} \phi & \Xi_1\Xi_2 \\ 3\times 3 & 3\times 4 \\ \mathbf{I} & \mathbf{0} \\ 6\times 6 & 6\times 1 \end{bmatrix} \tag{C.10}$$

Now the algorithm can proceed to determine the optimum control for the relay satellite to meet the desired end state.

C.3 Initial Conditions and Methodology for Relay and Collector Satellite's Mission with Ground Station

Throughout the ground station phase of the study, there is one set of initial conditions that is universal regardless of the relay's initial altitude, the guess at the ΔV and the initial guess at the rendezvous time. Specifically, the initial COEs for the collector satellite remain the same throughout the study. They are shown below in Table C.1[4].

As a result of the fixed initial conditions for the collector satellite, the orbital period for the collector satellite is also fixed at 5532.4 sec.

For this phase of the study, there are three specific relay satellite orbits being

Table C.1: Initial COEs for the Collector Satellite

Orbital Element	Collector Sat
Semi-Major Axis, a, km	6760.8
Eccentricity, e	.005
Inclination, i, Degrees	15
Right Ascension of Ascending Node, Ω , Degrees	45
Argument of Perigee, ω , Degrees	70
True Anomaly at Epoch, ν, Degrees	10

investigated. The first represents an orbital altitude of approximately 2000 km. The second is an orbital altitude of approximately 4000 km, which represents a relay satellite in an orbit with an orbital period nearly 2x's the collector's orbital period. The first two are identical to the high altitude phase of the study, while the third is the case that represents the relay and collector satellite being at nearly the exact same starting position. To further simplify the scenarios, the relay satellite and the ground station will begin on the same unit position vector as the collector satellite. This results in the COEs in Table C.2.

Provided the COEs, this phase of the study was conducted using a fixed initial ΔV of -50 $\frac{m}{sec}$. This is possible due to the negligible impact of the initial ΔV demonstrated in the first phase of the study. Therefore, the only variable to change is to alternate between the two guesses at the rendezvous time, including the collector's orbital period and the relay's orbital period. The test summary is outlined in Table C.3.

Table C.2: Initial COEs for the Relay Satellites

Orbital Element	Relay Sat 1	Relay Sat 2	Relay Sat 3 [4]
Semi-Major Axis, a, km	8378.1	10732.2	6830.35
Eccentricity, e	.0152	.0152	.0152
Inclination, i, Degrees	40.0519	40.0519	40.0519
Right Ascension of Ascending Node, Ω , Degrees	106.3808	106.3808	106.3808
Argument of Perigee, ω , Degrees	13.3168	13.3168	13.3168
True Anomaly at Epoch, ν, Degrees	10.0182	10.0182	10.0182

Table C.3: Test Methodology for Space to Ground Tracking

Test Case #	Relay Satellite	Initial Time Guess
1	Relay Sat 1	Collector Sat Period
2	Relay Sat 1	Relay Sat 1 Period
3	Relay Sat 2	Collector Sat Period
4	Relay Sat 2	Relay Sat 2 Period
5	Relay Sat 3	Collector Sat Period
6	Relay Sat 3	Relay Sat 3 Period

C.4 Relay Satellite 1 Results with Ground Station

Figure C.1 provides a view of the initial orbits without a maneuver for the first scenario. The collector's orbit is slightly more circular, while the relay's initial orbit is the other ellipse. This is the identical configuration explored in Section B.4 with the addition of the ground station.

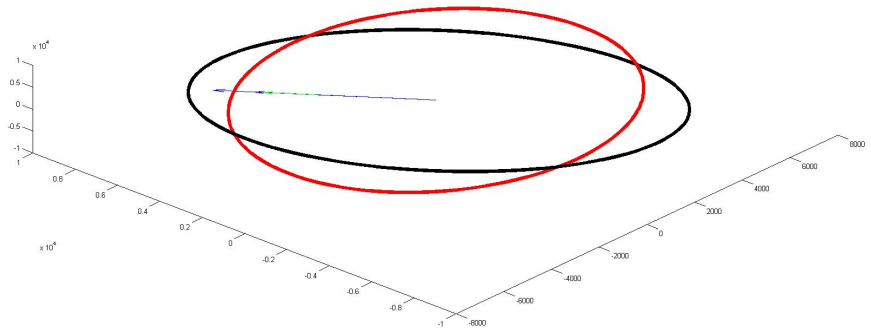

Figure C.1: Relay 1 and Collector Satellites' Orbits After One Orbital Period

In Figure C.1, notice that the original relay and collector satellites, and ground station position vectors are collinear at the starting time. Utilizing the modifications within the algorithm, test cases 1 and 2 were executed. The results from these scenarios are in Table C.4. Keep in mind that the semi-major axis for the collector satellite remains fixed at 6760.8 km. Test cases, 1 and 2 utilized arbitrary values for η and σ, $\eta = 0.333$ and $\sigma = 0.5$.

Table C.4: Results for Relay Satellite 1: Semi-Major Axis = 8378.1 km

#	Col t_0 (km)	Col t_f (km)	Gnd t_0 (km)	Gnd t_f (km)	ΔV $\frac{m}{sec}$	t Guess	t (sec)
1	1525.1	3991.3	1874.5	1629.1	-293.9	Col Period	5508.4
2	1525.1	3991.3	1874.5	1629.1	-294.6	Relay 1 Period	5510.2

Even though the results summarized in Table C.4 are promising, there is still an impact on the solution based on the initial time guess. However, the proposed algorithm

demonstrates convergence towards a solution given the paramaters of the problem. Figure C.2 provides an image for the solution summarized in Table C.4. In Figure C.2, the top solid line represents the original separation between the ground station and the relay satellite, while the rightmost solid line represents the final separation between the ground station and the relay satellite. The solid line between the two is the separation between the collector and relay satellites at the final time. The medium vectors are the position vectors of the collector satellite. The longest vectors are the position vectors of the relay satellite and the shortest vectors are the positions of the ground station at the initial and final times.

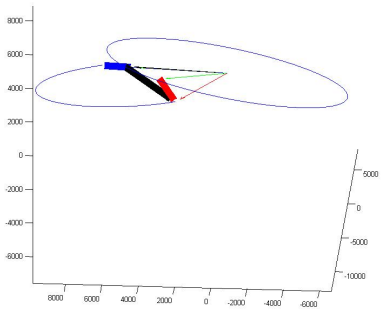

Figure C.2: Orbital Solution for Relay 1 with Collector Satellite and Ground Station

Figures C.3 and C.4 illustrate the evolution of the miss distance between the relay satellite and the collector satellite, and the relay satellite and the ground station through each iteration of the aglorithm.

Similarly to the high altitude solutions, the miss distance figures demonstrate that the algorithm is exploring an expansive search space for the final solution before converging.

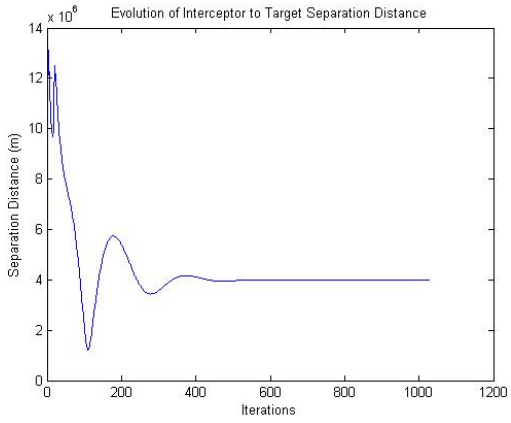

Figure C.3: Relay 1 to Collector Miss Distance per Iteration

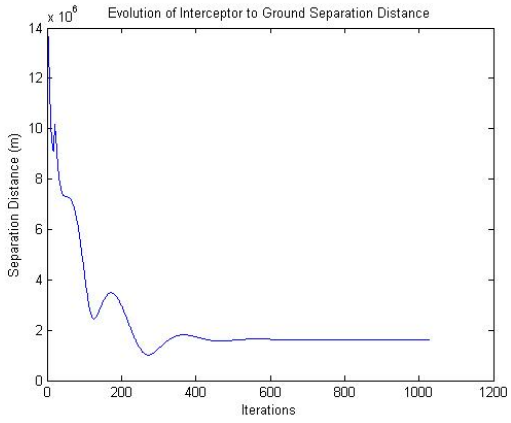

Figure C.4: Relay 1 to Ground Station Miss Distance per Iteration

C.5 Relay Satellite 2 Results with Ground Station

Figure C.5 provides a view of the initial orbits without a maneuver for the second ground station scenario. The collector's orbit is more circular than the elliptical relay orbit. This is the identical configuration explored in section B.5, with the addition of the ground station.

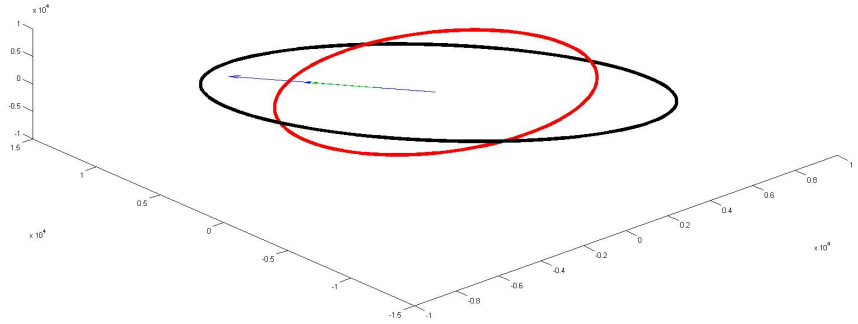

Figure C.5: Relay 2 and Collector Satellites' Orbits After One Orbital Period

In Figure C.5, notice that the original relay and collector satellites, and ground station position vectors are collinear at the starting time. The results from scenarios 3 and 4 are in Table C.5. Remember that the semi-major axis for the collector satellite remains fixed at 6760.8 km. These test cases, utilized arbitrary values for η and σ, $\eta = 0.333$ and $\sigma = 0.5$.

Table C.5: Results for Relay Satellite 2: Semi-Major Axis = 10732.2 km

#	Col t_0 (km)	Col t_f (km)	Gnd t_0 (km)	Gnd t_f (km)	ΔV $\frac{m}{sec}$	t Guess	t (sec)
3	3844.0	5896.1	4193.3	3638.3	-996.47	Col Period	5510.9
4	3844.0	5084.1	4193.3	3636.9	-946.59	Relay 2 Period	5636.8

Based solely on the results summarized in Table C.5, the algorithm demonstrates convergence to two separate solutions given the paramaters of the problem. Only further analysis outside the scope of this study could determine if the algorithm is actually finding

the same solution. Considering the difference in the final relay to collector distance, combined with the lower ΔV and the increased time, the results from this scenario could actually be converging towards very similar solutions.

Figure C.6 provides an image for the solution summarized in Table C.5. In Figure C.6, the leftmost solid line represents the original separation between the ground station and the relay satellite, while the rightmost solid line represents the final separation between the ground station and the relay satellite. The solid line in the middle is the separation between the collector and relay satellites at the final time. The medium vectors are the position vectors of the collector satellite. The longest vectors are the position vectors of the relay satellite and the shortest vectors are the positions of the ground station at the initial and final times.

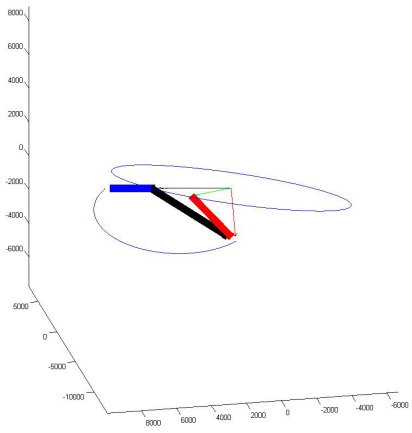

Figure C.6: Orbital Solution for Relay 2 with Collector Satellite and Ground Station

Figures C.7 and C.8 illustrate the evolution of the miss distance between the relay satellite and the collector satellite, and the relay satellite and the ground station through each iteration of the aglorithm.

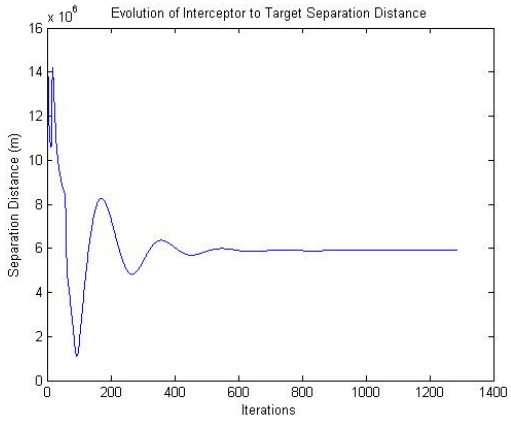

Figure C.7: Relay 2 to Collector Miss Distance per Iteration

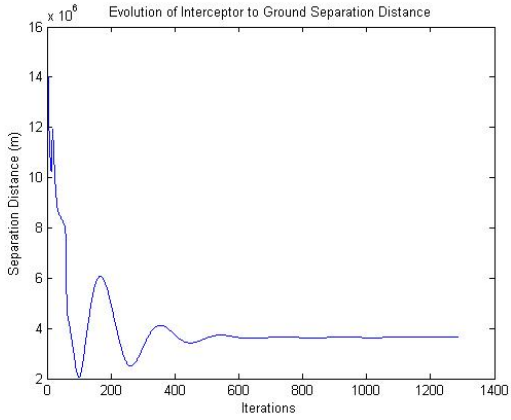

Figure C.8: Relay 2 to Ground Station Miss Distance per Iteration

C.6 Relay Satellite 3 Results with Ground Station

Figure C.9 provides a view of the initial oribits without a maneuver for the final ground station scenario. This is a unique scenario to this phase with the relay and collector satellites within very near proximity of each other but in separate orbital planes with differing inclinations and right ascension of the ascending nodes.

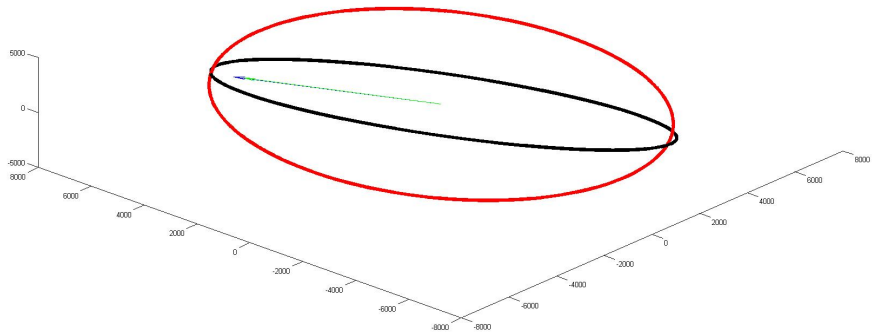

Figure C.9: Relay 3 and Collector Satellites' Orbits After One Orbital Period

In Figure C.9 notice that the original relay and collector satellites, and ground station position vectors are collinear at the starting time. The results from scenarios 5 and 6 are in Table C.6. These test cases, utilized $\eta = 0.333$, $\sigma = 0.5$ and a fixed collector orbit semi-major axis.

Table C.6: Results for Relay Satellite 3: Semi-Major Axis = 6830.35 km

#	Col t_0 (km)	Col t_f (km)	Gnd t_0 (km)	Gnd t_f (km)	ΔV $\frac{m}{sec}$	t Guess	t (sec)
5	.532	2804.5	449.92	407.8	-333.56	Col Period	5507.2
6	.532	2804.5	449.92	407.8	-333.56	Relay 3 Period	5507.2

The results in Table C.6 demonstrate no impact on the final solution from the initial time guess. The algorithm converges to one unique solution given the paramaters of the

problem. Figure C.10 provides an image for this solution. In Figure C.10, the solid line is the separation between the collector and relay satellites at the final time.

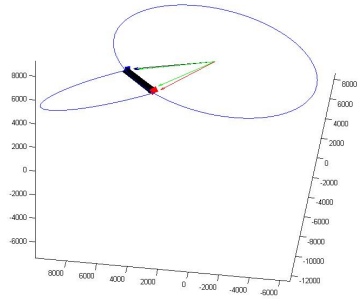

Figure C.10: Orbital Solution for Relay 3 with Collector Satellite and Ground Station

The convergence of the miss distance between the relay satellite and collector satellite, as well as the relay satellite and the ground station, is shown in Figures C.11 and C.12 respectively.

C.7 Introduction to Relay and Collector Model with Ground Station: Preliminary Conclusions and Way Forward

Throughout this section it has been sufficiently demonstrated that an algorithm can be produced to initiate a maneuver that aims to optimize the ΔV required to achieve a desired end state based on the dynamics of a relay and collector satellite with a ground station. However, the initial results still demonstrate that revisions are necessary in order to prove a design that is sustainable, the ΔV's identified through these results are too large.

Since the modified algorithm works and demonstrates convergence, the work that

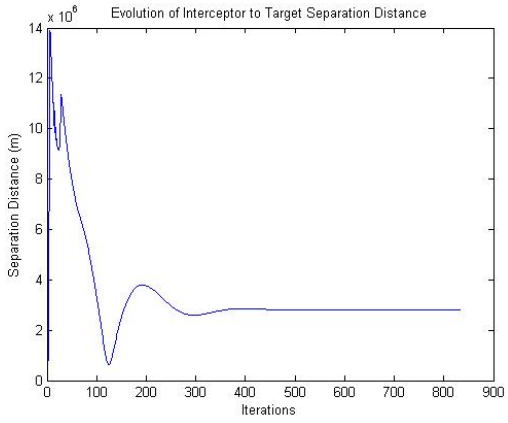

Figure C.11: Relay 3 to Collector Miss Distance per Iteration

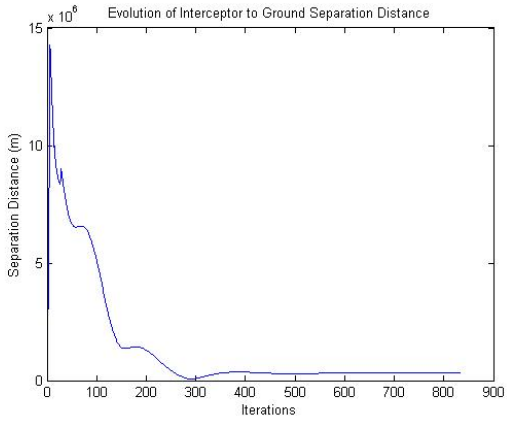

Figure C.12: Relay 3 to Ground Station Miss Distance per Iteration

needs to be completed hovers around the use of the η and σ variables. Similarly to the high altitude scenarios, the path forward is to better understand and modify the system's geometry to demonstrate an ability to implement a strategy to optimize the fuel consumed over the course of a responsive space scenario. Again, the goal was to demonstrate the a new algorithm could be presented, based on the principles of TMN, to apply differential

correction to execute a maneuver for one satellite versus the geometry of another satellite and a ground station.

Bibliography

[1] Leigh, A. M. and Black, J. T., "Navigation Solution to Solve Impulsive Tangential Orbital Maneuvers," Submitted for publication May 2013.

[2] Wagner, P., "The Operationally Responsive Space Office," November 2012.

[3] Bate, R. R., Mueller, D. D., and White, J. E., *Fundamentals of Astrodynamics*, chap. 2 and 3, Dover Publications, New York, 1st ed., 1971.

[4] Chioma, V. J., *Navigation Solutions to Enable Space Superiority Through the Repeated Intercept Mission*, Phd dissertation, United States Air Force Institute of Technology, 2007.

[5] Klumpp, A. R., "New Developments in Astrodynamics Algorithms for Autonomous Rendezvous," U.S. Automated Rendezvous and Capture Capabilities Review, November 1991.

[6] Engels, R. C. and Junkins, J. L., "The Gravity-Perturbed Lambert Problem: A KS Variation of Parameters Approach," *Celestrial Mechanics*, Vol. 24, 1981, pp. 3–21.

[7] Lawton, J. A. and Martell, C. A., "Hybrid Neighboring-Optimal-Control and Lambert-Based Interceptor Boost-Phase Guidance," Naval Surface Warfare Center, 1994.

[8] Lawton, J. A. and Byrum, C. A., "Anti-Tactical Ballistic Missile Global Effectiveness Model Intercept Algorithm," Naval Surface Warfare Center, July 1994.

[9] Kaplan, M. H., *Modern Spacecraft Dynamics and Control*, chap. 3, John Wiley and Sons, New York, 1976.

[10] Vallado, D. A., *Fundamentals of Astrodynamics and Applications*, chap. 6, 7, 8 and 10, Microcosm, Hawthorne, CA, 3rd ed., 2007.

[11] Prussing, J. E. and Conway, B. A., *Orbital Mechanics*, chap. 4, 6, 8 and 10, Oxford University Press, New York, 1993.

[12] Geisel, C. D., *Navigation Solutions to Enable Space Superiority Through the Repeated Intercept Mission From Highly Elliptical Orbits*, Master's thesis, United States Air Force Institute of Technology, 2008.

[13] Curtis, H. D., *Orbital Mechanics for Engineering Students*, chap. 6, Elsevier, Boston, MA, 2nd ed., 2010.

[14] Boulet, D., *Methods of Orbit Determination for the Micro Computer*, Willman-Bell Inc, Richmond, VA, 1991.

[15] Kirk, D. E., *Optimal Control Theory: An Introduction*, Dover Publications, Mineola, New York, 1970.

[16] Bryson, A. E., *Dynamic Optimization*, Addison-Wesley, Menlo Park, CA, 1999.

[17] Conway, B. A., "The Problem of Spacecraft Trajectory Optimization," *Spacecraft Trajectory Optimization*, edited by B. A. Conway, chap. 1, Cambridge University Press, New York, 2010, pp. 1–13.

[18] Conway, B. A. and Paris, S. W., "Spacecraft Trajectory Optimization Using Direct Transcription and Nonlinear Programming," *Spacecraft Trajectory Optimization*, edited by B. A. Conway, chap. 3, Cambridge University Press, New York, 2010, pp. 37–76.

[19] Izzo, D., "Global Optimization and Space Pruning for Spacecraft Trajectory Design," *Spacecraft Trajectory Optimization*, edited by B. A. Conway, chap. 7, Cambridge University Press, New York, 2010, pp. 178–200.

[20] Gilbert, E. G., Howe, R. M., Lu, P., and Vinh, N. X., "Optimal Aeroassisted Intercept Trajectories at Hyperbolic Speeds," *AIAA Guidance, Navigation and Control Conference*, 1989.

[21] Arora, J. S., *Introduction to Optimum Design*, Elsevier, Boston, MA, 2nd ed., 2004.

[22] Prussing, J. E. and Chiu, J.-H., "Optimal Multiple-Impulse Time-Fixed Rendezvous Between Circular Orbits," *AIAA/AAS Astrodynamics Conference*, 1984.

[23] Boden, D. G. and Larson, W. J., *Cost-Effective Space Mission Operations*, chap. 10, McGraw-Hill, New York, 1996.

[24] Humble, R. W., Henry, G. N., and Larson, W. J., *Space Propulsion Analysis and Design*, chap. 2 and 10, McGraw Hill Companies, New York, 1995.

[25] Sellers, J. J., *Understanding Space: An Introduction to Astronautics*, chap. 6 and 7, McGraw-Hill Companies, Inc, New York, 2nd ed., 2000.

[26] Wertz, J. R. and Larson, W. J., *Space Mission Analysis and Design*, chap. 6, 11 and Appendix, Microcosm Press, El Segundo, CA, 3rd ed., 2003.

[27] Sidi, M. J., *Spacecraft Dynamics and Control: A Practical Engineering Approach*, chap. 3, Cambridge University Press, New York, 2006.

[28] Alfano, S., *Hypervelocity Orbital Intercept Guidance*, Phd dissertation, University of Colorado, 1988.

[29] Alfano, S. and Fosha, C. E., "Hypervelocity Orbital Intercept Guidance Using Certainty Control," *Journal of Guidance, Control and Dynamics*, Vol. 14, No. 3, 1993, pp. 574–580.

[30] Alfano, S., "Two Variations of Certainty Controll," *Journal of Guidance, Control and Dynamics*, Vol. 15, No. 4, 1992, pp. 1040–1043.

[31] Lawton, J. A., Martell, C. A., and Jesionowski, R. J., "Optimal Thrust Allocation for TBM Interceptor Midcourse Guidance," Naval Surface Warfare Center, 1996.

[32] Thorne, J. D., *Optimal Continous-Thrust Orbit Transfers*, Phd dissertation, United States Air Force Institute of Technology, 1996.

[33] Jezewski, D. J., "Guidance Equations for Quasi-Optimum Space Manuevers," Tech. rep., National Aeronautics and Space Administration, Washington D.C., August 1964.

[34] Ng, L., Breitfeller, E., and Ledebuhr, A. G., "An Optimal t-Dv Guidance Law for Intercepting a Boosting Target," *AIAA/Missile Defense Agency Technology Conference*, 2002.

[35] Deaton, A. W., Lomas, J. J., and Mullins, L. D., "A Plan for Spacecraft Automated Rendezvous," Tech. rep., National Aeronautics and Space Administration, Washington D.C., October 1992.

[36] Alfano, S. and Thorne, J. D., "Constant-Thrust Orbit-Raising Transfer Charts," Tech. rep., Phillips Laboratory, Kirtland AFB, NM, July 1993.

[37] Kluever, C. A., "Low-Thrust Trajectory Optimization Using Orbital Averaging and Control Parameterization," *Spacecraft Trajectory Optimization*, edited by B. A. Conway, chap. 5, Cambridge University Press, New York, 2010, pp. 112–138.

[38] Kechichian, J., "Analytic Representations of Optimal Low-Thrust Transfer in Circular Orbit," *Spacecraft Trajectory Optimization*, edited by B. A. Conway, chap. 6, Cambridge University Press, New York, 2010, pp. 139–177.

[39] McAdoo, S., "Development of a Method for Optimal Manuever Analysis of Complex Space Missions," Tech. rep., National Aeronautics and Space Administration, Washington D.C., April 1975.

[40] Jezewski, D., "Primer Vector Theory and Applications," Tech. rep., National Aeronautics and Space Administration, Washington D.C., November 1975.

[41] Prussing, J. E., "Primer Vector Theory and Applications," *Spacecraft Trajectory Optimization*, edited by B. A. Conway, chap. 2, Cambridge University Press, New York, 2010, pp. 16–36.

[42] Barbee, B. W., Alfano, S., Pinon, E., Gold, K., and Gaylor, D., "Design of Spacecraft Missions to Remove Multiple Orbital Debris Objects," *35th Annual AAS Guidance and Control Conference*, 2012.

[43] Eagle, D. C., "Orbital Mechanics with Numerit: Drag Perturbed Orbital Motion of Earth Satellites," Nov 2012.

[44] Fichtl, G. H., Antar, B. N., and Collins, F. G., editors, *Spacecraft Dynamcis as Related to Laboratory Experiments in Space*. NASA Marshall Space Flight Center, 1979.

[45] Wiesel, W. E., *Modern Astrodynamics*, chap. 1, 4 and 5, Aphelion Press, Beavercreek, OH, 2nd ed., 2010.

[46] Meirovitch, L., *Methods of Analytical Dynamics*, Dover Publications, Mineola, NY, 1970.

[47] Sengupta, P., Vadali, S. R., and Alfriend, K. T., "Semi-Analytical Approach to Target Access in the Responsive Space Problem," *6th Responsive Space Conference*, 2008.

[48] Bowman, B. R., "True Satellite Ballistic Coefficient Determination for HASDM," *AIAA/AAS Astrodynamics Specialist Conference and Exhibit*, 2002.

[49] Roscoe, C. W. T., Vadali, S. R., and Alfriend, K. T., "Third-Body Perturbation Effects on Satellite Formations," *American Astronautical Society*, 2012.

[50] Ocampo, C., "The Clohessy Wiltshire Model," September 2003.

[51] Thorne, J. D. and Hall, C. D., "Minimum-Time Continous-Thrust Orbit Transfers Using the Kustaanheimo-Stiefel Transformation," *Journal of Guidance, Control and Dynamics*, Vol. 20, No. 4, 1997, pp. 836–838.

[52] Wiesel, W. E., *Spaceflight Dynamics*, McGraw Hill, New York, 2nd ed., 1997.

[53] Schaub, H. and Alfriend, K. T., "J2 Invariant Relative Orbits for Spacecraft Formations," *Journal of Celestial Mechanics*, 1999.

[54] Vadali, S. R., Vaddi, S. S., and Alfriend, K. T., "An Intelligent Control Concept for Formation Flying Satellite Constellations," *International Journal of Robust and Nonlinear Control*, December 2000.

[55] Schaub, H. and Alfiend, K. T., "Hybrid Cartestian and Orbit Element Feedback Law for Formation Flying Spacecraft," *Journal of Celestial Mechanics*, 2000.

[56] Schaub, H. and Alfiend, K. T., "Impulsive Spacecraft Formation Flying Control to Establish Specific Mean Orbit Elements," *Journal of Celestial Mechanics*, 2000.

[57] Alfriend, Kyle T, S. H. and Gim, D.-W., "Gravitational Perturbations, Nonlinearity and Circular Orbit Assumption Effects on Formation Flying Control Strategies," *American Astronautical Society*, 2012.

[58] Vadali, S. R., Schaub, H., and Alfriend, K. T., "Initial Conditions and Fuel-Optimal Control for Formation Flying Satellites," *AIAA Guidance, Navigation and Control Conference*, 1999.

[59] France, M. E. B., "Back to the Future: Space Power Theory and A.T. Mahan," Tech. rep., National Defense University: National War College, Washington D.C., 2000.

[60] Turner, A. E., "Development of Geosynchronous Satellite Servicing," Tech. rep., National Aeronautics and Space Administration, Washington D.C., 2002.

[61] Richharia, M., *Satellite Communications Systems*, McGraw-Hill, New York, 2nd ed., 1999.

[62] Ippolito, L. J., *Satellite Communications Systems Engineering*, Wiley and Sons, West Sussex, United Kingdom, 2008.

[63] Sears, G. B., *Optimal Non-Coplanar Launch to Quick Rendezvous*, Master's thesis, United States Air Force Institute of Technology, 1997.

[64] Wiesel, W. E., *Modern Orbit Determination*, chap. 1 and 3, Aphelion Press, Beavercreek, OH, 2003.

[65] Hoffman, K. and Kunze, R., *Linear Algebra*, Prentice Hall, Upper Saddle River, NJ, 2nd ed., 1971.

[66] Zill, D. G. and Cullen, M. R., *Advanced Engineering Mathematics*, Jones and Bartlett Publishers, Sudbury, MA, 2nd ed., 2000.

[67] Hughes, P. C., *Spacecraft Attitude Dynamics*, Dover Publications, Mineola, NY, 2nd ed., 2004.

[68] Chioma, V. J. and Titus, N. A., "Navigation Solutions for the Repeated-Intercept Mission with Constrained Maneuver Time," *Journal of Spacecraft and Rockets*, Vol. 45, 2008, pp. 116–121.

[69] Chioma, V. J. and Titus, N. A., "Expected Maneuver and Maneuver Covariance Models," *Journal of Spacecraft and Rockets*, Vol. 45, 2008, pp. 409–412.

[70] Chioma, V. J., *Orbit Estimation Using Track Compression and Least Squares Differential Correction*, Master's thesis, United States Air Force Institute of Technology, 1997.

[71] Martin, C. and Conway, B., "Optimal Low-Thrust Trajectories Using Stable Manifolds," *Spacecraft Trajectory Optimization*, edited by B. A. Conway, chap. 9, Cambridge University Press, New York, 2010, pp. 238–261.

Vita

Abraham M. Leigh is a Captain in the U.S. Air Force studying at the Air Force Institute of Technology, Wright-Patterson AFB, OH. His areas of interest are Orbital Mechanics, Space Operations and Optimal Trajectories. Prior to his study at AFIT he served in several capacities within the Air Force.

Most recently, he was a Space Systems Engineer at the Aerospace Data Facility, Buckley AFB, CO. There he was responsible for the command and control team for a national space system. His duties also included the identification, development and delivery of future capabilities to meet emerging needs.

Prior to assignment to Buckley AFB, Captain Leigh was the representative to the Operationally Responsive Space Office to deliver responsive space capabilities directly to a Combatant Commander. His job required the development of tactics, techniques and procedures for the tasking, collection, processing, exploitation and dissemination of intelligence directly to fielded users.

His career began at Schriever AFB, CO where he led a team to manage a test range of post-operational satellites to execute testing for the DoD, NASA and other national agencies. The capstone of this assignment was his role as the responsible engineer for the Orbital Express On Orbit Demonstration Satellite System. Orbital Express was the first satellite system to perform on-orbit autonomous capture, refueling and satellite servicing.

Captain Leigh completed his Master's in Space Operations Engineering from the University of Colorado at Colorado Springs. He is an Astronautical Engineering graduate of the United States Air Force Academy where he played on the offensive line for the Fighting Falcons. Throughout his career he has shared his love for football by coaching varsity football teams in various capacities. His players have made both the All-Conference and All-State teams.

REPORT DOCUMENTATION PAGE

Form Approved
OMB No. 0704–0188

1. REPORT DATE *(DD–MM–YYYY)*	2. REPORT TYPE	3. DATES COVERED *(From — To)*
14–09–2014	Doctoral Dissertation	Oct 2011–Sep 2014

4. TITLE AND SUBTITLE

Navigation Solution for a Multiple Satellite and Multiple Ground Architecture

5a. CONTRACT NUMBER

5b. GRANT NUMBER

5c. PROGRAM ELEMENT NUMBER

6. AUTHOR(S)

Leigh, Abraham M., Captain, USAF

5d. PROJECT NUMBER

5e. TASK NUMBER

5f. WORK UNIT NUMBER

7. PERFORMING ORGANIZATION NAME(S) AND ADDRESS(ES)

Air Force Institute of Technology
Graduate School of Engineering and Management (AFIT/EN)
2950 Hobson Way
WPAFB, OH 45433-7765

8. PERFORMING ORGANIZATION REPORT NUMBER

AFIT-ENY-DS-14-S-1

9. SPONSORING / MONITORING AGENCY NAME(S) AND ADDRESS(ES)

Dr. Greg Spanjers
AFRL/RV
3550 Aberdeen Ave SE
Kirtland AFB, NM 87117-5776
gregory.spanjers@us.af.mil
DSN 246-9330

10. SPONSOR/MONITOR'S ACRONYM(S)

AFRL/RV

11. SPONSOR/MONITOR'S REPORT NUMBER(S)

12. DISTRIBUTION / AVAILABILITY STATEMENT

DISTRIBUTION STATEMENT A:
APPROVED FOR PUBLIC RELEASE; DISTRIBUTION UNLIMITED

13. SUPPLEMENTARY NOTES

14. ABSTRACT

This research presents the phased development of an algorithm to plan impulsive orbital maneuvers based on the relative motion between multiple satellites and multiple ground locations. The algorithm leverages the state transition matrix derived from the equations of motion and the equations of variation for the non-spherical Earth and air drag effects. The algorithm determines the impulsive maneuver to achieve the user-defined terminal conditions. The first phase solves for the first burn of an orbital transfer between user-defined altitudes. The optimum trajectory is determined and compared to the first burn in a Hohmann Transfer. The results are expanded to include varying the inclination and eccentricity of the initial orbit. The second phase solves for the minimum time trajectory resulting from a fixed fuel maneuver to transfer a satellite between user-defined altitudes. The results include the transfer time and transfer angle for the minimum time trajectory. The third phase places a satellite within a sphere, of user-defined radius, centered on a non-maneuvering satellite within a constrained time. The results are presented for prograde orbits. An empirical method to determine the optimum ΔV is provided. The fourth phase places a satellite within the overlapping spheres, of user-defined radii, centered on multiple non-maneuvering satellites, within a constrained time. Empirical methods are presented to determine the separation distance and optimum ΔV. The final phase culminates by delivering a satellite within the overlapping spheres, centered on multiple non-maneuvering satellites and ground locations, constrained by range and elevation angle, within a constrained time. An empirical model to calculate the optimum ΔV is shown. All results illustrate mission design trade-offs including ballistic coefficient, orbit inclinations, eccentricity and orbit sizes.

15. SUBJECT TERMS

Optimal Trajectory; Space Navigation; Orbit Estimation Theory

16. SECURITY CLASSIFICATION OF:			17. LIMITATION OF ABSTRACT	18. NUMBER OF PAGES	19a. NAME OF RESPONSIBLE PERSON
a. REPORT	b. ABSTRACT	c. THIS PAGE			Dr. Jonathan T. Black (ENY)
U	U	U	UU	271	19b. TELEPHONE NUMBER *(include area code)* (937) 255-3636 x3645 jonathan.black@afit.edu